DEVELOPMENT OF A REACTION SIGNATURE

FOR COMBINED CONCRETE MATERIALS

A Dissertation

by

HASSAN A. GHANEM

Submitted to the Office of Graduate Studies of
Texas A&M University
in partial fulfillment of the requirements for the degree of

DOCTOR OF PHILOSOPHY

May 2009

Major Subject: Civil Engineering

DEVELOPMENT OF A REACTION SIGNATURE

FOR COMBINED CONCRETE MATERIALS

A Dissertation

by

HASSAN A. GHANEM

Submitted to the Office of Graduate Studies of
Texas A&M University
in partial fulfillment of the requirements for the degree of

DOCTOR OF PHILOSOPHY

Approved by:

Chair of Committee,	Dan G. Zollinger
Committee Members,	Robert L. Lytton
	Dallas N. Little
	Bruce Herbert
Head of Department,	David V. Rosowsky

May 2009

Major Subject: Civil Engineering

ABSTRACT

Development of a Reaction Signature for Combined Concrete Materials. (May 2009)

Hassan A. Ghanem, B.E., M.E., Beirut Arab University, Lebanon;

M.S., Texas Tech University

Chair of Advisory Committee: Dr. Dan G. Zollinger

Although concrete is widely considered a very durable material, if conditions are such, it can be vulnerable to deterioration and early distress development. Alkali-Silica Reaction (ASR) is a major durability problem in concrete structures. It is a chemical reaction between the reactive silica existent in some types of rocks and alkali hydroxides in the concrete pore water. The product of this reaction is a gel that is hygroscopic in nature. When the gel absorbs moisture, it swells leading to tensile stresses in concrete. When those stresses exceed the tensile strength of concrete, cracks occur. The main objective of this study was to address a method of testing concrete materials as a combination to assist engineers to effectively mitigate ASR in concrete. The research approach involved capturing the combined effects of concrete materials (water cement ratio, porosity, supplementary cementitious materials, etc.) through a method of testing to allow the formulation of mixture combinations resistant to ASR leading to an increase in the life span of concrete structures.

To achieve this objective, a comprehensive study on different types of aggregates of different reactivity was conducted to formulate a robust approach that takes into account the factors affecting ASR; such as, temperature, moisture, calcium concentration and alkalinity. A kinetic model was proposed to determine aggregate ASR characteristics which were calculated using the System Identification Method. Analysis of the results validates that ASR is a thermally activated process and therefore, the reactivity of an aggregate can be characterized in terms of its activation energy (E_a) using the Arrhenius equation. Statistical analysis was conducted to determine that the test protocol is highly repeatable and reliable.

To relate the effect of material combinations to field performance, concrete samples with different w/cm's and fly ash contents using selective aggregates were tested at different alkalinities. To combine aggregate and concrete characteristics, two models

iv

were proposed and combined. The first model predicts the E_a of the aggregate at levels of alkalinity similar to field conditions. The second model, generated using the Juarez-Badillo transform, connects the ultimate expansion of the concrete and aggregate, the water cement ratio, and the fly ash content to the E_a of the rock. The proposed models were validated through laboratory tests. To develop concrete mixtures highly resistant to ASR, a sequence of steps to determine threshold total alkali in concrete were presented with examples. It is expected that the knowledge gained through this work will assist government agencies, contractors, and material engineers, to select the optimum mixture combinations that fits best their needs or type of applications, and predict their effects on the concrete performance in the field.

DEDICATION

To my parents

Akram Ghanem and Salam Sayadi

who dedicated their lives for the education of their two children

And to my beloved sister

Noha

For their endless love, encouragement and support

ACKNOWLEDGEMENTS

First and foremost, I thank the Lord (Allah) for his continuous bounties and guidance in my life.

This dissertation concludes my learning journey at Texas A&M University (TAMU). I am grateful to many individuals who contributed to my learning experience at TAMU.

At the top of the list is my advisor, Dr. Dan G. Zollinger, for giving me this wonderful opportunity to work on this research project, and for his invaluable guidance, inspiration, and advice. He is a symbol of humbleness, intelligence, and creativeness that inspired me all the time. What I learned from him exceeds by far the contents of this dissertation. What I have learned from him can be summarized in two words: "THINK BIG". I am very honored to know Dr. Zollinger and I will always treasure my association with him.

I am indebted to Dr. Robert L. Lytton for his constant support, valuable insight and encouragement he offered me in the past four years. He was always ready and happy to answer all my questions and I have gained a lot from our discussions. What I learned from him in the modeling part is more than I ever thought was possible.

I want to also thank the distinguished professors, Dallas Little and Bruce Herbert, for serving as valuable committee members and for their very kind advice and helpful ideas. Another thanks goes to Dr. Anal for his suggestions.

I want also to take this opportunity to thank my former advisors at Texas Tech University, Dr. Scott Phelan and Dr. Sanjaya Senadheera for their continuous encouragement.

I would like to express my sincere gratitude to the crew of McNew and Civil Engineering lab: Lee Gustavus, Jeff Perry, Gerry Harrison, Tony Barbosa, Rick Seneff and Scott Cronauer, for their tremendous help and input in the instrumentation part. They taught me some tips that made my life easier in the lab. Also, I want to thank Pam Kopf, Teresa Boriski, Cathy Bryan, and Pamela Fritcher for their kind assistance, whether it was related to scheduling field trips, using printers, or helping me making arrangement for my defense. Another big thanks goes to Dr. Ruth Schemmer for her help in preparing

my academic application documents. The help that I received from the staff of the business office in the Civil Engineering Department, especially from Anni Brunker and Mary Louise Sims is highly appreciated.

I would like to express my sincere gratitude to many people for their support and assistance that I received during my stay in college station. Those include our current research group and some friends: Dr. Emad Kassem, Dr. Enad Mahmoud, Dr. Abdallah Farraj, Dr. Selcuk Dincal, Dr. Juanyu Liu, Dr. Dan Ye and Dr. Reza Ashtiani. The unconditional help and advice that I receive from my buddies at Texas Tech University, especially Mr. Sanad Shamsan, Dr. Mohammed Zain and Dr. Abdul Rahman Habshi, is highly appreciated.

My appreciation goes to my dear cousin Dr. Amine Ghanem for our endless discussions about: "Life", "Honda", "Japanese conspiracy against Lebanon" etc. It was fun.

I am ever indebted to my family for their continuous support and patience during my study in the US. Thanks Mom and Dad for everything: the financial support, the encouragement sheer and love. I can't ever repay for what y'all have done for me. Without a doubt, it would not be possible to complete this dissertation successfully without the invaluable tactical advice from my beloved sister Noha. Thank you Lili.

TABLE OF CONTENTS

LIST OF FIGURES

LIST OF TABLES

CHAPTER I

INTRODUCTION

General

Portland cement concrete being used in almost every structure, ranging from commercial buildings, bridges, to pavements is considered a very important structural material. Unfortunately, concrete like any other material is subjected to environmental conditions that make it vulnerable to deterioration, potentially reducing significantly its service life. As the cost of demolishing and reconstruction concrete structures continually increase, concrete durability becomes a key issue among engineers, owners, and government agencies.

Alkali-silica reaction (ASR) is one of the most recognized durability issues in portland cement concrete that contributes to premature degradation. It is a chemical reaction between reactive silica existent in some types of rocks and alkali hydroxide in the concrete pore water. The product of this reaction is a gel that can be in a liquid or solid state depending on the concentrations of its components (sodium, potassium, calcium, hydroxide, silica, etc) (Mindess, Young, and Darwin 2006). The get itself is not harmful but at the same time, it is hygroscopic in nature. When the gel absorbs moisture, it swells. Swelling leads to tensile stresses in concrete. When those forces exceed the tensile strength of concrete, cracks occurs. Further damage occurs because ASR doesn't stop at this point as those cracks create fresh surfaces and act as open passages for other chemicals (chloride ions, sulfate ions, etc) to attack the matrix of the concrete leading to more damage. Unfortunately, ASR damage may exponentially shorten the life of a concrete structure to survive at least 15 years to needing replacement only after 5 to 10 years (Young, et al. 1998). Consequently, tremendous pressure is placed on the shoulder of design engineers and contractors to select the right materials (type of aggregate, type of cement, supplementary cementitious materials (SCM), chemical admixtures, etc) that will lead to the most durable concrete possible that lasts for many decades.

———————

This dissertation follows the style and format of *Journal of Transportation Engineering*.

This dissertation is the result of a research project sponsored by the Innovative Pavement Research Foundation (IPRF) entitled *"Mitigation of ASR in Concrete - Combined Materials Test Procedure"*. The main objective of this research is to address a method of testing concrete materials as a combination to assist engineers to effectively mitigate ASR in concrete. The research approach involved capturing the combined effects of concrete materials (water cement ratio, porosity, supplementary cementitious materials, etc) through a method of testing to allow the formulation of mixture combinations resistant to ASR leading to an increase in the life span of concrete structures.

Research Significance and Problem Statement

As mentioned above, ASR is a major issue of worldwide interest. Consequently, many researchers and agencies have invested significant amount of time and energy to develop test procedures and approaches to mitigate this chemical reaction.

One technique was to use non-reactive aggregate removing a key component deemed necessary to initiate the ASR reaction. This solution is perhaps ideal, as long non-reactive aggregate are available however the majority of rocks contain some forms of reactive silica in different forms and structure (Swamy 1992).

Another approach has been to use low alkali cement in concrete mixtures leading to a decrease of ASR potential. However, this may not be achievable as alkali may come from outside sources like deicers salts used during winter to remove ice formed at the top of the pavement. A study conducted by Rangaraju and Olek in 2007 indicated that the use of low alkali cement in concrete specimens subjected to deicers only delays ASR expansion and does not prevent it.

A third approach is the introduction of supplementary cementitious materials (SCM) like fly ash, slag and silica fume in the mixtures to minimize the incidence of ASR. The results are promising although it is mentioned in the literature that SCM's sometimes contribute to the total amount of alkali in the concrete matrix. The addition of lithium recently was seen an important tool in mitigating ASR (Desai 2007).

Most of the available laboratory test methods are focused on aggregate reactivity. The most common procedure is ASTM C 1260 "Standard Test Method for Potential

Alkali Reactivity of Aggregates (Mortar- Bar Method)" (ASTM 2000b). However, results obtained from this test have little correlation to actual field performance. Most of the ASR research conducted using ASTM C1260 has involved some form of modification (i.e. increasing the testing duration) in order to predict the behavior of the tested aggregate field conditions. The result of this method of testing often only provides a clue as whether the aggregate is reactive or not.

An alternative to ASTM C 1260 is ASTM C1293 "Standard Test Method for Concrete Aggregate by Determination of Length Change of Concrete Due to Alkali-Silica Reaction" (ASTM 2000a).It is considered a good index of field performance however the duration of the test extends to one year and this is considered a major drawback.

Clearly, these short comings warrant a completely different approach to ASR testing. Current testing methodology apply to only a narrow band of conditions making the risk associated with the use of a new source of untested aggregate unacceptably high. Better tools are needed to evaluate concrete materials for ASR that are both robust and useful in the prediction of concrete field performance of concrete subjected to ASR and this research is a step in this direction. The major outcome of this research is to provide an approach in which to develop recommendations for using combined concrete materials while keeping ASR in check.

Objectives

The ultimate objective of this study was to develop a method of testing to assist mitigation of ASR. This was achieved by developing a robust and reliable test protocol that can be performed within a reasonably short period of time and have the capability of capturing the effect of combined concrete materials on ASR potential. The developed protocol can assist pavement engineers, owners and government agencies to quantify the potential for concrete degradation as a consequence of ASR. To this end, the following steps are accomplished:

- Development of a test protocol to measure ASR expansion using dilatometry.
- Identifying key material related parameters that affect ASR. The parameters are determined using a mathematical procedure entitled "System Identification Method".

- Predicting potential ASR aggregate reactivity in terms of their activation energy making use of the Arrhenius equation.
- Determining of the ultimate expansion of aggregate subjected to ASR.
- Determining of an alkali threshold for design that will lead eventually to the development of concrete mixtures highly resistant to ASR.

Organization of the Dissertation

This dissertation consists of seven chapters. Each chapter is briefly summarized below.

Chapter I is an introduction addressing a statement of the research followed by a description of project objectives and outline.

Chapter II presents a review of the available literature relevant to the study of ASR in pavement structures. The first part defines and introduces the main requirement deemed necessary by previous researchers to initiate the chemical reaction followed with a brief overview of the chemistry of ASR and the current mechanisms of ASR expansion. Chapter II also includes a complete review of the main experimental, technical, and traditional test methods to assess ASR. The last part of this chapter summarizes the role and effectiveness of using mineral admixtures like fly ash, slag and silica fume in decreasing the deleterious effects of ASR.

Chapter III describes the materials and their properties used in the test program undertaken for this project. It also includes the experimental design and the laboratory testing to achieve the objectives of the investigation. Description of the equipment and test procedures to measure ASR expansion for aggregate and concrete including the calibration procedure to calculate ASR expansion is also provided.

Chapter IV describes the methodology proposed to develop a strategy in which to mitigate ASR. To this end, a kinetic model was developed taking into consideration the main parameters that have significant effect on ASR. Those variables are determined using the system identification procedure (SID). Also aggregate reactivity was characterized based on their measured activation energy. A new generalized model that connects aggregate reactivity, alkalinity of the pore water and the ratio of the ultimate expansion concrete to ultimate expansion of the aggregate is also introduced. The

algorithm used to determine the parameters of the above models are thoroughly discussed and outlined.

Chapter V presents the analysis and interpretation of the aggregate solutions tests. The results of the analysis carried out are presented in the forms of graphs and tables. The chapter starts by displaying the ASR time-expansion data for aggregate expansion at different temperatures and alkalinities followed by a discussion of the effect of alkalinity on activation energy. Ranking of the four aggregates against each other based on their reactivity is also presented. The effect of temperature on the rate constant and the effect of calcium hydroxide on the ultimate expansion of aggregate are also discussed thoroughly. To check the reliability and the repeatability of the test protocol and procedure proposed in Chapter IV, an intra and inter-laboratory comparisons between Texas Transportation Institute (TTI) and University of New Hampshire (UNH) is conducted. Analysis is also performed on the chemistry of the pore water and results are tabulated.

Chapter VI presents and discusses the results of the concrete tests proposed in the experimental plan. The parameters of the generalized concrete model were determined using the SID method. Using these parameters, a set of relationships linking alkalinity, aggregate reactivity, and the ratio of the ultimate expansion of concrete to the ultimate expansion of the aggregate are proposed. The effects of the combined concrete materials (water cement ratio, fly ash, etc) on ASR performance are also presented. Based on these effects, concrete mixtures highly resistant to ASR can be developed and formulated.

Chapter VII is a summary of the knowledge obtained through this study. The main conclusions and findings are presented and discussed. Recommendations are proposed in this chapter to answer a key question of: "How to predict the ASR-related performance of concrete for a given set of exposure conditions?" This chapter also provides crucial information concerning the selection of concrete materials to mitigate ASR. Suggestions for further investigation are also provided.

CHAPTER II

LITERATURE REVIEW

This chapter provides in 4 parts a comprehensive literature review of alkali-silica reaction (ASR) in concrete. The first part defines and introduces the nature of ASR in concrete and the main requirement needed for the ASR chemical reaction to initiate and spread. The second part deals specifically with the chemistry of the alkali ASR and its relationship to the chemistry of cement and aggregate. The third part provides a detailed explanation regarding current test methods for assessing ASR including both experimental and analytical techniques; traditional methods, and rapid test methods. Lastly, this chapter addresses the role and effectiveness of mineral admixtures (fly ash, silica fume and slag) in reducing or eliminating the deleterious effect of ASR expansion.

Introduction

Alkali-silica reaction is a combination of chemical reactions that occur within the microstructure of the concrete matrix. It involves alkali hydroxide coming most of the time, from the cement used in the concrete and some reactive form of silica existing within the aggregate structure. The product of this reaction is a gel known as "Alkali Silica Gel" which is not harmful. However, this gel has a tendency to swell in the vicinity of concrete moisture coming from the pores in the concrete, causing internal stresses within the matrix. These swelling pressures depend on many factors: gel composition, temperature, type and composition of reacting materials. With further absorption of moisture, these pressures increase and become high enough to induce the development of microcracks in the concrete and eventually its failure. A schematic drawing of ASR is shown in Figure 2.1.

Typical characteristics of ASR include cracking (Figure 2.2), misalignment of structural elements (Figure 2.3), and spalling at the concrete surface. The alkali-silica reaction is slow and takes many years to develop and it is very devastating when alkalis are found in high concentration in the pore fluid.
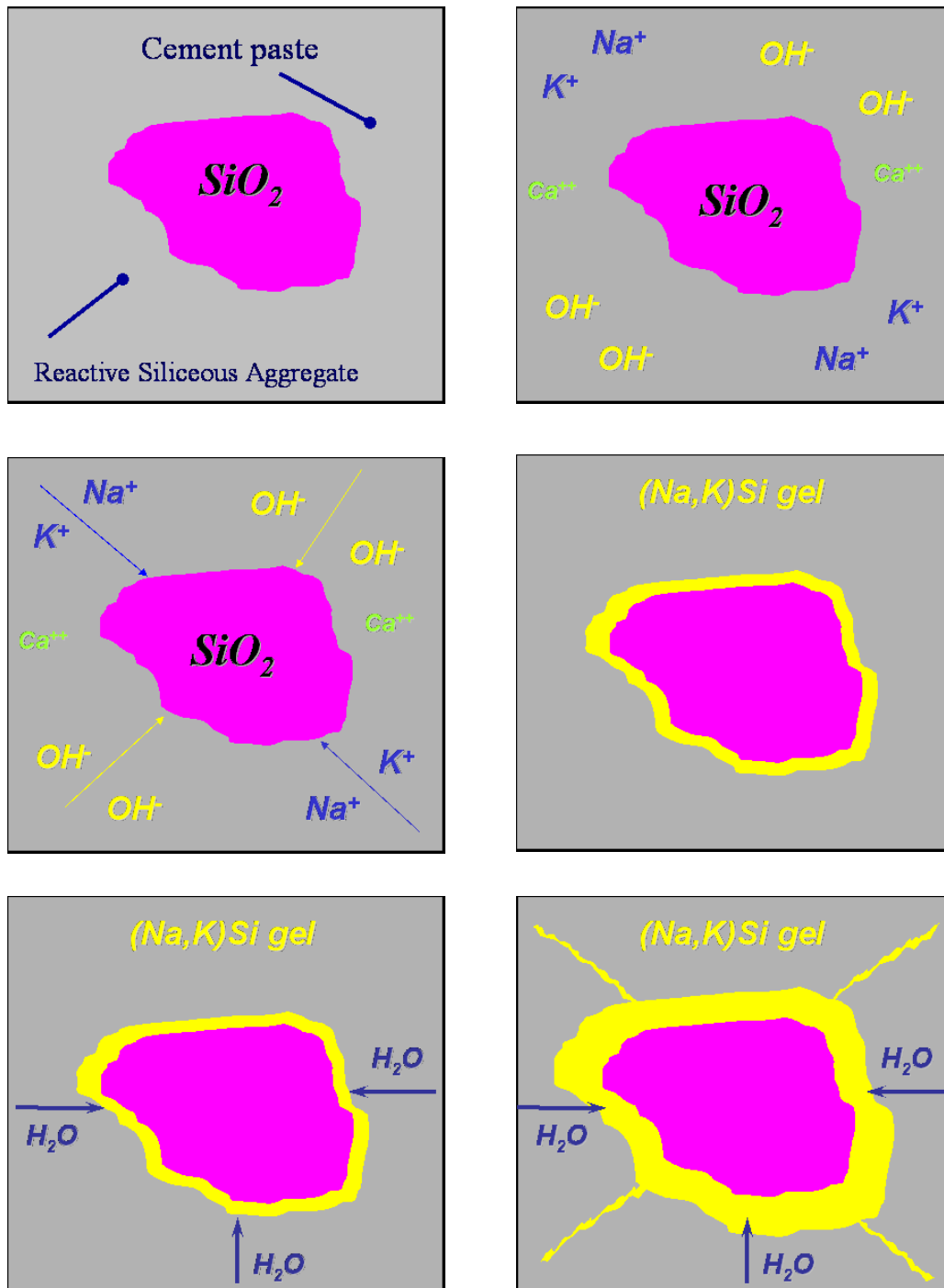
Figure 2.1 Schematic of Alkali-Silica Reaction (Modified from Thomas et al. 2007).
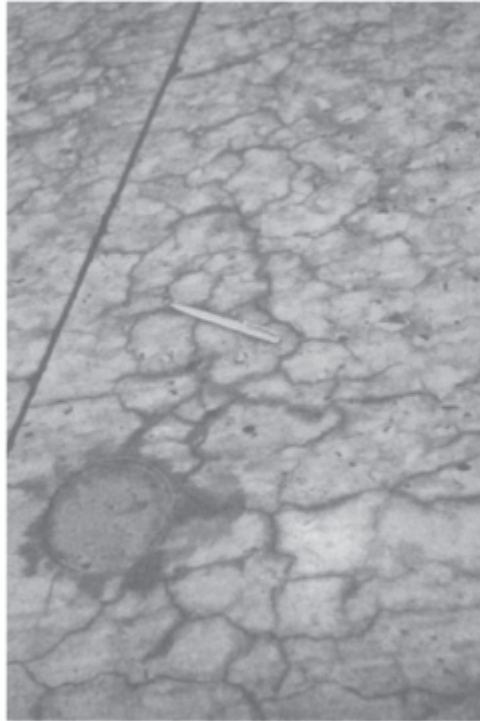
Figure 2.2 Map Cracking, Portion of Concrete Road Pavement (Swamy 1992).

Figure 2.3 Misalignment of Adjacent Sections of a Parapet Wall on a Highway Bridge
Due to ASR (Strategic Highway Research Program (SHRP)-315, 1991).

Alkali - Silica Reaction

In early 1900, it was noticed that although concrete is a durable material, it was still
susceptible to deterioration due to a combination of exposure to seawater and frost

thought at that time as the primary agent for degradation. At the same time however, many other cases of concrete failures were left without explanation.

In California, late 1930's, it was observed that relatively new concrete structures began developing severe cracking, although these new structures met the standard of construction at that time. It was Stanton in 1940 that established the existence of the alkali-silica-reaction as an internal deleterious process within the structure of concrete. From that point forward, it was clear to researchers and scientists that concrete exposure to harsh environment was of less importance than the characteristics and properties of the aggregate and cement used. Research studies followed and progressed rapidly in a couple of different directions, ranging from understanding the chemical reaction of alkali-silica reaction itself, assessing the reaction effects of ASR to identifying the aggregate mineral components involved in the reaction.

Major Components of ASR

Many researchers have different opinions about the mechanisms that govern ASR and different schools of thought are found in the literature about which mechanism is most prevalent in initiating ASR, but all researchers have agreed that the major components necessary for ASR-induced damage in the structure of the concrete are (Figure 2.4):

    a) Reactive Silica

    b) Sufficient Alkali

    c) Sufficient moisture

Figure 2.4 The Three Necessary Components for ASR-induced Damage in Concrete (Folliard et al, 2006).

Reactive Silica

Silica (SiO_2) constitutes about 65% by weight of the quantifiable components of the earth (Swamy 1992). Silica occurs mainly in nature as the mineral quartz. The physical property and atomic structure of silica is known. It consists of Silicon (Si) at the center of a tetrahedron of four oxygens. The bonds between oxygen and silicon are semi covalent. Each tetrahedron is connected to the one adjacent to it, in fact, the oxygen is shared among two other tetrahedrals. The tetrahedrals are fully cross linked into a three dimensional framework. The cross-linking of these frameworks is not the same among all; in fact, it depends on the temperature and pressure. Quartz, which is found in great quantity, is one of the polymorphs where the cross-linking is strong; hence it is dense and unreactive, being insensible to the presence of the majority of alkalis. On the other side, two other framework types, named tridymite and cristoballite are more open (i.e. less dense) relative to Quartz, and therefore, they expose significantly enhanced reactivity towards alkali (Swamy 1992). In addition to the above crystalline polymorph, some disordered frameworks also take place. These disordered structures increase the potential for reaction with cement alkali.

In addition, silica displays a unique structural relationship with water. The structure of water molecule consists of an oxygen atom surrounded by two hydrogens atoms and two electrons in an approximately tetrahedral array. This geometric similarity between water and silica make it possible for water to be substituted to some degree in silica. In crystalline silica (i.e. Quartz), the amount of this substitution is extremely small (parts per million). However, these replacements in less crystalline silica will be much higher (several per cent or more). In reality, the Si-O-Si bonds which are considered strong are destroyed by hydroxylation and substituted by the more reactive Si-OH ***Si-OH bonds where *** corresponds to a weak hydrogen bond. The mentioned amorphous hydrous silicas in contact with alkalis are very reactive. Their most common names, depending on their physical form and origin are: opal, chert and chalcedony. The above disordered silica have one main feature in common: they are extremely difficult to qualify and determine by methods such as X-ray diffraction because they have a low degree of crystallinity (Swamy 1992).

Although silica is present in the majority of rock, most aggregate used in concrete structures are composed of more than just one mineral. Limestone, which is a sedimentary rock composed largely of calcium carbonate, contains also a small amount of other minerals, and clay and quartz are the most common. Similarly, quartzites and sandstones, although considered monomineralic, contain also a small percentage of feldspar and micas (Swamy 1992).

The majority of coarse aggregate used in concrete mixes contains small amounts of silica. But one of the most important requirements for the alkali-silica reaction to take place in concrete is the presence of "reactive silica". The requirement for a siliceous material to be reactive is that the form of silica should be either a) poorly crystalline or contains a lot of lattice defects or b) glassy or amorphous in character. It was also mentioned that silica should be micro porous to provide a high surface area for the reaction. Therefore, most researchers state that it is inaccurate to consider the rock type as a criterion for aggregate reactivity, but rather attention should go to the reactivity of the mineral components of the rock itself. It was reported that as a little as 2 % of reactive silica is enough to observe distress in concrete structures (Swamy 1992). The most common type of rock and reactive minerals are compiled and summarized in Table 2.1.

Table 2.1 Rock Types and Reactive Minerals Susceptible to ASR (CSA, 2000).

Rocks	Reactive Minerals
Arenite	Crisobalite
Argillitequartz opal	Cryptocrystalline (or
Arkose	microcrystalline)
Chert	Strained quartz tridymite
Flint	Volcanic glass
Gneiss	
Granite	
Greywacke	
Hornfels	
Quartz-arenite	
Quartzite	
Sandstone	
Shale	
Silicified carbonate	
Siltstone	
Limestone	

Sufficient Alkali

Many concrete structures displaying severe distress due to alkali-silica reaction were made using high-alkali cement. The presence of alkali is necessary for the ASR to start. Alkalis are basic, ionic salt of an alkali metal. They are well known for being bases (i.e. their pH is higher than 7). They are located in the Group 1 in the periodic table (Figure 2.5).

Figure 2.5 Location of Alkali in the Periodic Table (group1).
http://www.dayah.com/periodic/

The alkalis are: lithium, sodium, potassium, rubidium, cesium and francium.

Alkali from concrete structures can come from:

a) Ordinary Portland cement

b) Aggregates

c) Mineral admixtures (Fly Ash, Silica fume, slag)

d) Chemical admixtures (Superplasticizers, etc)

e) De-icing salts

f) Water

Ordinary portland cement contains a small amount of alkali (sodium and potassium) present as sulphates $(K, Ka)SO_4$. These alkalis originate from the raw material used in the cement manufacture. If the raw material contains illitic clay or mica, the clinker (product of the kiln) will be rich in potassium. If the material contains feldspar, the clinker will contain, depending on the composition of feldspar more sodium, potassium or both. The final proportion of alkali in the clinker will depend on the proportion of mineral in the rock and on the manufacture of cement in the plant referred.

In general, alkali content in the clinker is divided into two types (Swamy 1992): alkali that are found and condensed on the clinker grain's surface as sulfate salts, and alkali that are restricted and secured within the clinker mineral's crystal structure. When clinker comes in contact with water, hydration occurs, and both types of alkalis behave differently from each other with respect to their release rates. The ones present as water soluble sulphates will be available for solution right away, but the ones secured into the grain becomes available in much slower rate during the process of hydration. The release rate is not constant and depends on the type of cement and the percentage of each type of alkali. Since alkali-silica reaction is a very slow process, Swamy assumes that it is safe to assume that all cement alkali will be available for release.

The total amount of cement alkali is the summation of potassium and sodium oxide and is generally expressed in terms of "sodium equivalent"

$$\% \ Na_2O_{equivalent} = \%Na_2O + 0.658 \ \%K_2O \qquad (2.1)$$

where:

$\% \ Na_2O_e$ = weight percentage of total sodium oxide equivalent

$\% \ Na_2O$ = weight percentage of sodium oxide content

$\% \ K_2O$ = weight percentage of potassium oxide content

The alkali concentration needs to reach a certain threshold value if the alkali-silica reaction is to proceed. Stanton in 1940 in his research stated that ASR will likely not occur in the structure if the alkali content of cement is less than 0.6% $Na_2O_{equivalent}$. Based on his work, the American Society for Testing and Materials (ASTM) C 150 recommend

the above threshold 0.6%. Experience with the mitigation of ASR, suggests that putting a threshold on the amount of alkali in cement is not effective in preventing the deleterious effects of ASR and is not the correct approach to specify alkali levels. The focus should rather be to control the total amount of alkali in concrete mixtures. Many agencies and countries specified that total permissible alkali to be between 2.5 and 4.5 kg/m^3. They also stated that the previous boundaries are not rigid but depends on the aggregate reactivity (Nixon and Sims 1992).

In his report in 2005, Folliard presented a plot (Figure 2.6) showing the relationship between the alkali content in concrete and the % expansion at 2 years. This plot shows clearly that the threshold of 3.0 kg/m^3 Na$_2$O$_{equivalent}$ withstands expansion up to two years. However, others have reported continuing expansion even with the total alkali content less then 3 kg/m^3 (Swamy 1992). It is interesting to notice that the curve follows an S-shape pattern.
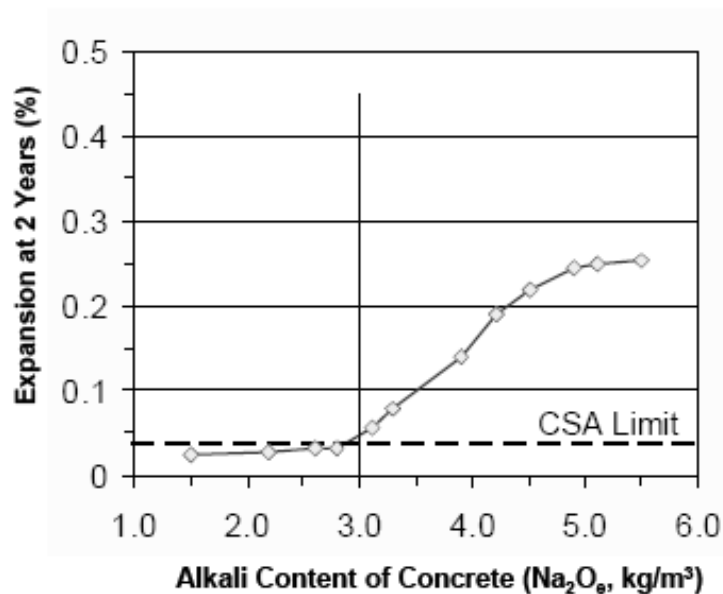
Figure 2.6 Effects of Alkali Content on Expansion of Prisms Stored Over Water at 38 °C (Folliard et al. 2006).

Despite the fact that in some cases, the total alkali in the cement paste may be very low, reactive aggregate may contain large amounts of alkalis (French 1986). Some mineral components of the rock, mainly feldspar, mica and illitic clay contain some alkalis in their structure. Researchers are divided whether these alkalis will be available

for release in the concrete and therefore increasing the alkali amount in the matrix or, locked within the crystal lattice (Thomas, Blackwell, and Pettifer 1992). But there is a general agreement that where the aggregate is subjected to "geological weathering" for a long period of time, the debasement of the mineral inside the rock will help by leaching some of the alkali in the pore water of the concrete. Under extreme conditions, some aggregates can release up to 10% of the total alkali into the cement (Stark and Bhatty 1986).

Mineral admixtures (silica fume, slag, fly ash), as by-products of industrial processes, contain some alkali. The alkali content of each is different because the chemical and physical properties of the above admixtures are variable. Silica fume, a byproduct of producing silicon metal, has a simple composition. It consists mainly of silicon dioxide (SiO_2) with a small amount of aluminum and magnesium, and its alkali content is normally low. Slag is a by-product of smelting ore. Depending on the plant practice and the ore origin, their composition is variable. The alkali content of slag is evenly distributed and reasonably high and may exceed 1% and is higher than the alkalis found in the portland cement. But at the same time, alkalis are restricted in slags and their release in the concrete is very slow and may take decades (Idorn 1967). Fly ash is a by-product from the combustion of coal and its composition is even more variable than that of slag. Both types (silica rich fly ash designated Class F and calcium rich ash designated Class C) may contain significant alkalis located at the surface of the particles. Researchers agreed that the alkali content of both types should be considered available for release in the concrete and therefore increasing the total alkali content in the mixtures. (Swamy 1992). The effect of alkalis coming from fly ash, slag and silica fume on the alkali-silica reaction is a point of controversy among researchers even though in many instances their effect is simply ignored. Nonetheless, the Canadian Standards Association (CSA) guidelines limit the amount of alkali of supplementary cementitious materials based on their chemistry and replacement levels.

The presence of alkalis in the pore fluid in concrete is well established in the literature and has led researchers to focus on the chemistry of the pore fluid (Diamond, 1983). At the beginning, the pore solution is composed of calcium, sulphate and alkali hydroxides (Figure 2.7), but after two days, the concentration of those elements remains

constant for a long time period (Figure 2.8); around 0.8 N for hydroxide, 0.2 N for sodium and 0.4 N for potassium while the concentration of calcium is almost negligible. The above values are for a cement paste with w/cm = 0.5 and type I cement and 0.91% Na_2O_e.
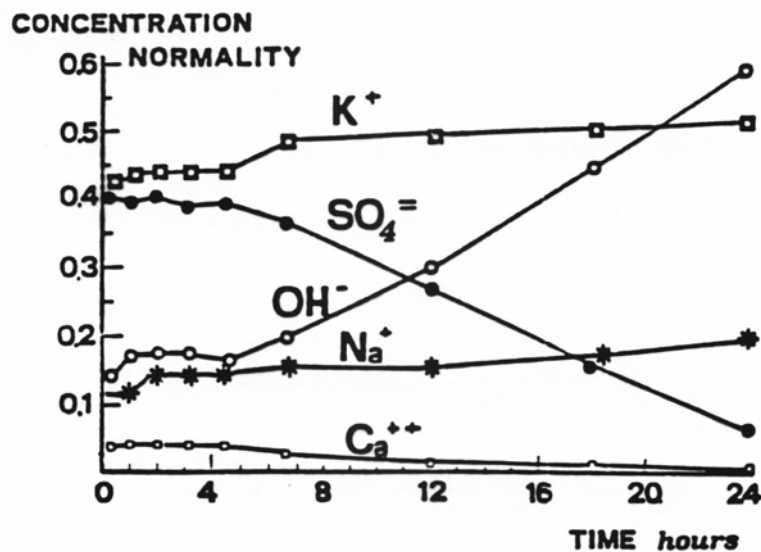
Figure 2.7 Pore Solution Concentration for the First 24 h (Diamond 1983).
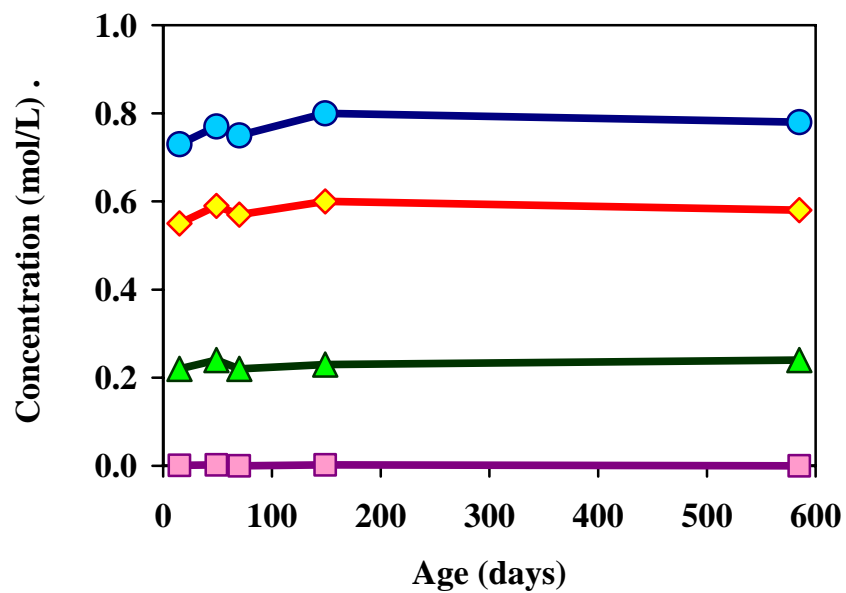
Figure 2.8 Pore Solution Concentration for the First Two-Years (Diamond 1983).

The Role and Effect of Moisture in Alkali-Silica Reactivity

The presence and role of moisture is very important in ASR. Swamy (1992) mentioned that ASR may occur at a very low humidity, but for the gel to absorb water and expand, high moisture level is necessary. It was reported that in a very dry environment, ASR expansion was negligible, although a highly reactive aggregate and high alkali cement have been used (Folliard et al. 2006). Different areas in the same structure have displayed different kinds of performance: areas exposed to a high level of moisture displayed ASR-induced damage, whereas areas that remained dry or not exposed to moisture showed little or no damage (Folliard et al. 2006). Therefore one can deduce that exposure to environmental conditions is an important parameter in the durability of concrete with respect to ASR.

Most chemical reactions need water to proceed and the alkali-silica reaction is no different. In fact, water has a double role: first, water is the main carrier of hydroxyl and cations in the pore water to the reaction site and second, it is absorbed by the ASR gel causing swelling. This swelling can develop pressure high enough to produce cracks and eventually those will deteriorate the concrete.

Although concrete looks dry during its service years, it still retains some pore fluids in the inner portions where the relative humidity (RH) is around 80-90%. In 1996, Pedneault described in detail the importance of moisture on expansion (Figure 2.9). As it can be seen from the plot, concrete made with four different types of aggregates displayed very small expansion at a relative humidity less then 80%. On the other side, expansion increases exponentially as the RH increases above 80%, emphasizing the enormous effect of RH on expansion.

Reducing the exposure of concrete structures to moisture is helpful in reducing ASR-induced damage. Although it may be feasible to reduce the moisture level below 80% in concrete, any effort to reduce any additional moisture, through the use of low permeability concrete or proper design of drainage, will ameliorate the durability aspects of concrete due to ASR.
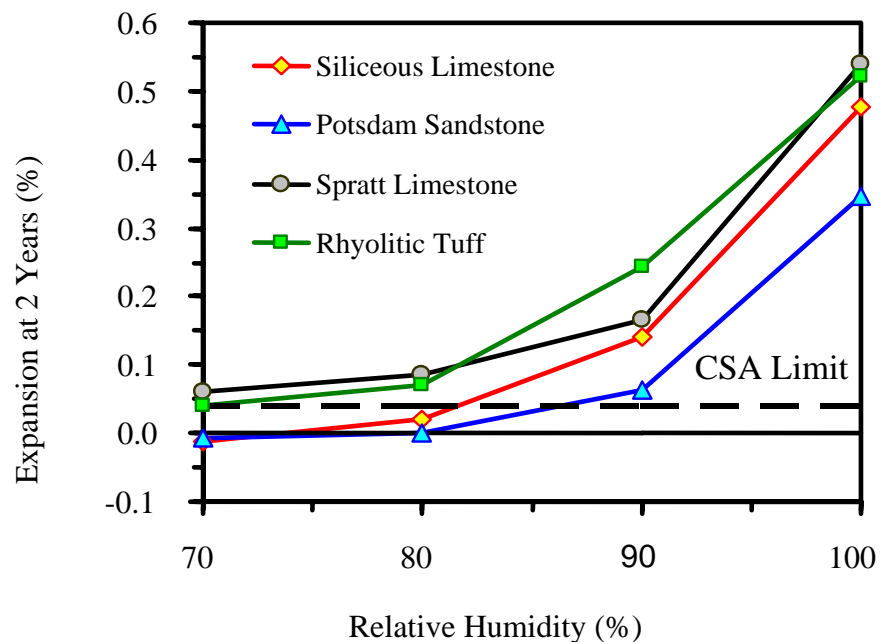
Figure 2.9 Effects of Relative Humidity on Expansion Using the ASTM C 1293 Storage Regime (Pedneault 1996).

Chemistry of Alkali-Silica Reaction

The previous section covered the main components of ASR: a) reactive silica, b) sufficient alkali and c) sufficient moisture. This section will cover in detail the chemical mechanism of the ASR (dissolution of silica, formation of gel) and the current proposed mechanisms of expansion.

First of all, one has to mention that the alkali-silica reaction is not a reaction between the alkalis (i.e. sodium, potassium and calcium) and the reactive siliceous components existent in some types of aggregate. The fact is that the main reaction is between the hydroxyl (OH⁻) ions found in the pore water and siliceous aggregates. The alkali metal cations are important because their presence in high concentration leads to an equally high concentration of hydroxyl to maintain equilibrium in the pore water. The role of alkali becomes relevant when they are incorporated into the gel.

Mass transport is a prominent aspect of ASR. Studies have shown that aggregates containing SiO_2 are considered in the concrete environment "thermodynamically unstable" (Swamy, 1992). When ASR begins, the free energy of the system decreases. This is accompanied by mass transport of alkali and hydroxyl ions. The main agent of the

transport mentioned above is the pore fluid which is perhaps in direct contact with aggregates and cement hydration product (Figure 2.10).
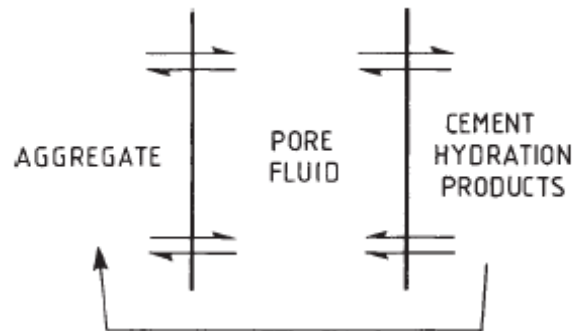
Figure 2.10 Mass Transport in ASR (Swamy 1992).

Figure 2.11 displays in detail the microstructure and mineralogy of the aggregate-paste interface. As seen from the picture, the main cement hydration products are calcium silicate hydrate (C-S-H) and calcium hydroxide (CaOH$_2$). The aggregate surface is composed of the siliceous mineral (SiO$_2$) and the pore volume (i.e. meso and micropores) in the concrete is partially filled by water molecules (H$_2$O).

When water comes into contact with siliceous aggregate particle, the surface of the rock is hydroxylated. This leads to the development of a disturbed region at the surface of the aggregate which is several atoms deep. When the rock is placed into contact with high hydroxyl concentration solution, the hydroxylation is intensified. This hydroxylation occurs in all types of siliceous aggregates, but in well-crystallized quartz, the rate of this reaction is very slow. On the other hand, finely ground crystalline quartz is very reactive at high temperatures.

The result of the above reaction is well documented in the literature and the chemical mechanisms are clarified by Dent-Glasser and Kataoka in 1981. The hydrolysis of reactive silica by OH- forms an alkali-silica gel located at the cement paste-aggregate interface. As this gel is formed, it absorbs water and other alkali cations, mainly sodium, potassium and calcium. Dent Glassier et al. mentioned that the ASR gel is not very soluble and is mainly located around susceptible siliceous aggregate.
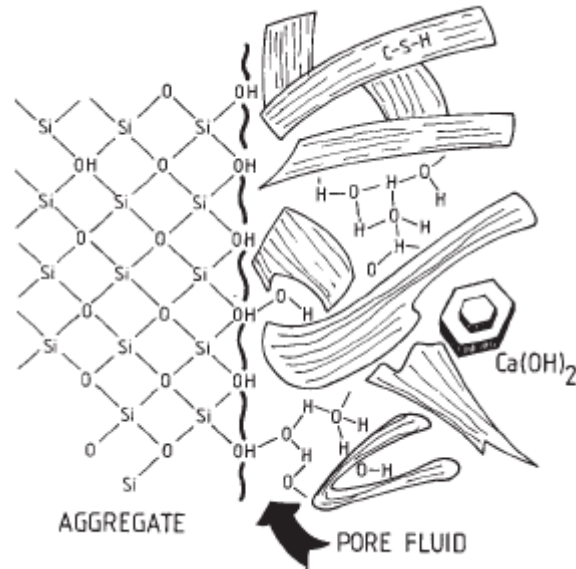
Figure 2.11 Microstructure and Mineralogy of the Aggregate-paste Interface
(Swamy 1992).

The alkali-silica reaction is composed of three major components. In the first reaction, the pore fluid solution reacts with Si-O-Si bonds to create silanol bonds:

$$Si - O - Si + H_2O \rightarrow Si - OH ....OH - Si$$
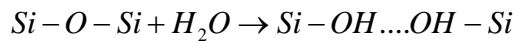
Some silanol bonds are already existent on the surface of hydrous silica aggregate. These silanol groups are considered acidic. The second reaction is an acid base reaction between the acidic silanol groups (Si-OH) and the hydroxyl ion (OH⁻)

$$Si - OH + OH^- \rightarrow Si - O^- + H_2O$$
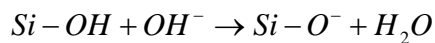
The products of the above acid base reaction are a molecule of water and the negatively charged Si-O-. These negative charges attract positive alkali cations such as sodium, potassium, and calcium. The number of positive cations should be sufficient enough to maintain a charge equilibrium in the system. The third stage of this reaction occurs when the silixane bonds are attacked by hydroxyl ions.

$$Si - O - Si + 2OH^- \rightarrow Si - O^- + {}^-O - Si + H_2O$$
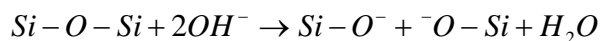
The major consequence of the above three reactions is the dissolution of silica in the pore solution. The amount of this dissolution depends on many factors: a) temperature b) particle size of silica c) whether the silica inside the aggregate is well crystallized (i.e.

macrocrystalline quartz) or amorphous (i.e. poorly crystallized like cristobalite, opal and volcanic glass). The main difference between the two mentioned categories is that the solubility of well crystallized silica is negligible in high alkali solution (High pH) and if it occurs, it would be only at the surface of the aggregate while the solubility of amorphous silica increments dramatically with pH, as shown in Figure 2.12.
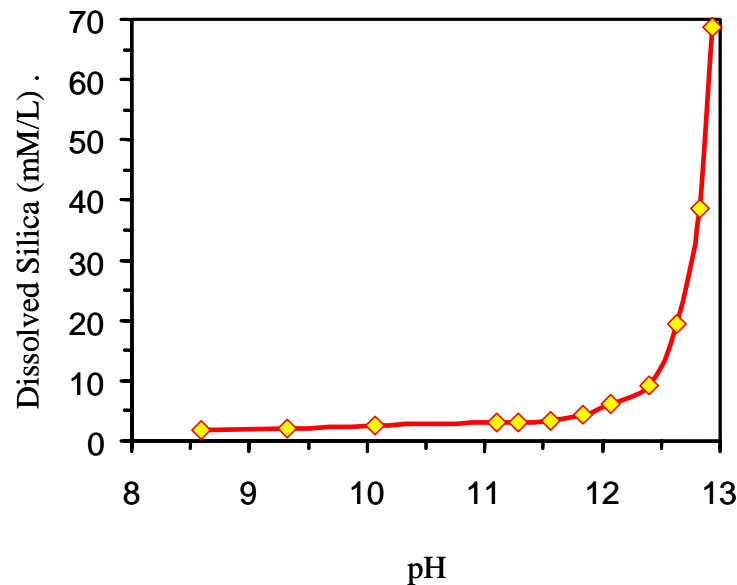
Figure 2.12 Effects of pH on Dissolution of Amorphous Silica (Tang and Su-Fen 1980).

As the $Si-O^-$ are generated and to achieve balance, these negative charges begin attracting positive alkali cations such as sodium, potassium, etc to form ASR gel. The entire ASR chemical reaction was summarized by Dent-Glasser and Kataoka (1981) as:

$$H_{0.38}SiO_{2.19} + 0.38Na_2O \rightarrow Na_{0.38}SiO_{2.19} + _{0.38}H_2O$$
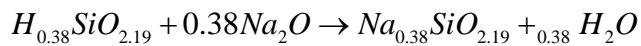
As shown in the above equation, sodium was involved to achieve charge compensation, but at the same time, some other cations may also contribute. The major product of the above reaction is the ASR product. According to many researchers, this product may take the form of either a gel or crystalline material (Stewart 2005). This ASR product itself is not deleterious. The problem occurs when this gel absorbs water, resulting in greater volume than the one that it replaces, creating high swelling pressure and expansion, notorious of the alkali-silica reaction. The ASR product is composed of the main components: Silica (SiO_2), Lime (CaO), Alkali (NaO_e) and water. Studies have

shown these gels maintained quasi-state equilibrium with water. During drying cycles, the alkali concentration increases and therefore the ionic content of the gel increase. On the other side, during wetter cycles, the reverse reaction happens. Since these gels have different chemical composition and different densities at different periodic cycles, the amount of swelling is extremely difficult to predict. (Swamy 1992).

Current Mechanisms of Expansion

The main chemical reactions that govern ASR are well accepted and understood by the majority of researchers. However, the mechanism of expansion is a point of controversy among researchers. The five most common and circulated theories in the literature regarding the mechanism of expansion are:

Hansen Theory

In 1940, Hansen discovered that some cracking in concrete structures in California is due to chemical reaction between alkali hydroxide released by cement during its hydration and some siliceous types of aggregates. In his research following his discovery, Hansen (1944) proposed a new mechanism for ASR: osmotic pressure theory, in which the hardened cement paste plays the role of a semi-permeable membrane toward the complex silicate ions. The membrane will allow molecules of water in addition to alkali hydroxides ions to diffuse through, but will prevent the passage of silicate ions surrounding the grains to diffuse through. Therefore an osmotic pressure cell around the aggregate will be developed. As more solution is drawn from the cement paste to the reaction site around the grains, hydrostatic pressure increases dramatically against the confined cement paste leading unavoidably to cracking in the matrix of the cement paste.

McGowan and Vivian Theory

In 1952, McGowan and Vivian challenged the Hanson theory on the basis that cracking in cement paste will release pressure and rule out any further expansion and in case elastic distention of the paste impacts the mechanism of expansion, it will be to a very limited extent. Instead, they proposed the "Swelling theory" in which alkali-silica gel, product of reacted aggregates" absorb water, leading to swelling in the gel which causes

cracking and expansion in the mortar. Tang (1981) also mentioned that he is in agreement with the above theory.

Powers and Steinour Theory

In 1955, both researchers mentioned that the swelling theory introduced by McGowan and Vivian and the osmotic theory proposed by Hansen are fundamentally alike. They were of the belief that the key to the mechanism of ASR is the nature of the alkali-silica gel itself and whether it acts as a solid or fluid which depends on the ratio of calcium to alkali.

When sodium hydroxide attacks an aggregate that is also reactive (in the presence of a high calcium concentration), the complex generated from the chemical reaction is a non-swelling lime-alkali-silica combination forming a layer around the reactive grains. This layer separates the reactive silica from the pore water rich in alkalis. The nature of the complex is fluid-like and its chemical composition is very close to C-S-H and in this case, it is considered non-expansive or at most a very limited swelling product as long as chemical equilibrium is reached between the alkali-silicate and lime.

On the other hand, when calcium (unlike other alkalis such as sodium and potassium) was unable (probably because of the low solubility of calcium hydroxide in alkali solution) to diffuse through the cement paste to the reaction site where alkali silicate are generated, the calcium to alkali ratio becomes very low and an alkali-silica complex is formed in the dry state. This complex upon absorbing water, swells apparently without limit. Powers and Steinour (1955) added that expansion in concrete occurs when this reaction product is still solid and cracking occurs primarily because of the swelling of the gel. But in some isolated cracks inside the concrete matrix, the gel in the crack may generate hydraulic pressure produced by osmosis where the concrete plays the role of a semi-permeable membrane.

Chatterji Theory

The theory proposed by Powers and Steinour was challenged by Chatterji (Chatterji et al, 1986, Chatterji 1989) in the 80's based on: i) The expanding gel contains none or very little lime (ii) alkali does not play a role in the alkali-silica reaction, instead only alkali

hydroxide takes part. To provide an explanation of the above two points and a better understanding of the alkali-silica reaction, Chatterji (1989) proposed another mechanism. The main points are summarized as follows:

(i)   As the PH and ionic strength of the pore solution increases, hydroxyl ions attack and penetrate reactive aggregates. The rate of (OH^-) penetration depends on the size of the alkali hydrated cations in the pore solution. i.e. the rate decreases in the series potassium, to sodium, to lithium, to calcium. Chatterji mentioned that sodium ions are less aggressive than potassium ions and therefore cement containing a large amount of potassium is much more harmful than that containing sodium. This last point also suggests that the ASR reaction will lessen from potassium to lithium salt (Chatterji 1989). This previous deduction was confirmed: low ASR expansion using lithium salt (i.e. $LiNO_3$, $LiCl$, etc) was noted by Folliard et al (2006). This inefficiency of lithium salt in producing ASR damage was attributed to the large size of hydrated lithium ions (Chatterji 1989) and to the fact that lithium salt does not increase the PH of the pore solution (Folliard et al. 2006).

(ii)   When both alkali metal salt (i.e. $NaCl$) and calcium hydroxide $(Ca(OH)_2)$ are found at the same time in the pore water, they penetrate the reactive grain leaving behind the calcium ions and anions in a liquid phase. The higher the concentration, the higher is the rate of penetration of alkali and hydroxyl ions (Chatterji, Thaulow, and Jensen 1988).

(iii)   This attack of the above mentioned ions leads to the destruction of the structure of the reactive grains (i.e. disruption of the siloxane bonds) according to the following chemical reaction: $Si - O - Si + OH^- \rightarrow Si - OH + Si - O^-$. As a result of the structure breakdown, more hydrated ions and water molecules penetrate the interior of the aggregate, leading to the dissolution of silica. This dissolved silica has two roads to follow (i) either to migrate out of the reaction site or (ii) internally within the grain (Chatterji, Thaulow, and Jensen 1988).

(iv)   The rate of diffusion of silica out of the reactive grain is inversely proportional to the concentration of $Ca(OH)_2$ in the pore water around the reactive aggregate. Chatterji (1979) in a previous research mentioned that the existence of free

$Ca(OH)_2$ in the pore water is a prerequisite condition for the destruction of concrete structure because of the alkali-silica reaction. He added that ASR can be suppressed by a complete removal of $Ca(OH)_2$ either by using a pozzolanic material (i.e. fly ash) or by leaching using calcium chloride concentrated solution.

(v)   Whether expansion occurs or not, depends on the rate of pumping and diffusion. Pumping refer to the penetration of Na^+, OH^-, Ca^{+2}, and H_2O and diffusion refers to migration of Si^{+4} out of the grain. Expansion happens when more materials penetrate the grain than the amount of silica outward diffusion. The rate of pumping and diffusion is completely controlled by the amount of $Ca(OH)_2$ in the pore solution.

When an ample amount of $Ca(OH)_2$ is present with high alkali ion concentration, a minimal amount of Si^{+4} can diffuse out allowing for more Na^+, OH^-, Ca^{+2}, and H_2O to be pumped in which yields expansion. On the other hand when the amount of $Ca(OH)_2$ is very limited, the pumping of Na^+, OH^-, Ca^{+2}, and H_2O will be at its minimum and at the same time, the amount of silica diffusing out increases significantly. This movement of silica from one place to another will stop the development of any expansive forces (Chatterji et al. 1986).

In the mechanism proposed by Chatterji, $Ca(OH)_2$ plays three major roles: (i) it restrains the diffusion of silica ions out of the reactive aggregates (ii) it speeds up the penetration Na^+, OH^-, Ca^{+2}, and H_2O into the reactive grain, (iii) it encourages prejudiced penetration of Na^+, OH^-, and H_2O.

Diffuse Double Layer Theory

In an attempt to provide a better explanation of the mortar bar expansion containing reactive siliceous aggregate, Prezzi (1997) proposed a theoretical model based on Gouy-Chapman double layer theory. Her model is mainly based on the chemical composition of the ASR gel and on the surface properties of colloidal systems. The expansion of the mortar bar was attributed to the gel swelling induced by electrical double layer repulsive theory.

Since the ASR reaction is first of all a chemical reaction where ions from different chemical substances react together, the expansion of the gel should be related to the

surface characteristics of the reactants (Prezzi, 1997). In her proposed mechanism to explain concrete degradation, Prezzi mentioned that the interface between solid and liquid is charged with electricity and the surface of the solid material holds excess charge. Monteiro et al. (1997) mentioned that surface charges can be originated from ion adsorption. In his research, Monteiro et al. (1997) defines three modes of adsorption of monovalent cations by a glass surface (Figure 2.13) a) by an inner sphere complex where are water is not allowed between the surface and the ion, b) outer sphere complex where one H_2O exists between the ion and the surface and c) ion adsorbed into the cloud of the double layer to offset the negative surface (silica) charges.
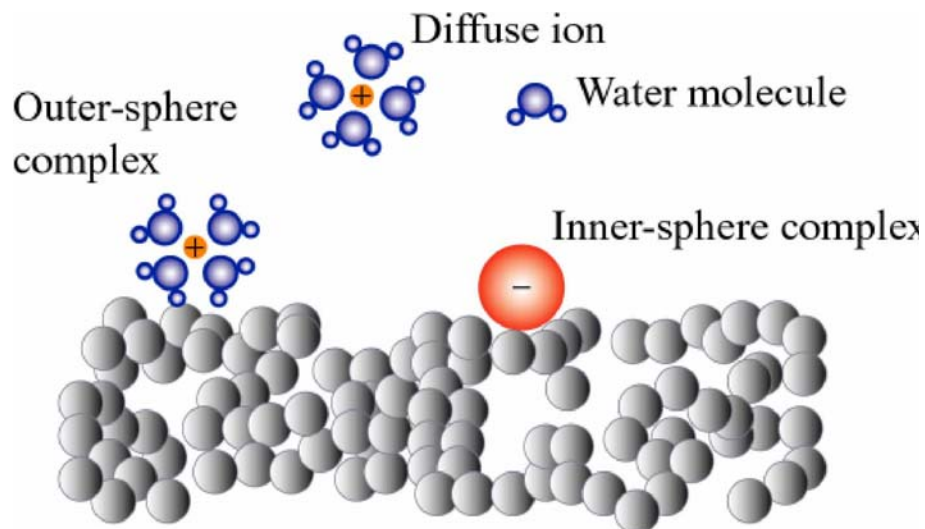
Figure 2.13 Three Modes of Adsorption of Monovalent Cations by a Glass Surface
(Monteiro et al. 1997).

Very high negative charges are observed at the surface of the silica grains (Rodrigues, Monteiro, and Sposito 1999). These highly charged silicas react with the alkaline solution found in the pore solution of the concrete leading to the dissolution of the silica and the formation of gel. To counterbalance the negative silica charges, an electric double layer of positive charges (cations) develop and adsorb around the silica surface. The double layers are composed of calcium, potassium and sodium and some other onions, but the net charge of the whole system (sum of negative charges of silica + anions + sum of all cations) is equal to zero. This system will form a colloidal suspension

and then conglomerate into a gel (Prezzi, Monteiro, and and Sposito 1997). The chemistry of this gel depends on the chemistry of the pore solution, pore structure in the concrete and environmental condition. As this gel absorbs water, it expands leading to internal stresses in the concrete matrix. Once these stresses exceed the tensile strength of concrete, cracks occur leading to other processes of deterioration (Swamy 1992). Diamond (1989) indicates that the expansive pressures because of gel swelling are in the range 6-7 MPa, but expansive pressure of 10.3 MPa was calculated by Prezzi using conventional double layer equations (Rodrigues, 2001).

The electric double layer developed is not static. In fact, it is affected by the alkali concentration in the pore solutions which is in turn affected by environmental conditions (Prezzi, Monteiro, and and Sposito 1997). Swamy indicates that cycles of wetting and drying greatly affect the alkali concentration in the pore solution.

During drying cycles, the local alkali concentration tends to increase with time in the pore solution while the double layer thickness and the repulsive forces decrease (Prezzi, Monteiro, and and Sposito 1997). This will lead to localized alkali-silica reaction even though the amount of alkali in the concrete structure stays low. As more silica grains dissolve and react with alkali, gels are formed in localized regions in the matrix of the concrete structure. However, this gel will not cause any damage or expansion since the likelihood of its interaction with water is very small (Swamy 1992).

On the other hand, during wetting cycles, the opposite reaction occurs. Water percolates through the interior of the concrete and the local pore water is diluted and therefore its ionic content decreases (Swamy 1992). As water arrives to the reaction site, it adsorbs around the gel particles and the distance among gel particles increases. As more water is adsorbed, the electrical double layer thickness increases and the repulsion forces dominate leading to swelling of the gel which occupies the empty pores. No damage occurs up to this point. In the following drying cycle, as more silica is being continuously dissolved, more gel is produced. In the next wetting cycle, as the gel absorbs water, it expands trying to make room for itself. As no more empty pores are available to accommodate the gel, expansive pressures are developed. As these wetting and drying cycles occur, pressure increases until fracture and fissures occur in the concrete. Gels can then be developed in the cracks. As water is now more accessible to

the gel, the repulsion forces and the thickness of the double layer increase significantly, leading eventually with time to the failure of the concrete structure (Prezzi, Monteiro, and and Sposito 1997).

Prezzi mentioned that the amount of repulsive forces and the thickness of the electric double layer depend on the valence of the cations in the gel and their concentration in the double layer. Rodrigues, Monteiro, and Sposito 2001 agrees with the above statement and cited that the amount of expansion increases as cations valence decrease following the sequence: Trivalent < divalent < monovalent. Consequently, bivalent ions (Ca^{++}) will generate more repulsive forces and a larger electric double layer thickness than monovalent ions (Na^+). Therefore gels with high concentration of calcium will produce lower expansive forces than those containing high amount of sodium and vice versa (Rodrigues, Monteiro, and Sposito 1999).

Prezzi, Monteiro and Sposito (1998) based on her ASTM 1260 mortar bar tests showed that chloride salts with monovalent cations (NaCl) displayed the largest expansion followed by those with divalent and trivalent cations ($CaCl_2$, $AICI_3$). This difference in the behavior of monovalent and bivalent ions is caused by their effects on the surface charge density. i.e. monovalent cations produce much higher surface charge density than bivalent cations, leading to more expansive gels (Rodrigues, Monteiro, and Sposito 2001). Prezzi, Monteiro and Sposito (1998) also observed from her mortar bar tests that the gel that expands the most (using a NaCl solution) had the highest amount of Silica (SiO_2) whereas its amount of calcium oxide is minimum. On the other side, the bars prepared using $AICI_3$ solutions had the lowest amount of silica and the highest amount of calcium oxide.

Testing for Alkali-Silica Reaction

This section provides an overview of the main laboratory test methods that are currently used to recognize reactive aggregate and their expected role in the alkali-silica reaction that occur in the matrix of concrete structures. Since many aggregates are by nature heterogeneous, laboratory test methods of aggregate and/or cement aggregate-combinations are the only possible ways to measure aggregate reactivity prior to their use in concrete structures. At the same time, one has to acknowledge that lab procedures may

in some cases be time consuming and difficult to conduct, but are necessary to limit damage to concrete construction because of ASR.

Today, there are many standard procedures to test reactivity of aggregate and/or cement-aggregate combinations. Of the many laboratory tests methods available to assess alkali-silica reaction, two procedures are the most common among researchers to conduct (a) ASTM C 1260 (Accelerated Detection of Potentially Deleterious Expansion of Mortar Bars due to Alkali-Silica Reaction), and (b) ASTM C 1293 (Test Method for Concrete Aggregates by Determination of Length Change of Concrete Due to Alkali-Silica Reaction).

In recent years, many researchers (Andersen and Thaulow 1989) have proposed and developed new and rapid test methods. Most of these procedures depend on accelerating the ASR reaction by increasing temperature and pressure.

With the intent of reducing the test time, greater expansions were observed than those obtained with standards test methods (Swamy 1992). Lab tests may in some cases be inconclusive, especially when evaluating structures showing symptoms of ASR like map cracking or gel exudations. Such tests may lead to erroneous results; for instance, structures attacked by ASR can be mis-diagnosed as not to be suffering from ASR while others show serious of cracking and be diagnosed as ASR caused but is not (Tordoff, 1990). Consequently, a petrographic study on the aggregate used, field performance, and a reliable test which can model the main parameters of ASR are highly desired.

Rating the Alkali-Reactive Aggregates

The first step in evaluating the suitability of an aggregate for concrete construction is to perform a petrographic analysis, together with other complementary techniques such as X-ray diffraction (XRD) and infra-red spectroscopy. The above mentioned tests will provide the necessary information to identify the deleterious components in the rock and what specific test needs to be conducted (Dolar-Mantuani 1978).

The different types of reactive aggregates, their mineral composition and the problems involved in their recognition are well established and documented in the literature. The majority of standards and codes like the American Society for Testing and

Materials (ASTM C 289, C295), and the British Code (British Standard (1984), British Standard (1989)) supply a lot of information about the origin and formation of the rocks and their mineral composition and classification including the siliceous phases, such as quartz, chert, flint and quartzite. Aggregates that contain at least 95% of a specific type are considered not reactive if they contain less than 2% by weight of flint, chalcedony or chert or if they are not contaminated by silica minerals like cristobalite, opal, etc. (Swamy 1992).

To detect reactive aggregate and to confirm or reject the presence of ASR in concrete, two techniques are available. The first method is by examining reactive aggregate by petrographic scrutiny of thin sections of contaminated concrete. The objective of this study is to locate the different deleterious components, to locate (if any) the fracture in the rock, to identify any alteration zones around the siliceous grains and to look for any gel deposit. Petrographic study on virgin aggregates should include a full analysis of the fraction of the rock. Thin section study will also help identify any potential reactive components in the aggregate. The second technique is the use of XRD. The charts obtained from the analysis will provide a deep perception on the mineral present and the location and arrangement of secondary minerals (Swamy 1992).

Both methods are useful in providing information about the list of minerals found in the rock, but there is no guarantee if ASR will occur or not in the structure, in fact one has to keep in mind that other important characteristics of the aggregates such as particle size distribution, environmental effect, porosity, amount of reactive minerals, etc., have a significant effect on future observed expansions (Shon 2008).

Established Mortar-Concrete Tests

The four common tests for mortar-concrete tests are:

a) ASTM C 227 "Standard Test Method for Potential Alkali Reactivity of Cement-Aggregate Combinations (Mortar-Bar Method)".

b) ASTM C 441 "Effectiveness of Mineral Admixtures or GBFS in Preventing Excessive Expansion of Concrete due to Alkali-Silica Reaction.

c) ASTM C 1260 "Standard Test Method for Potential Alkali Reactivity of Aggregates (Mortar- Bar Method).

d) ASTM C 1293 "Standard Test Method for Concrete Aggregate by Determination of Length Change of Concrete Due to Alkali-Silica Reaction.

The objective of the ASTM C 227 is to provide information about the probability that a cement-aggregate combination is capable of producing deleterious expansion in concrete because of ASR. The mortar bars in this test are composed of aggregates that are crushed to meet some grading requirements. Then the mortar bars are stored in closed containers with wicks above water at 100 F. Measurements are then taken at 1 and 14 days. One, two, three, four, six and nine months are recommended. In ASTM C33, it is stated in the appendix that the expansion limits are 0.05% at 3 months and 0.1% at 6 months.

The results of the mortar bar test were seen to be not always reliable (Grattan-Bellew, P.E, 1989). Storage containers with efficient wick systems, were found to cause excessive leaching of alkali out of the mortar bar and consequently, the measured expansion was considerably reduced. However, bars sealed in plastic bags have displayed higher expansion (Rogers and Hooton 1989). The test period of this procedure is another disadvantage: in the case of opaline aggregate, a period of three to six months (six to twelve months in case of quartz bearing aggregate) is needed to obtain conclusive results (Oberholster and Davies 1986).

ASTM C 411 is mainly used as a preliminary test to assess the efficiency of mineral admixture or slag in reducing expansion because of ASR. The bars are made with a combination of cement, mineral admixtures and reactive aggregate (pyrex glass) and then the bars are stored in closed containers above water at 100 F. Like ASTM C 227, readings were taken at 1 and 14 days. Hooton, R.D. (1986) had found that pyrex glass aggregates are not appropriate for this test because pyrex contains high amount of alkali and they maybe released during the test and contribute to the chemical reaction and therefore leading to higher expansion. Rogers, C.A. and Hooton, 1989, in their mortar bar test, measure a 0.3% expansion with pyrex glass aggregate, while less than 0.1% expansion was measured in the other containers. For the above two mortar tests to be successful, Swamy (1992) suggests the complete removal of wicks from the container and storage of the mortar samples in plastic bags.

The accelerated mortar bar test method (ASTM C1260) is very common and is a standard in the US and Canada. The procedure came originally from a method developed by Oberholster and Davies (1986). The test consists of casting mortar bars using 1:2.25 parts of cement to sand with a water cement ratio of 0.47. The aggregate (whether it is course or fine) used in the test should be crushed to meet some grading requirement. The samples are kept in their molds for 24 hrs in the curing room at 100% RH. Then, the bars are removed from the molds and placed in a closed container in a water bath at 80^0C for another 24 hrs. After the first initial storage period, the bars were again removed from the water bath and an initial reading using a vertical comparator is taken. The bars are then fully submerged in 1N NaOH at 80^0C for 14-day period. Length measurements are taken during the 14 day storage period. Expansion limits are mentioned in the appendix of ASTM C 1260 as follows: less than 0.1% at 16 days for innocuous aggregates, 0.1-0.2% for slowly expansive aggregates and greater then 0.2% for potentially high expansive aggregates. This procedure has a couple of drawbacks: a) the test conditions are severe (1N NaOH at 80^0C) and b) the aggregate has to be crushed to meet certain gradation requirements and both previously mentioned factors make it difficult to interpret the results relative to the conditions that the concrete will be subjected to under field conditions.

The concrete prism test, described in ASTM C1293 is another popular procedure to evaluate the potential of an aggregate to deleterious expansion due to alkali-silica reaction. The test procedure consists of casting concrete prisms at a specific mix proportion. Following demolding, the prisms are then stored above water at 100 F and the length change of concrete prisms is measured at specific intervals. This method is seen as the best index for field performance but at the same time, the length of the procedure (12 months) represents a major drawback. It was mentioned in the appendix of ASTM C1293 that an average expansion equal to or greater than 0.04% at 1 year is a reasonable value to classify the deleterious reactive aggregate from those that are not reactive.

The results obtained, whether they came from the mortar bar or the concrete prism test, may be problematic. Mortar bar incorporates high amount of cement, much higher then those used in concrete construction and consequently, the results obtained from the test can't be applied to concrete (Swamy 1992). Although the use of high alkali levels in the concrete prism tests (1.25% by weight of cement) is unrealistic, there are other causes why researchers prefer this test over the mortar bar test (Swamy and Al-Asali 1988): a) alkali, not only comes from cement, but also from aggregate, mineral and chemical admixtures, water, de-icing salts and seawater (Stark et 1986) b) environmental conditions (relative humidity and temperature) have great power on the progress of alkali-silica reaction and its resulting expansion. And the concrete test is the test where all the above influences can be realistically modeled and reproduced (Swamy and Al-Asali 1986). A summary of the American standards for Evaluating Alkali-Silica Reaction is presented in Table 2.2 (ASTM (2000a), ASTM (2000b), ASTM (2000c), ASTM (2000d), ASTM (2000e), ASTM (2000f), ASTM (2000g), ASTM (2000h), ASTM (2000i), ASTM (2000j), ASTM (2006)).

Table 2.2 Available Test Methods for Evaluating Alkali-Silica Reaction.

Test Type	Test Name	Significance and use	Test Procedure	Test Duration	Additional Comments
Aggregate	ASTM C289 (2000d): Standard Test Method for Potential Alkali-Silica Reactivity of Aggregates (Chemical Method)	To assess the reactivity of Siliceous aggregate with Alkali in concrete	o Aggregate should be sieved and crushed to pass a 300 um and retained on 150 um sieve o Crushed agg soaked in a 1N NaOH for 24 hrs. o Solution analyzed to determine alkali and dissolved silica	24 hrs	o Quick results o Not completely reliable o Severe test o During crushing, some reactive phases may be lost
	ASTM C294 (2000e): Standard Descriptive Nomenclature for Constituents of Concrete Aggregates	To describe natural materials of which mineral aggregate are composed	Visual Observation	Short but depends on the examiner and its experience	o The identification of rock and minerals should be made by qualified petrographer, geologist and mineralogist
	ASTM C 295 (2000f): Standard Guide for Petrographic Examination of Aggregates for Concrete	o To recognize the reactive components in the rock o To determine the physical and chemical characteristics of the material	o X-Ray diffraction (XRD) o Scanning electron microscopy (SEM) o Differential thermal Analysis (DTA) o Energy dispersive x-ray analysis (EDX)	Short but depends on the examiner and its experience	o Very useful to identify many reactive aggregates o Reliability depends on the quality of the petrographer. Other tests (1260 and 1293) should be conducted to confirm the results

Table 2.2 (Cont'd).

Test Type	Test Name	Significance and use	Test Procedure	Test Duration	Additional Comments
Cement-Aggregate Combinations	ASTM C227 (2000c): Standard Test Method for Potential Alkali-Reactivity of Cement-Aggregates Combinations (Mortar Bar Method)	To provide information about the probability that a cement-aggregate combination is capable to produce deleterious expansion in concrete because of ASR	Agg should be crushed to meet some grading requirements Mortar bars are stored in closed containers above water at 100 F	Measurements are taken at 1 and 14 days. 1,2,3,4,6,9 and 12 months are recommended	o long test method o Expansion due to alkali-carbonate reaction is minimal compared to Alkali-silica reaction
	ASTM C856 (2000h): Standard Practice for Petrographic Examination of Hardened Concrete	To describe the petrographic examination of concrete samples (from laboratory or field) and to identify the presence of reactive products in the specimens	Visual and microscopic examinations	Time depends on the sample preparation and microscopic examination.	o Mandatory to relate aggregate reactivity to field performance. o Reliability depends on the petrographer qualifications
	ASTM C 441 (2000g) Effectiveness of Mineral Admixtures or GBFS in Preventing Excessive Expansion of Concrete due to Alkali-Silica Reaction	To be used as a preliminary test to assess the efficiency of mineral admixture or slag in reducing expansion because of ASR	o Mortar bars made with a combination of cement, mineral admixtures and reactive aggregate (pyrex glass). o Mortar bars are stored in closed containers above water at 100 F	Readings are taken at 1 and 14 days. 1,2,3,4,6,9 and 12 months are recommended	o High alkali cement. o Alkali maybe released from the Pyrex glass which is sensitive to test conditions.

Table 2.2 (Cont'd).

Test Type	Test Name	Significance and use	Test Procedure	Test Duration	Additional Comments
Cement-Aggregate Combinations	ASTM C342 (2000i): Standard Test Method for Potential Volume Change of Cement-Aggregate Combinations	To find out the possibility of expansion of cement-aggregate combination subjected to changes of temp and water saturation	o Mortar bars are stored in water at 23 C for 28 days. o The temp will be then raised to 55 C for 7 days followed by 24 hr at 23 C before taking reading. Any further reading will follow the above cycle	52 weeks	o Test used on aggregates coming from Kansas, Oklahoma, Iowa and Nebraska. o No limits for expansion have been developed
	ASTM C1260 (2000b): Standard Test Method for Potential Alkali Reactivity of Aggregates (Mortar-Bar Method)	To give us a way to find the potential of the aggregate for experiencing ASR leading to deleterious expansion.	o Aggregate are crushed to meet the grading requirements. o Mortar bars are soaked in 1 N NaOH for 14 days.	16 days	o It is a considered a screening test o Very utile for slowly reacting aggregate. o Test conditions are very severe. o The fastest available test procedure
	ASTM C 1293 (2000a): Standard Test Method for Concrete Aggregate by Determination of Length Change of Concrete Due to Alkali-Silica Reaction.	To assess the potential of an aggregate to deleterious expansion due to alkali-silica reaction	o The length change of concrete prisms is measured. o Prisms are stored above water at 100 F.	12 months	o Considered the best index for field performance. o Main disadvantage is the test duration (12 months).

Table 2.2 (Cont'd).

Test Type	Test Name	Significance and use	Test Procedure	Test Duration	Additional Comments
Cement-Aggregate Combinations	ASTM C1567 (2006) Potential alkali-silica reactivity of Combinations of cementitious materials and Aggregate (Accelerated mortar-bar test)	to assess the use of cementitious materials in controlling or reducing expansion due to ASR	o Mortar bars at 80C soaked in alkaline solution	16 days	Fast alternative to 1293
Gel Recognition	ASTM C856 (2000h): Annex A1 A Technique for Detecting Alkali Silica Gel Subject to Confirmation by Other Methods.	To find alkali silica gel products coming from the reaction of silica with alkali in the cement	o The surface of the specimens is treated with Uranyl-acetate solution. o The treated surfaces are subjected to ultraviolet light. o The ASR gel around the aggregate will glow bright greenish-yellow	Quick Results	o Ultraviolet light risky to the skin and eyes. o Uranyl-acetate needs special manipulation and disposition. o Test results not conclusive: should be confirmed by petrographic methods.

Kinetics Models

Many researchers had focused over the years on the kinetics of alkali-silica reaction. Today, many models are available in the literature but each of those models has limitation in their scope and their applicability. The most current models are the ones developed by Sorrentino, Clement, and Golber 1992, Johnston, Stokes, and Surdahl 2000 and Mukhopadhyay, Shon, and Zollinger 2006.

The chemical method ASTM C289 "Standard Test Method for Potential Alkali-Silica Reactivity of Aggregates" is very popular since it is fast, easy to conduct and requires small amount of material. It consists of measuring the amount of silica dissolved into 1 N NaOH at 80C for 24 hours. However, some researchers have mentioned that its results are in some cases unreliable (Bellew 1983) and the detection of slow/late reactive aggregate is difficult. Consequently, Sorrentino et al. in 1992 introduced the French kinetic chemical test. The procedure, almost similar to the chemical method, consists of measuring the dissolved silica for 96 hrs and therefore the time parameter is included in the chemical procedure. After conducting a huge number of tests, Sorrentino et al suggested a chart (Figure 2.14) displaying the different degree of reactivity. They also mentioned based on their test results that their new test procedure was able to detect aggregates that displayed a pessimum effect.

To overcome some of the deficiencies run across using a % expansion for specifying reactive aggregates in ASTM C1260, Johnston, Stokes, and Surdahl 2000 proposed a kinetic based method using the Kolmogorov-Avrami-Mehl-Johnson model. This procedure based on growth and nucleation where the power of time and the % expansion are related to each other exponentially as follows:

$$\alpha = \alpha_0 + (1 - \alpha_0).(1 - e^{-k(t-t_0)^M}) \qquad (2.2)$$

where: α_0 is the degree of reaction at time t_0; k is the rate constant; t_0 is the time when growth and nucleation are dominant and M is an exponential factor. The researchers found that by applying a least square fit to the logarithmic form of the kinetic model, two parameters were generated ln k and M. By plotting M against ln k, two distinctive areas were noticed (see Figure 2.15). From their test data, they found that reactive aggregates are associated with ln k > -6 and non-reactive aggregates are associated with ln k < -6. In their conclusions, they mentioned that this new method was effective in determining the

amount of mineral admixtures necessary to mitigate ASR. The main disadvantage of this procedure is that the analysis was done using ASTM C1260 data which requires that the aggregate be crushed and therefore the surface area and the reactivity of the aggregate were altered and no longer represented real concrete.
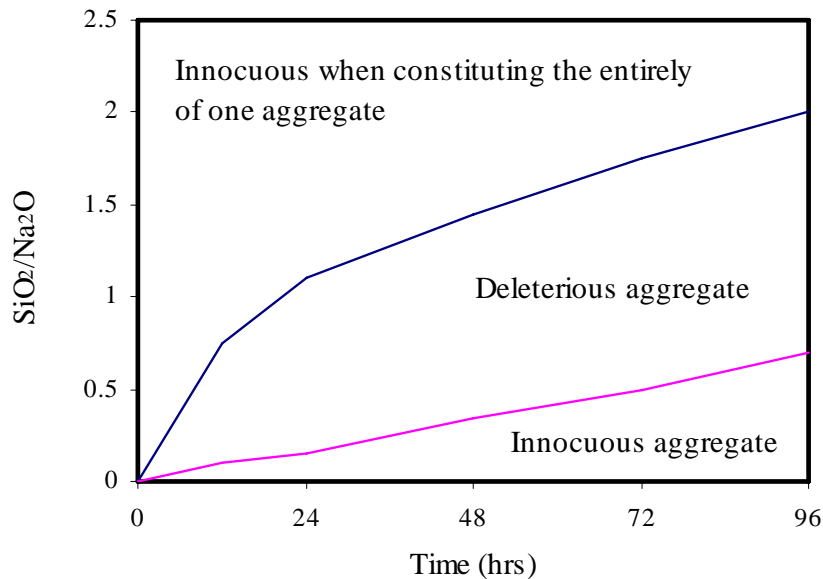
Figure 2.14 Diagram of the Kinetic Test (Sorrentino, Clement, and Golber 1992).
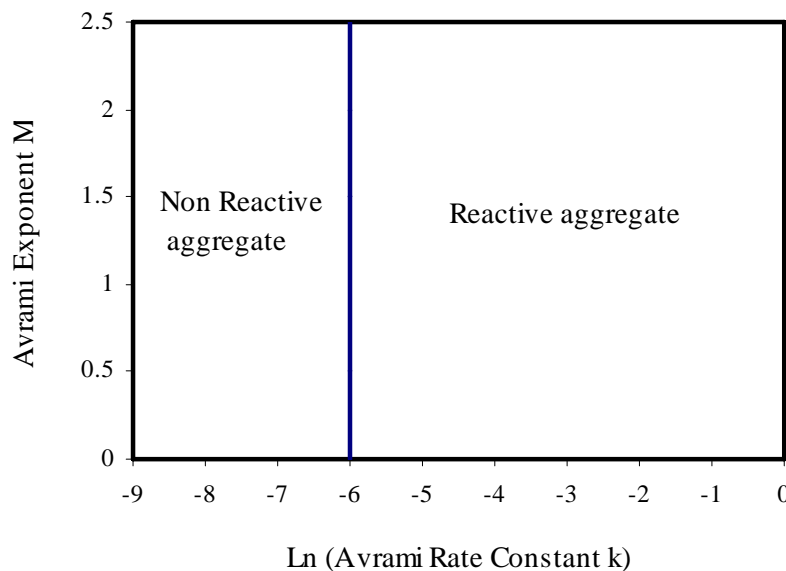
Figure 2.15 Avrami Exponent Versus Rate Constant
(Johnston, Stokes, and Surdahl 2000).

In 2006, Mukhopadhyay, Shon, and Zollinger introduced the concept of activation energy (E_a) for ASR. E_a was defined as the energy required to initiate ASR. To determine the (E_a) for aggregate, the following steps were followed. They proposed an empirical model based on the maturity concept (Carino and Lew 2001):

$$\varepsilon(t) = \varepsilon_a \frac{K_T(t - t_0)}{1 + K_T(t - t_0)} \tag{2.3}$$

where: $\varepsilon(t)$ = ASR expansion at time t; ε_a = ASR ultimate expansion of the aggregate; K_T = rate constant; t = actual reactive age at temperature t; and t_0 = theoretical initial reaction time.

The rate constant and the ultimate expansion at three different temperatures from the above model were determined using linear regression (Figure 2.16). The E_a was then calculated from the slope of the linear regression of Ln (K_T) versus 1/T (Figure 2.17) and therefore they were able to rank different types of aggregates based on their reactivity. Although this concept of ASR E_a was creative and innovative, the model has two major drawbacks: a) the fit of the model to the expansion data is poor and b) in some cases the intercept for some types of aggregate turns out to be negative resulting in a negative ultimate expansion.
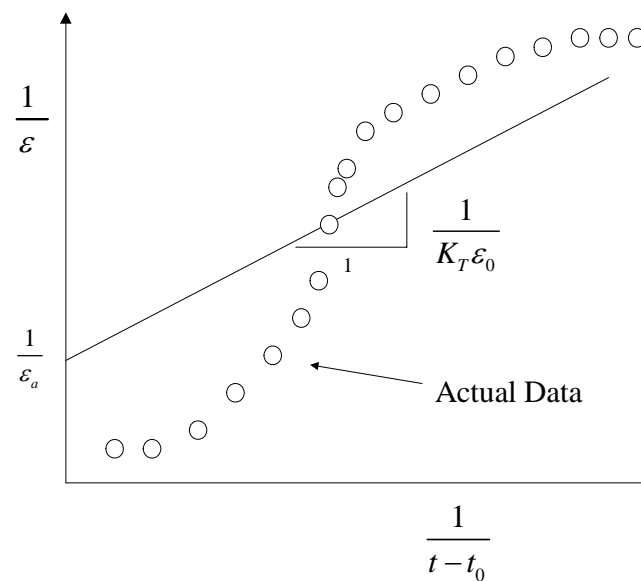
Figure 2.16 Reciprocal of Expansion Versus Reciprocal of Age (Modified from Mukhopadhyay, Shon, and Zollinger 2006).
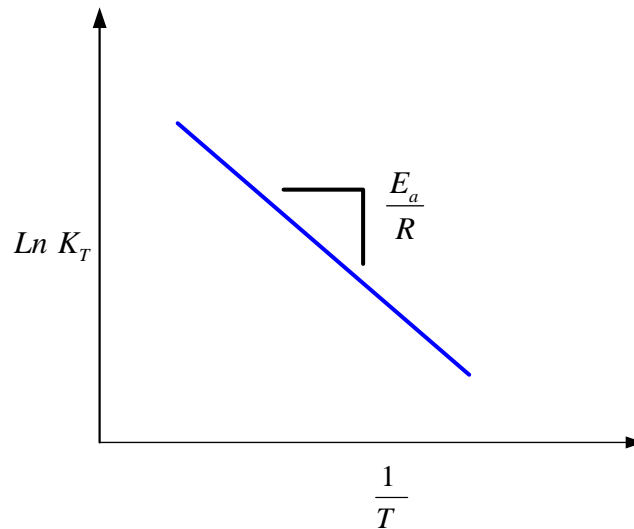
Figure 2.17 Plot for Determining the Value of Activation Energy
(Mukhopadhyay, Shon, and Zollinger 2006).

Chemical Shrinkage

During chemical reaction between the participating components, there is a decrease in the volume of reactants and an increase in the volume of the products and consequently, the total volume of the reacting system before and after the chemical reaction is not the same. If the net volume difference is negative, this would be attributed to the occurrence of chemical shrinkage in the system. It should be mentioned that the idea of chemical shrinkage is not new as it was noticed during cement hydration in concrete as hydration products occupy less volume than the initial starting materials like water and cement (Geiker 1983). Powers in 1935, released chemical shrinkage data identifying the importance of chemical composition on cement hydration. Currently, there is no ASTM standard to measure chemical shrinkage but the volume change can be measured in two different means, either directly as an increase or decrease in the level of a liquid in a capillary tube or indirectly as a decrease in the buoyancy of a specimen soaked in oil (Geiker and Knudsen 1985).

In the 1985's, Geiker and Knudsen at the Technical University of Denmark extended the concept of chemical shrinkage that takes place in cement hydration to that which occurs in alkali-silica reaction for aggregate soaked in an alkaline solution in a closed system. They developed a commercial device called the Kanemeter to measure

chemical shrinkage (Knudsen 1986). The device is composed of a glass flask and a pipette closed by a piston connected to a data acquisition system (Figure 2.18). The test consists of placing reactive sand particles in a 10N NaOH solution. The flasks are then placed in a thermostatic bath at 50^0C. As ASR occurs in the pipette, they discovered that the height of oil in the piston falls resulting in the measured chemical shrinkage. The higher is the value, the more reactive is the aggregate. Based on this finding, they developed reaction curves for different sands widely used in Denmark.

To provide an explanation for the apparent contradiction between the measured ASR contraction in their new test procedure and the well know ASR expansion in concrete, they stated that their measured chemical shrinkage is very similar to the cement hydration system where the total volume (cement + water) decreases whereas there is an increase in the volume of solids. On the other hand, in the alkali-silica reaction occurring in concrete, water coming from outside the system allows the gel to swell and to occupy a volume greater than the amount of water consumed in the initial reaction (Knudsen 1986).

Although their proposed procedure is innovative, the two major difficulties while conducting this experiment lies in 1) removing completely the air void in their system as they used only vibrating table instead of using it with a closed vacuum system and 2) achieving complete water saturated samples.
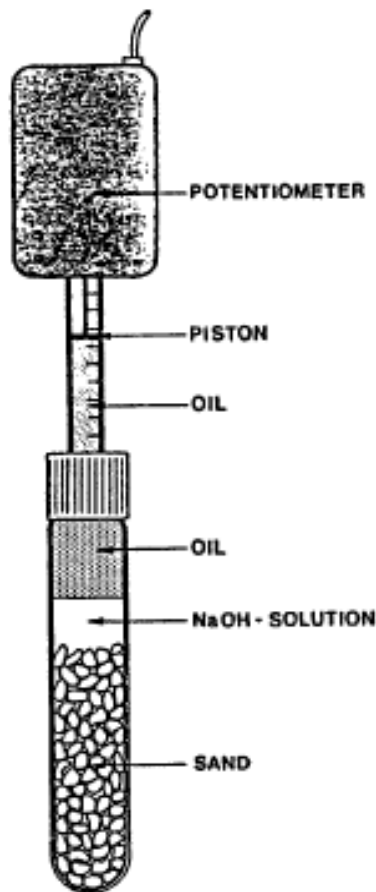
Figure 2.18 Konometer to Measure the Chemical Shrinkage of Danish Sand
(Geiker and Knudsen 1985).

Mitigation of Alkali-Silica Reaction

As mentioned earlier in this chapter, four prerequisites are needed for the alkali-silica reaction to proceed: a) reactive silica b) high concentration of alkali, c) water and d) the presence of calcium hydroxide. Any deficiency in any of the four components may lead to the reduction or elimination of the expected expansion. Currently, there are many ways to mitigate ASR. The most common ones are:

a) Restricting the movement of water molecules and alkali ions. The amount of water molecules and ions can be reduced by decreasing the water cement ratio leading to a lower porosity and consequently, the movement of ions is much more restricted (Gjorv 1983).

b) Removing the calcium hydroxide from the pore solution. This can be obtained by using a slag portland cement or a cement-pozzolanic cement mixture. If the amount of these mineral admixtures is high enough to consume the calcium hydroxide in the concrete structure, expansion will be prevented, even if a high alkali concentration comes into contact with the structure (Chatterji, et al. 1986).

c) Using air-entrained admixtures: the addition of air entrained admixture will create air bubbles into the concrete matrix and those bubbles may stick on the surface of the rock. Therefore, a partial isolation will be achieved between the aggregate and the matrix and the overall expansion will be reduced. It was shown that the air entrained performed much better and is more effective in fine aggregate than coarse rock mixtures (Jensen et al. 1984).

d) Using nonreactive aggregates. One of the best methods to mitigate ASR is to use non-reactive aggregate. However, this is not possible most of the time because non-reactive aggregate are rare to find and the vast majority of aggregates contains some form of reactive silica. Even if nonreactive aggregates are found, they should be tested and have displayed good field performance before their use in concrete mixtures (Folliard et al, 2006).

e) Using Supplementary Cementitious Materials (SCM). The use of SCM (fly ash, slag and silica fume) is very common not only to reduce the deleterious effect of ASR, but also to improve resistance of concrete structures to other durability problems such as freezing and thawing, corrosion and sulfate attack.

Among the mineral admixtures mentioned above, fly ash is the most commonly used. Two different types of fly ash are available: Class C and Class F where the amount of lime, silica and alkali vary among them. Shehata and Thomas in 2000 mentioned that Class F Fly ashes (low lime) are more effective in controlling ASR than the higher lime fly-ashes (Class C) because low lime fly ash has a greater amount of silica and therefore more CSH (with low calcium to silicon ratio) are generated during the hydration process (Glasser 1992). Diamond (1981) added that low calcium fly ash (Class F) are more effective in controlling ASR because the alkali of ashes will not be available in the pore water unlike high calcium ashes where alkali would be available.

Slag is also used to extenuate the effects of ASR, but its dosage is relatively high (35-50%) (Folliard et al, 2006). The exact amount needed depends on the total alkali content of concrete and on the reactivity of aggregate. Slag is rich in silica and its effect leads to a reduction of calcium hydroxide in the concrete matrix and enhance the alkali-binding capacity of concrete (Odler 2000).

Silica fume can also be used to minimize the risk of ASR. The total amount of alkali and the reactivity of aggregate are two major factors that decide the efficiency of silica fume. Thomas and Bleszynski in 2001 proposed an upper and lower limit on the percentage of silica fume added to the concrete mixture:

- Lower limit: % SF = 2 x (alkali expressed as kg of Na_2O_e per m^3 of concrete).

- Upper limit: % SF = 3 x (alkali expressed as kg of Na_2O_e per m^3 of concrete).

Attention should me made to the maximum amount of silica fume added to the concrete mixtures, as too much silica fume raises workability and shrinkage concerns during field applications (i.e. high water demand may be difficult to deal with).

To reduce the amount of silica fume, the use of ternary blends, where silica fume is used in conjunction with fly ash and/or slag, was introduced and has gained popularity as of late. The advantage of these types of blend is early strength development, improved durability, better workability and economic (Folliard, et al. 2006). Bleszynski, Thomas, and Hooton 2000 has found that adding slag (20 to 35%) combined with 4 to 6 % silica fume is very effective to mitigate ASR with a highly reactive aggregate.

This literature review provides an overview about ASR, its chemical reaction, its major components, the main factors affecting it, the latest test procedures and methods developed to identify it and the mitigation techniques to reduce or eliminate its deleterious effect. Although some of the new methods and procedures showed some improvement over current standard test methods (ASTM C1260 and ASTM C1293), their application to field condition is very limited. It is obvious that there is a need to study the effect of different combinations of concrete materials (w/cm, SCM, etc) that affect ASR. Therefore, it is imperative to develop a protocol that captures the effect of different concrete materials which will lead ultimately to the development of concrete mixtures highly resistant to ASR.

CHAPTER III

MATERIALS, TEST PROGRAM AND INSTRUMENTATION

In a combined effort between Texas A&M University (TAMU) and Innovative Pavement Research Foundation (IPRF), TAMU researchers began a process that will potentially lead to the development of concrete mixtures highly resistant to ASR, therefore enhancing the concrete durability of pavement structures.

To achieve this objective, different series of expansions measurements were conducted on different types of aggregates widely used in concrete mixtures. These aggregates originate form different locations in the United States and Canada, representing different mineralogies and reactivity. In addition, concrete samples with different water cement ratios and supplementary cementitious materials using selective types of aggregates were tested using the dilatometer to measure expansions. By casting and testing concrete, as opposed to simply testing aggregates, realistic field and environmental effects are inherently considered when evaluating the resistance of different concrete mixture to ASR.

This chapter describes the materials, the test program, the test procedure and the different types of equipment used to carry out the above mentioned objective. The tests methods are classified into three categories: aggregates tests, concrete tests and other tests related to aggregates like pH measurements and chemical analysis of the soak solutions.

Materials

The material used in this study are a) four reactive aggregates (New Mexico Rhyolite, Platte River Gravel, Spratt Limestone, Sudbury Gravel), reagent grade sodium hydroxide (NaOH), low alkali type I/II cement and class F fly ash. This study also involved the use of hydrated lime (calcium hydroxide) to saturate alkali solutions with calcium.

Aggregates

In this research, four reactive aggregates having a record of their reactivity with respect to ASR were selected. The aggregates used in the study are listed below:

(a) New Mexico Rhyolite (NMR). This reactive aggregate was brought from New Mexico from Las Placitas Gravel Pit from the Bernalillo County in New Mexico. The major reactive component is Rhyolite (acid volcanic) and it is considered a highly reactive aggregate (Barringer 2000)

(b) Platte River Gravel (PRG). This aggregate was brought from Nebraska. The main reactive constituent in this aggregate is strained quartz (Mukhopadhyay, Shon, and Zollinger 2006).

(c) Spratt Limestone (SL). This aggregate came from the Spratt quarry in Ontario, Canada. It is used in many ASR studies. Like all sedimentary rocks, Spratt limestone is composed mainly of calcite with small amount of dolomite. 3 to 4% of microscopic chalcedony and black chert, found in the matrix of the aggregate is the reactive constituent of the rocks (Rogers 1999).

(d) Sudbury Gravel (SuG). This aggregate is obtained from the Sudbury area of Ontario, Canada. It is considered a slow/late reactive aggregate. The major reactive aggregates in the gravel consist mainly of quartz arenites, argillites, quartz wackes and feldspathic quartzites (Swamy 1992). The major reactive component is microcrystalline quartz (Gillott, Duncan, and Swenson 1973).

To check if the aggregates selected meets ASTM C33 Standard Specification for Concrete Aggregates, a sieve analysis was conducted on the four aggregates. The results are presented in Figure 3.1. As shown from the gradation curves, NMR, SL and SG falls within the limits specified by ASTM C33 (2000j), while the PRG fall out of the specifications indicating the gravel is slightly coarser than sand.

An understanding of the material properties is an important parameter in order to measure ASR potential of aggregate and concrete. Therefore, all related properties (Specific Gravity, Absorption Capacity, Unit weight) are measured and summarized. The physical properties of aggregates tested are tabulated in Table 3.1.
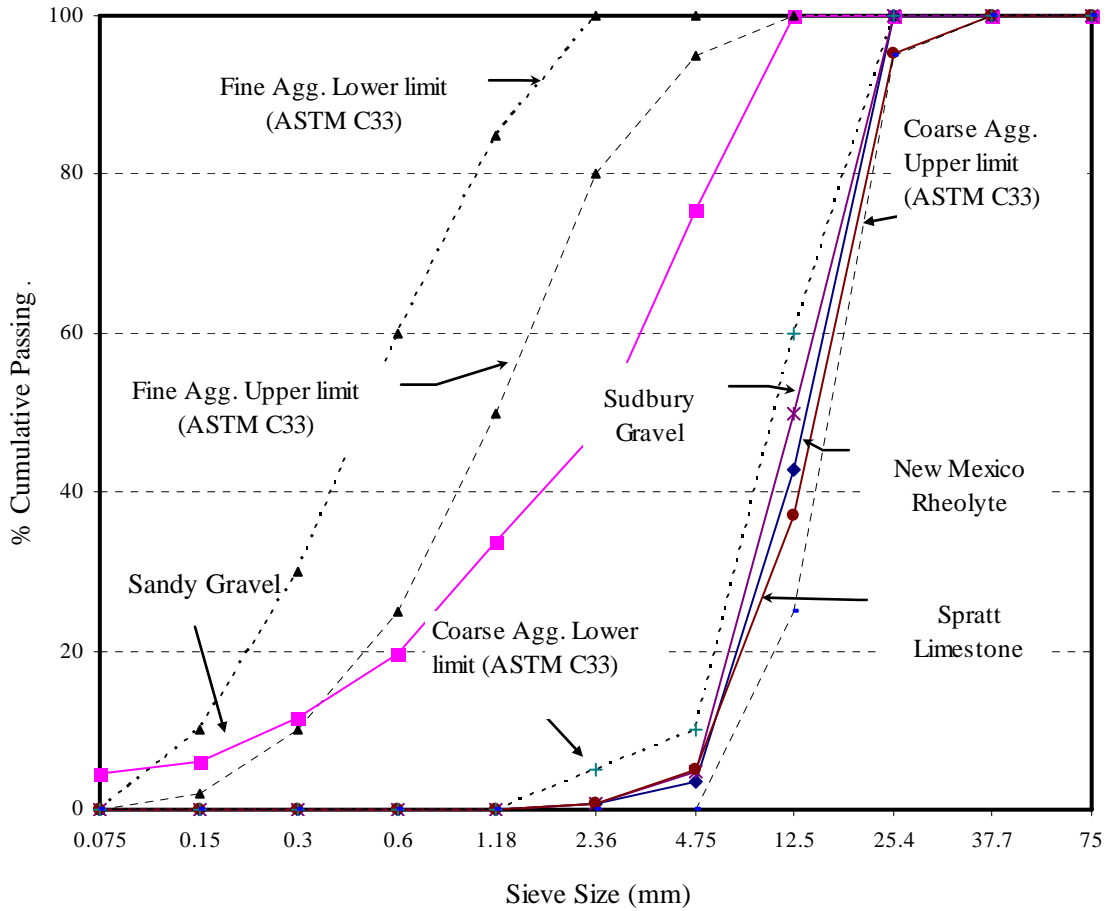
Figure 3.1 Gradation Curves of Aggregates.

Table 3.1 Properties of Aggregates.

Aggregate Property	New Mexico Rhyolite	Platte River Gravel	Sudbury Gravel	Spratt Limestone
Water absorption (%)	1.06	0.72	0.50	0.64
Bulk specific gravity (OD)	2.54	2.47	2.62	2.67
Bulk specific gravity (SSD)	2.56	2.48	2.63	2.68
Dry Rodded Unit Weight, lb/ft^3	99.45	129.4	99.09	98.54

Cement

Low alkali cement (Type I/II) with a Na_2O equivalent of 0.54% (Na_2O_{eq}) and an autoclave expansion of -0.01% was used for this study. It was obtained from Texas Industries (TXI), TX. The source of the cement was from the Midlothian cement Plant in Midlothian, TX. The chemical and physical properties of cement are provided in Tables 3.2 and 3.3 respectively. As shown from both tables, the cement meets the minimum requirements of ASTM C150 specifications.

Table 3.2 Chemical Properties of Cement.

Chemical Requirement	*Spec, Limit (ASTM C150)*	*Test Result*
Al_2O_3	6 max	4.3
Fe_2O_3	6 max	3.9
MgO	6 max	1.4
SO_3	3 max	2.7
Loss on Ignition, (%)	3 max	1
Insoluble Residue, (%)	0.75 max	0.37
C_3A, (%)	8 max	5
CO_2, (%)		0
Limestone, (%)	5 max	0
$CaCO_3$ in Limestone, (%)	70 min	
$C_3S + 4.75(C_3A)$	100 max	92.5
Total Alkalies (Na_2O_e), (%)	0.60 max	0.54

Table 3.3 Physical Properties of Cement.

Physical Requirement	*Spec, Limit (ASTM C150)*	*Test Result*
Air Content, Volume, (%)	12 max	8
Average Fineness (Blaine**,**	280 min	377
Autoclave Expansion, (%)	0.80 max	-0.01
Vicat Initial Set	45 min	116
Compressive Strength (psi)	3 max	1
3 days	1740 min	3630
7 days	2760 max	4450

Fly Ash

The fly ash used in this study was Class F fly ash, as designated by ASTM-C-618-99. The lime (CaO) content was noted to be 10.39%, indicating very good cementitious potential. The fly ash was obtained from Headwaters Resources, Jewett, Texas. The chemical and physical analysis of the fly ash is shown in Tables 3.4 and 3.5 respectively as provided by the manufacturer.

Table 3.4 Chemical Analysis of Class F Fly Ash.

CHEMICAL TESTS	RESULTS	ASTM C 618 Class F Fly Ash
Silicon Dioxide (SiO_2), %	54.12	
Aluminum Oxide (Al_2O_3), %	18.90	
Iron Oxide (Fe_2O_3), %	8.36	
Sum of SiO_2, Al_2O_3, $Fe_2O_{3,}$ %	81.38	70 Min
Calcium Oxide (CaO), %	10.39	
Magnesium Oxide (MgO), %	2.49	
Sulfur Trioxide (SO_3), %	0.5	5.0 Max
Moisture Content	0.14	2.0 Max
Loss of Ignition	0.13	3.0 Max
Available Alkalies (as Na_2O), %	0.34	

Table 3.5 Physical Analysis of Fly Ash.

PHYSICAL TESTS	RESULTS	ASTM C 618 Class F Fly Ash
Fineness (Amount retained on #325 sieve %)	11.21	34 %
Water Requirement, % Control	95.00	105 % Max
Specific Gravity	2.66	
Autoclave Expansion, %	0.00	0.8 % Max
Strength Activity Index with Portland Cement,	81%	75% Min
7 days	88%	75% Min

Sodium Hydroxide

The sodium hydroxide used in this study was obtained from Mallinckrodt Baker, Inc., Phillipburg, NJ. It is a white, high purity pellet with 99 to 100 weight percent NaOH. An analysis of the sodium hydroxide is presented in Table 3.6 and was provided by Mallinckrodt Baker, Inc.

Table 3.6 Physical and Chemical Properties of Sodium Hydroxide, Pellet.

Property	Description
Appearance	White, deliquescent pellets or flakes
Odor	Odorless
Solubility	111 g/100 g of water
Specific Gravity	2.13
pH	13 - 14 (0.5% soln.)
% Volatiles by volume @ 21^0C (70F)	0
Boiling Point	1390C (2534F)
Melting Point	318C (604F)
Vapor Density (Air=1)	> 1.0
Vapor Pressure (mm Hg)	Negligible

Experimental Design and Laboratory Testing

As described previously, to initiate ASR, some conditions (types of reactive aggregate, alkalinity, temperature and exposure conditions) must be available. Since the ultimate objective is to develop concrete mixtures highly resistant to ASR, it is extremely important to understand how the combinations of the above conditions affect and control ASR expansion. Consequently, the factors and the levels in the experimental program for both aggregate and concrete were chosen to take into account the effect of those on ASR. The design factors and levels for aggregates are presented in Table 3.7. For aggregates, 36 test runs were made according to the factorial design, as listed in Table 3.8. The design factors for concrete are shown in Table 3.9. For concrete, 14 test runs were made according to the factorial design, as listed in Table 3.10.

Table 3.7 Experimental Design Factors for Aggregates.

Factor	No. of levels	
Aggregate type	4	New Mexico Rhyolite Platt River Gravel Spratt Limestone Sudbury Gravel
Temperature	3	60, 70 and 80^0C
Normality (NaOH)	3	0.25, 0.5, and 1N
Calcium Hydroxide Ca(OH)$_2$	2	NaOH with and without Ca(OH)$_2$

Table 3.8 Test Runs of Experimental Design for Aggregates.

Tests	Aggregate type	Temperature	Normality	Ca(OH)$_2$
1.	NMR	60	1	With
2.		70		
3.		80		
4.		60	0.5	
5.		70		
6.		80		
7.		60	0.25	
8.		70		
9.		80		
10-11.	PRG	60	1	With and Without
12-13.		70		
14-15.		80		
16-17.		60	0.5	
18-19.		70		
20-21.		80		
22-23.	PRG	60	1	With and Without
24-25.		70		
26-27.		80		
28-29.		60	0.5	
30-31.		70		
32-33.		80		
34.	SL	60	1	Without
35.		70		
36.		80		

All tests (except NMR) in Table 3.8 were repeated twice to establish intra-laboratory comparison

Table 3.9 Experimental Design Factors for Concrete.

Factor	No. of levels	
Aggregate type	2	New Mexico Rhyolite Platt River Gravel
Water cement ratio (w/cm)	1	0.45
Alkalinity	3	0.25, 0.5, and 1N NaOH + CH
Fly Ash (% by weight replacement of cement	3	0, 25 and 50 %
Fixed Parameters		Cement factor, coarse aggregate factor, a non-reactive sand from lattimore materials

Table 3.10 Test Runs of Experimental Design for Concrete.

Tests	Aggregate type	(w/cm)	Fly Ash (%)	Alkalinity
1.	NMR	0.45	0	0.25 N NaOH + CH
2.				0.5 N NaOH + CH
3.				1 N NaOH + CH
4.		0.45	25	0.25 N NaOH + CH
5.				0.5 N NaOH + CH
6.				1 N NaOH + CH
7.	PRG	0.45	25	0.5 N NaOH + CH
8.				1 N NaOH + CH
9.		0.45	50	0.5 N NaOH + CH
10.				1 N NaOH + CH

All combinations for mortar PRG tests were repeated twice to verify repeatability

Equipment Description

This section provides a detailed description of the apparatus and accessories used in the test program to measure ASR expansion of aggregate and concrete.

The device used in this study to measure ASR expansion is called "the dilatometer". It was originally developed at Texas Transportation Institute and has shown great potential to be a successful and a rapid method for assessing aggregate reactivity. In fact, this procedure was included as an appendix in FAA's recently published Advisory Circular "Handbook for Identification of Alkali Silica Reactivity in Airfield Pavement" by Sarkar et al. (2004).

The modified dilatometer (Figure 3.2) used in this study consists of a pot, a Teflon-coated brass, a hollow tower and a steel float (Figure 3.3). The pot is made of Stainless steel. The type of brass used for the lid is the Naval brass; similar to admiralty brass; is a 40% zinc brass and 1% tin. To ensure that air bubbles can be easily removed, the inner surface of the lid will be designed at a specific angle upwards.

The tower was made from Stainless steel S31600. At the top of the tower, a casing is installed to ensure proper alignment of the linear variable differential transducer (LVDT) and the float. The LVDT used is the SCHAEVITZ Model 1000 HCA, which has a maximum range of 2 inch. The LVDT is then pushed into an O-ring located at the bottom of the casing and then secured with six set screws that come though the side of the cylinder. A thermocouple is inserted from the side of the dilatometer to measure the temperature of the solution. The TJ36-CPSS-18G-6 T/C Assembly w/trans joint is used and it is tied to the dilatometer using the SSLK -18-18 1/8*1/8 Compression Fitting. A detailed drawing of the assembled parts of the dilatometer is shown in Figure 3.4.

As the chemical reaction between the aggregate and the NaOH solution is in progress, ASR gel is formed. This gel absorbs water leading to an increase in total volume. As the stainless steel rod moves inside the LVDT, electrical signals are generated. Therefore the physical phenomenon (i.e. movement of the rod) is converted into a measurable signal.

Figure 3.2 Dilatometer Picture.

Figure 3.3 Stainless Steel Float.

2.250"

0.745" 0.760" 0.745"

0.500"

2.546" 2.500"

1.125"

0.250"

3.750"

LVDT
Casing

0.454"

0.875"

0.750"

0.750"

0.350" 0.350"

7.000"

Tower

0.140"

1.275"

0.712"

Brass
Lid

0.550"

2.325"

0.500"

6.449"

Chamber

0.250"

6.000"

6.500"
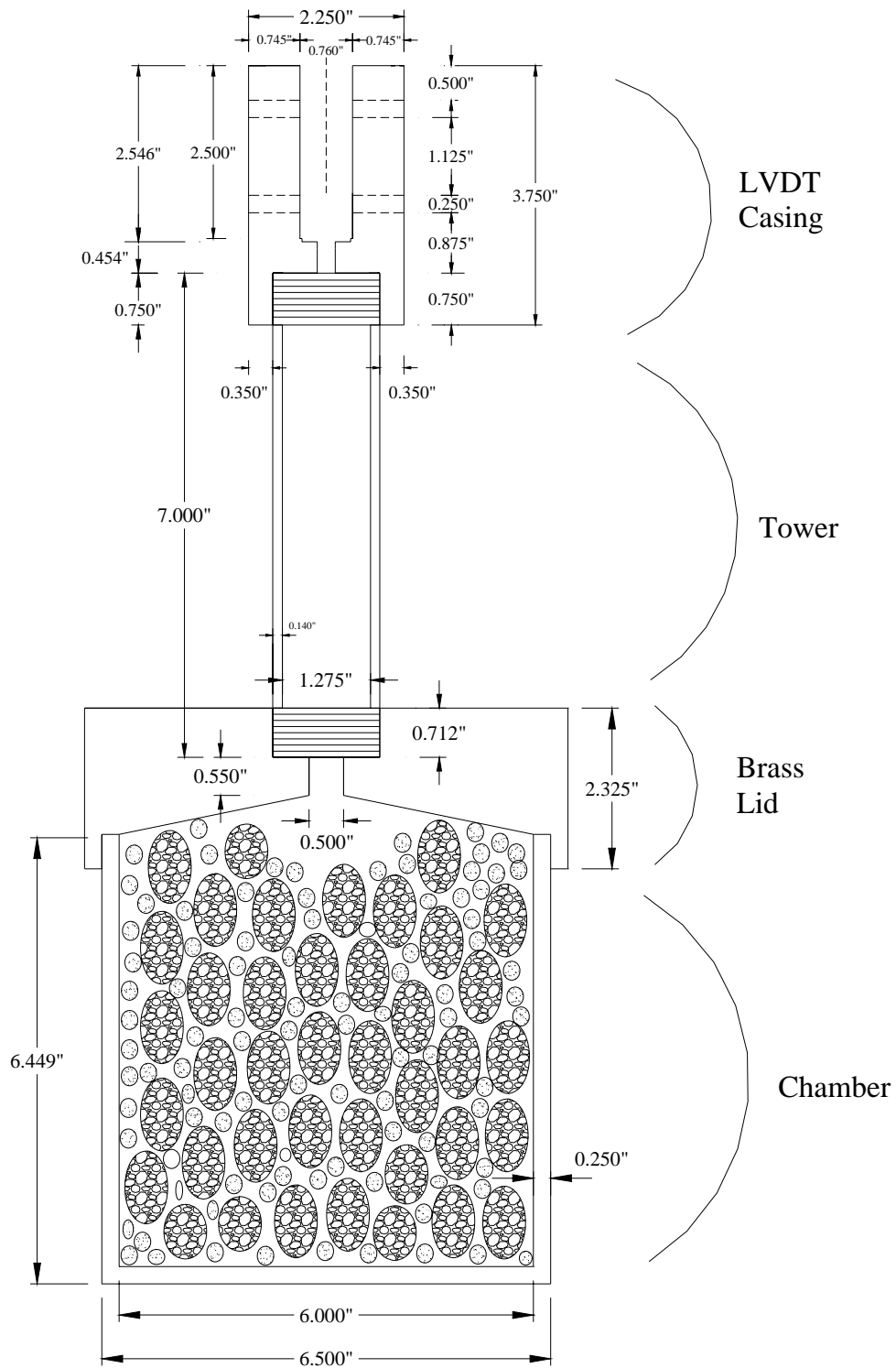
Figure 3.4 Cross-sectional Area of the Dilatometer.

The signals generated are so small in magnitude that the Analog-to-Digital. converter (ADC) of SCXI-1600, USB Data Acquisition and Control Module can't process them. Therefore, signal conditioners are needed to:

a) Amplify the current.

b) Filter and/or remove the noise of a signal.

c) Make the sensor output available for reading by computer boards.

The signal conditioners for the thermocouple and LVDT used are the SCXI-1102 32 Channel Thermocouple Amplifier and the SCXI-1540 8-Channel LVDT Input Module respectively. All signal conditioner and the DAQ card are hold together in the SCXI-1000 4-Slot Chassis. The use of Chassis is to provide power to the signal conditioner and to hold the terminal block, the DAQ card and the SCXI's tight together (Figure 3.5). All LVDT and thermocouples signals are then transferred though a USB cable to a workstation where a program in LabVIEW was developed to display, analyze and store the data generated.
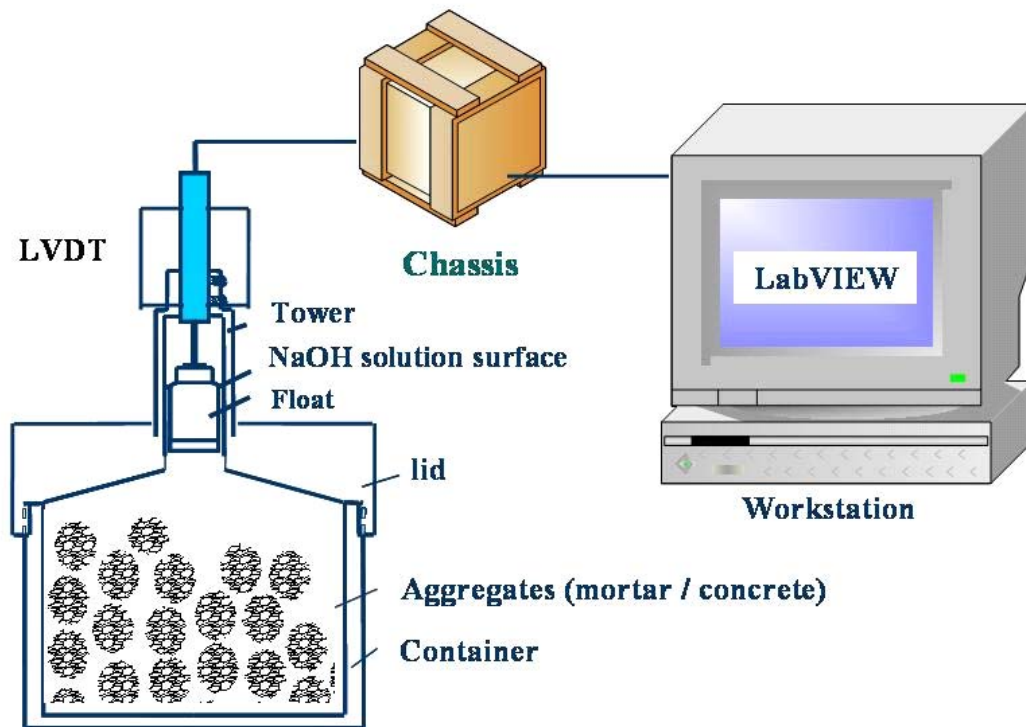
Figure 3.5 Test Setup.

Test Procedure to Measure ASR Expansion for Aggregate and Concrete

This section covers the preparation of the test solution at a different alkalinity, the testing procedure of aggregate and concrete samples in the dilatometer, the calibration procedure and the calculation of ASR expansion.

Preparation of Alkalinity Solutions

The 1 N, 0.5N and 0.25N NaOH solutions mentioned in the experimental designs are prepared by diluting 40, 20 and 10g of sodium hydroxide crystals into 0.9 liter of distilled water. Then water is added to raise the total volume of solution to 1 liter. To achieve calcium hydroxide saturated solutions, 1 gram of $Ca(OH)_2$ crystals is added to the above alkalinity solutions. To achieve homogeneity, all prepared solutions are stirred thoroughly on a magnetic stirrer for 1 minute.

Aggregate Preparation

It is known that the reactivity of aggregate decreases when the size of rock increases (Swamy 1992). Some test procedures like the ASTM C1260 require the aggregate to be crushed to meet certain gradation requirements, therefore changing the total surface area and therefore the reactivity of the aggregate is affected and may not represent anymore their true reactivity under field conditions. To solve the problem, the four types of aggregates in this study are tested uncrushed in the dilatometer and the amount retained on each sieve was kept constant for all types. This will allow a comparison of the activation energy of different aggregate and to rank them based on their reactivity. The amount of aggregate in the dilatometer was selected to be 80% by volume of the stainless steel pot. The sample preparation of aggregates is as follows:

    a)   The weight of the oven dried aggregate is measured and then placed in the dilatometer.

    b)   The aggregate is soaked for 24 hr into an alkaline solution at room temperature.

    c)   The dilatometer is subjected to 3 hrs vacuuming the following day to remove entrapped air (Figure 3.6).

    d)   The dilatometer is then placed in a water bath to raise the temperature to the target temperature.

e) A second round of vacuuming will be applied for 1 hr to remove any remaining or dissolved air bubbles into the solution.

f) The stainless steel float is weighted and then inserted into the tower and the casing is securely placed at the top of the tower using set of screws that come through the side of the cylinder.

g) The free movement is assured by rotating the LVDT and by shaking the whole system in a smoothly manner.

h) The dilatometer is then placed in the oven (Figure 3.7). It takes around 4-5 hrs for the alkalinity solution to be equilibrated with the temperature of the oven.

i) In Measurement and Automation Explorer (MAX); the driver software that recognize the DAQ card; the "rate" (Hz), the "Samples to Read" and the "Acquisition Mode" are selected based on the user needs.

j) In LabVIEW, the "Samples to Read" and the "Timeout" are selected to match the setting inputted in MAX.

k) LVDT readings after the stabilizing period represent the ASR LVDT movement.

A summary of the above steps is presented in Table 3.11.

Table 3.11 Sample Preparation of Aggregates.

Step	Time	Temp.	Purpose/ process
Aggregate Saturation	24 hrs.	Room	Saturation
Vacuuming (Agg. + sol.)	3 hrs.	Room	Remove entrapped air
Preheating dilatometer	2 hrs	Room to Target	Remove entrapped air
Vacuuming (Agg. + sol.)	1 hr.	Target	Remove entrapped air
Dilatometer stabilization	5 hrs.	Target	Set LVDT
ASR Measurement	75-100 hrs	Target	Measure ASR expansion

* For concrete, sample preparation begins from step 2.

Figure 3.6 Dilatometer under Vibration.

Figure 3.7 Dilatometer Placed in the Oven.

Concrete Preparation

Fourteen concrete samples were cast according to the experimental design (Table 3.9): 6 specimens using New Mexico Rhyolite (NMR) and 8 specimens using Platte River Gravel (PRG). Two different types of molds are used: one for each type of aggregate.

For concrete samples using the NMR aggregate, a special mold was designed. The cylindrical specimen consists of a 4 in diameter and 4.5 in length. To accelerate the ASR reaction, a stainless steel insert and a plastic pad with one inch diameter hole were constructed to increase the exposure area of concrete specimens to alkaline solutions. The insert and the pad are placed into the plastic container and concrete samples were cast based on the mixture design provided in Table 3.10. Three to four hours following casting, the inserts are removed and the concrete samples are covered by plastic sheets to reduce evaporation overnight. The following day, the concrete specimens are extracted by breaking the plastic mold from the sides and placed in a water bath at 23^0C saturated with calcium hydroxide to prevent leaching. The molds, the pad, the inset and the procedure of casting and de-molding the concrete specimens are shown in Figure 3.8. After 14 days of curing, concrete samples were taken out of the water bath, any excess water was dried off and the weight of the concrete specimens is recorded in order to calculate the specific gravity and the initial volume of concrete samples. The concrete sample preparation in the dilatometer is exactly the same as the aggregate sample preparation (Table 3.11). The specimens were tested in the dilatometer for 7-10 days.

For concrete samples using the PRG aggregate, ASTM C1260 molds were used to cast the specimens. 8 mortar mixtures were cast using the paddle, mixing bowl and mixer. The mortar bars (1x1x11.25") were prepared according to the experimental design. After casting, the ASTM C1260 molds were transferred to the 100% humidity chamber (Figure 3.9). After 24 hours, specimens were demolded and fully immersed in a lime saturated water bath. After 14 days of curing, the mortars bars were retrieved from the bath and tested in the dilatometer for 4-5 days following the procedure outlined in Table 3.11.

Mold, Pad and Insert

Insert and pad are assembled

All parts are assembled

Casting of the molds

Demolding of concrete samples

Concrete samples after demolding

Figure 3.8 Steps of Casting NMR Concrete Samples.

Mortar mixer

ASTM 1260 molds + bars

ASTM 1260 mold in the Curing Room

ASTM 1260 Bars
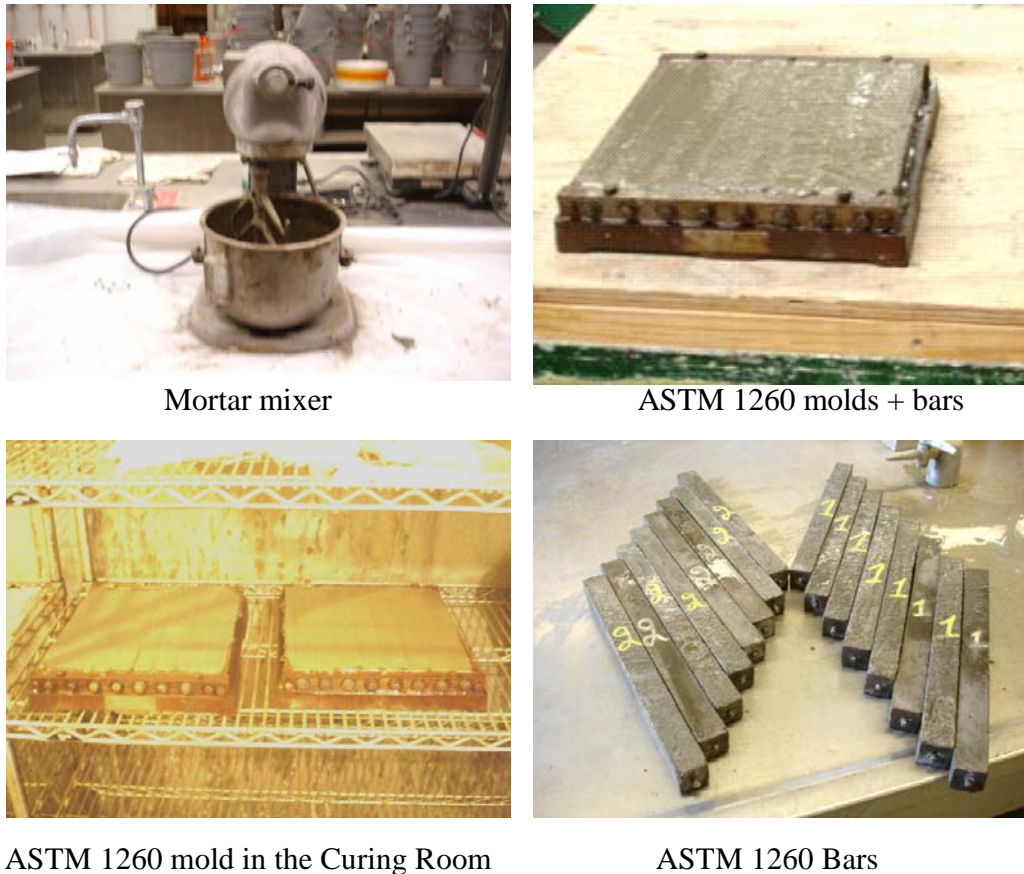
Figure 3.9 Steps of Casting for Platte River Gravel Concrete Samples.

Determination of ASR Expansion

This section covers the calibration procedure and the calculation of ASR expansion followed for aggregate and concrete specimens. Additionally, this section covers the additional test conducted on the aggregate soak solutions.

Calibration Procedure

Since the dilatometer is a very sensitive test procedure, it is imperative to apply a calibration curve for both aggregate and concrete samples to ensure accurate measurement of the expected expansion. The steps below were followed:

    a) For each combination in the experimental design for aggregate, two dilatometer tests were conducted: the first is with aggregate soaked at a specific alkaline solution and the second with aggregate soaked in water at the same temperature.

b) For concrete tests, two dilatometer tests were conducted: the first contained a concrete sample soaked at a specific alkaline solution and the second concrete specimen was soaked in saturated calcium hydroxide solution at the same temperature.

c) The data were recorded and monitored for at least 4-5 day.

d) Once the test was stopped, the linear movement (inch) versus time (hours) was plotted for the above mentioned tests.

e) A reference point was chosen when the dilatometer temperature reached the target temperature.

f) All future LVDT readings were subtracted from the reference point reading. The above analysis was conducted on all aggregate and concrete solution test results.

g) The expansion was determined by calculating the difference in the magnitude between the two movements (Figure 3.10).
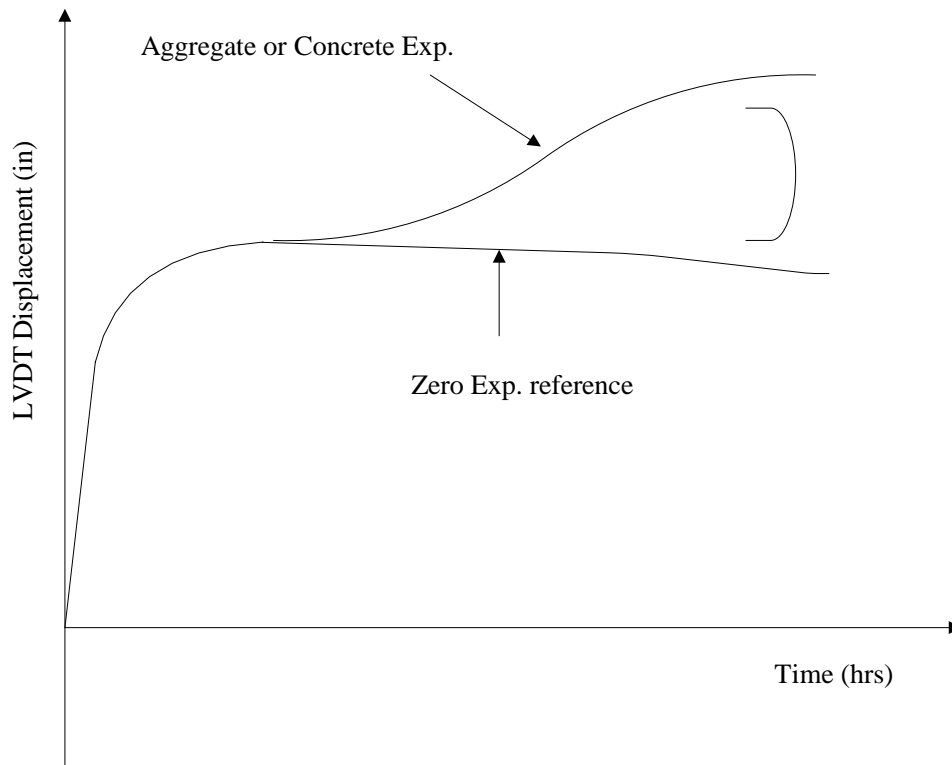
Figure 3.10 Schematic Drawing of the Calibration Procedure.

Calculation of ASR Expansion

The volume change of aggregate because of ASR expansion is an important parameter of internal cracking in concrete structures. The ASR expansion was calculated as follows (Figure 3.11).

$$E_n(\%) = \frac{\Delta V_{ASR}}{V_{aggregate}} \times 100$$

where:

$E_n(\%) = $ Percent Expansion at n hours

$V_{aggregate} = $ Initial Volume of Aggregate

$\Delta V_{ASR} = $ Volume change of Aggregate at n hours
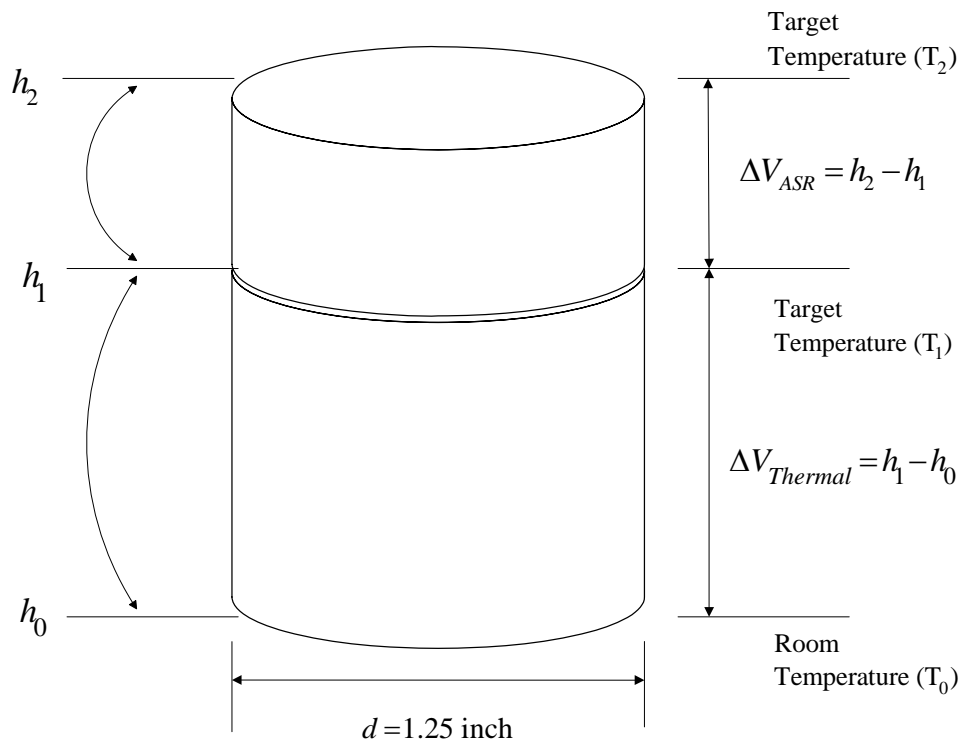
Figure 3.11 ASR Expansion.

pH Measurements

As mentioned in Chapter II, to initiate ASR, a high pH environment is necessary. The selection in the experimental program of 1, 0.5 and 0.25 N NaOH provides a highly

alkaline environment (pH between 13 and 14). To check if any drastic change in hydroxyl ions occurs from the interaction of alkaline solution and the aggregate and concrete samples, it is vital to measure the pH of solution before and after conducting the dilatometer test to see if there is any correlation between the expected expansion observed during the test and pH.

The pH of all soaked solutions was determined using a Fisher Scientific Accumet Excel XL25 pH meter, calibrated to buffer solutions 12 and 14 levels of pH. pH 14 was prepared by diluting 40 gm of NaOH into 1 Liter of distilled water and pH 12 buffer solutions was prepared by taking 1 mL of the above solution using a micropipette and then diluted it 100 times in a volumetric flask.

CHAPTER IV

DEVELOPMENT OF A METHODOLOGY TO MITIGATE ASR

To initiate ASR, certain conditions need to be met: nature and amount of reactive silica, sufficient alkali existent in the pore solution and sufficient moisture. ASR damage is directly linked to ultimate expansion of concrete. The expansion of concrete is a function of concrete material properties (i.e. pH of pore solution, aggregate reactivity, amount of coarse and fine aggregate, water cement ratio, amount and type of supplementary cementitious materials, types of admixtures, etc). To formulate concrete mixtures highly resistant to ASR, the complex interactions of the above concrete properties need to be evaluated thoroughly. Consequently, a methodology to mitigate ASR was developed and proposed in this chapter.

This study will lead to the development of a reaction signature for combined concrete materials using dilatometer test. And this objective is accomplished though four main steps:

- Step 1: Developing a model to determine ASR main parameters.
- Step 2: Determination of the main parameters of the ASR model using system identification method.
- Step 3: Predicting potential ASR aggregate reactivity in terms of their activation energy.
- Step 4: Determination of alkaline reactive signature.

Developing a Model to Determine ASR Expansion

Any mathematical structure of any phenomena can take any of the following forms: non-parametric models, differential equations, transfer functions, exponential functions, linear or nonlinear functions (Unbehauen 1982). To have an accurate and an optimized form of the proposed model, all major properties and characteristics of the phenomena (i.e. ASR) are identified and taken into account.

An initial attempt to include the main parameters that affect ASR into a single model was made by Mukhopadhyay, Shon, and Zollinger 2006. In their paper, they

proposed a model (described in details in Chapter II) based on a maturity concept to predict the ultimate expansion of aggregate. For some types of aggregates, the ultimate expansion turned out to be negative because they used linear regression to fit non-linear expansion data from the dilatometer. Consequently, their model has very limited practicality.

The ultimate expansion of aggregates, the theoretical initial time of ASR expansion, the rate constant (Beta) are all important parameters and have to be determined. Therefore the following model is used to fit the measured expansion data from the dilatometer (Figure 4.1).

$$\frac{1}{\varepsilon} = \frac{1}{\varepsilon_0} . e^{\left(\frac{\rho}{t-t_0}\right)^{\beta}} \qquad (4.1)$$

where:

ε_0 = ASR Ultimate Expansion

β = Rate Constant

t_0 = Initial time of ASR Expansion (hr)

ρ = Time corresponding to an expansion (ε_0 / e)
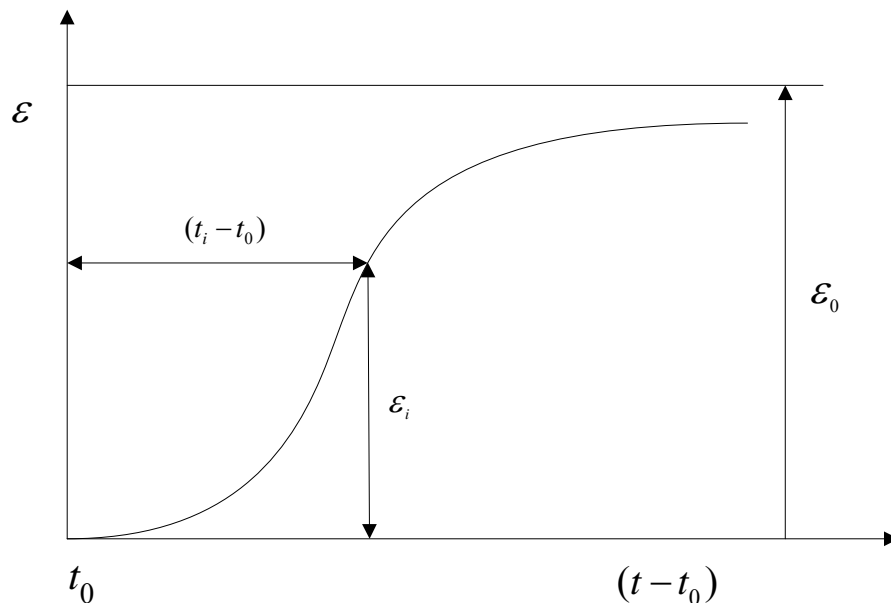
Figure 4.1 Proposed ASR Model to Fit the Expansion Data History of the Dilatometer.

The parameters of the proposed model are determined using a mathematical procedure called System Identification (SID) method. The proposed kinetic model has

two major advantages over other models mentioned in the literature. The current kinetic model has two major advantages over other models mentioned in the literature:

1. The model fit of the expansion data obtained by the dilatometer is of high quality.

2. The parameter β, defined in the model as the "ASR rate constant" remains constant over the full range of collected data, asserting a basic law in chemistry that the rate of a chemical reaction is constant (β in this case).

Revealing the threshold level of expansion where cracking will be initiated is of paramount importance. This can be achieved by taking the double natural logarithm of equation (4.1). Therefore, the above kinetic performance model is transformed into the following linear form:

$$Ln\left[-Ln\left(\frac{\varepsilon}{\varepsilon_0}\right)\right] = \beta Ln\alpha - \beta Ln(t - t_0) \qquad (4.2)$$

Figure 4.2 displays the linear relationship between $Ln\left[-Ln\left(\varepsilon/\varepsilon_0\right)\right]$ and $Ln(t - t_0)$. Preliminary test results indicate that time expansion data falls on the linear regression line. Any expansion data that shows signs of double hump or major deviation in the slope (β) will be attributed to the initiation of microcracks in the concrete. This justifies only modeling the first hump since this is the behavior that most are interested in at least in terms of expansion related to cracking behavior. Thus, for each set of measured ASR concrete and aggregate data, the linear trends will be assessed and examined to make sure that the kinetic performance model will fit only the linear portion of the data.
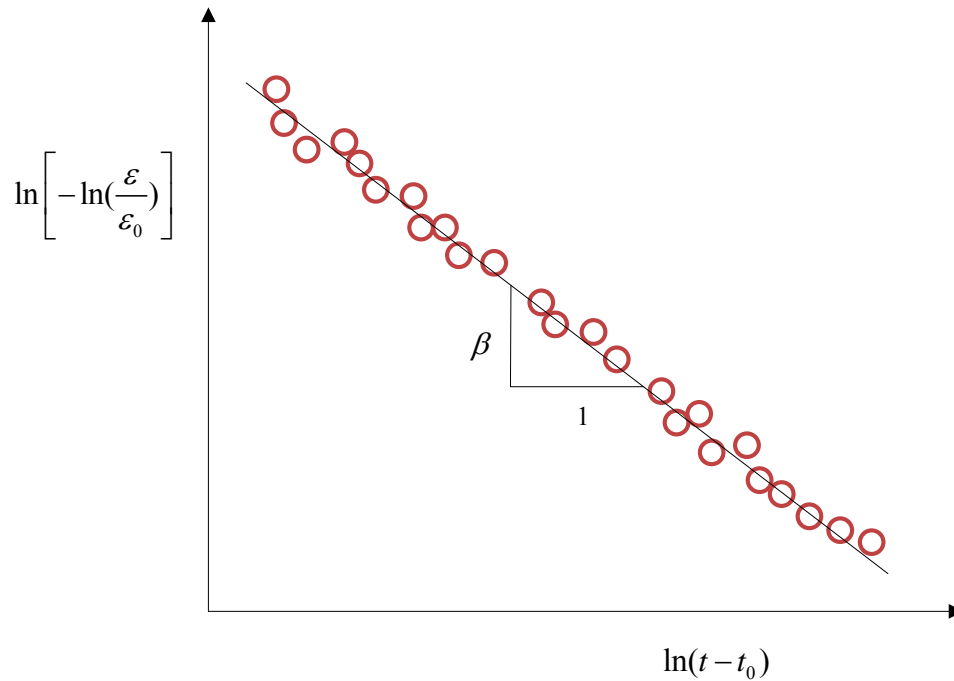
Figure 4.2 Linearization of the Kinetic Performance Model.

Determination of the Main Parameters of the ASR Model Using SID

This section covers in details the background and the principle of the system identification procedure and the parameters calculations.

Principle of the Method

The advancement of computer technology in the last century has boosted the usage of computers to store, display, process and analyze huge amount of data in a very short period of time. A key point in the optimum process operation is the knowledge of the processes or phenomena (whether it is static, dynamic, linear, non linear, etc) in the past, present and in the future. Most processes are time continuous systems.

The utilization of computers make it possible to identify the process by assessing the input and output signals of the system. The general consequence of the process identification is a mathematical model. The main reasons for setting up these models for processes are listed as follow (Unbehauen 1982):

a) The model gives us the chance to understand how the internal behavior of the system works.

b) The model provides us an opportunity to simulate future process behavior in special conditions (i.e. simulation of malfunctions in an experiment or test).

c) The determination of the main parameters affecting the process can be only determined accurately based on an accurate model.

Depending on the types of processes and applications, the mathematical model can take many forms i.e. non-parametric models, differential equations, transfer functions, exponential functions, linear or nonlinear functions, etc. To have an accurate and an optimized form of the model, all major properties and characteristics of the phenomena should be identified and taken into account. Therefore, the objective of system identification is to formulate a mathematical model which describes in a sufficiently precise manner, the behavior of the system (Unbehauen 1982). The accuracy of the developed model is determined by a comparison of the system output (i.e. measured expansion) and the model output (i.e. predicted expansion) when both the system and the model are excited by the same input signal (Figure 4.3). The output signal error is calculated as:

$$E = Y(t) - Y_M(t) \qquad\qquad (4.3)$$

where:

Y = Measured System Output

Y_M = Model Output

When the output signal error is minimal, it will be assumed that the optimum model was obtained. If this is not the case (i.e. significant error), the parameters of the model must be adjusted and corrected by a parameter factor. This rectification will continue until the error is reduced to a minimum value.
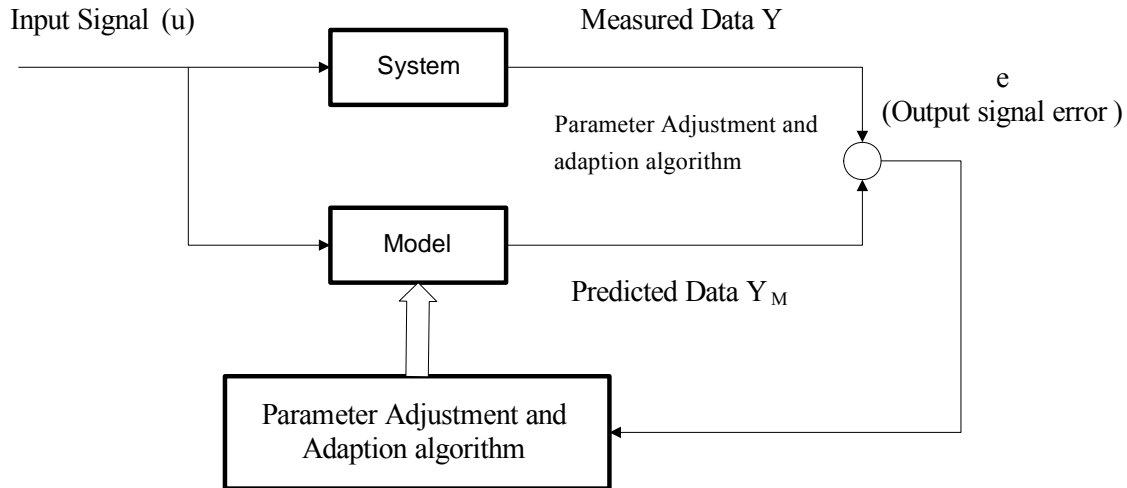
Figure 4.3 System Identification Procedure Using Parameter Estimation Method
(modified from Unbehauen 1982).

When knowledge about the system is not available, the system identification is composed
of three steps (Unbehauen 1982):

a) Determination of the model equation. The choice of the model depends mainly on the
    physical characteristics of the phenomena under study. And this is determined during
    the first step of the identification procedure.

b) Determination of the structural coefficients. These include the model order and the
    deadtime d of your signal.

c) Calculation of the equation parameters in the proposed model. The parameters are
    determined using the parameter estimation methods. This is obtained by minimizing
    the quadratic function of the error. The numerical calculation of this optimization
    problem can be performed using many methods: Least square methods is the most
    common and is obtained from:

$$\begin{Bmatrix} \text{New} \\ \text{estimated} \\ \text{value} \end{Bmatrix} = \begin{Bmatrix} \text{Old} \\ \text{estimated} \\ \text{value} \end{Bmatrix} + \begin{bmatrix} \text{Correction} \\ \text{vector} \end{bmatrix} \times \begin{Bmatrix} \begin{pmatrix} \text{new} \\ \text{sample} \end{pmatrix} \end{Bmatrix} \qquad (4.4)$$

Parameters Calculations

As mentioned in section 4.1, the model used to fit the expansion data is:

$$\frac{1}{\varepsilon} = \frac{1}{\varepsilon_0}.e^{(\frac{\rho}{t-t_0})^\beta} \tag{4.5}$$

To simplify the above equation, first define $z = \frac{1}{\varepsilon}$ and $z_0 = \frac{1}{\varepsilon_0}$, the transformed equation

becomes:

$$Z_i = Z_0.e^{(\frac{\rho}{t-t_0})^\beta} \tag{4.6}$$

The coefficients to be determined are z_0, ρ, β, t_0. As shown from Eq 4.5, it is a non-linear least square error problem, and for it, there is no closed-form solution. Instead, initial values must be chosen for the parameters. Then, the parameters are refined iteratively, that is, the values are obtained by successive approximation. Equation (4.7) displays the relationship between F, α and r. F is usually called the sensitivity matrix, because its elements reflect the sensitivity of the output. α is defined as the parameter vector and represents the % change of the parameters (z_0, ρ, β, t_0) to be determined. r is called the residual vector and represents the % change of the data (i.e. the ratio of the difference of the observed expansion and calculated expansion from the model to the calculated expansion).

$$F.\alpha = r \tag{4.7}$$

where:

$F =$ Sensitivity Matrix or Data Matrix

r $=$ Residual Vector

α $=$ Parameter Vector

Writing out Eq. 4.7 in detail, we obtain

$$
\begin{bmatrix}
\dfrac{\delta Z_1}{\delta Z_0}\cdot\dfrac{Z_0}{\hat Z_1} & \dfrac{\delta Z_1}{\delta\rho}\cdot\dfrac{\rho}{\hat Z_1} & \dfrac{\delta Z_1}{\delta(t_0)}\cdot\dfrac{t_0}{\hat Z_1} & \dfrac{\delta Z_1}{\delta\beta}\cdot\dfrac{\beta}{\hat Z_1} \\[2mm]
\dfrac{\delta Z_2}{\delta Z_0}\cdot\dfrac{Z_0}{\hat Z_2} & \dfrac{\delta Z_2}{\delta\rho}\cdot\dfrac{\rho}{\hat Z_2} & \dfrac{\delta Z_2}{\delta(t_0)}\cdot\dfrac{t_0}{\hat Z_2} & \dfrac{\delta Z_2}{\delta\beta}\cdot\dfrac{\beta}{\hat Z_2} \\[2mm]
\dfrac{\delta Z_3}{\delta Z_0}\cdot\dfrac{Z_0}{\hat Z_3} & \dfrac{\delta Z_3}{\delta\rho}\cdot\dfrac{\rho}{\hat Z_3} & \dfrac{\delta Z_3}{\delta(t_0)}\cdot\dfrac{t_0}{\hat Z_3} & \dfrac{\delta Z_3}{\delta\beta}\cdot\dfrac{\beta}{\hat Z_3} \\[2mm]
\vdots & \vdots & \vdots & \vdots \\
\vdots & \vdots & \vdots & \vdots \\
\vdots & \vdots & \vdots & \vdots \\
\dfrac{\delta Z_n}{\delta Z_0}\cdot\dfrac{Z_0}{\hat Z_n} & \dfrac{\delta Z_n}{\delta\rho}\cdot\dfrac{\rho}{\hat Z_n} & \dfrac{\delta Z_n}{\delta(t_0)}\cdot\dfrac{t_0}{\hat Z_n} & \dfrac{\delta Z_n}{\delta\beta}\cdot\dfrac{\beta}{\hat Z_n}
\end{bmatrix}
\times
\begin{bmatrix}
\dfrac{Z_0^{i+1}-Z_0^{i}}{Z_0^{i}} \\[3mm]
\dfrac{\rho^{i+1}-\rho^{i}}{\rho^{i}} \\[3mm]
\dfrac{t_0^{i+1}-t_0^{i}}{t_0^{i}} \\[3mm]
\dfrac{\beta^{i+1}-\beta^{i}}{\beta^{i}}
\end{bmatrix}
=
\begin{bmatrix}
\dfrac{Z_1-\hat Z_1}{\hat Z_1} \\[3mm]
\dfrac{Z_2-\hat Z_2}{\hat Z_2} \\[3mm]
\dfrac{Z_3-\hat Z_3}{\hat Z_3} \\[3mm]
\vdots \\ \vdots \\ \vdots \\
\dfrac{Z_n-\hat Z_n}{\hat Z_n}
\end{bmatrix}
$$

| Sensitivity Matrix | Change Vector | Residual Vector |

To calculate the elements of the sensitivity matrix, the partial derivatives of Z with respect to the parameters are determined as follows:

$$
\frac{\delta Z}{\delta Z_0}=e^{(\frac{\rho}{t-t_0})^{\beta}}
$$

$$
\frac{\delta Z}{\delta\rho}=Z_0\cdot\left(\frac{\rho}{t-t_0}\right)^{\beta}\cdot\frac{\beta}{\rho}\cdot e^{(\frac{\rho}{t-t_0})^{\beta}}
$$

$$
\frac{\delta Z}{\delta(t_0)}=Z_0\cdot\frac{\beta\cdot\rho^{\beta}}{(t-t_0)^{\beta+1}}\cdot e^{(\frac{\rho}{t-t_0})^{\beta}}
$$

$$
\frac{\delta Z}{\delta(\beta)}=Z\cdot\left(\frac{\rho}{t-t_0}\right)^{\beta}\cdot\ln\left(\frac{\rho}{t-t_0}\right)
$$

The elements of the sensitivity matrix are determined as follows:

$$
\frac{\delta Z_i}{\delta Z_0}\cdot\frac{Z_0}{\hat Z_i}=e^{(\frac{\rho}{t_i-t_0})^{\beta}}\cdot\frac{Z_0}{Z_0\cdot e^{(\frac{\rho}{t_i-t_0})^{\beta}}}=1
$$

$$\frac{\delta Z_i}{\delta \rho} \cdot \frac{\rho}{\hat{Z}_i} = \hat{Z}_i \cdot (\frac{\rho}{t_i - t_0})^\beta \cdot \frac{\beta}{\rho} \cdot \frac{\rho}{\hat{Z}_i}$$

$$= \beta \cdot (\frac{\rho}{t_i - t_0})^\beta$$

$$\frac{\delta Z_i}{\delta(t_0)} \cdot \frac{t_0}{\hat{Z}_i} = \hat{Z}_i \cdot \frac{\beta \cdot \rho^\beta}{(t_i - t_0)^{\beta+1}} \cdot \frac{t_0}{\hat{Z}_i}$$

$$= \frac{\beta \cdot \rho^\beta \cdot t_0}{(t_i - t_0)^{\beta+1}}$$

$$\frac{\delta Z_i}{\delta \beta} \cdot \frac{\beta}{\hat{Z}_i} = Z_i \cdot (\frac{\rho}{t_i - t_0})^\beta \cdot \ln(\frac{\rho}{t_i - t_0}) \cdot \frac{\beta}{\hat{Z}_i}$$

$$= \beta \cdot (\frac{\rho}{t_i - t_0})^\beta \cdot \ln(\frac{\rho}{t_i - t_0})$$

The above determined coefficients are used in the System Identification Method. The sensitivity matrix, change vector, and residual vectors becomes as follows:

$$
\begin{bmatrix}
1 & \beta(\frac{\rho}{t_1-t_0})^\beta & \frac{\beta\rho^\beta t_0}{(t_1-t_0)^{\beta+1}} & \beta(\frac{\rho}{t_1-t_0})\ln(\frac{\rho}{t_1-t_0}) \\
1 & \beta(\frac{\rho}{t_2-t_0})^\beta & \frac{\beta\rho^\beta t_0}{(t_2-t_0)^{\beta+1}} & \beta(\frac{\rho}{t_2-t_0})\ln(\frac{\rho}{t_2-t_0}) \\
1 & \beta(\frac{\rho}{t_3-t_0})^\beta & \frac{\beta\rho^\beta t_0}{(t_3-t_0)^{\beta+1}} & \beta(\frac{\rho}{t_3-t_0})\ln(\frac{\rho}{t_3-t_0}) \\
\vdots & \vdots & \vdots & \vdots \\
\vdots & \vdots & \vdots & \vdots \\
\vdots & \vdots & \vdots & \vdots \\
\vdots & \vdots & \vdots & \vdots \\
1 & \beta(\frac{\rho}{t_n-t_0})^\beta & \frac{\beta\rho^\beta t_0}{(t_n-t_0)^{\beta+1}} & \beta(\frac{\rho}{t_n-t_0})\ln(\frac{\rho}{t_n-t_0})
\end{bmatrix}
\times
\begin{bmatrix}
\frac{Z_0^{i+1}-Z_0^i}{Z_0^i} \\
\frac{\rho^{i+1}-\rho^i}{\rho^i} \\
\frac{t_0^{i+1}-t_0^i}{t_0^i} \\
\frac{\beta^{i+1}-\beta^i}{\beta^i}
\end{bmatrix}
=
\begin{bmatrix}
\frac{Z_1-\hat{Z}_1}{\hat{Z}_1} \\
\frac{Z_2-\hat{Z}_2}{\hat{Z}_2} \\
\frac{Z_3-\hat{Z}_3}{\hat{Z}_3} \\
\vdots \\
\vdots \\
\vdots \\
\vdots \\
\frac{Z_n-\hat{Z}_n}{\hat{Z}_n}
\end{bmatrix}
$$

Sensitivity Matrix   Change Vector   Residual Vector

Multiplying Eq. (4.7) by F^T, the eq. can be written as:

$$F^T.F.\alpha = F^T.r \tag{4.8}$$

Multiplying Eq (4.8) by $\left[F^T.F\right]^{-1}$, it can be written as:

$$\left[F^T.F\right]^{-1}.\left[F^T.F\right].\alpha = \left[F^T.F\right]^{-1}.F^T.r \tag{4.9}$$

Simplifying the above Eq, the vector change is obtained

$$\alpha = \left[F^T.F\right]^{-1}.F^T.r \tag{4.10}$$

If every value in the α vector is less than 0.01 (1%), it is assumed that optimum model is obtained. If this is not the case, the parameters of the model are adjusted and corrected by a parameter factor as follows:

$$Z_0^{i+1} = (1+0.6\alpha_1).Z_0^i$$
$$\rho^{i+1} = (1+0.6\alpha_2).\rho^i$$
$$t_0^{i+1} = (1+0.6\alpha_3).t_0^i$$
$$\beta^{i+1} = (1+0.6\alpha_4).\beta^i$$

The above constant value "0.6" used in the parameter adjustment was chosen to make the convergence toward the optimum solution faster. The core structure of all algorithmic estimation methods is presented in Figure 4.4. Since solving the above equations manually is very involved and time consuming, a program in matlab was generated for that purpose.
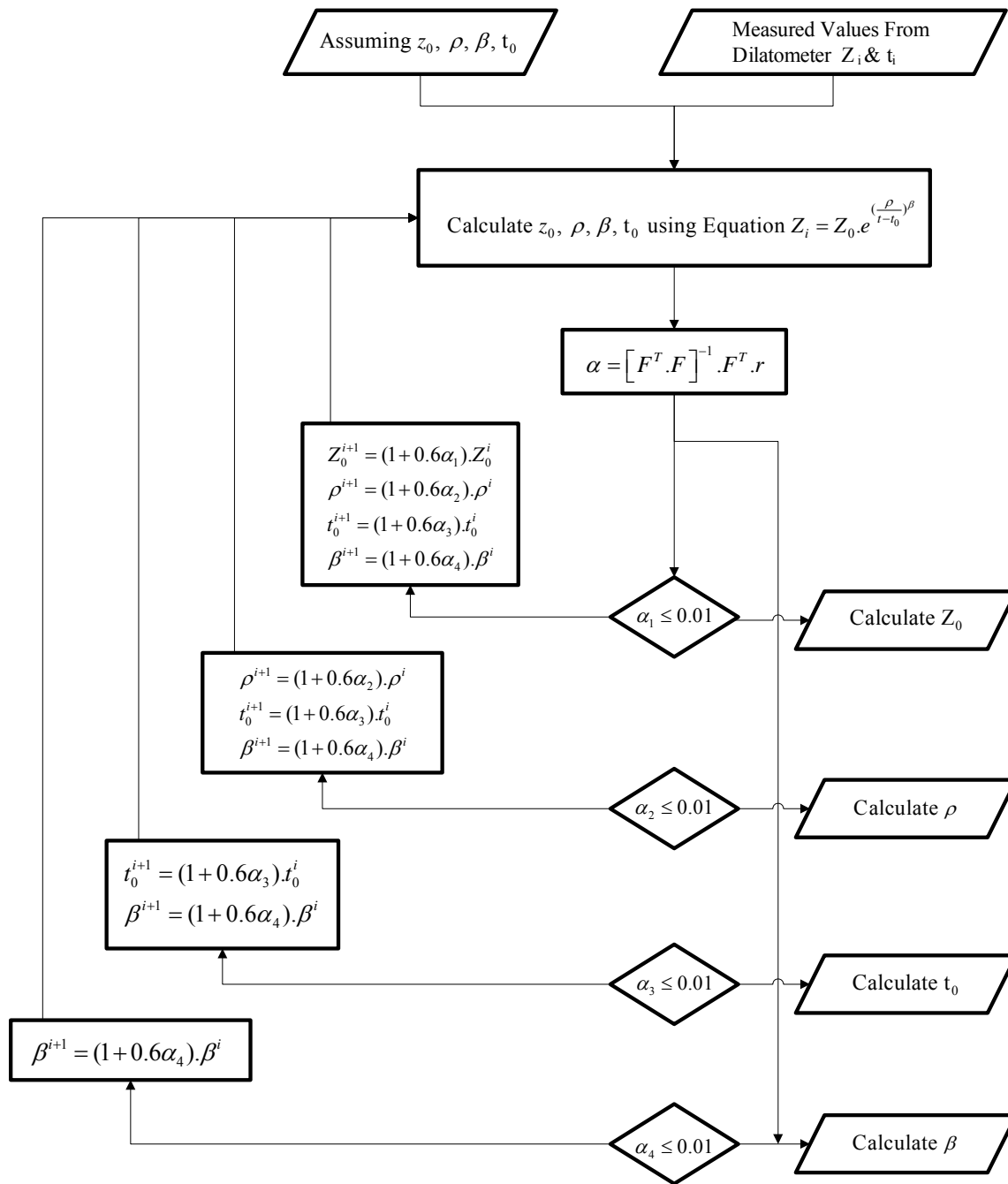
Figure 4.4 Flowchart of the Algorithm to Determine the Parameters of the ASR Model.

Predicting Potential ASR Aggregate Reactivity in Terms of Their Activation Energy

In analytical chemistry, activation energy (E_a) is defined as the minimum energy required to overcome for a chemical reaction to proceed (Ebbing and Gammon 2005). Consequently, it can be considered as an energy barrier (Figure 4.5). For exothermic chemical reaction, more energy is needed to convert the products to reactants. On the other side, for an endothermic reaction (like ASR), E_a ($X \rightarrow Y$) is higher than the E_a ($Y \rightarrow X$).

The concept of ASR related activation energy was introduced as a representative single parameter of the ASR (Shon 2008). For ASR, E_a is considered as the energy required to initiate ASR taking into account the combined effect of alkalinity, temperature and time. The Arrhenius equation provides us the relationship between the rate constant, temperature and activation energy (Ebbing et al. 2005). To solve the relationship, three tests are conducted at three temperatures (60, 70 and 80^0C) for different alkalinities mentioned in the experimental design in Chapter III to determine the rate constants.
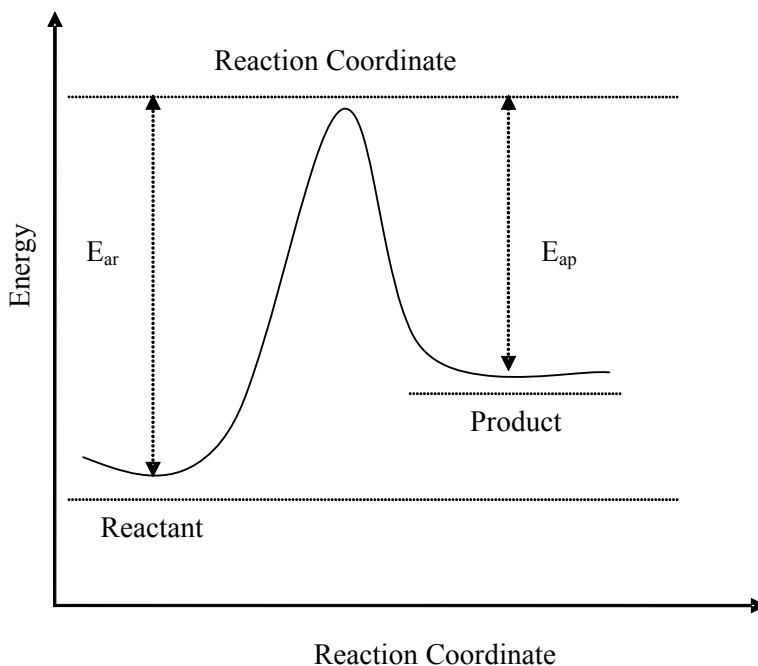
Figure 4.5 Reaction Coordination Diagram (Ebbings and Gammon 2005).

Based on the proposed ASR model, the rate constant is defined as Beta. The activation energy is calculated by plotting ln (Beta) versus (1/T). The slope of this equation is obtained by linear regression and is equal to $(-E_a/R)$ where R is the universal gas constant (Figure 4.6).
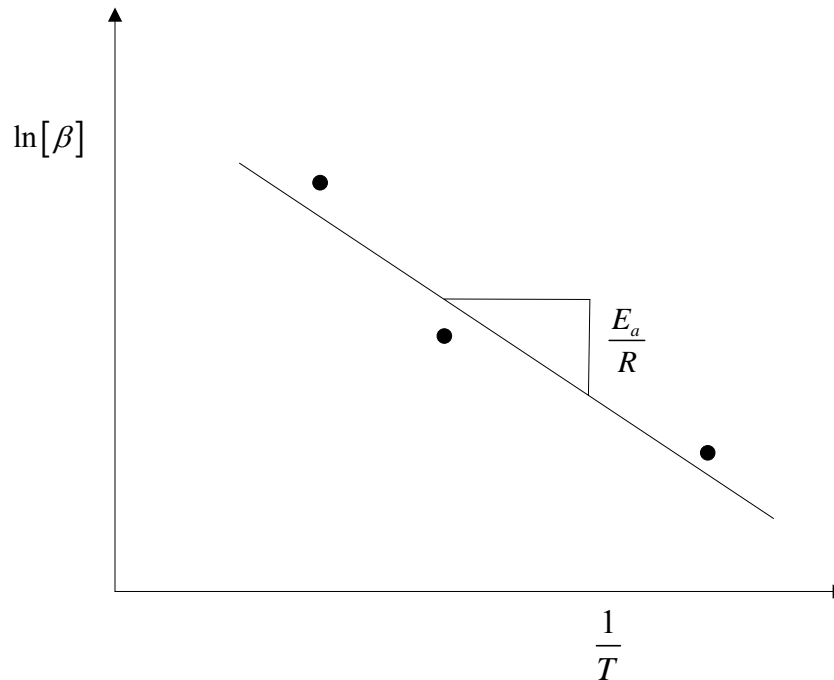
Figure 4.6 Determination of Activation Energy.

Determination of Alkaline Reactive Signature

One of the ultimate objectives of this study is to incorporate the effect of aggregate reactivity, water cement ratio and supplementary cementitious materials on ASR to develop concrete mixtures highly resistant to ASR. To achieve this objective, the ultimate expansion of concrete, alkalinity and activation energy of aggregate should be related and this was performed into two steps.

Proposed Model to Determine E_a of Aggregate under Field Conditions

It is known that the natural pH of concrete is around 12.4. If the cement contains a high amount of alkali, the concentration of sodium and potassium hydroxide in the pore solution will be significant and the pH may reach well above 13. An increase in pH will increase the rate of ASR. The normality of sodium hydroxide in this study is 0.5 and 1 N

corresponding to a pH of 13.7 and 14 respectively, well above the pH of concrete in field conditions. Therefore, it is important to determine the activation energy of the aggregate covering the whole pH spectrum that the concrete will be subjected to. Therefore the following model is used determine E_a at different levels of alkalinity (Figure 4.7).

$$E_a = E_{a_0} + \frac{C_1}{C^n} \tag{4.11}$$

where:

E_a = Activation Energy $\left[\dfrac{KJ}{mol}\right]$

E_{a_0} = Activation Energy - Threshold $\left[\dfrac{KJ}{mol}\right]$

C_1 = Activation Energy Curvature Coefficient $\left[\dfrac{KJ}{(mol)^{1-n}}\right]$

n = Activation Energy Curvature Exponent

C = Alkalinity (mol)

Figure 4.7 Activation Energy vs. Alkalinity.

The coefficients to be ascertained are E_{a_0}, C_1, n and are determined using the system identification method. The sensitivity matrix, change vector, and residual vectors are defined as follows:

$$
\begin{bmatrix}
\dfrac{\delta E_{a_1}}{\delta E_{a_0}}\cdot\dfrac{E_{a_0}}{\hat{E}_{a_1}} & \dfrac{\delta E_{a_1}}{\delta C_1}\cdot\dfrac{C_1}{\hat{E}_{a_1}} & \dfrac{\delta E_{a_1}}{\delta n}\cdot\dfrac{n}{\hat{E}_{a_1}} \\[3mm]
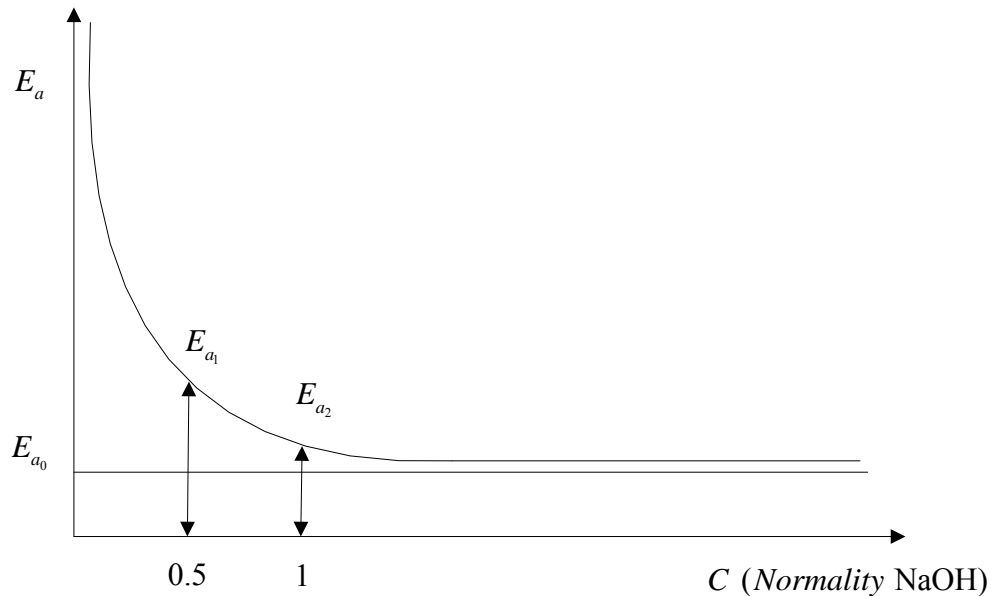\dfrac{\delta E_{a_2}}{\delta E_{a_0}}\cdot\dfrac{E_{a_0}}{\hat{E}_{a_2}} & \dfrac{\delta E_{a_2}}{\delta C_1}\cdot\dfrac{C_1}{\hat{E}_{a_2}} & \dfrac{\delta E_{a_2}}{\delta n}\cdot\dfrac{n}{\hat{E}_{a_2}}
\end{bmatrix}
\times
\begin{bmatrix}
\dfrac{E_{a_0}^{i+1}-E_{a_0}^{i}}{E_{a_0}^{i}} \\[3mm]
\dfrac{C_1^{i+1}-C_1^{i}}{C_1^{i}} \\[3mm]
\dfrac{n^{i+1}-n^{i}}{n^{i}}
\end{bmatrix}
=
\begin{bmatrix}
\dfrac{E_{a_1}-\hat{E}_{a_1}}{\hat{E}_{a_1}} \\[3mm]
\dfrac{E_{a_2}-\hat{E}_{a_2}}{\hat{E}_{a_2}}
\end{bmatrix}
$$

Sensitivity Matrix   Change Vector   Residual Vector

The partial derivatives of E_a with respect to the coefficients are:

$$
\frac{\delta E_a}{\delta E_{a_0}}=1, \quad \frac{\delta E_a}{\delta C_1}=\frac{1}{C^n}, \quad \frac{\delta E_a}{\delta n}=\frac{-C_1}{C^n}\cdot\ln(C),
$$

For the sensitivity matrix, the following terms are formed.

$$
\frac{\delta E_{a_i}}{\delta E_{a_0}}\cdot\frac{E_{a_0}}{\hat{E}_{a_i}}=\frac{E_{a_0}\cdot C^n}{E_{a_0}\cdot C^n+C_1}, \quad
\frac{\delta E_{a_i}}{\delta C_1}\cdot\frac{C_1}{\hat{E}_{a_i}}=\frac{E_{a_0}}{E_{a_0}\cdot C^n+C_1}, \quad
\frac{\delta E_{a_i}}{\delta n}\cdot\frac{n}{\hat{E}_{a_i}}=\frac{-n\cdot C_1\cdot\ln(C)}{E_{a_0}\cdot C^n+C_1}
$$

These above relative coefficients are used in the System Identification Method. The sensitivity matrix, change vector, and residual vectors becomes as follows:

$$
\begin{bmatrix}
\dfrac{E_{a_0}\cdot C_1^n}{E_{a_0}\cdot C_1^n+C_1} & \dfrac{E_{a_0}}{E_{a_0}\cdot C_1^n+C_1} & \dfrac{-n\cdot C_1\cdot\ln(C^1)}{E_{a_0}\cdot C_1^n+C_1} \\[3mm]
\dfrac{E_{a_0}\cdot C_2^n}{E_{a_0}\cdot C_2^n+C_1} & \dfrac{E_{a_0}}{E_{a_0}\cdot C_2^n+C_1} & \dfrac{-n\cdot C_1\cdot\ln(C^2)}{E_{a_0}\cdot C_2^n+C_1}
\end{bmatrix}
\times
\begin{bmatrix}
\dfrac{E_{a_0}^{i+1}-E_{a_0}^{i}}{E_{a_0}^{i}} \\[3mm]
\dfrac{C_1^{i+1}-C_1^{i}}{C_1^{i}} \\[3mm]
\dfrac{n^{i+1}-n^{i}}{n^{i}}
\end{bmatrix}
=
\begin{bmatrix}
\dfrac{E_{a_1}-\hat{E}_{a_1}}{\hat{E}_{a_1}} \\[3mm]
\dfrac{E_{a_2}-\hat{E}_{a_2}}{\hat{E}_{a_2}}
\end{bmatrix}
$$

Sensitivity Matrix   Change Vector   Residual Vector

The change vector is previously mentioned in the first model $\alpha=\left[F^T.F\right]^{-1}.F^T.r$.

To determine the optimum values of the parameters (E_{a_0}, C_1, n), a matlab program was developed, following the below flowchart (Figure 4.8).
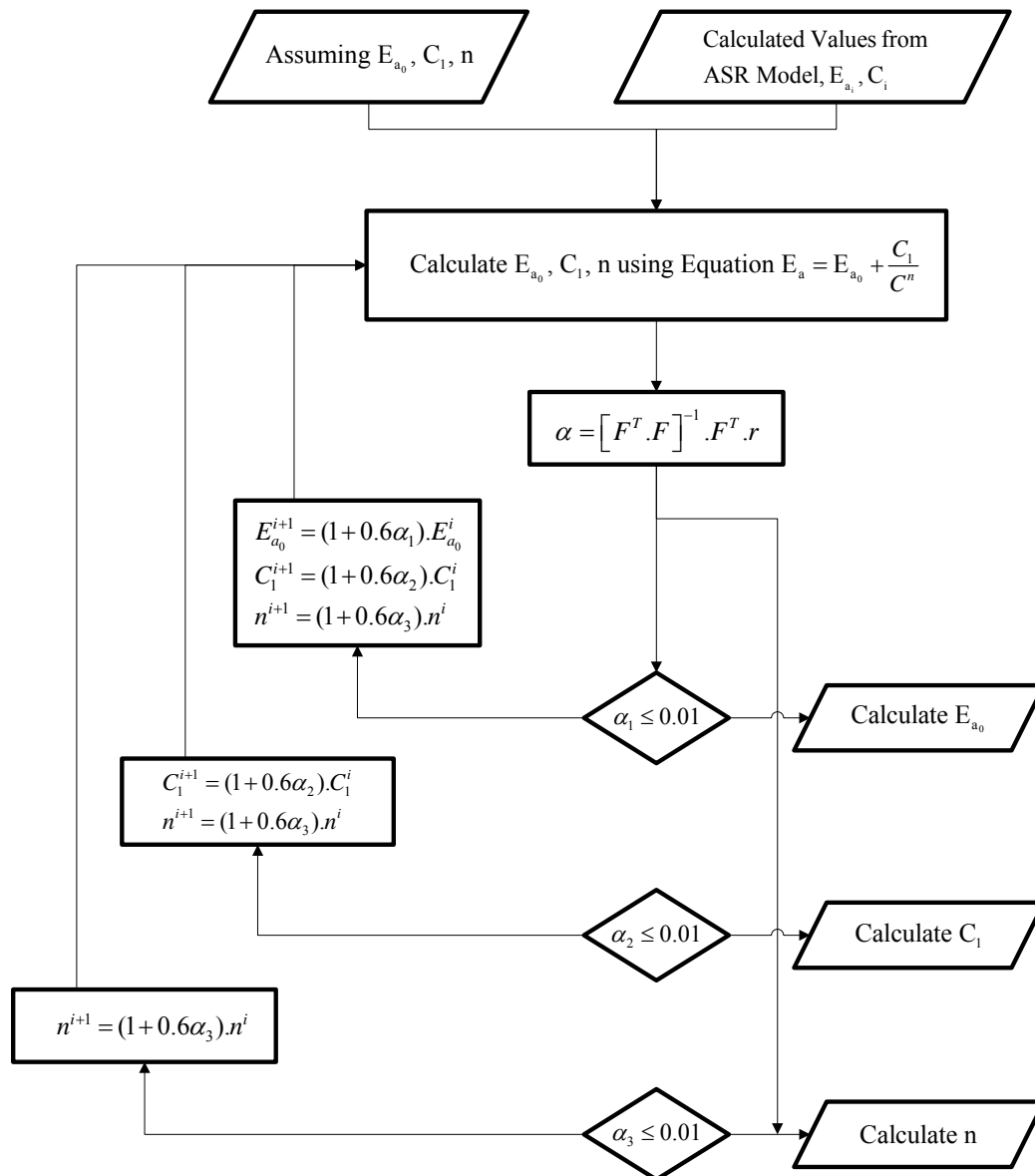
Figure 4.8 Flowchart to Determine the Parameter of the Model (Alkalinity vs. E_a).

Development of a Reaction Signature for Combined Concrete Materials

The ultimate expansion of concrete depends on many factors: a) aggregate reactivity b) alkalinity of the pore solution, water cement ratio, fly ash, etc. The aggregate reactivity is in turn directly related to alkalinity and activation energy. The variable r is introduced and defined as the ratio of the ultimate expansion of concrete to ultimate expansion of

aggregate $(\dfrac{\varepsilon_u}{\varepsilon_a})$. Both ε_u and ε_a are determined, from concrete and aggregate tests using the model proposed in step 1. The minimum value r_{min} can be equal to zero which corresponds to "no cracking in the pavement" and this can be achieved theoretically by using non-reactive aggregate, very low water cement ratio, high percentage of supplementary cementitious materials. On the other side, r_{max}, which corresponds to "complete cracking in the pavement" can be achieved by choosing highly reactive aggregate, high water cement ratio and without using any pozzolanic materials. It should be mentioned here that r is unlikely to exceed 1 since aggregate in concrete is always surrounded partially or totally by the cement paste depending on the porosity of the mixture. Therefore, aggregate in the concrete is always in the restrained stage unlike aggregate tested alone in the dilatometer where expansion can freely occur depending on the amount of gel formed.

Introducing a universal equation connecting the combined effects of concrete materials on ASR has been a dream for decades. The solution to the previous statement is to find the infinitesimal change in the ratio $(\dfrac{\varepsilon_u}{\varepsilon_a})$ under an infinitesimal change in activation energy (E_a), fly ash (f) and water cement ratio (w). The above philosophical idea of relating variables to each other is not new. Juarez-Badillo (1981) used the above principle to determine the general compressibility equations for soils under isotropic stresses, where he related the change in volume of the soil to the change of stress through a non dimensional parameter. In this study, a general relationship was developed to connect the above four parameters (r, E_a, f and w). The connection of those parameters is not direct because each one has a different boundary condition. The domain of r, E_a, f and w are from r_{min} to r_{max} , E_{amin} to ∞, 0 to f_{max}, and w_{min} to w_{max} respectively. Consequently, a set of functions for all parameters has to be found with the boundary conditions (i.e. 0 to ∞) the same for all proposed functions. For example, choose the variable r. The simplest form of f(r) is: $f(r) = \dfrac{1}{r_{max} - r} - \dfrac{1}{r_{max} - r_{min}}$ obtained as shown Figure 4.9. New functions were developed for the other parameters to make the domain and limits for all functions the same (Figure 4.10).
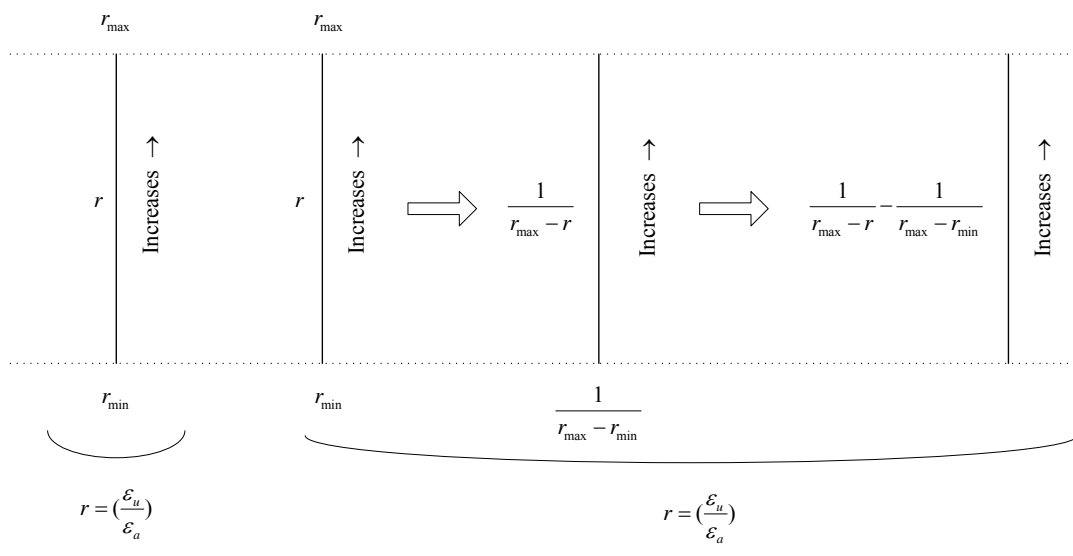
Figure 4.9 Scheme for the Obtention of $f(r) = \dfrac{1}{r_{max} - r} - \dfrac{1}{r_{max} - r_{min}}$.
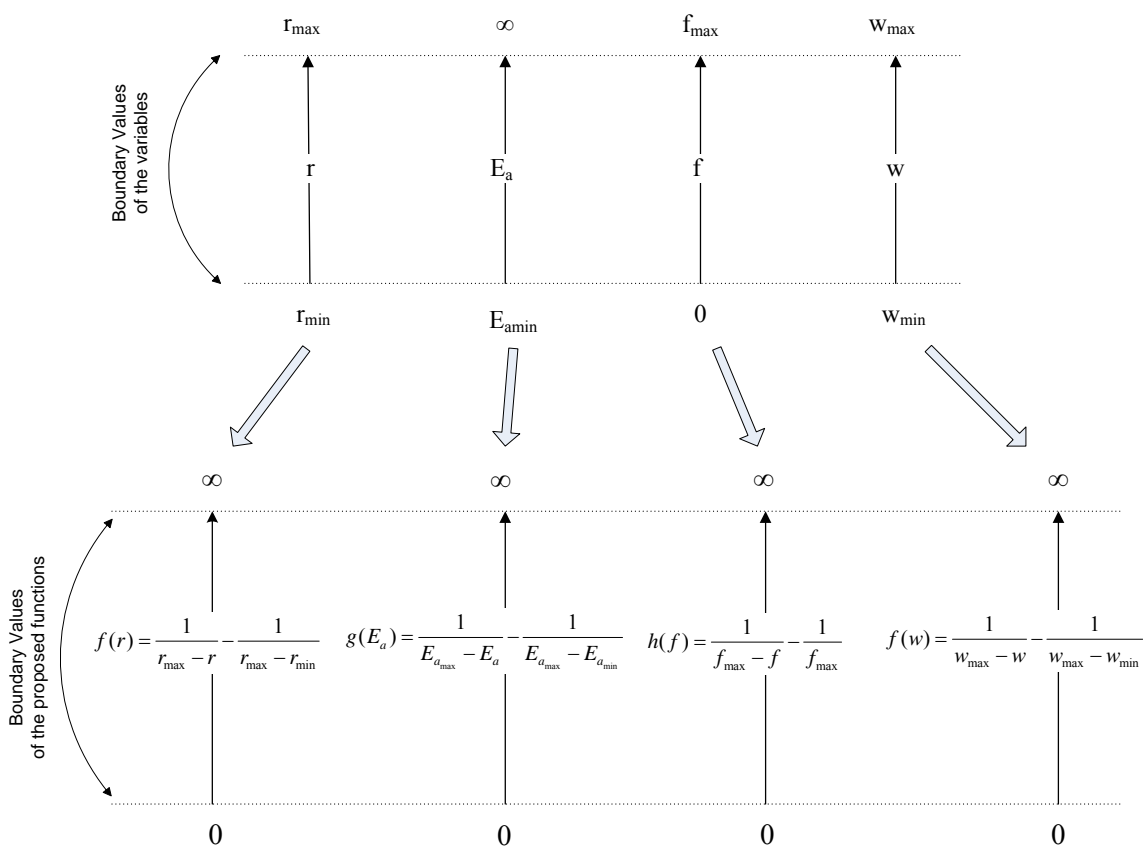
Figure 4.10 Domain of Variables and Their Functions.

Now that all functions are defined with their domain, straight and complete, the mathematical relationship connecting r to E_a, f and w is as follows:

$$\frac{df(r)}{f(r)} = \lambda \frac{dg(E_a)}{g(E_a)} + \beta \frac{dh(f)}{h(f)} + \gamma \frac{df(w)}{f(w)} \tag{4.12}$$

where:

β, λ, γ are non dimensional parameters of proportionality.

Integrating the above equation as follows:

$$\int_{r_1}^{r} \frac{df(r)}{f(r)} = \lambda \int_{E_{a_1}}^{E_a} \frac{dg(E_a)}{g(E_a)} + \beta \int_{f_1}^{f} \frac{dh(f)}{h(f)} + \gamma \int_{w_1}^{w} \frac{df(w)}{f(w)} \tag{4.13}$$

where: r_1, E_{a_1}, f_1, w_1 are the expansion ratio, the aggregate activation energy, the amount of ash and the water cement ratio for a specific concrete mixture.

Expanding (eq. 4.13) yields the following:

$$\ln \left[\frac{\frac{1}{r_{max} - r} - \frac{1}{r_{max} - r_{min}}}{\frac{1}{r_{max} - r_1} - \frac{1}{r_{max} - r_{min}}} \right] = \alpha \ln \left[\frac{E_a - E_{a_{min}}}{E_{a_1} - E_{a_{min}}} \right] + \cdots$$

$$+ \beta \ln \left[\frac{\frac{1}{1-f} - 1}{\frac{1}{1-f_1} - 1} \right] + \gamma \ln \left[\frac{\frac{1}{w_{max} - w} - \frac{1}{w_{max} - w_{min}}}{\frac{1}{w_{max} - w_1} - \frac{1}{w_{max} - w_{min}}} \right] \tag{4.14}$$

Eq 4.14 may be written as:

$$\left[\frac{(r - r_{min})(r_{max} - r_1)}{(r_{max} - r)(r_1 - r_{min})} \right] = \left[\frac{E_a - E_{a_{min}}}{E_{a_1} - E_{a_{min}}} \right]^{\alpha} \cdot \left[\frac{f(1 - f_1)}{(1 - f)f_1} \right]^{\beta} \cdot \left[\frac{(w - w_{min})(w_{max} - w_1)}{(w_{max} - w)(w_1 - w_{min})} \right]^{\gamma} \tag{4.15}$$

After simplifying and arranging the terms, Eq. 4.15 may be written as:

$$r = \frac{r_{min} + r_{max} \left[C \cdot (\frac{f}{f_{max} - f})^{\beta} \cdot (\frac{E_a - E_{a_{min}}}{E_{a_{max}} - E_a})^{\alpha} \cdot (\frac{w - w_{min}}{w_{max} - w})^{\gamma} \right]}{1 + C \cdot (\frac{f}{f_{max} - f})^{\beta} \cdot (\frac{E_a - E_{a_{min}}}{E_{a_{max}} - E_a})^{\alpha} \cdot (\frac{w - w_{min}}{w_{max} - w})^{\gamma})} \tag{4.16}$$

where:

$$r = (\frac{\varepsilon_u}{\varepsilon_a})$$

$\varepsilon_u =$ Ultimate Expansion of Concrete (%)

$\varepsilon_a =$ Ultimate Expansion of Aggregate (%)

$f =$ % of Fly Ash used in the Mixture

$f_{max} =$ Max % of Fly Ash

$E_a =$ Activation Energy $\left[\dfrac{KJ}{mol}\right]$

$E_{a_{min}} =$ Min. Activation Energy $\left[\dfrac{KJ}{mol}\right]$

w = Water cement ratio (w/cm)

$w_{min} =$ Min. w/cm

$w_{max} =$ Max. w/cm

C, β, α, γ = non dimensional parameters of proportionality

Figure 4.11 displays the shape of the generalized concrete model. The parameters of proportionality are determined using the system identification method. Like the previous model, the sensitivity matrix, change vector, and residual vectors are set up as seen below. The algorithm used is shown in Figure 4.12. A matlab routine was developed for that purpose.

$$\begin{bmatrix} \dfrac{\delta r_1}{\delta C} \cdot \dfrac{C}{\hat{r}_1} & \dfrac{\delta r_1}{\delta \beta} \cdot \dfrac{\beta}{\hat{r}_1} & \dfrac{\delta r_1}{\delta \lambda} \cdot \dfrac{\lambda}{\hat{r}_1} & \dfrac{\delta r_1}{\delta \gamma} \cdot \dfrac{\gamma}{\hat{r}_1} \\[2mm] \dfrac{\delta r_2}{\delta C} \cdot \dfrac{C}{\hat{r}_2} & \dfrac{\delta r_2}{\delta \beta} \cdot \dfrac{\beta}{\hat{r}_2} & \dfrac{\delta r_2}{\delta \lambda} \cdot \dfrac{\lambda}{\hat{r}_2} & \dfrac{\delta r_2}{\delta \gamma} \cdot \dfrac{\gamma}{\hat{r}_2} \\[2mm] \dfrac{\delta r_3}{\delta C} \cdot \dfrac{C}{\hat{r}_3} & \dfrac{\delta r_3}{\delta \beta} \cdot \dfrac{\beta}{\hat{r}_3} & \dfrac{\delta r_3}{\delta \lambda} \cdot \dfrac{\lambda}{\hat{r}_3} & \dfrac{\delta r_3}{\delta \gamma} \cdot \dfrac{\gamma}{\hat{r}_3} \end{bmatrix} \times \begin{bmatrix} \dfrac{C^{i+1} - C^i}{C^i} \\[2mm] \dfrac{\beta^{i+1} - \beta^i}{\beta^i} \\[2mm] \dfrac{\lambda^{i+1} - \lambda^i}{\lambda^i} \\[2mm] \dfrac{\gamma^{i+1} - \gamma^i}{\gamma^i} \end{bmatrix} = \begin{bmatrix} \dfrac{r_1 - \hat{r}_1}{\hat{r}_1} \\[2mm] \dfrac{r_2 - \hat{r}_2}{\hat{r}_2} \\[2mm] \dfrac{r_3 - \hat{r}_3}{\hat{r}_3} \end{bmatrix}$$

Sensitivity   Change   Residual

Matrix   Vector   Vector

$$r = \frac{r_{\min} + r_{\max}\left[C.(\frac{f}{f_{\max} - f})^{\beta}.(\frac{E_a - E_{a_{\min}}}{E_{a_{\max}} - E_a})^{\alpha}.(\frac{w - w_{\min}}{w_{\max} - w})^{\gamma}\right]}{1 + C.(\frac{f}{f_{\max} - f})^{\beta}.(\frac{E_a - E_{a_{\min}}}{E_{a_{\max}} - E_a})^{\alpha}.(\frac{w - w_{\min}}{w_{\max} - w})^{\gamma})}$$

$\frac{\varepsilon_u}{\varepsilon_a}$

E_a(Activation Energy)

Figure 4.11 Generalized Concrete Model.

Assuming $C, \beta, \lambda, \gamma$

Calculated value from ASR model $(\frac{\varepsilon_u}{\varepsilon_a})_i$

Calculate $C, \beta, \lambda, \gamma$ using Equation

$$r = \frac{r_{min} + r_{max}\left[C.(\frac{f}{f_{max}-f})^{\beta}.(E_a - E_{a_{min}})^{\lambda}.(\frac{w-w_{min}}{w_{max}-w})^{\gamma}\right]}{1 + C.(\frac{f}{f_{max}-f})^{\beta}.(E_a - E_{a_{min}})^{\lambda}.(\frac{w-w_{min}}{w_{max}-w})^{\gamma})}$$

$$\alpha = \left[F^T.F\right]^{-1}.F^T.r$$

$C^{i+1} = (1+0.6\alpha_1).C^i$
$\beta^{i+1} = (1+0.6\alpha_2).\beta^i$
$\lambda^{i+1} = (1+0.6\alpha_3).\lambda^i$
$\gamma^{i+1} = (1+0.6\alpha_4).\gamma^i$

$\alpha_1 \leq 0.01$ — Calculate C

$\beta^{i+1} = (1+0.6\alpha_2).\beta^i$
$\lambda^{i+1} = (1+0.6\alpha_3).\lambda^i$
$\gamma^{i+1} = (1+0.6\alpha_4).\gamma^i$

$\alpha_2 \leq 0.01$ — Calculate β

$\lambda^{i+1} = (1+0.6\alpha_3).\lambda^i$
$\gamma^{i+1} = (1+0.6\alpha_4).\gamma^i$

$\alpha_3 \leq 0.01$ — Calculate λ
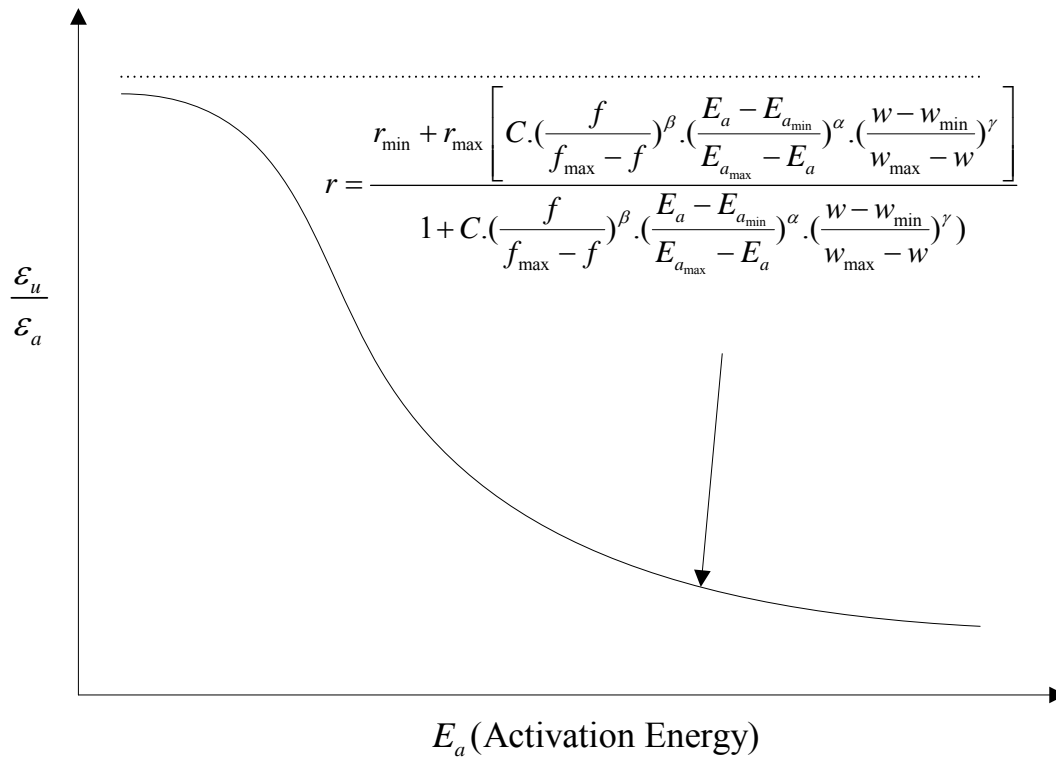
$\gamma^{i+1} = (1+0.6\alpha_4).\gamma^i$

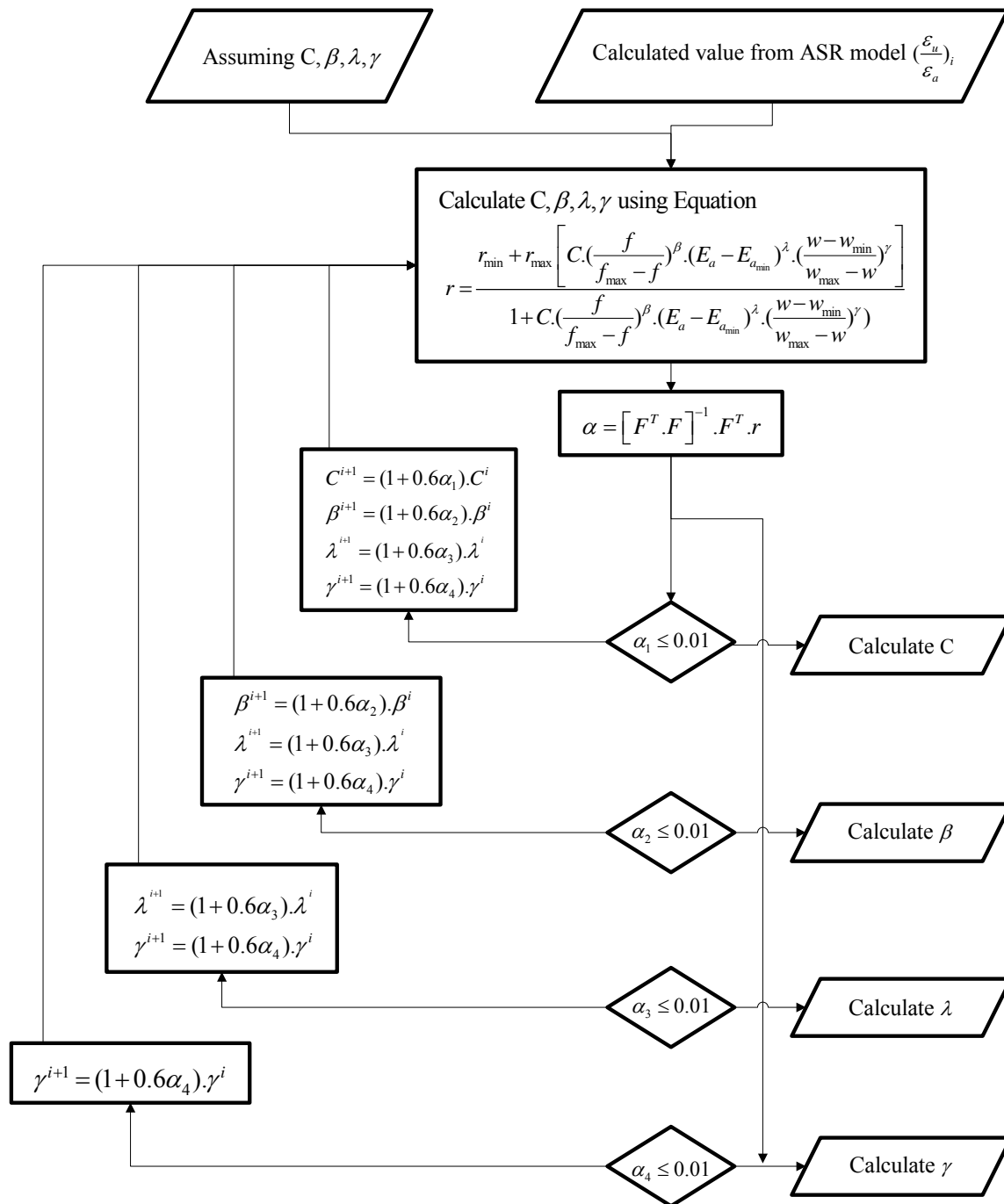$\alpha_4 \leq 0.01$ — Calculate γ

Figure 4.12 Flowchart to Determine the Generalized Concrete Model.

Once the parameters of the generalized concrete model are determined, a design procedure can be outlined leading to the formulation of ASR safe concrete mixtures. To achieve this objective, the following steps should be followed.

a) The concrete and aggregate model and combined together where the x axis represents the activation energy (E_a) for both models as shown in Figure 4.13.

b) The concrete reactivity model leads to the following relationship:

$$(\frac{\varepsilon_u}{\varepsilon_a}) = \text{function } (f, E_a, w) \tag{4.17}$$

where:

f = Fly ash

E_a = Activation energy of aggregate at a specific alkalinity

W = Water cement ratio

For a specific concrete mixture, the amount of fly ash and water cement ratio is known from the design procedure and therefore, those variables are constant in Eq. 4.16 which yields the following:

$$(\frac{\varepsilon_u}{\varepsilon_a}) = \text{function } (f, E_a) \tag{4.18}$$

$$(\frac{\varepsilon_u}{\varepsilon_a}) = \text{function } (E_a, w) \tag{4.19}$$

Each of the above equations leads to the generation of:

i) A set of curves between ($\varepsilon_u / \varepsilon_a$) and E_a for different fly ash content for concrete mixtures with a specific water cement ratio.

ii) A set of curves between ($\varepsilon_u / \varepsilon_a$) and E_a for different water cement ratio for concrete mixtures with a specific fly ash content.

c) The designer will select the appropriate ($\frac{\varepsilon_u}{\varepsilon_a}$) which represents the percentage cracking over the life span of the pavement, the fly ash content and the water cement ratio and based on the aggregate model, he will select the corresponding alkalinity of the mixture. The above outlined procedure is shown in Figure 4.14. The main benefits of the above method is that it allows the user to determine the effect of fly ash and water cement ratio on the without physically conducting the dilatometer test, thus saving invaluable amount of time for the contractor who needs the optimum safe mix as soon as possible.

$$r = \cfrac{r_{min} + r_{max}\left[C.(\cfrac{f}{f_{max}-f})^{\beta}.(\cfrac{E_a-E_{a_{min}}}{E_{a_{max}}-E_a})^{\alpha}.(\cfrac{w-w_{min}}{w_{max}-w})^{\gamma}\right]}{1+C.(\cfrac{f}{f_{max}-f})^{\beta}.(\cfrac{E_a-E_{a_{min}}}{E_{a_{max}}-E_a})^{\alpha}.(\cfrac{w-w_{min}}{w_{max}-w})^{\gamma})}$$

Concrete Reactivity

Aggregate Reactivity

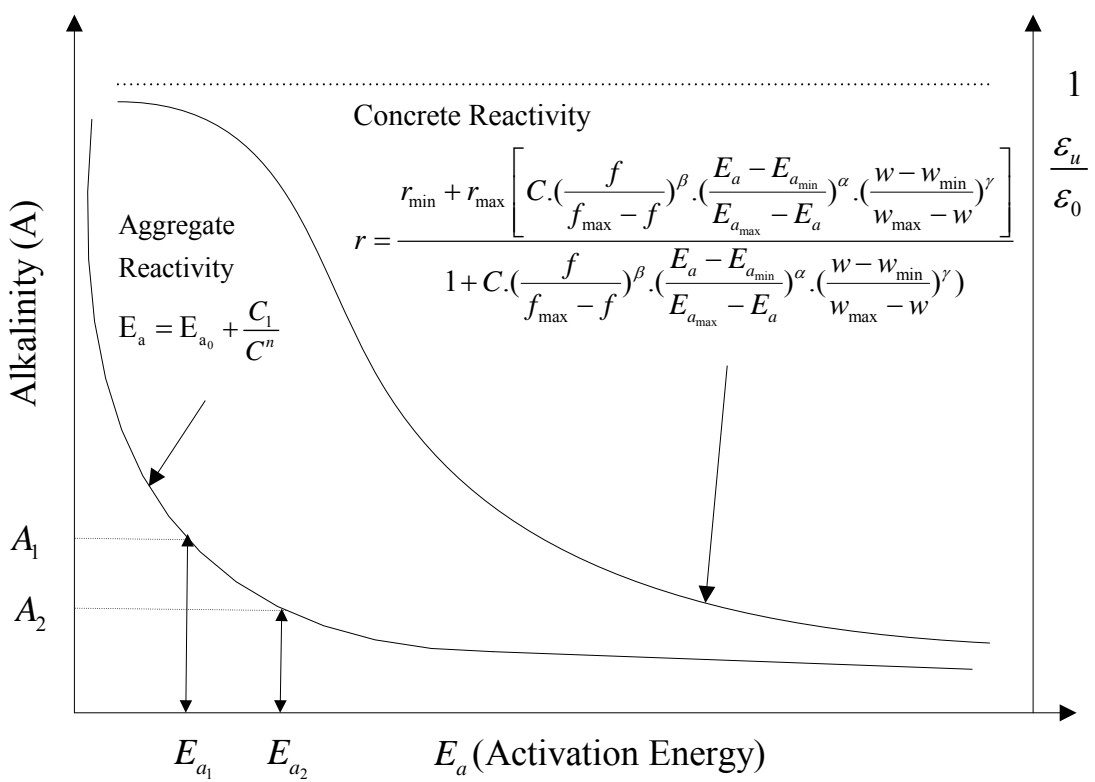$$E_a = E_{a_0} + \frac{C_1}{C^n}$$

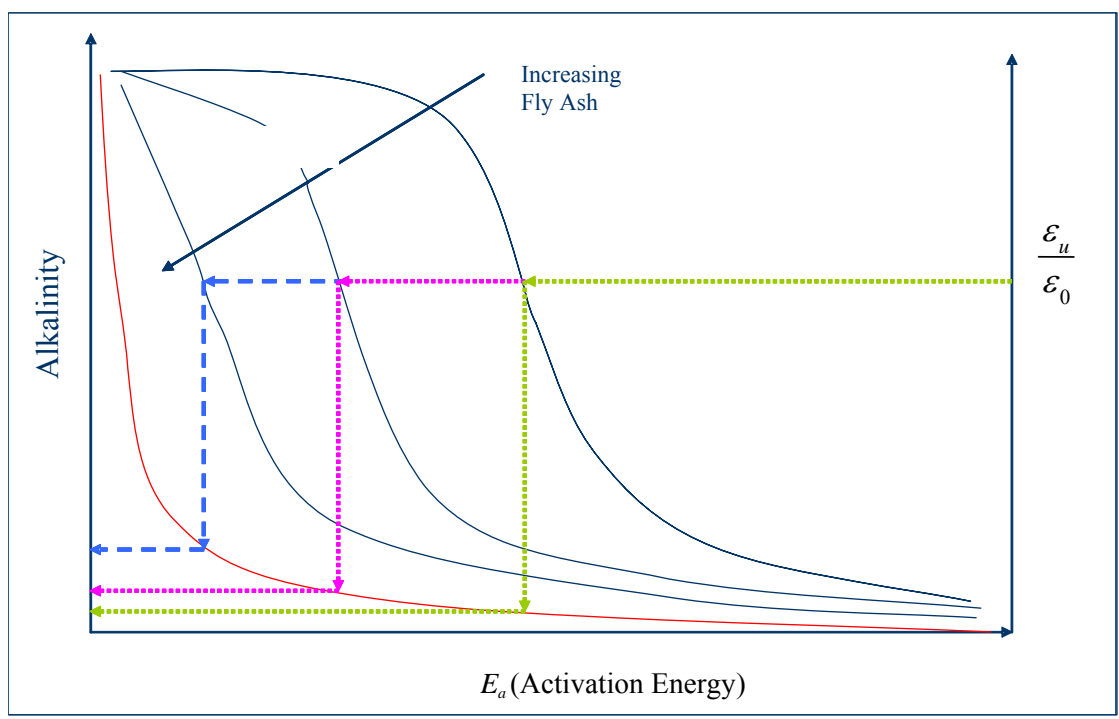Figure 4.13 Combined Concrete and Aggregate Model.

Figure 4.14 Design Procedure (w = constant).

CHAPTER V

**DETERMINATION OF AGGREGATE ASR MATERIALS PROPERTIES**

The interpretation and analysis of the four aggregates conducted in this research study are presented in this chapter. This chapter begins by presenting the ASR time-expansion data for the rocks at different temperature and alkalinities, followed by a discussion of the effect of test conditions (calcium hydroxide, temperature and alkalinity) on the main ASR materials properties. Using the Arrhenius equation, the aggregate activation energy was determined and the aggregates ranking based on their reactivity was presented. Results of the chemistry of the test solution before and after each test are included in the following section. To check the reliability of the test protocol and procedure presented in Chapter IV, an intra and inter-laboratory comparisons between Texas A&M University (TAMU) and University of New Hampshire (UNH) was conducted and results were presented in the last section of this chapter.
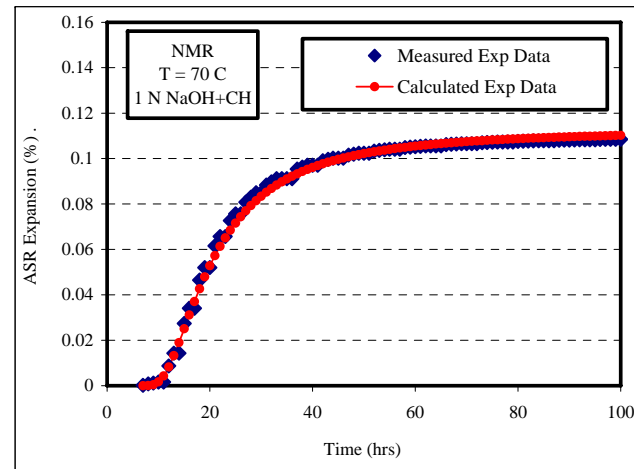
Expansion Characteristics

This section presents the generated ASR time expansion data using the dilatometer for New Mexico Rhyolite, Spratt Limestone, Platte River Gravel and Sudbury Gravel.

New Mexico Rhyolite (NMR)

For the NMR aggregate, the tests were conducted at three different alkalinities (1 NaOH + CH, 0.5 NaOH + CH, and 0.25 NaOH + CH) to illustrate the effect of alkalinity on ASR expansion. For each alkalinity, three tests were performed at three different temperatures (60^0C, 70^0C and 80^0C) to determine the rate constant and consequently the reactivity of the rock. The time expansion data of NMR are shown in Figures 5.1, 5.2 and 5.3. Also displayed in the plots, are the calculated volumetric ASR expansions using the model proposed in Chapter IV. As it can be seen from the plots, the model fit to the measured data is very promising and the difference between the measured and the predicted expansion is negligible, demonstrating the accuracy of the proposed model.
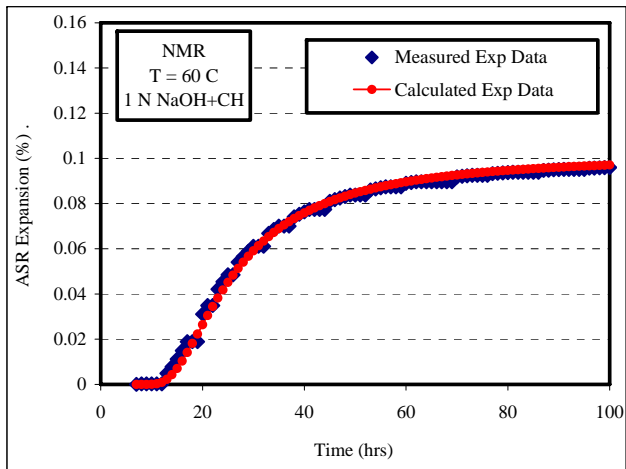
(a) NMR expansion at 60 ^{0}C

(b) NMR expansion at 70 ^{0}C
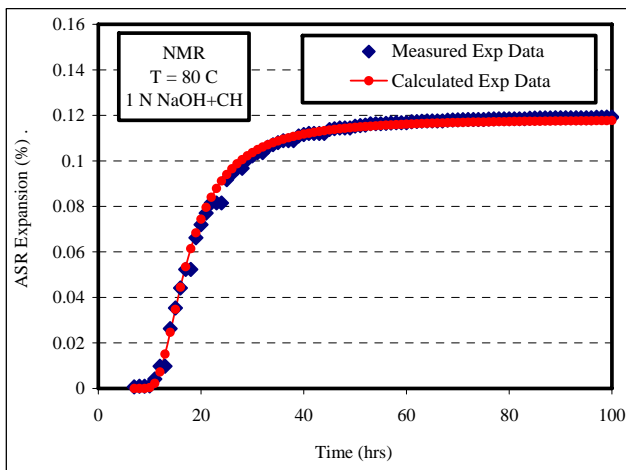
(c) NMR expansion at 80 ^{0}C

(d) Determination of activation energy

Figure 5.1 NMR Characteristics (1N NaOH + CH).

(a) NMR expansion at 60 ^{0}C

(b) NMR expansion at 70 ^{0}C

(c) NMR expansion at 80 ^{0}C

(d) Determination of activation energy

Figure 5.2 NMR Characteristics (0.5 N NaOH + CH).

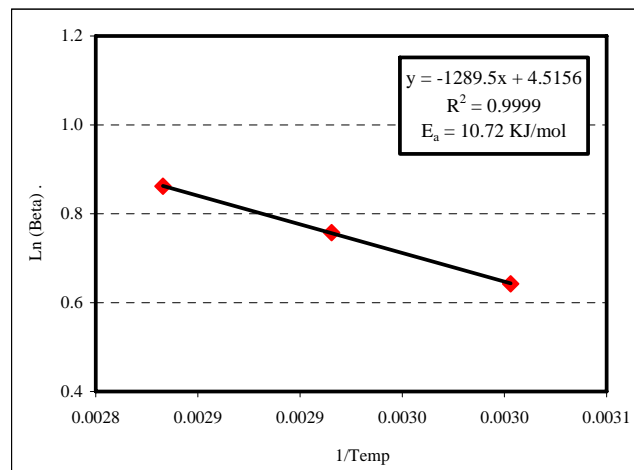(a) NMR expansion at 60 ^{0}C

(b) NMR expansion at 70 ^{0}C
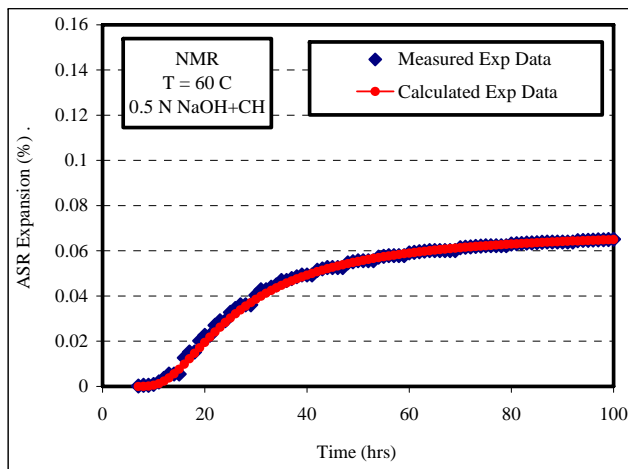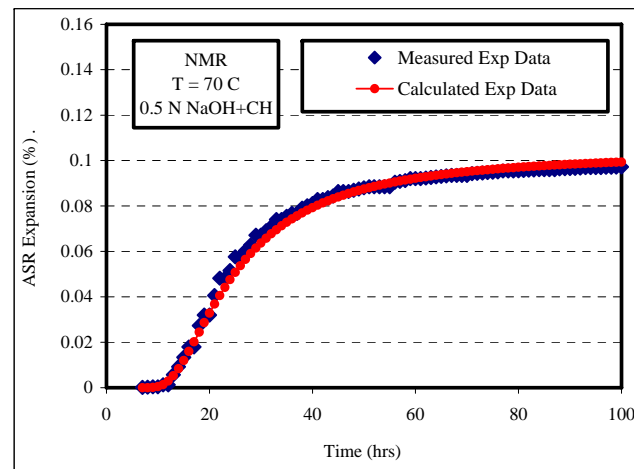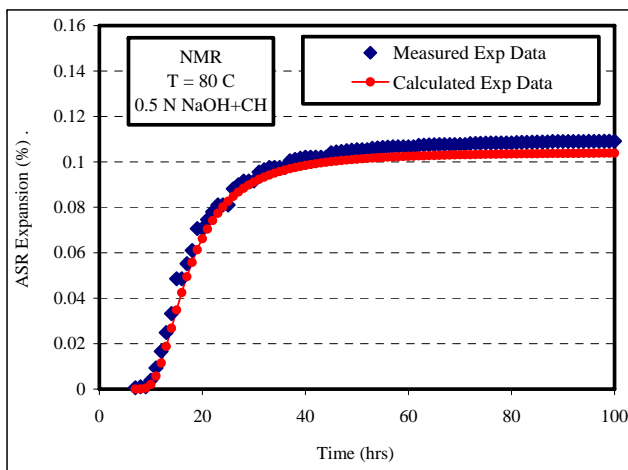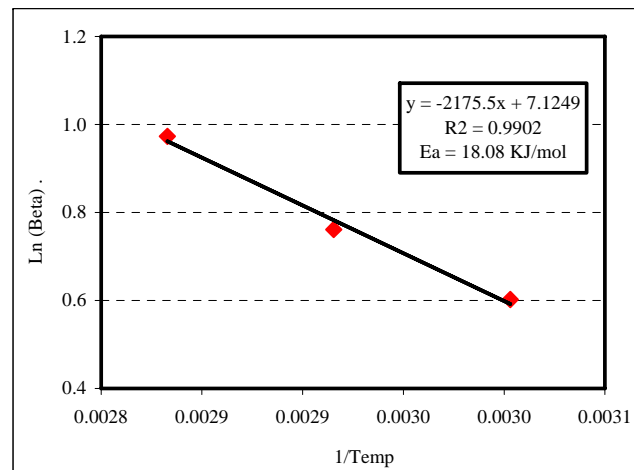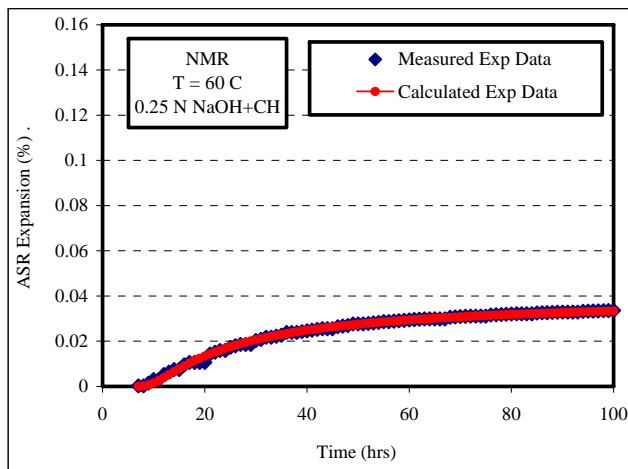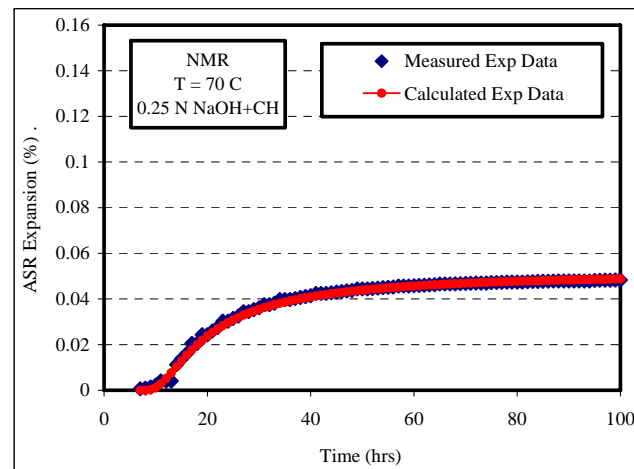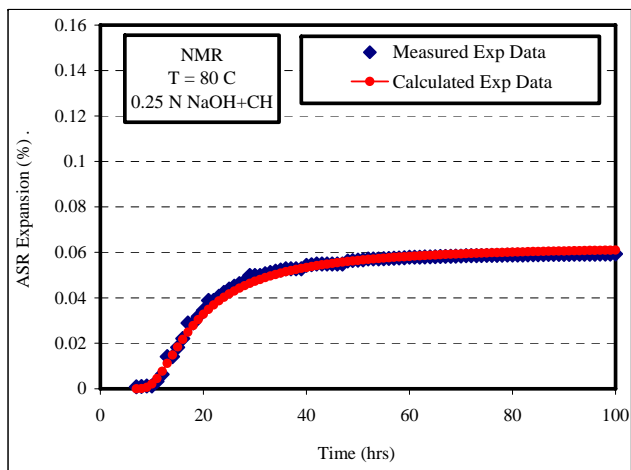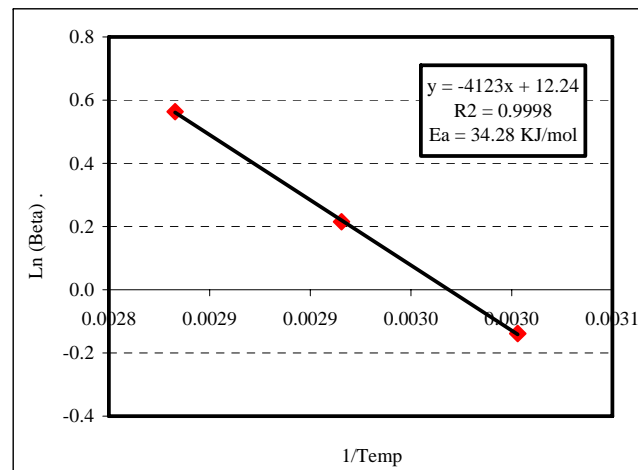

(c) NMR expansion at 80 ^{0}C

(d) Determination of activation energy

Figure 5.3 NMR Characteristics (0.25N NaOH + CH).

As shown in Figures 5.1 through 5.3, all plots show similar characteristic patterns. Almost no expansion was measured in the initial hours. This was followed by a rapid increase in volume expansion up to 60-80 hrs. Then the expansion was stabilized around the 90-100 hrs. For example, for NMR tested in 1 NaOH + CH at 80C, the expansion was negligible in the first 5-7 hrs, followed by a sharp increase in the expansion between 10-50 hrs, then a mild increase was noticed after that where expansion reached the 0.12% level at the 100 hrs. This increase in volumetric expansion with time is due to the following set of reactions. At the beginning of the test, some silanol bonds are already existent on the surface of hydrous NMR aggregate. As hydroxyl ions coming from the NaOH solutions attack the surface of the rock, an acid-base reaction occurs resulting in the release of one molecule of water and the negatively charged Si-O⁻. As the above reaction progresses, the silixane bonds are also attacked by hydroxyl ions. The output of the previous reactions is the dissolution of the silica, creating a negative charge on the surface of the aggregate. Since the whole system needs to be in equilibrium all the time, positive cations are attracted from the surrounding (sodium ions coming from the NaOH solution) forming the gel around the aggregate. When the latter absorbs water, the resultant is a volume greater then the original one. Consequently, expansion occurs and it is this expansion that was recorded by the data acquisition system during the dilatometer test.

The dissolution of silica depends on many parameters: a) temperature, b) alkalinity and c) the silica inside the aggregate whether it is amorphous or well crystallized. It should be mentioned here that the reactive component in NMR aggregate is the volcanic glassy material (amorphous). To illustrate the effect of both temperature and alkalinity on NMR ASR expansion, the main parameters of the proposed model in Chapter IV were determined using the system identification procedure.

$$\frac{1}{\varepsilon} = \frac{1}{\varepsilon_0}.e^{(\frac{\rho}{t-t_0})^{\beta}}$$

The results are shown in Table 5.1. The fourth, fifth, sixth and seventh column show the ultimate expansion ε_0 (%), the time scale parameter ρ, the theoretical initial time t_0 and the rate constant β respectively. As shown from the table, the effect of test solution

alkalinity is evident on the ultimate expansion of NMR; e.g. at 60^0C, the ε_0 (%) increases from 0.0418% at 0.25N + CH to 0.0695% at 0.5N + CH and then jumps to 0.1030% at 1N + CH. This increase in volumetric expansion is simple to understand. In fact, the more alkaline the solution, the more the hydroxyl ions becomes available; i.e. 1N + CH contain almost double the amount of hydroxyl ions than the 0.5N + CH solution. and as more OH$^-$ are available, the reaction sites around the aggregates increase leading to a quicker chemical reaction and this in turn leads to the formation to a large quantity of gel, and thus higher expansion.

The effect of temperature on ASR characteristics is very important to observe. As shown from Table 5.1, as temperature increases, the ultimate expansion increases; i.e. for NMR tested at 0.5N+CH, the ε_0 increase from 0.0695% at 60^0C to 0.1070% at 80^0C. Same deduction can be made for other tests conducted at different alkalinities. This previous finding leaves no choice other than to conclude with confidence that ASR is a thermally activated process. This means that for ASR to go forward, the whole system has to overcome an energy barrier. Increasing the temperature will provide the energy necessary for the chemical reaction to occur. As a result, the rate of reaction as well as the rate constant will increase with temperature. Results in Table 5.1 are consistent with the findings. For example, for NMR tested at 0.5N+CH, the rate constants β are 0.87, 1.23 and 1.75 for T = 60^0C, 70^0C and 80^0C.

One of the objectives of this study is to rank the different type of aggregates based on their reactivity. Shon (2008) introduced the concept of activation energy (E_a) for aggregate as a single parameter. E_a will be determined using the same concept and based on the new proposed kinetic model in Chapter IV. Since ASR was shown above to follow a "Thermally activated process", the Arrhenius equation is used to determine the E_a of the rock. The E_a was determined from the slope of the plot of Ln (β) versus 1/T. the results are displayed in Table 5.1 (eighth column) and Figure 5.1.d, 5.2.d and 5.3.d. As shown from the three plots, the coefficient of determination R^2 is around 0.99 for tests conducted at different alkalinities, illustrating the dependence of the rate constant β on temperature. The E_a values for NMR aggregate were 34.28, 18.09 and 10.72 (KJ/mol) for tests performed at 0.25N+CH, 0.5N+CH, and 1N+CH. These results indicate that the

activation energy of aggregate is a function of alkalinity. As alkalinity of the solution increase, the E_a decreases. This deduction is consistent with the activation energy of ASR as the energy necessary to initiate this reaction. As a result, aggregate tests conducted at higher alkalinity (i.e. 1N+CH) needs less energy (10.72 KJ/mol) to initiate the ASR reaction, since there is an abundant amount of hydroxyl ions in the solution. On the other side, at lower alkalinity solution (i.e. 0.25N+CH) higher energy is required for the reaction to proceed (i.e. 34.28 KJ/mol). From a practical point of view, it is would be very interesting to determine the minimum activation energy required to initiate this reaction as well as its corresponding level of alkalinity. This last point will be elaborated in detail in the first section of Chapter VI.

Table 5.1 New Mexico Rhyolite Main Parameters.

Aggregate type	Alkalinity (NaOH)	Temp (^{0}C)	ASR aggregate parameters				E_a (KJ/mol)
			ε_0 (%)	ρ	t_0	β	
New Mexico Rhyolite	0.25N + CH	60	0.0418	16.8	5.43	0.87	34.28
		70	0.0537	12.6	5.40	1.23	
		80	0.0625	12.9	3.52	1.75	
	0.5N + CH	60	0.0695	21.8	0.52	1.82	18.09
		70	0.1023	20.5	0.68	2.14	
		80	0.1070	13.3	1.85	2.64	
	1N + CH	60	0.1030	20.1	3.04	1.90	10.72
		70	0.1134	16.4	1.65	2.13	
		80	0.1190	11.5	4.41	2.36	

* CH = calcium hydroxide

Spratt Limestone (SL)

For the SL aggregate, the tests were conducted at three different temperatures (60^0C, 70^0C and 80^0C) in 1 N sodium hydroxide solution. It should be mentioned here that 3 to 4% of microscopic chalcedony and black chert imbedded within the rock matrix are the reactive component of the SL (Rogers 1999). Figure 5.4 shows the time expansion history up to 100 hrs for S.L. As shown in the figure, the plots at the three temperatures display similar trend. In the first 10 hr of testing, negligible expansion was recorded. This was followed by an irregular increase up to the 80 hrs. The readings then stabilize around 90-100 hrs. This non uniform increase in the SL expansion maybe possibly due to non-homogenous distribution of the reactive component in the SL. Also superimposed on the plots in Figure 5.4, are the calculated ASR expansions using the kinetic model. It can be seen from the plots that the model fit to the measured data is pretty good.

ASR characteristics are presented in Table 5.2. The effect of temperature is very evident on the theoretical initial time of expansion t_0. As the temperature of the test solutions increase, t_0 decreases; i.e. for SL conducted at 60^0C, t_0 was 7.16 hrs, while t_0 was equal to 3.12 hrs at 80^0C. This can be explained from a kinetic point of view. As the temperature of the system (i.e. dilatometer) increases, the amount of additional energy needed to initiate ASR decreases because the energy barrier that the system has to overcome is much smaller at a higher temperature and consequently the time that it takes for ASR to initiate will be smaller. On the other side, when the temperature is low, the energy barrier is higher and therefore more time is needed for ASR to proceed and therefore the theoretical initial time of expansion is higher. The results obtained are consistent with the above analysis.

The consequence of increasing the temperature can also be seen on the rate constant (β). As shown from Table 5.2, the relationship between β and temperature is proportional. At 80^0C, β was 2.92 while at 60^0C, it was 0.92. The results are logical with our previous conclusion that ASR is a "Thermally Activated Process". The Arrhenius equation was used to calculate the activation energy. From the relationship between log (β) and 1/T, the E_a was calculated to be 53.46 KJ/mol. The high value of the coefficient of determination ($R^2 = 93.5\%$) indicates the strength and the almost linear relationship between the two variables: log of the rate constant and 1/T.

The significance of the above method is not limited to calculating the E_a. Since the E_a will be ultimately a material property for an aggregate and by knowing the rate constant at a specific temperature, the rate constant and the time to initiation at any other temperature can be determined using the Arrhenius equation. This is extremely important as the aggregate in concrete structures will be subjected probably to ambient temperature. The temperature selection of 60^0C, 70^0C and 80^0C were only chosen to increase the rate of reaction in order to measure significant ASR expansion within a short period of time. Consequently, the rate constant at ambient temperature can be calculated and the theoretical initial time of expansion in the field can be determined.

Table 5.2 Spratt Limestone Characteristics.

Aggregate type	Alkalinity (NaOH)	Temp (^0C)	ASR aggregate parameters				E_a (KJ/mol)
			ε_0 (%)	ρ	t_0	β	
Spratt Limestone	1 N	60	0.033	51.5	7.16	0.98	53.46
		70	0.032	31.8	4.21	2.21	
		80	0.039	45.2	3.12	2.92	
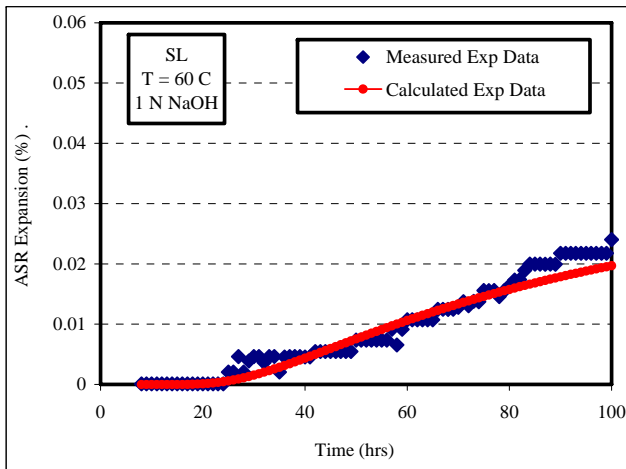
(a) SL expansion at 60 ^{0}C
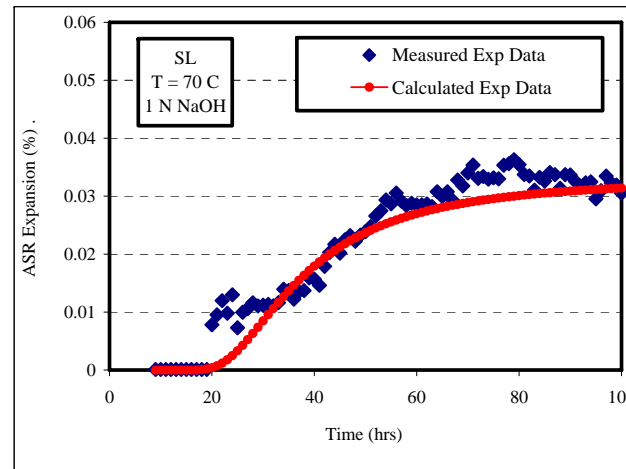
(b) SL expansion at 70 ^{0}C
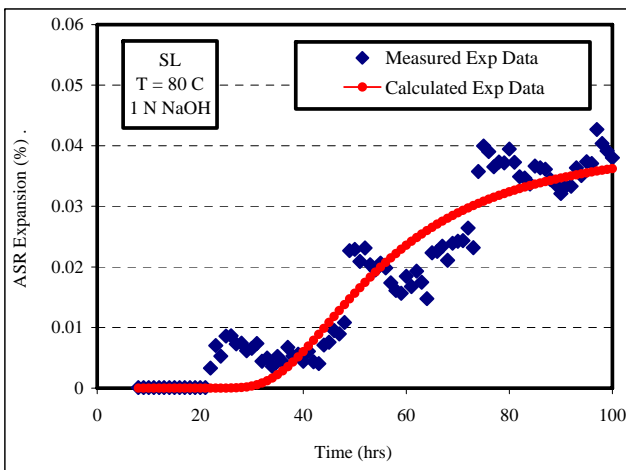
(c) SL expansion at 80 ^{0}C
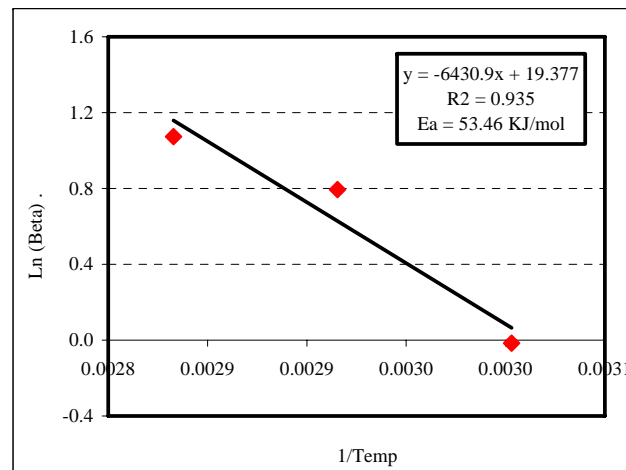
(d) Determination of activation energy

Figure 5.4 Spratt Limestone (SL) (1 NaOH).

Platte River Gravel (PRG)

For PRG aggregate, the tests were conducted at four different alkalinities: 1 N NaOH + CH, 1 N NaOH, 0.5 N NaOH + CH and 0.5 N NaOH. For each alkalinity, three tests were conducted to determine the reactivity of the aggregate. Expansion data were collected to the 100 hrs. One has to mention here that strained quartz is the reactive component of PRG. Also, it should be stated here that the addition of calcium hydroxide (CH) to the alkaline solution was to simulate the pore solution of the concrete and to study the effect (if any) of CH on the ASR expansion since the role of CH is a point of controversy among researchers in the field.

Figures 5.5, 5.6, 5.7 and 5.8 show the measured volumetric expansion of Platte river gravel. It can be seen that although all plots display similar behavior, the ultimate measured expansion is different depending on the alkalinity of the solution. The % expansion increases with an increase of the alkalinity of the test solutions; i.e. for PRG tested at 80^0C, the % expansion was 0.05% and 0.042% for experiments conducted at 1 N NaOH and 0.5 NaOH respectively. This can be explained as follows: as more hydroxyl ions become available, the sooner the reaction will take place and therefore more gel will be formed and thus more expansion is measured. As a result, pavement structures subjected to high alkali environment will exhibit earlier expansion and consequently, earlier cracking can be expected as opposed to other concrete structures subjected to mild alkali environment. Another important conclusion can be made. The % ASR expansion was recorded and measured without the presence of calcium hydroxide. This indicates that the ASR can be expansive without the existence of CH. It would be interesting to determine the contribution of CH on ASR expansion.
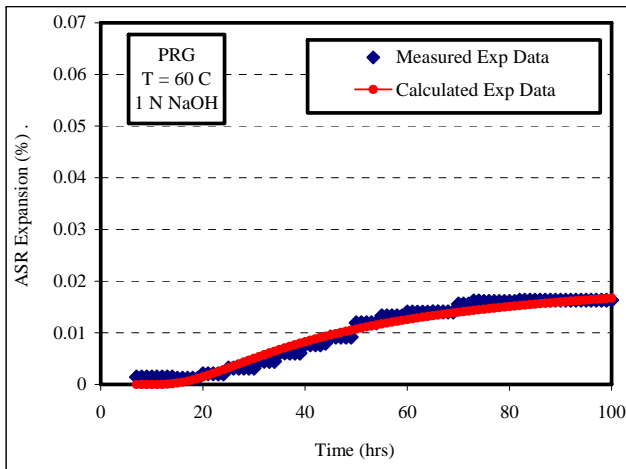
(a) PRG expansion at 60 ^{0}C
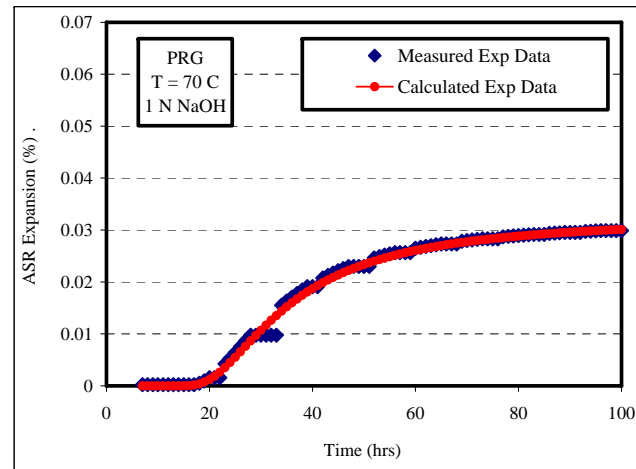
(b) PRG expansion at 70 ^{0}C
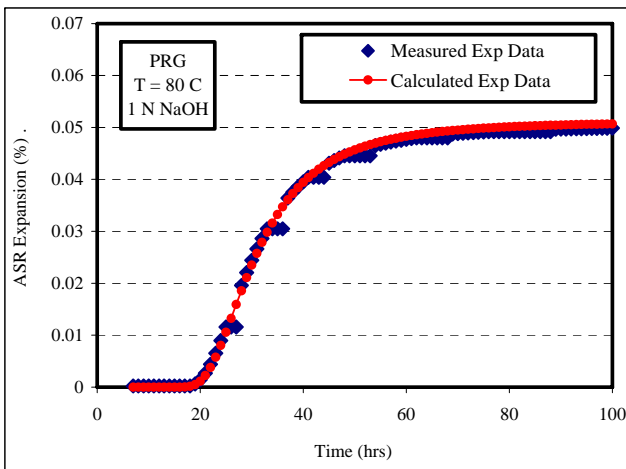
(c) PRG expansion at 80 ^{0}C
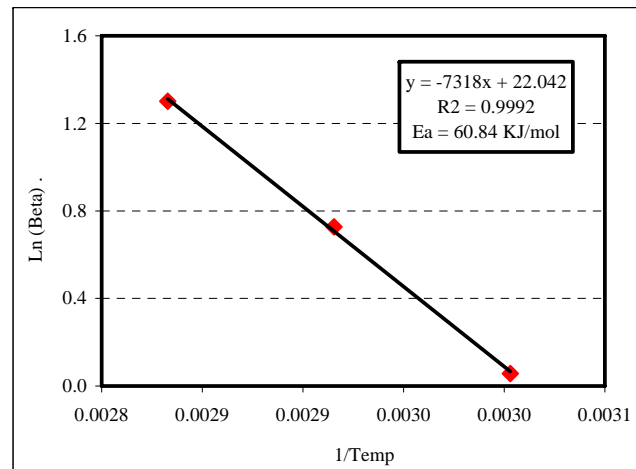
(d) Determination of activation energy

Figure 5.5 Platte River Gravel (PRG) Characteristics (1 NaOH).

(a) PRG expansion at 60 ^{0}C

(b) PRG expansion at 70 ^{0}C

(c) PRG expansion at 80 ^{0}C

(d) Determination of activation energy

Figure 5.6 Platte River Gravel (PRG) Characteristics (0.5 NaOH).

(a) PRG expansion at 60 ^{0}C

(b) PRG expansion at 70 ^{0}C
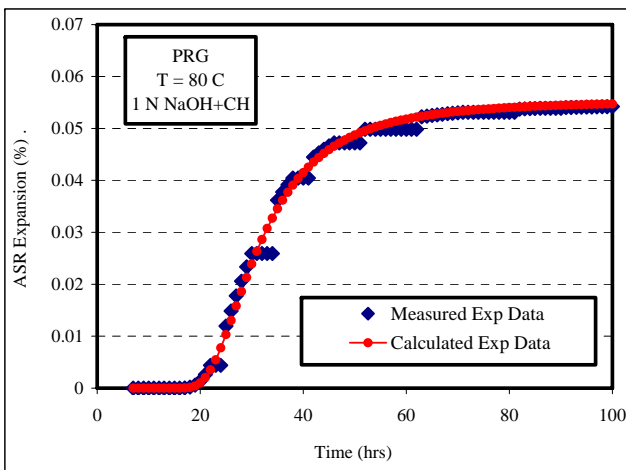
(c) PRG expansion at 80 ^{0}C
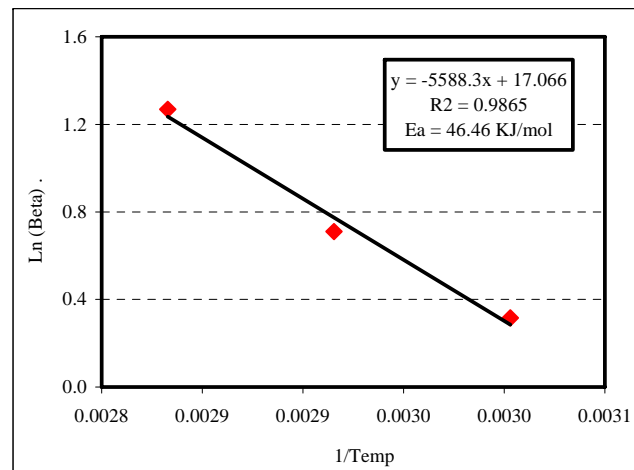
(d) Determination of activation energy

Figure 5.7 Platte River Gravel (PRG) Characteristics (1 NaOH + CH).
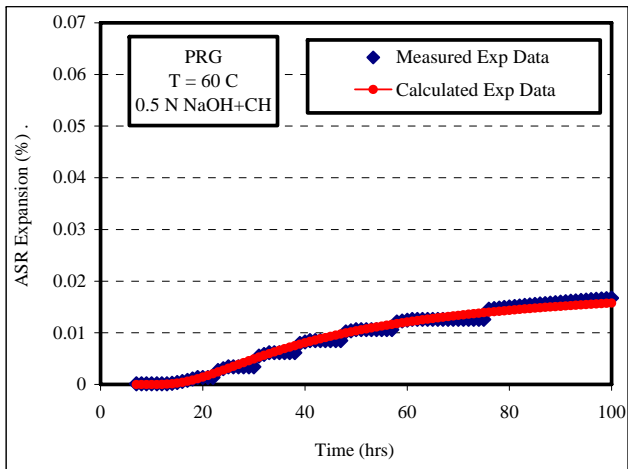
(a) PRG expansion at 60 ^{0}C
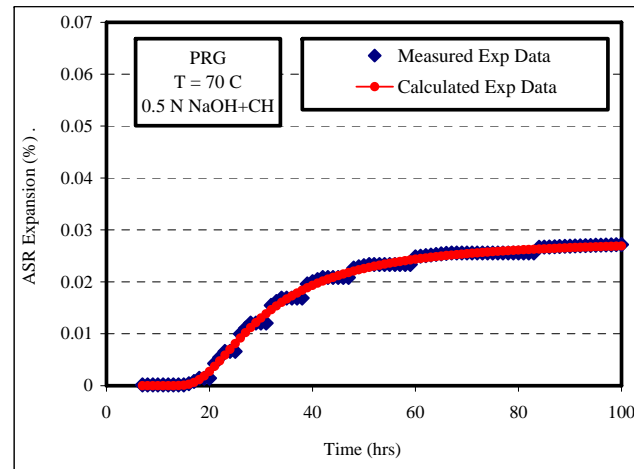
(b) PRG expansion at 70 ^{0}C
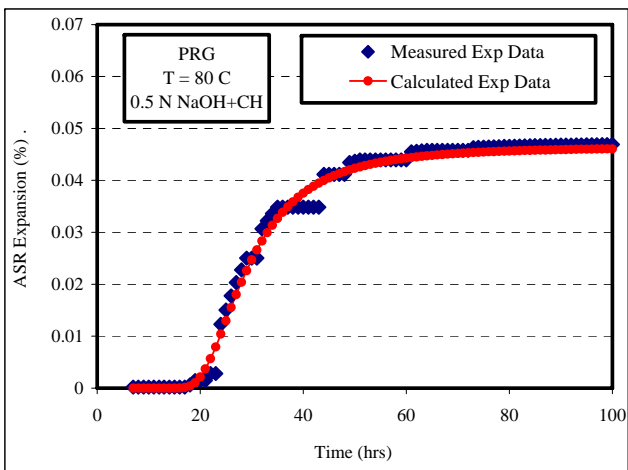
(c) NMR expansion at 80 ^{0}C
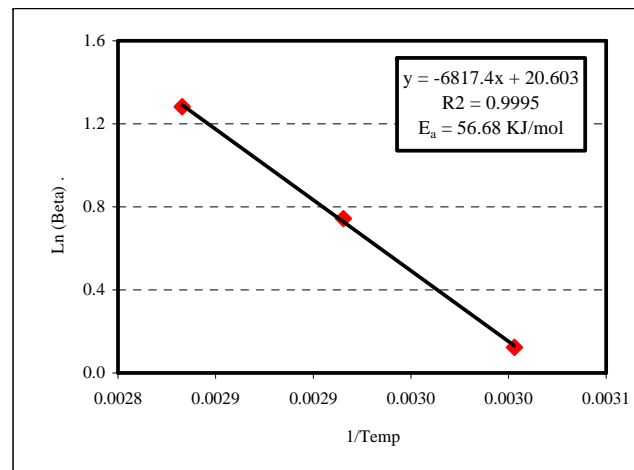
(d) Determination of activation energy

Figure 5.8 Platte River Gravel (PRG) Characteristics (0.5 NaOH + CH).

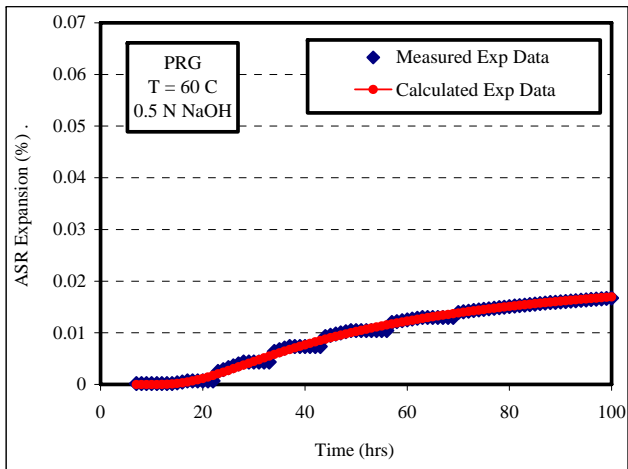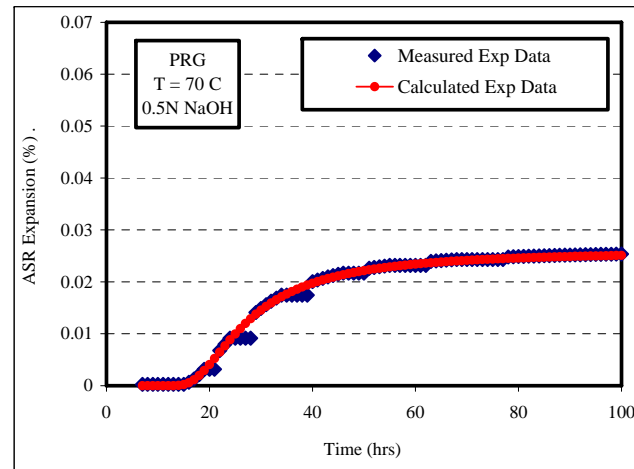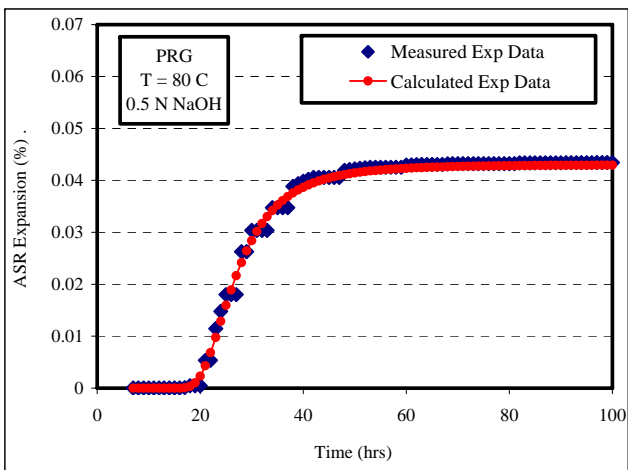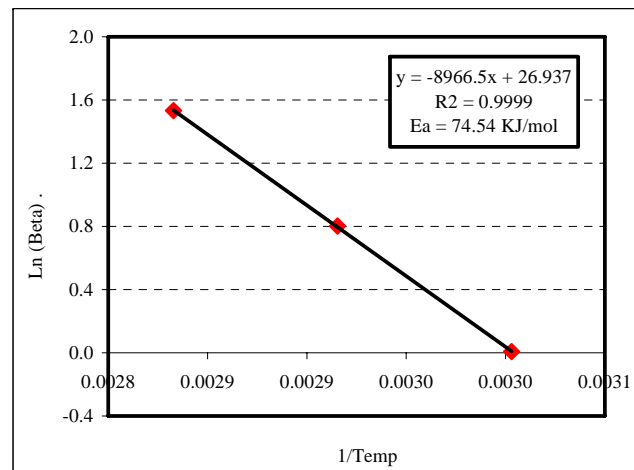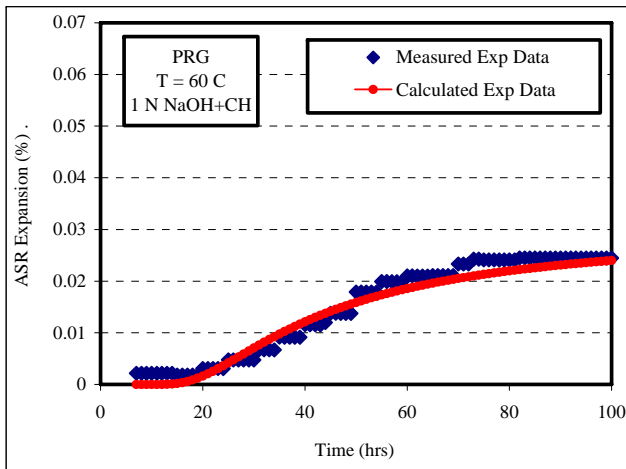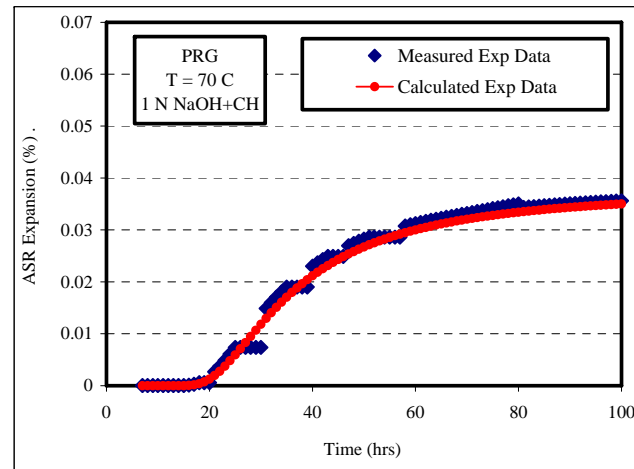To determine PRG characteristics, the measured expansion data were fitted using the proposed kinetic model mentioned previously and the calculated expansion plots were superimposed on the measured data in Figures 5.5, 5.6, 5.7 and 5.8. The main parameters of PRG gravel are presented in Table 5.3. Important conclusion can be made by looking at the results. It can be seen that the presence of calcium hydroxide enhances ASR expansion; i.e. for tests conducted at 80^0C, the ultimate expansion (ε_0) at 1 N NaOH + CH was 0.053% while it was only 0.049% at 1N NaOH. This is equivalent to 8.16% increase in expansion. The same comparison can also be made for runs at 0.5 N NaOH + CH and 0.5N NaOH. At 0.5 N NaOH + CH, the ε_0 was 0.053% while at 0.5 N NaOH, the ε_0 was 0.049%. This corresponds to a 9.75% growth. Therefore, from the previous results, it can be deduced that the presence of CH increases ASR expansion slightly, but is not major a factor or a prerequisite to initiate ASR as expansion was recorded without CH in the solution.

The importance of temperature as an accelerator of ASR is also illustrated in Table 5.3. It can be seen as that the ultimate expansion increases when the temperature goes up from 60^0C to 70^0C and then from 70^0C to 80^0C. This is attributed to the fact the speed of the reaction increases with temperature leading to the formation to larger amount of reaction products (gel) around the rock. This last deduction is consistent with the results of the rate constant (β) calculated. The ε_0 (%) and β have a proportional relationship with temperature. As temperature decreases, both parameters (ε_0) and β go down as well; i.e. for PRG at 0.5 N NaOH, the ε_0 (%) and β were 0.041% and 4.63 at 80C while at 60^0C, they were equal to 0.027% and 1. This indicates that any change in temperature affects all of the parameters of the kinetic model, mainly the rate constant since ASR is first of all a chemical reaction. Accordingly, a set of relationships can be developed for ε_0 (%), ρ, t_0 as function of β and the latter can be calculated at any other temperature using the Arrhenius equation.

To determine the E_a of PRG, the rate constant β was plotted against (1/T), and best-fit was performed using linear regression analysis (Figures 5.5.d, 5.6.d, 5.7.d and 5.8.d). The coefficient of determination R^2 was 0.99 (i.e. the three points almost lay on a straight line) for all cases indicating a strong correlation between the variables. The E_a

was determined by multiplying the slope of the regression line by the gas constant. As shown from Table 5.3, the E_a for PRG was equal to 60.84, 74.55, 46.46, 56.68 KJ/mol for tests conducted at 1N, 0.5N, 1N + CH and 0.5N + CH respectively. It can be seen from the results that the E_a decreases as the alkalinity of solution increases. This deduction is made for both set of tests conducted with and without CH. The results look logical and can be explained as follows: less energy (46.46 KJ/mol) is required at higher alkalinity (1N+CH) to overcome the barrier to initiate ASR. On the other side, at lower alkalinity (0.5N+CH), the system needs more energy to overcome the barrier and thus the E_a is higher (56.68 kJ/mol).

The results also indicate that there is a possibility that a relationship exists between the alkalinity of test solution and E_a of the aggregate. Also, it would be of great interest for the pavement engineer to determine the alkalinity and its corresponding E_a to initiate ASR as this will help in developing concrete mixtures highly resistant to ASR. The above mentioned points will be discussed in detail in the following chapter (Chapter VI).

Table 5.3 Platte River Gravel Characteristics.

Aggregate type	Alkalinity (NaOH)	Temp (^{0}C)	ASR aggregate parameters				E_a (KJ/mol)
			ε_0 (%)	ρ	t_0	β	
Platt River Gravel	1N	60	0.024	37.6	5.33	1.05	60.84
		70	0.031	24.2	5.88	2.06	
		80	0.049	25.4	2.01	3.67	
	0.5N	60	0.027	45.1	5.21	1.00	74.55
		70	0.024	18.0	5.85	2.23	
		80	0.041	23.5	1.13	4.63	
	1N + CH	60	0.030	33.2	4.30	1.37	46.46
		70	0.036	25.0	5.91	2.03	
		80	0.053	25.9	2.20	3.55	
	0.5N + CH	60	0.022	35.8	5.02	1.13	56.68
		70	0.027	20.4	5.86	2.10	
		80	0.045	24.0	2.16	3.60	

* CH = calcium hydroxide

Sudbury Gravel (SuG)

For the SuG aggregate, the major reactive component is microcrystalline quartz (Gillott, Duncan, and Swenson 1973). To emphasize the effect of alkalinity on ASR, the SuG were tested at realistic levels of alkalinity (1 NaOH + CH, 0.5 NaOH + CH, 1 NaOH, 0.5 NaOH) to which the concrete will be subjected in the field conditions. To accelerate the chemical reaction, three temperatures were selected: 60^0C, 70^0C and 80^0C. All tests were conducted for a period of four days.

The results of SuG are presented in Figure 5.9, 5.10, 5.10 and 5.11 for tests conducted at 1 NaOH, 0.5 NaOH, 1 NaOH + CH and 0.5 NaOH + CH respectively. It can be seen from the figure that all expansion data curve follow an S-curve; i.e. minimum or negligible expansion was recorded in the initial hours (0-15 hrs), then a steep rise occurs (20-70 hrs). Then the % expansion values stabilize around the 4 days. This S-curve shape can be explained as follow: initially, the hydroxyl attacks and penetrates the surface of the aggregate resulting in the dissolution of silica. No expansion is measured in this initial period. This dissolution of silica leads to the creation of negative charge. To maintain equilibrium around the particle, cations around the particle (i.e. sodium) are attracted to achieve neutrality forming a hygroscopic gel, resulting in the rapid expansion. The stabilizing period following the 70 hr testing period maybe due to the following: as silica from the aggregate dissolves, at the same time, some calcium and potassium cations leach out of the aggregate (PRG contains small amount of CaO) and are absorbed by the gel. The gel surrounding the aggregate prevents the dissolution of any more silica, therefore preventing temporarily any further gel development.
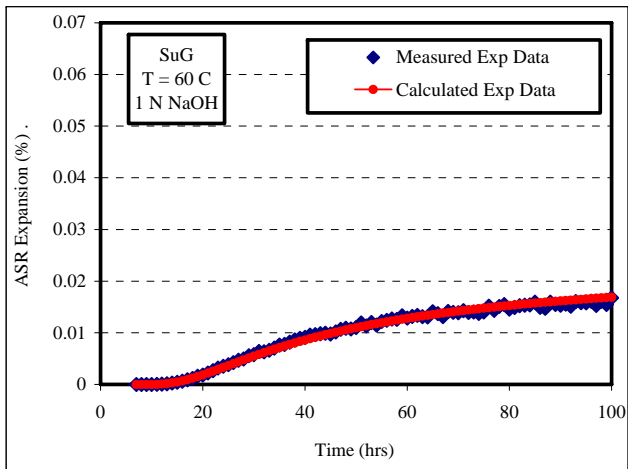
(a) SuG expansion at 60 ^{0}C
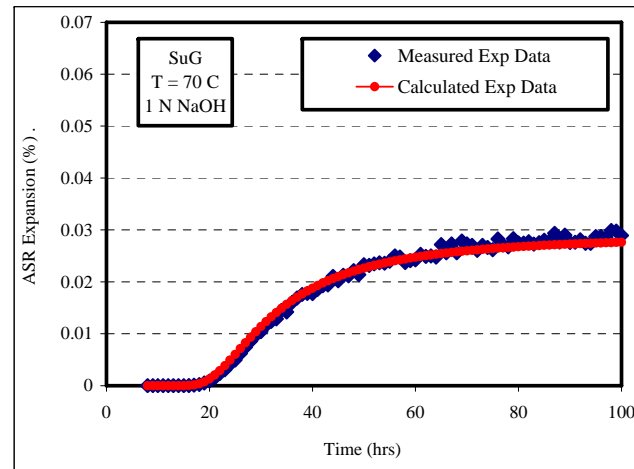
(b) SuG expansion at 70 ^{0}C
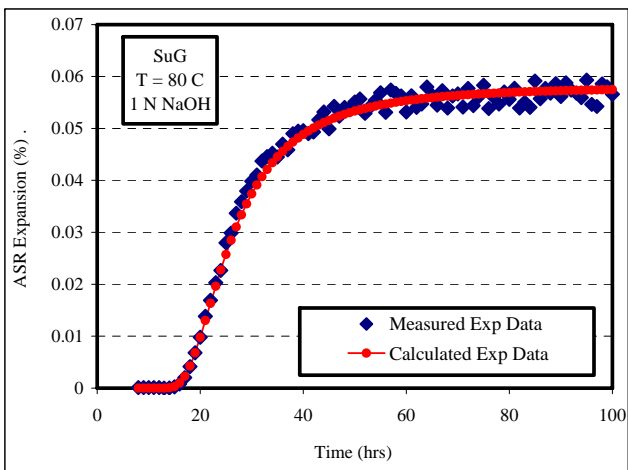
(c) SuG expansion at 80 ^{0}C
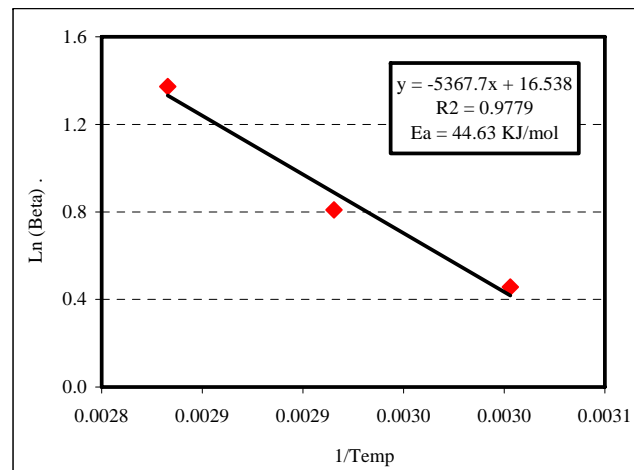
(d) Determination of activation energy

Figure 5.9 Sudbury Gravel (SuG) Characteristics (1 NaOH).
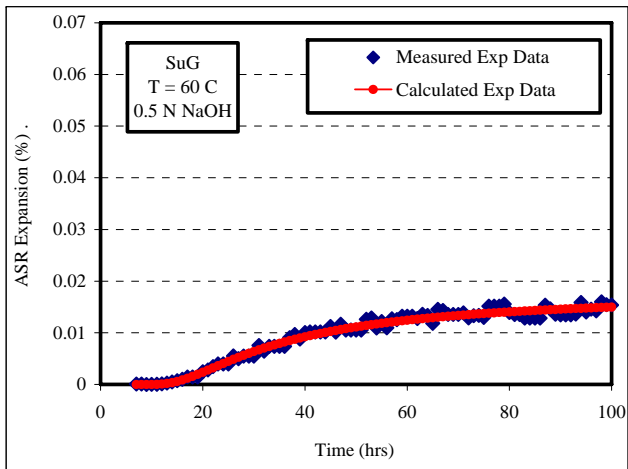
(a) SuG expansion at 60 ^{0}C
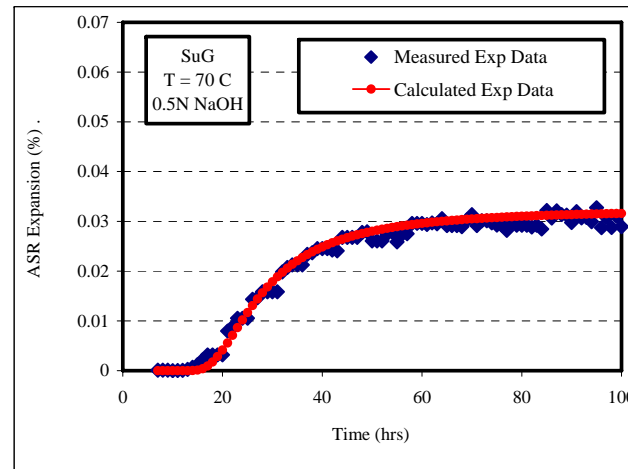
(b) SuG expansion at 70 ^{0}C
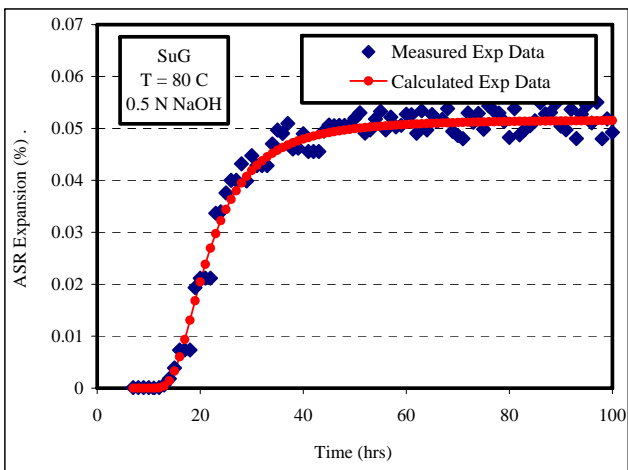
(c) SuG expansion at 80 ^{0}C
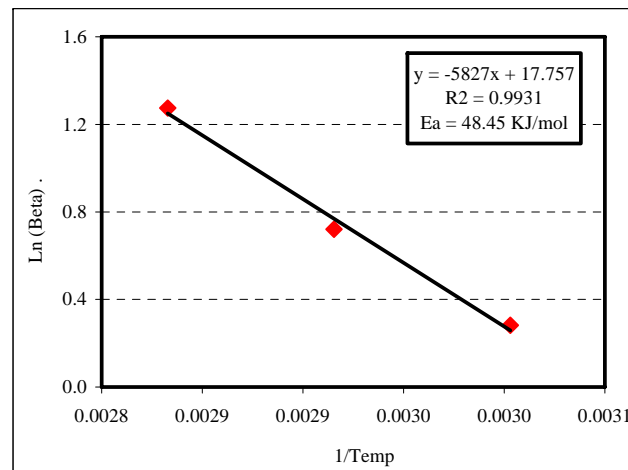
(d) Determination of activation energy

Figure 5.10 Sudbury Gravel (SuG) Characteristics (0.5 NaOH).
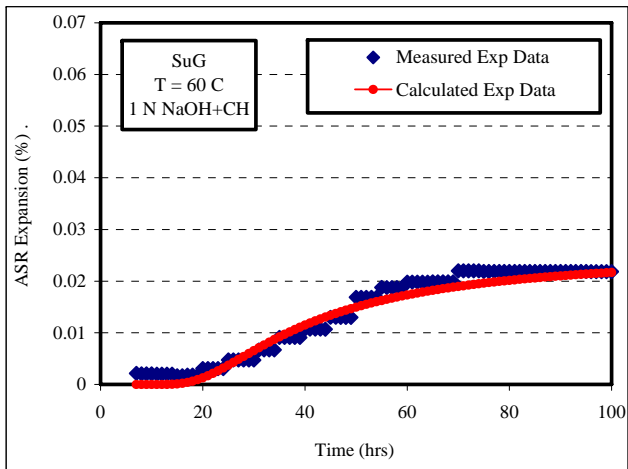
(a) SuG expansion at 60 ^{0}C
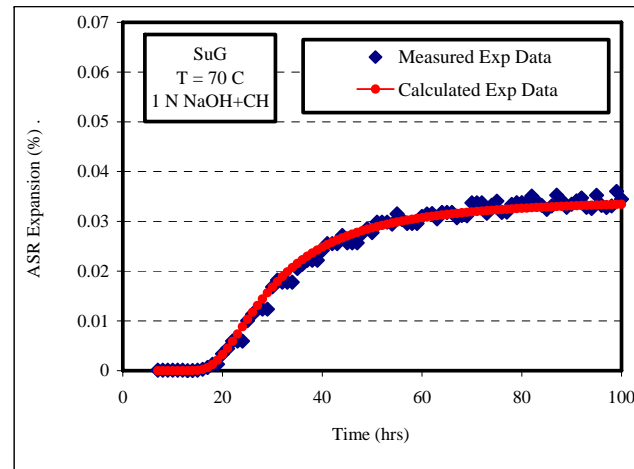
(b) SuG expansion at 70 ^{0}C
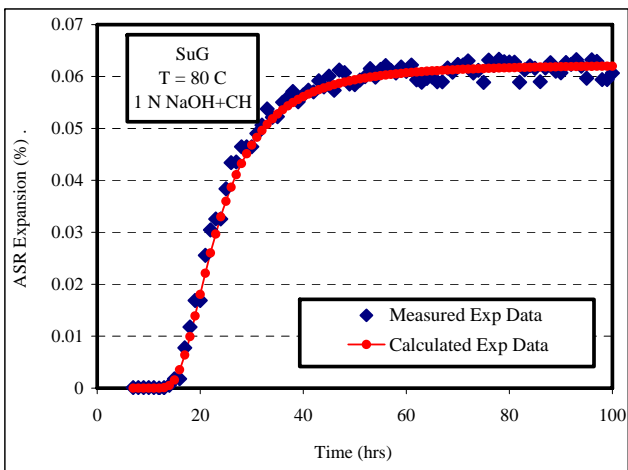
(c) SuG expansion at 80 ^{0}C
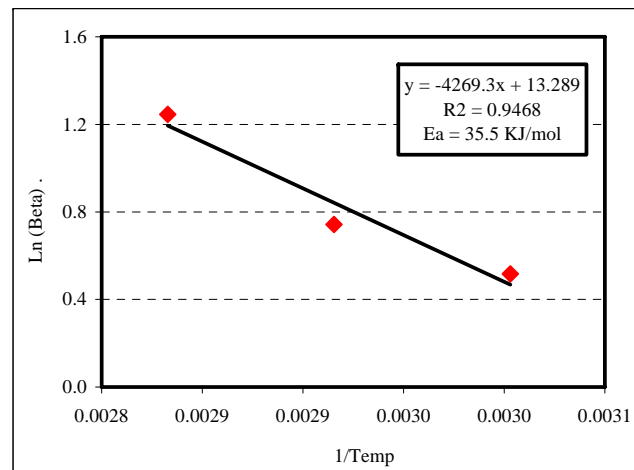
(d) Determination of activation energy

Figure 5.11 Sudbury Gravel (SuG) Characteristics (1 NaOH + CH).
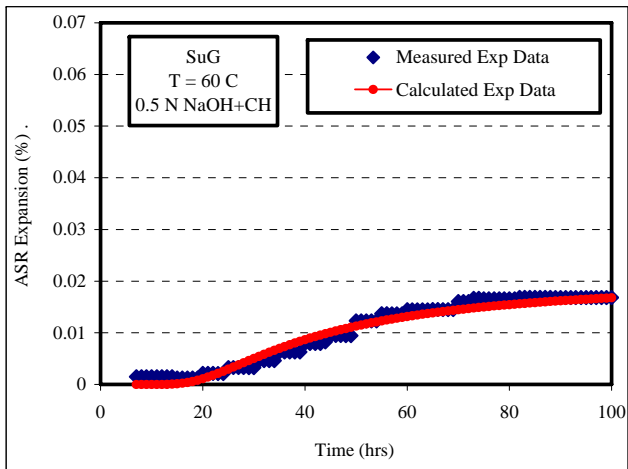
(a) SuG expansion at 60 ^{0}C
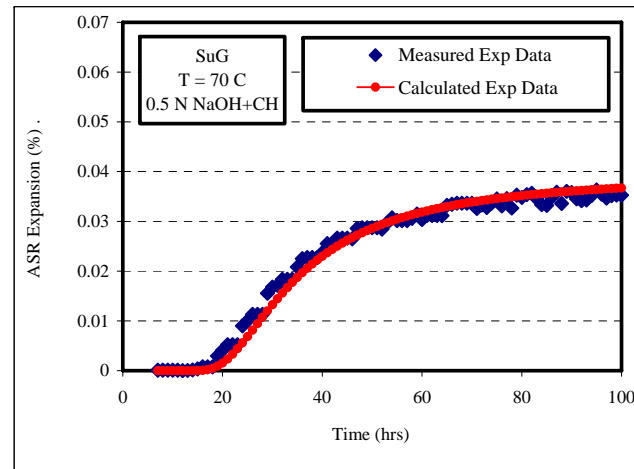
(b) SuG expansion at 70 ^{0}C
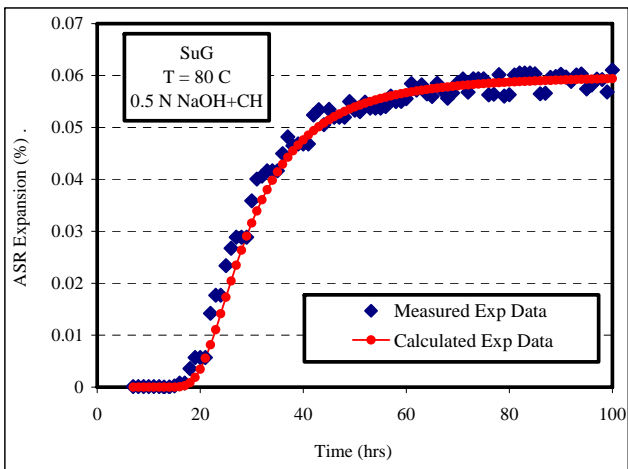
(c) SuG expansion at 80 ^{0}C
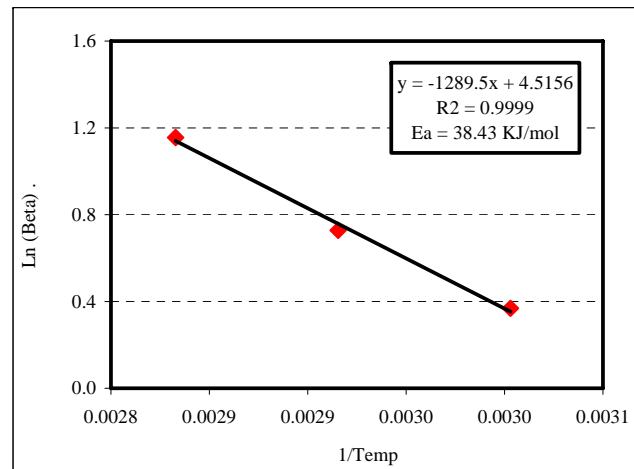
(d) Determination of activation energy

Figure 5.12 Sudbury Gravel (SuG) Characteristics (0.5 NaOH + CH).

Using the system identification procedure, SuG characteristics were determined. The results are shown in Table 5.4. The difference in ultimate expansion ε_0 (%) between tests conducted at 1N+CH and 1N NaOH are important to observe and illustrate the effect of calcium hydroxide on ASR. i.e. at 60^0C, the ε_0 (%) is 0.02% at 0.5N+CH while it is 0.016% at 0.5N. This corresponds to 25% increase. This is due to the fact that calcium hydroxide speeds up the penetration of hydroxyl ions into the aggregate grains leading to a quicker reaction. This conclusion on the role of CH is also supported by the values of the rate constant (β). At 60^0C, β is 1.44 at 0.5N+CH while it is 1.32 at 0.5N. The results are also consistent with Chatterji theory regarding this point (Chatterji et al, 1986, Chatterji 1989).

The activation energy for SuG was calculated by plotting ln(β) versus (1/T). The plots are displayed in Figures 5.9.d, 5.10.d, 5.11.d and 5.12.d. The coefficient of determination R^2 was 0.99. Its importance is that it provides us an indication about the regression line. Theoretically, if the regression line passes exactly through the three points, all variation in the data would be explained by the line. As the point scatter away from the regression line, the variation can't be explained. The high value of R^2 indicates that the dilatometer test and the new proposed kinetic model are very promising tools within the hands of the researchers and practitioners. Both (dilatometer + kinetic) model will have the capability to determine the speed of ASR at temperature close to the field conditions. It is highly unlikely that the dilatometer test will be performed at room temperature as this will require a significant amount of time (i.e. weeks or months) before any volumetric expansion is recorded. Since R^2 is almost close to 1 for all vast majority of tests, the rate constant (β) can be predicted from the regression equation at any other temperature. As shown from Table 5.4, the E_a for SuG was equal to 44.62, 48.44, 35.49 and 38.42 KJ/mol for tests conducted at 1N, 0.5N, 1N + CH and 0.5N + CH respectively. The results indicate that the activation energy of aggregate is inversely proportional to alkalinity of the test solution for both sets of testing, with and without calcium hydroxide. This suggests the presence of an equation relating the two parameters together and also implies that the concept of ASR activation energy can be very useful in detecting the reactivity of aggregate in concrete subjected to different level of alkalinity.

Aggregate reactivity can be determined by either comparing the ultimate expansion of the rock at a specific alkalinity or by comparing their activation energy at the same level of alkalinity. For tests conducted at 80^0C in 1 N NaOH+CH, the ε_0 (%) for NMR, PRG and SuG were 0.1190%, 0.053% and 0.059%. As seen from the data, NMR displays the highest volumetric expansion among other aggregate in this study, therefore NMR is more reactive than PRG and SuG. On the other side, the ε_0 (%) of PRG is less than the ε_0 (%) of SuG. Consequently, PRG is less reactive than SuG. From the above results, it can be stated that the ε_0 (%) is a good index number to predict ASR reactivity of aggregate.

Table 5.4 Sudbury Gravel Characteristics.

Aggregate type	Alkalinity (NaOH)	Temp (^{0}C)	ASR aggregate parameters				E_a (KJ/mol)
			ε_0 (%)	ρ	t_0	β	
Sudbury Gravel	1N	60	0.019	31.2	3.70	1.57	44.62
		70	0.029	22.2	5.61	2.2	
		80	0.054	27.5	1.29	3.94	
	0.5N	60	0.016	32.7	4.59	1.32	48.44
		70	0.030	24.5	5.89	2.05	
		80	0.048	24.3	2.17	3.57	
	1N + CH	60	0.025	30.7	3.31	1.67	35.49
		70	0.034	23.6	5.85	2.10	
		80	0.059	25.4	2.75	3.47	
	0.5N + CH	60	0.020	32.1	4.14	1.44	38.42
		70	0.036	24.2	5.88	2.07	
		80	0.057	27.1	3.20	3.17	

* CH = calcium hydroxide

Effect of Test Condition on ASR Expansion

As shown in Chapter II, there are certain requirements or conditions that need to be present in concrete structures for ASR to proceed. Those are: a) reactive silica, b) alkalinity and c) moisture. Temperature is also considered a factor since it helps accelerate the chemical reaction. Since the main target of this research is to mitigate ASR and to study the combination of the above conditions to control ASR, the above factors with their corresponding levels were chosen in the experimental program to study their effect on ASR. The effect of reactive silica was taken into account by selecting four different types of aggregates with different reactivity. Three different alkali concentration were selected (0.25 N, 0.5N and 1N NaOH) to simulate alkalinity of the pore solution of concrete. Calcium hydroxide was also added to selected alkali solution to study its outcome on ASR. To speed up the ASR reaction, three levels of temperatures were chosen: 60^0C, 70^0C and 80^0C. The effect of alkalinity was covered in detail in the previous part of this chapter. This section covers the effect of temperature and calcium hydroxide on ASR characteristics.

Effect of Temperature

It is known that the rate of reaction depends on the temperature. The rate of reaction and the rate constant (β) are related through the rate law. The effect of temperature on β and on the theoretical initiation time of ASR (t_0) is presented in Figures 5.13 and 5.14 respectively. As seen from the results (without any exception), the rate constant and temperature have a proportional relationship; i.e. when temperature increases from 60^0C to 70^0C, β goes up as well. A similar deduction can be made when the temperature increases from 70^0C to 80^0C.

The dependence of β on temperature is important to observe and can be explained by the collision theory. This theory which was proposed in 1916 and 1918 by Max Trautz and William Lewis, was based on the concept that reactant molecules must collide for the reaction to occur, but only a proportion of the total number of collisions will have the energy necessary for the molecules to react effectively and for the products to be transformed into products. This minimum amount of energy required for the collision to occur effectively is called the activation energy (E_a) (Ebbing and Gammon

2005). The rate constant in the collision theory is composed of three elements and is as follows (Ebbing and Gammon 2005):

$$\beta = Z \times f \times p$$

where:

Z = The collision frequency.

f = The % of collisions having energy greater than E_a

p = The % of collision that takes place when the reactant particles are properly oriented.

The collision frequency depends on temperature. This can be easily explained in the case of aggregate soaked in alkaline solution. As temperature goes up, the hydroxyl ions moves faster because their kinetic energy increases and thus, they collide more frequently with the reactive silica located at the surface of the aggregate.

The second factor f is highly dependent on temperature and is related to the activation energy (E_a) through the following equation:

$$f = e^{-\frac{E_a}{R.T}}$$

where:

T = Temperature

R = Gas constant, which is equal to 8.314 J/(mol.K)

In the dilatometer test, this is explained as follows. When there is rise in the temperature, the fraction of particles possessing energy higher than the (E_a) is much higher than those having that energy at lower temperature. The third factor p, which depends on the orientation on the reactant particles, does not depend on temperature, although it is an important parameter.

In this study, the four types of aggregates have different reactivity and this is well illustrated by the values of the rate constant at different temperature for each type of aggregate. For example, for NMR at 1N NaOH+CH, the rate constant increase from 1.9 at 60^0C to 2.5 at 80^0C. This corresponds to a 26.3% increase. However, for PRG at 1N NaOH+CH, the rate constant increases from 1.1 at 60^0C to 3.7 at 80^0C. This is equivalent to 236% growth. As a result, it can be concluded that the rate constant for PRG is much more sensitive to temperature comparing to NMR and consequently, it can be stated that NMR is more reactive than PRG. The same analogy can be made for the other types of rocks and it can be determined that New Mexico Rhyolite is the most reactive among all aggregates tested, followed by Spratt Limestone, Sudbury Gravel and then Platte River Gravel.

By looking at Figure 5.14 and by comparing t_0 at 60^0C and 80^0C, it can be seen that t_0 is much lower at 80^0C than at 60^0C. This is due to the fact that when temperature increases, the rate constant goes up as well, resulting in the ASR occurring sooner, thus the lower t_0 value of at 80^0C.
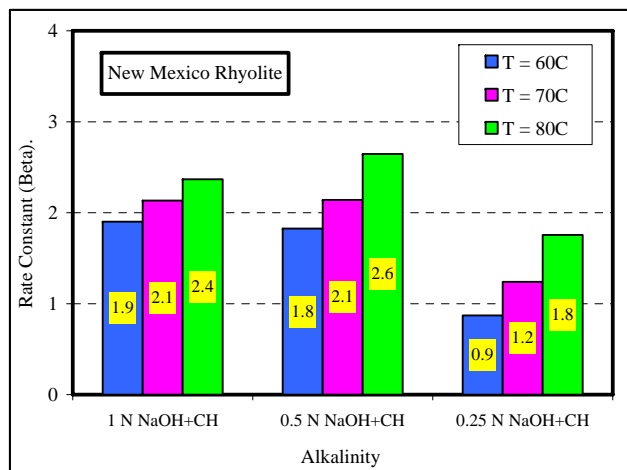
(a) New Mexico Rhyolite
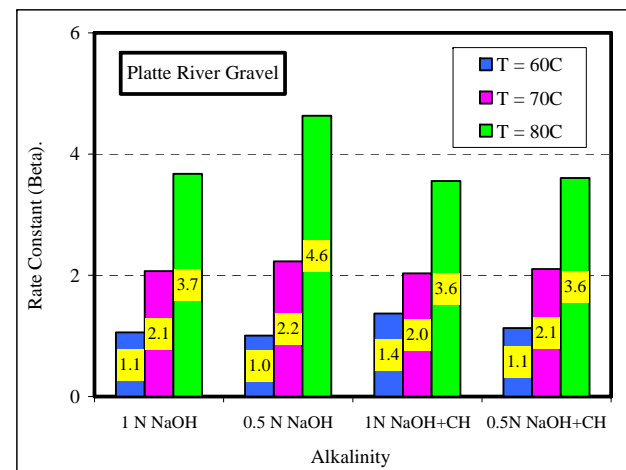
(b) Platte River Gravel
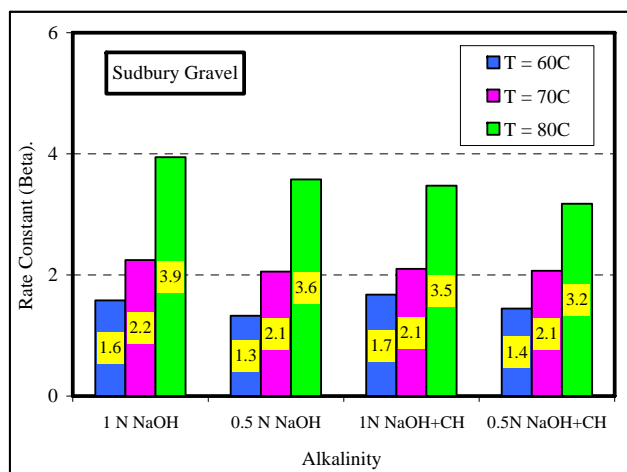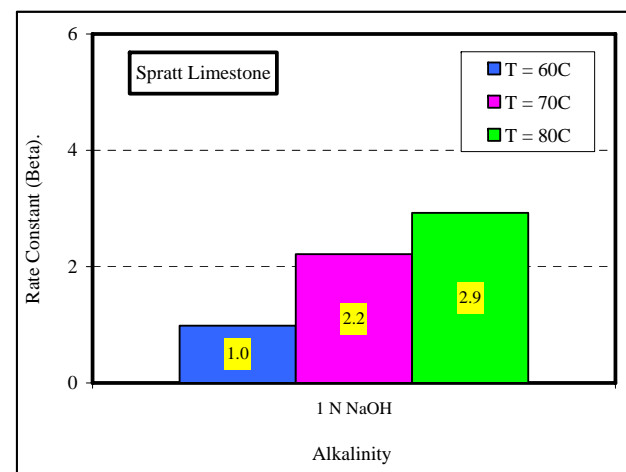
(c) Sudbury Gravel

(d) Spratt Limestone

Figure 5.13 Effect of Temperature on the Rate Constant (Beta).
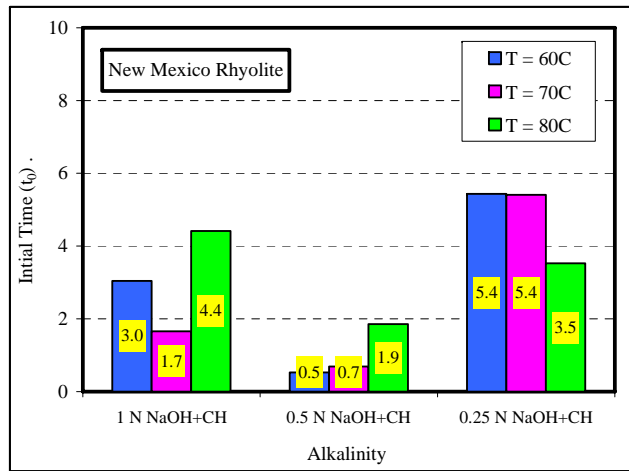
(a) New Mexico Rhyolite
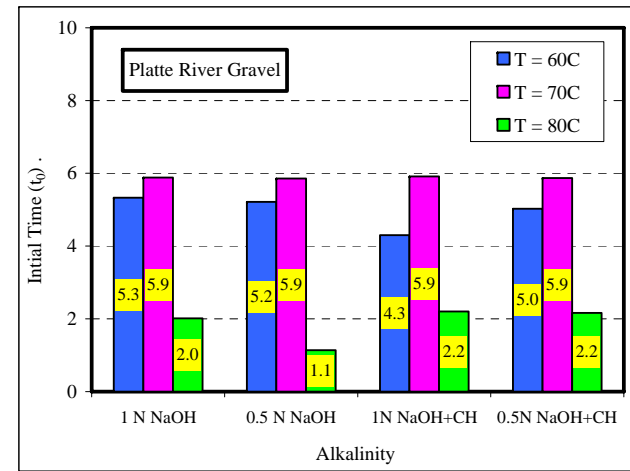
(b) Platte River Gravel
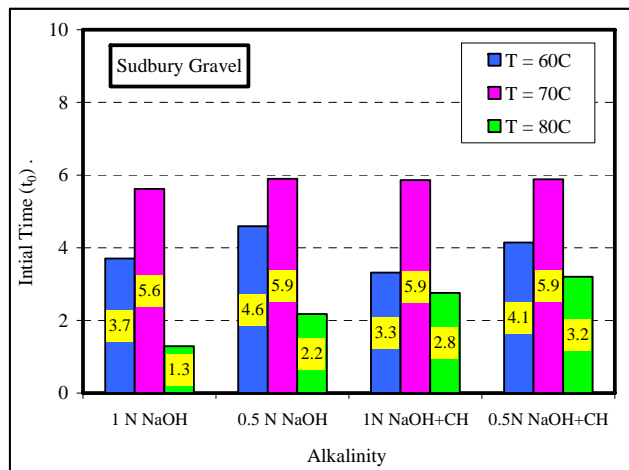
(c) Sudbury Gravel
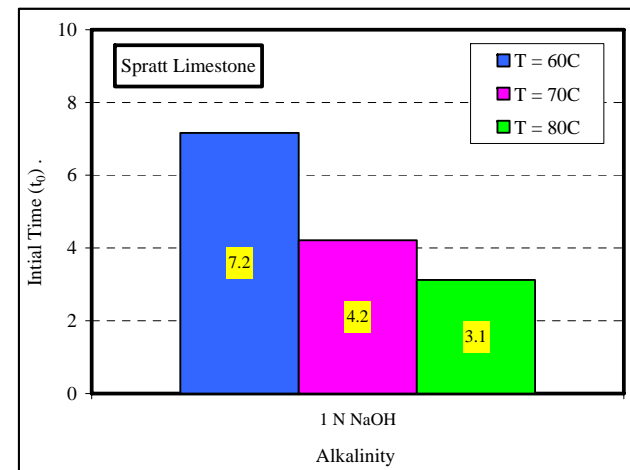
(d) Spratt Limestone

Figure 5.14 Effect of Temperature on the Theoretical Initial Time (t_0).

Effect of Calcium Hydroxide

When cement comes into contact with water, hydration begins. The major hydration products are calcium silicate hydrate (C-S-H) and calcium hydroxide (CH). The initial theories (McGowan and Vivian, 1952) didn't consider calcium to play a role in the chemistry of ASR. However, later research conducted by Power and Steinour (1955) showed that the main factor affecting the "expansivity" of ASR is the ratio of calcium to silica. They found that if the ratio is very low, the gel can be very expansive; however, if this ratio is high, the gel won't be expansive. Other researchers in later years had different thoughts about this issue. Since the role of CH has been a point of controversy among researchers since Hanson discovered ASR in 1940, CH was introduced as a parameter in the experimental design.

The effect of CH on ASR characteristics is presented in Figure 5.15. As seen from the figure, the ultimate expansion increases slightly when CH is present in the alkaline solution. For example, for SuG conducted at 80^0C, the ε_0 (%) is 0.057% at 0.5N NaOH+CH, while the ε_0 (%) is 0.049 at 0.5N NaOH. This is equivalent to a 16.3% increase. The same conclusion on the effect of ASR can be made for other types of aggregates tested at different alkalinities at all temperatures. This increase may be due to the following reason: as the gel is formed around the rock, calcium ions in the alkaline solution in addition to calcium leaching out from the aggregate, are taken into the gel and prevent the diffusion of dissolved silica ion into the solution, therefore creating a barrier around the aggregate. Pore solution chemistry (provided in the next section) supports this point of view. Results show calcium concentration reduces significantly after the test indicating that it participated in the chemical reaction. The above results are consistent with the ASR theory developed by Chatterji. In his theory, Chatterji et al. 1986 and Chatterji 1989 mentioned that the rate of diffusion of silica out of the reactive grain is inversely proportional to the concentration of $Ca(OH)_2$ in the pore solution around the reactive aggregate. He added that when there is an ample amount of CH, a minimal quantity of Si^{+4} can diffuse out of the grain. Another important conclusion that can be stated here is that expansion is also measured in the absence of CH. This indicates that at least the gel did not dissolve into the high alkaline solution. Otherwise, shrinkage would have been measured instead of expansion.
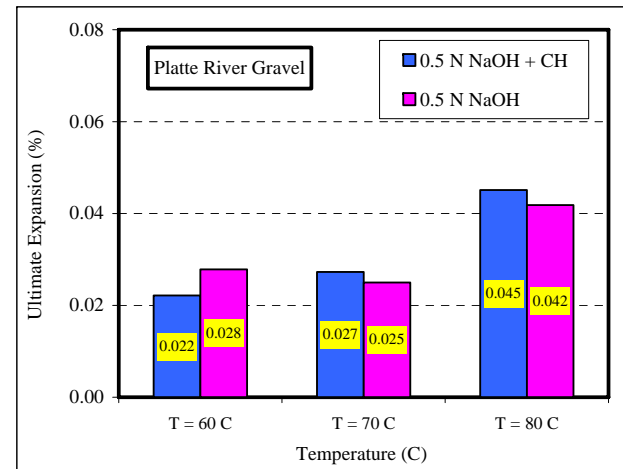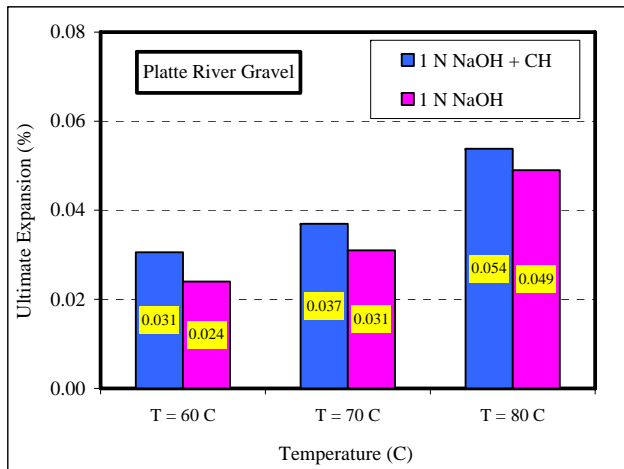
(a) Platt River Gravel
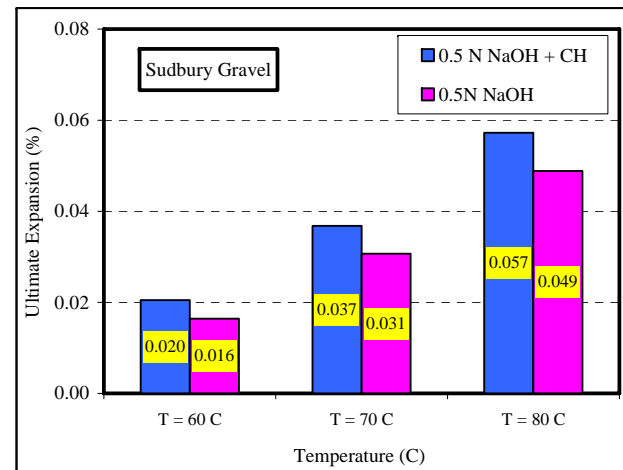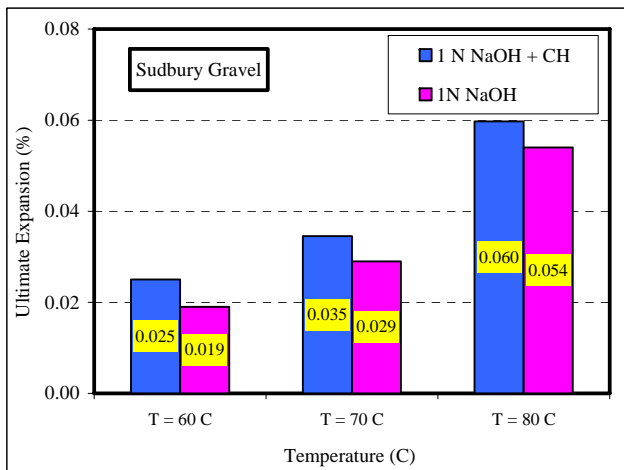
(b) Sudbury Gravel

Figure 5.15 Effect of Calcium Hydroxide (CH) on Ultimate Expansion.

Chemistry of Test Solution

As described previously in Chapter II, a high pH value facilitates the development of ASR, as high pH values increase the dissolution of amorphous silica in the aggregate. Therefore, it is imperative to measure pH values to check if there is any correlation between pH values and ASR characteristics. For that reason, pH values were measured before and after each test using an Accumet pH meter. It is also known that the presence of alkali ions is mandatory for ASR gel development; consequently, it is vital to study the change in alkali concentration after the dilatometer test. Sodium (Na^+), potassium (K^+) and calcium (Ca^{+2}) were measured before and after each experiment using a four element flame photometer. This section presents the results and discussion of the pH and of the chemistry of the test solution before and after testing.

pH test results are presented in Table 5.5. It should be mentioned here that pH values are a representation of the hydroxyl ions in the solution. As shown in the table, the pH values decrease for all tests, regardless of the alkalinity and temperature of the test solutions. This is a clear indication that hydroxyl ions were consumed in the chemical reaction. However, the rate of decrease of pH values is different for each type of aggregate. For example, the pH value for New Mexico Rhyolite at 1N NaOH+CH at 80^0C was measured to be 14.009 before testing. Then it dropped significantly to 13.087. One has to mention here that 1N NaOH yields a pH 14 and 0.1 N NaOH gives a pH of 13. Thus, from NMR pH results, this drop in pH values is equivalent to a 90% reduction in hydroxyl ions concentration. On the other side, for Platt River Gravel, the pH values at 1 N NaOH+CH at 80^0C dropped from 14.009 to 13.514. This is equal to a 70% decrease in OH⁻. Based on the above pH measurements, it can be seen that (OH⁻) ions were consumed more during the chemical reaction in the dilatometer test where NMR is the aggregate. Consequently more gel is expected to be formed in the NMR case, and more expansion is anticipated to be measured, which was the case. This comparison of the % decrease of OH⁻ concentration is very consistent with ASR characteristics discussed earlier in the chapter. In fact, the ultimate expansion ε_0 was 0.1190 % for NMR at 1N NaOH+CH at 80^0C while it was 0.053 % for PRG at the same alkalinity and temperature. This clearly indicates that NMR is more reactive than PRG as more (OH⁻) were consumed (lower pH values) and higher measured expansion was recorded.

An important piece of information can be deduced from the analysis of the test solution. (K^+) was measured in all tests, although the alkali test solutions before the test don't contain any (K^+) ions. This is an indication that those ions were leached out from the aggregate during testing. This finding is consistent with a previous study by Berube et al. 2002 that shows that some types of aggregate (i.e. volcanic glass, micas, alterated feldspars, etc) can supply a substantial amount of alkalis into the pore solution of concrete.

$Ca(OH)_2$ was added to the NaOH solutions of respective strengths (e.g., 1N, 0.5N, and 0.25N) at room temperature. It is known that CH solubility is very low in water (i.e., around 1gm / liter) which matches with concrete pore solution. A comparison is conducted between the amount of calcium measured after the test for NMR at 1N NaOH+CH at 60, 70 and 80 ^{0}C. Results indicate that Ca^{+2} ions concentrations decrease as temperature increases. This is an indication that more Ca^{+2} ions have participated in the reaction. The results are consistent with pH values obtained at 60 ^{0}C (pH = 13.141) and 80 ^{0}C (pH = 13.087). This indicates that more OH^- ions were consumed and more gel was formed. Therefore, one can conclude that the presence of CH enhances ASR expansion slightly. But this increase is not significant. Results of ASR characteristics support this point of view. It is also interesting to notice that higher Ca^{+2} ions concentration are measured in PRG than NMR. Consequently, it can be concluded that more calcium has participated in the case of NMR. Therefore, it can be deducted from this observation that NMR is more reactive than PRG (pH values after the test supports this deduction).

The solubility of gel in alkali solution is a point of interest. Therefore, alkali ions were measured after the test. Results are presented in Table 5.5. It can be seen that (Na^+) concentration decreases significantly, irrespective of the test conditions (i.e. temperature, alkalinity, CH). This can be explained as follows: as hydroxyl ions attack the grains of the aggregate, siloxane bridges are broken and eventually silica dissolves creating a negative charge (SiO^-). To maintain equilibrium in the system, Na^+ ions were attracted and taken into the gel, resulting in the measured decrease of (Na^+) concentration after the test. Another conclusion can be stated here is that the gel did not dissolve (at least fully) in the alkali solution, otherwise (Na^+) should be at least the same or maybe higher as some (Na^+) ions may also leach out of the rock. To investigate the effect of test

parameters on the alkali concentration, the % decrease in Na$^+$ was determined using the following equation:

$$\% \ R_{Na^+} = \left[\frac{C_{initial_{Na^+}} - C_{final_{Na^+}}}{C_{initial_{Na^+}}} \right] \times 100$$

where:

$\% \ R_{Na^+}$ = % reduction in Na$^+$concentration

$C_{initial_{Na^+}}$ = Na$^+$concentration in the alkaline solution before dilatometer testing

$C_{final_{Na^+}}$ = Na$^+$concentration in the alkaline solution after dilatometer testing

The results are displayed in Figure 5.16. It can be seen that % Na$^+$ reduction increases with increasing alkalinity and temperature of test solution; i.e. the % R_{Na^+} was 23% for Spratt Limestone at 80C whereas it was 10% at 60^{0}C. Similar behavior for other aggregates tested at different alkalinity was noticed. Thus, it can be concluded that increasing temperature and alkalinity enhance ASR, as the driving force of the diffusion of the alkali hydroxide ions into the aggregate grains becomes higher and faster.

Table 5.5 Test Solution Chemistry Before and After the Test.

Aggregate type	Alkalinity N = NaOH	Temp (°C)	Alkali Concentration (ppm) before testing				Alkali Concentration (ppm) after testing			
			pH	Na$^+$	K$^+$	Ca^{+2}	pH	Na$^+$	K$^+$	Ca^{+2}
New Mexico Rhyolite	1N + CH	60	14.009	23605	0	486	13.141	16068	52.8	68.7
		70	14.009	23605	0	486	13.135	14481	55.9	59.5
		80	14.009	23605	0	486	13.087	13438	51.7	51.4
	0.5N + CH	60	13.708	11755	0	486	13.319	8911	62.8	106.2
		70	13.708	11755	0	486	13.271	7916	54.5	93.4
		80	13.708	11755	0	486	13.201	7394	62.6	85.8
	0.25N + CH	60	13.399	5877	0	486	13.291	5124	12.0	137.5
		70	13.399	5877	0	486	13.277	4982	13.7	119.0
		80	13.399	5877	0	486	13.189	4674	35.6	102.9
Platte River Gravel	1N	60	14.004	23605	0	0	13.778	22183	5.1	1.3
		70	14.004	23605	0	0	13.687	21804	5.8	1.6
		80	14.004	23605	0	0	13.652	20666	5.6	2.9
	0.5N	60	13.701	11755	0	0	13.356	11329	1.3	1.7
		70	13.701	11755	0	0	13.381	11080	1.3	1.6
		80	13.701	11755	0	0	13.369	10475	1.2	1.5
	1N + CH	60	14.009	23605	0	486	13.71	21377	3.7	339.9
		70	14.009	23605	0	486	13.617	19813	3.9	285.3
		80	14.009	23605	0	486	13.514	19244	3.6	276.8
	0.5N + CH	60	13.708	11755	0	486	13.303	11092	1.5	374.5
		70	13.708	11755	0	486	13.354	10582	1.3	311.4
		80	13.708	11755	0	486	13.305	10215	1.5	291.5

Table 5.5. (Cont).

Aggregate type	Alkalinity (NaOH)	Temp (^{0}C)	Alkali Concentration (ppm) before testing				Alkali Concentration (ppm) after testing			
			pH	Na$^+$	K$^+$	Ca^{+2}	pH	Na$^+$	K$^+$	Ca^{+2}
Sudbury Gravel	1N	60	14.004	23605	0	0	13.603	21093	465.5	1.5
		70	14.004	23605	0	0	13.576	20074	421.9	1.2
		80	14.004	23605	0	0	13.558	19339	448.2	1.4
	0.5N	60	13.701	11755	0	0	13.31	10463	312.4	1.5
		70	13.701	11755	0	0	13.265	9978	359.5	1.6
		80	13.701	11755	0	0	13.253	9504	347.7	1.1
	1N + CH	60	14.009	23605	0	486	13.701	18320	420.0	340.3
		70	14.009	23605	0	486	13.669	17727	430.6	296.2
		80	14.009	23605	0	486	13.507	16898	480.2	258.8
	0.5N + CH	60	13.708	11755	0	486	13.251	10333	241.3	274.4
		70	13.708	11755	0	486	13.252	9907	310.9	247.9
		80	13.708	11755	0	486	13.217	9018	342.7	221.4
Spratt Limestone	1 N	60	14.004	23605	0	0	13.687	21211	1.2	1.8
		70	14.004	23605	0	0	13.683	19505	1.0	3.2
		80	14.004	23605	0	0	13.609	18107	1.1	3.8
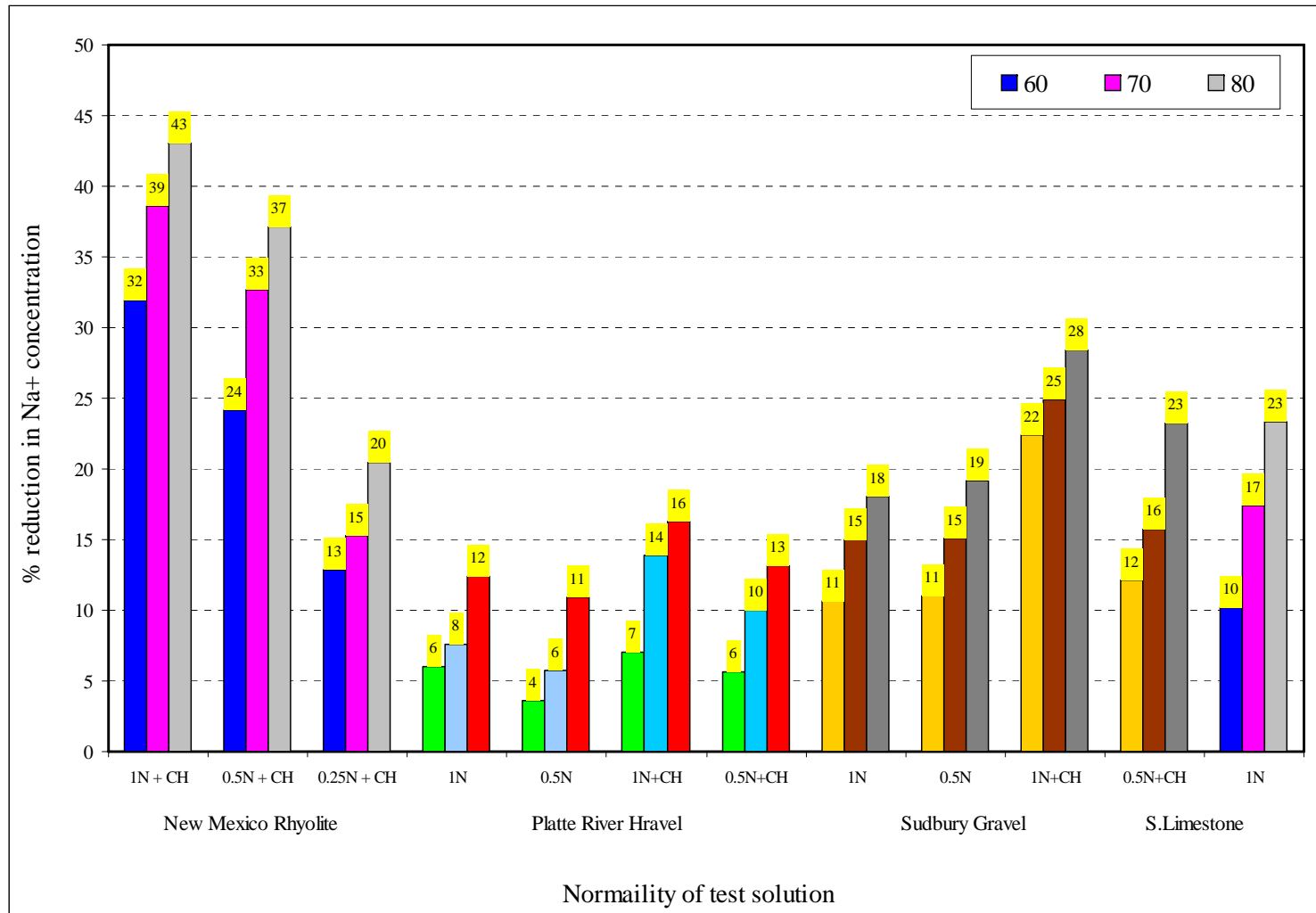
Figure 5.16 Effect of Temperature and Alkalinity on Sodium Concentration.

Comparison of ASR Activation Energy (E$_a$) for Aggregate

The Arrhenius equation which was formulated after the Swedish chemist Svante Arrhenius, was used to determine the E$_a$ of aggregate. The E$_a$ was determined from the slope of the plot of ln(β) versus 1/T. the plots and the results of E$_a$ were displayed and calculated earlier in the chapter. To compare the reactivity of the aggregate, the E$_a$ of all aggregates in this study were compared against each other.

A summary of the comparison is shown in Figure 5.17. As seen from the figure, the E$_a$ of NMR (10.7 KJ/mol) conducted at 1N NaOH+CH is less than the E$_a$ of SuG (35.5 KJ/mol) and the latter is less than the E$_a$ of PRG (45.6 KJ/mol). Therefore it can be concluded that NMR is more reactive than SuG and PRG, and SuG is in turn more reactive than PRG as a lower E$_a$ indicates that less energy is needed to initiate ASR and less energy is required to overcome the barrier. Another comparison can be made between S.L and SuG at 1 N NaOH alkalinity. The E$_a$ was 53.2 and 43.7 KJ/mol respectively. This indicates that SuG is more reactive than SL. From the above two comparisons, one can deduct that NMR is the most reactive aggregate tested in this research, followed by SuG, S.L and then PRG. Therefore, one can conclude that the concept of E$_a$ is a very useful tool and can be used as a screening indicator to determine the reactivity of the rock.

The alkalinity of test solutions appears to play a major role in the E$_a$ values and this is very interesting to notice. Regardless of the type of aggregate tested and irrespective of the presence or absence of CH in the solution, E$_a$ increases when alkalinity decreases. For example, the E$_a$ of PRG at 1 N NaOH is 58.08 KJ/mol and then goes up to 77.04 KJ/mol at 0.5 N NaOH. This signals the presence of a relationship between E$_a$ and alkalinity. Since aggregate in concrete structures will be subjected to different alkali level during the lifetime of the structure, it will be very beneficial to relate these two parameters through a mathematical model.
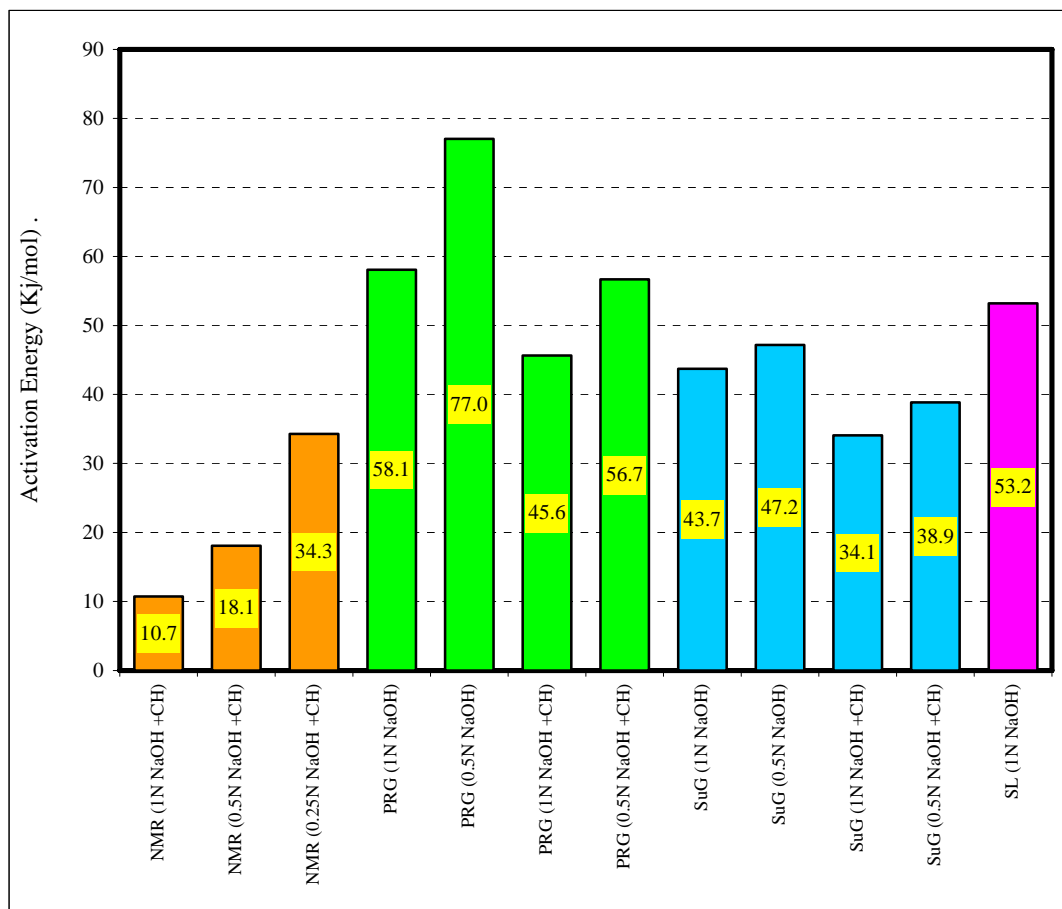
Figure 5.17 Comparison of E_a for All Aggregates at Different Alkalinities.

Intra and Inter-laboratory Comparison (TTI and UNH)

This IPRF project is a joint study between Texas Transportation Institute (TTI) and University of New Hampshire (UNH). One of the main objectives of this study is to develop a reliable test protocol that can be conducted within a short period of time. Consequently, the repeatability of this test protocol (i.e. dilatometer test method) and the reliability of the new kinetic model proposed in Chapter IV becomes a point of interest and an important component. To validate the proposed test protocol, two comparisons were conducted. The first is an intra-laboratory comparison of TTI activation energy (E_a) results obtained from the previous sections. The second is an inter-laboratory comparison between TTI and UNH (E_a) results. This section provides the results of the above two comparisons in addition to the results of the statistical analysis performed to find out if

the difference within TTI results and between the TTI-UNH results are statistically significant or not. All analysis was conducted using Microsoft Excel software packages.

Intra-laboratory comparisons

As mentioned previously in the experimental design, selected tests with different types of aggregates were repeated to check the procedure validation and the laboratory proficiency. Average, standard deviation and coefficient of variation of E_a (TTI) were determined for all repeated tests. Results are presented in Table 5.6. It can be seen from the analysis that the COV is less than 7% indicating that the results are highly repeatable.

Table 5.6 Intra-Laboratory Comparisons (E_a) - TTI.

Aggregate Type	Alkalinity (NaOH)	Average (μ)	Standard Deviation (σ)	$COV(\%) = \dfrac{\sigma}{\mu}$
Platt River Gravel	1N	58.08	3.90	6.72
	0.5N	77.04	3.52	4.57
	1N + CH	45.64	1.15	2.52
	0.5N +CH	56.22	0.64	1.14
Sudbury Gravel	1N	43.71	1.28	2.94
	0.5N	47.17	1.79	3.80
	1N + CH	34.09	1.97	5.78
	0.5N +CH	38.86	0.62	1.60
Spratt Limestone	1 N	53.21	1.01	1.9

* CH = calcium hydroxide

Inter-laboratory Comparisons

Inter-laboratory comparison is essential for standard reference material certification. To check the multi-laboratory precision, UNH conducted the dilatometer test under the same conditions as TTI for Platt River Gravel and Spratt Limestone at 1N NaOH. A summary of this comparison is presented in Table 5.7. As shown, this test procedure, although conducted in different laboratories by different personnel, can be easily described as highly reproducible as the average multi-laboratory coefficient of variation for Platte River gravel is less than 10%.

Table 5.7 Inter-Laboratory Comparisons of E_a (TTI versus UNH).

Type of Aggregate	Alkalinity (NaOH)	E_a TTI	E_a UNH	E_a Average	Standard Deviation	E_a COV
Platt River Gravel (PRG)	1N	58.08	66.4	62.24	5.88	9.45
Spratt Limestone (SL)	1N	53.2	54.3	53.75	0.78	1.45

- CH = calcium hydroxide

Although the results of the above intra and inter-laboratory are very promising, questions remain as a) whether the new test protocol and the new kinetic model used in the analysis are capable of distinguishing aggregates with different reactivity and b) whether this procedure can capture the effect of alkalinity and calcium hydroxide on the activation energy (E_a). In other words, from a statistical point of view, is the mean E_a for PRG conducted at TTI (58.08 KJ/mol) different than the mean E_a of PRG conducted at UNH (66.4 KJ/mol).

To answer the above questions, a detailed analysis on the data needs to be performed using appropriate statistical methods. Consequently, a hypothesis test (T test) for the two population means was performed. If the variance were equal, pooled method can be used. Since this was not the case, the Satterthwaite method was used to analyze the results. The level of significance (α) for all hypothesis testing was 0.05. α is considered the type 1 error probability. The Null hypothesis (H_o) assumes that the mean (E_a) for PRG at TTI is equal to mean (E_a) of PRG at UNH and the alternate hypothesis (H_a) was that the mean (E_a) of PRG for both universities are different. If the t value obtained from statistical tables (Montgomery and Runger 2002) was less than test statistics (T_0), the null hypothesis statement was rejected. On the other hand, if it was greater than or equal to T_0, we will say that there is not enough evidence to reject the (H_o). The above statistical procedure is outlined below in a step by step approach.

1. The parameter of interest is E_a, the activation energy of the aggregate

2. $H_0 : \mu_1 = \mu_2$ (μ_1 is the population mean of E_a - TTI)

3. $H_a : \mu_1 \neq \mu_2$ (μ_2 is the population mean of E_a - UNH)

4. Significance level α (i.e. 5%)

5. The Test Statistic is: $T_0 = \dfrac{X_1 - X_2}{\sqrt{\dfrac{s_1^2}{n_1} + \dfrac{s_2^2}{n_2}}}$

6. Reject H_0 that the means of (E_a) are equal if:

$$-t_{(\alpha/2, \upsilon)} < T_0 < t_{(\alpha/2, \upsilon)}$$

where:

$t_{(\alpha/2, \upsilon)}$ is the critical value of the t distribution and υ is the number of degrees of freedom

$$\upsilon = \frac{\left(\dfrac{s_1^2}{n_1} + \dfrac{s_2^2}{n_2}\right)^2}{\dfrac{(s_1^2 / n_1)^2}{n_1 - 1} + \dfrac{(s_2^2 / n_2)^2}{n_2 - 1}}$$

Results of the analysis are presented in Table 5.8. Several points can be observed. For the inter-laboratory comparison, it can be seen from the hypothesis testing that there was not enough evidence to reject the H_o since $-t = -4.3 < T_0 = -2.1 < t = 4.3$. Since T_0 falls within the acceptance region, it can be concluded from a statistical point of view that (E_a) for PRG of TTI and UNH are equal.

Table 5.8 Statistical (Hypothesis Test) Results for Both Inter and Intra-laboratory Comparison Using PRG and S.L. Aggregate.

	Combinations	T_0	t_0	T-test Output	Conclusion
Platte River Gravel	1N (TTI) vs. 1 N (UNH)	-2.1	4.3	Fail to reject Null hypothesis	Means are equal
	1N (TTI) vs. 0.5N (TTI)	-5.1	4.3	Reject Null hypothesis	Means are not equal
	1N (TTI) vs. 1N+CH (TTI)	-4.36	4.3	Reject Null hypothesis	Means are not equal
	1N (TTI) vs. 0.5N+CH (TTI)	0.52	4.3	Fail to reject Null hypothesis	Means are equal
Spratt Limestone	1N (TTI) vs. 1 N (UNH)	-0.74	4.3	Fail to reject Null hypothesis	Means are equal

For the intra-laboratory tests, hypothesis tests were done to check if the means (E_a) of PRG calculated at different alkalinities are significantly different from each other or not. Results are also displayed in Table 5.8. For all cases, the H_o was rejected (T_0 falls within the rejection region), indicating that the means are significantly different. Thus, it can be deduced that the new proposed protocol can distinguish the rock based on their reactivity and can capture the effect of alkalinity and CH on E_a.

Summary

This chapter presents the analysis and the interpretation of four aggregate types (NMR, PRG, SuG, SL) tested in the dilatometer test at different temperatures under different alkali levels with and without calcium hydroxide. A new kinetic model was introduced and used to rank the aggregates based on their reactivity using the activation energy concept (E_a). The latter was seen as the energy necessary to initiate ASR. Based on the analysis conducted, several conclusions can be made:

a) Results indicate that ASR expansion increases as the alkalinity of test solutions and time goes up and this gain was attributed to the formation and then expansion of ASR gel.

b) Increasing the temperature leads to an increase in the rate constant. This indicates that ASR is a thermally activated process.

c) From ASR characteristics and from the chemistry of the test solution, ASR was found to be expansive without the presence of calcium hydroxide, as the major ions (sodium and hydroxyls) were consumed during the chemical reaction. It should be noted that the presence of CH in the solution increases slightly the ASR expansion.

d) The E_a concept of ASR was seen to be a useful parameter and has the potential of playing the role of a screening parameter for rocks with different reactivity.

e) From the statistical analysis conducted on the mean E_a, this new test protocol is seen to be highly repeatable and reliable.

CHAPTER VI

DETERMINATION OF COMBINED CONCRETE
ASR MATERIAL PROPERTIES USING DILATOMETER

This chapter is divided into four major parts. The first division presents the results and analysis of the tests of concrete made with New Mexico Rhyolite (NMR) and Platte River Gravel (PRG) aggregates. The second section shows the results of the proposed model in Chapter IV linking the activation energy and the alkalinity of test solution. The third portion displays the results of the generalized ASR concrete generated from the Badillo transform and the additional concrete tests performed to corroborate the suggested model. To formulate concrete mixtures highly resistant to ASR, a sequence of steps to determine threshold total alkali are presented in the last section of this chapter.

Concrete Characteristics

The interpretation of NMR and PRG concrete expansion tests are presented in this section. For each experiment, pH readings were recorded using a pH meter. Following each test, alkali ions measurements (Na^+, Ca^{+2}, and K^+) were conducted using a flame photometer.

New Mexico Rhyolite

For New Mexico Rhyolite (NMR) testing, concrete was mixed at a water cement ratio of 0.45 and 25% of the cement content was replaced with class F Fly ash. Type I/II low alkali cement and non reactive sand were used in the mixture and the coarse aggregate factor was 0.7. The cement: fly ash: fine aggregate: coarse aggregate ratio was 1.00:0.46:5.51:3.69 (volumetric). To determine the effect of alkalinity on the concrete samples, three tests were conducted at three different alkalinity levels: 1 NaOH + CH, 0.5 NaOH + CH, and 0.25 NaOH + CH (CH = calcium hydroxide). All concrete tests were performed at 70 ^{0}C. The volume expansion test results for the NMR concrete are shown in Figure 6.1. For the concrete tested in the 1 NaOH + CH solution (Figure 6.1a), measurable expansion started after 12 hours. This was followed by a rapid increase in the
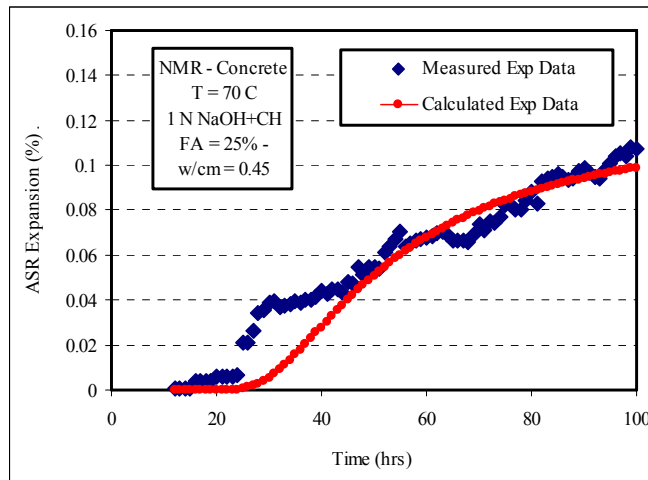
(a) NMR expansion at 1N NaOH + CH
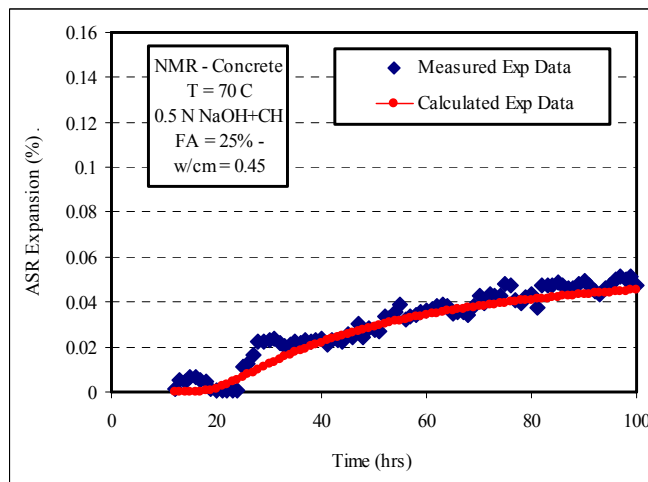
(b) NMR expansion at 0.5N NaOH + CH
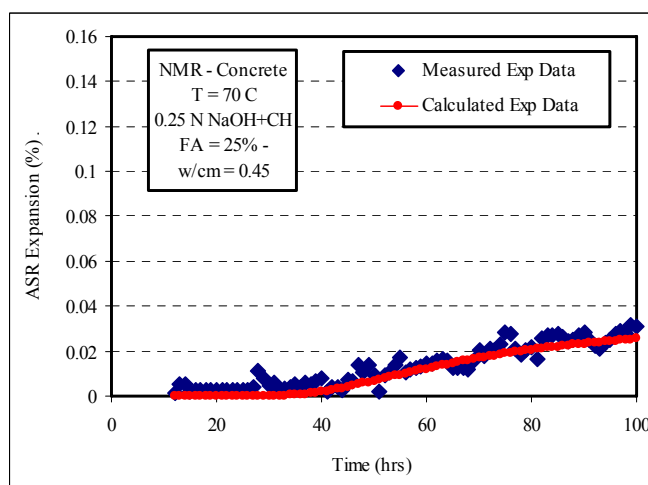
(c) NMR expansion at 0.25N NaOH + CH

Figure 6.1 Concrete NMR Expansion.

volume expansion until the end of the testing period of 100 hrs culminating at 0.1% volume expansion. On the other hand, the concrete specimens tested in 0.25 NaOH + CH solution showed no expansion until 40 hrs followed by an increase in expansion with constant slow rate till 100 hrs reaching around 0.03% volume expansion until 100 hrs. This difference between the time necessary to initiate ASR expansion for 1 NaOH + CH and 0.25 NaOH + CH is mainly because of the difference in concentration (e.g., normality) of the soak solutions. The higher the alkalinity of the solutions, the sooner the ASR is developed and consequently the ASR gel is formed. Therefore, one can expect that concrete structures in the field which are subjected to a high alkali environment will display expansion and cracking earlier as opposed to pavement structures exposed to mild alkali conditions.

To illustrate the effect of alkalinity of the test solution on NMR concrete, the ultimate expansion was determined for the three tests. The expansion data was fitted using the same numerical model proposed for the aggregate. The plots of the calculated ASR expansion are superimposed on the measured ASR expansion data as shown in Figure 6.1 and a reasonably good fit between calculated and measured plots is manifested.

The model parameters [ε_0, ρ, t_0, β] corresponding to the calculated expansion are presented in Table 6.1. Those were determined using the system identification method. A comparison of the ε_0 at three different alkalinities is presented in Figure 6.2. As shown, the concrete tested in the 1 NaOH + CH solution shows the highest ultimate expansion (i.e. 0.1126) and the one tested in 0.25 NaOH + CH solutions shows the lowest ultimate expansion ((i.e., 0.0345). The ultimate expansion of the concrete tested in the 0.5 NaOH + CH solution is 0.0756, which is in between the two limiting values. This observation suggests that alkalinity plays a major role in the expansion characteristics of concrete. As the alkalinity of the test solutions increase, more hydroxyl ions become available and diffuse into the matrix of the concrete along with the available alkali ions (e.g., Na^+) and attack the reactive aggregate leading to the dissolution of the silica. This is confirmed by the chemistry of the soak solutions presented in Table 6.2. For example, for the NMR concrete tested in the 1 NaOH + CH solutions, the pH was 14.009 at the beginning of the test, and then dropped down to 13.718, indicating that hydroxyl ions were consumed in the reaction and therefore, their concentration in the soak solutions diminish.

Table 6.1 NMR Concrete Parameters Results.

NMR Concrete - Type I/II cement - 25% FA (class F) - w/cm = 0.45			
	Alkalinity of Test Solution		
	0.25N NaOH + CH	0.5N NaOH + CH	1N NaOH + CH
$\varepsilon_{0\,(\%)}$	0.0345	0.0756	0.1126
ρ	49.936	36.131	33.536
t_0 (hrs)	8.623	11.758	9.707
β	2.102	0.919	1.952
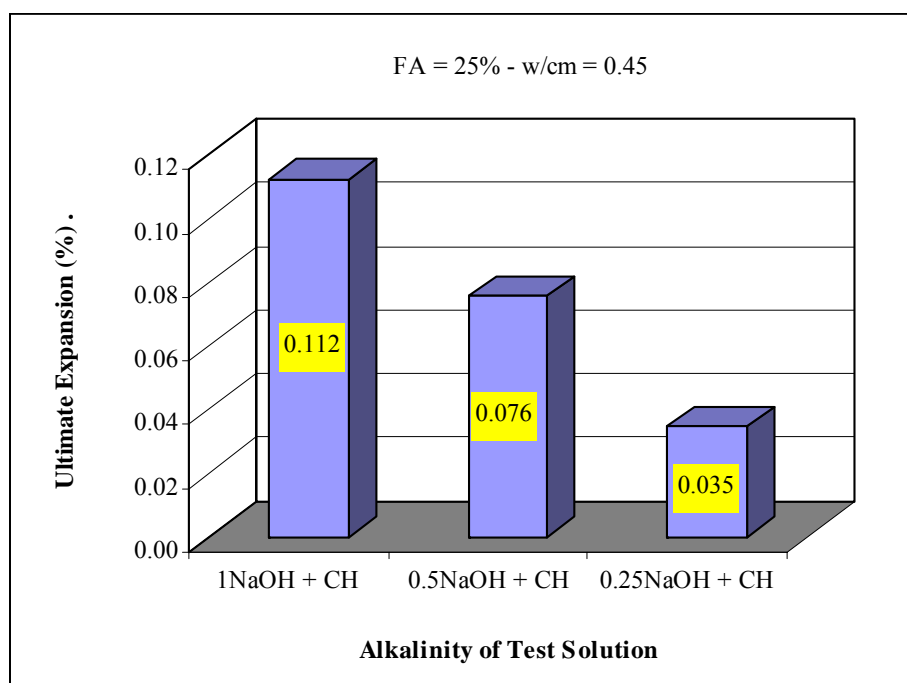
Figure 6.2 Effect of Test Solution Alkalinity on the ε_0 of NMR Concrete.

Since CH, one of the main chemical products of the hydration of cement is available in the concrete, it is possible that it blocks the diffusion of dissolved silica and consequently a thin layer of gel will be formed around the surface of the rock. The above theory is not new as it is initially proposed by previous research conducted with ASR (Chatterji et al. 1988, Chatterji et al 1986). In the case of test solutions with higher concentration than the concrete pore solution, a continuous supply of OH^-, Na^+, Ca^{2+} ions from the soak solution to the concrete specimens is maintained. The thickness of the gel layer increases with time. Since the ASR gel is hygroscopic, it absorbs water leading to

its expansion. Since the aggregate is surrounded by the mortar, tension stresses develop. As pressure builds up, micro-cracks appear in the paste as well as the aggregate. The gel diffuses through the cracks, absorbs more water and expands the concrete as a result. It should be mentioned here that all concrete samples were cured for 14 days after casting. Accordingly, the concrete is in a saturated condition and the diffusion of ions in or out of the concrete becomes much faster.

In a previous part of this study, the NMR aggregates were tested in the dilatometer at 70 ^{0}C in three different alkali solutions (1 NaOH + CH, 0.5 NaOH + CH, and 0.25 NaOH + CH) similar to the concrete testing. CH was added to the NaOH solution to simulate the pore solution of the concrete. The ultimate expansion of the aggregate was equal to 0.0537 %, 0.1023 %, 0.1134 % for 0.25 NaOH + CH, 0.5 NaOH + CH, and 1 NaOH + CH respectively.

To compare the ultimate expansion of aggregate and concrete, the expansion ratio $r = \left[\dfrac{\varepsilon_0(conc)}{\varepsilon_0(agg)} \right]$ introduced previously in Chapter IV is calculated. The results are shown in Figure 6.3. Some important observations can be made based on the results in Figure 6.3. The ratio r at 1 NaOH + CH is equal to 0.987 indicating that the ultimate expansion of concrete is almost equal to the ultimate expansion of aggregate. This appears to be surprising because the aggregate is surrounded by the cement paste and the latter was expected to provide restraining effects as well as some barrier against hydroxyl and other ions coming from the alkali solutions. But this doesn't look to be the case. The most reasonable explanation is the concrete at this stage is still very porous, especially at a water/cement ratio of 0.45 and the transition zone between the aggregate and the paste is still very weak, although the mix contains 25% class F fly ash. It is known that fly ash increases the durability of concrete through the pozzolanic reaction. At the same time, it is known from the literature, that the mechanical properties of concrete (i.e. compressive strength) are much weaker in its earlier stage than the concrete containing no fly ash. But once the pozzolanic reaction initiates, concrete microstructure becomes more dense with time as calcium hydroxide is transformed to calcium silicate hydrate. The same analogy can be applied here, in relation to the diffusion of ions though the interior of the concrete.

Table 6.2 NMR Soak Solution Chemistry Before and After the Test.

Aggregate type	Test Conditions	Alkalinity (NaOH)	Temp (^{0}C)	pH	Alkali Concentration (ppm) before testing			pH	Alkali Concentration (ppm) after testing		
					Na^+	K^+	Ca^{+2}		Na^+	k^+	Ca^{+2}
New Mexico Rhyolite	w/cm = 0.45 FA =25%	1N + CH	70	14.009	23605	0	486	13.718	18770	79.9	253.1
		0.5N + CH	70	13.708	11755	0	486	13.611	9883	71.1	240.8
		0.25N + CH	70	13.399	5877	0	486	13.354	5962	94.3	255.5
	w/cm = 0.45 FA =0%	1N + CH	70	14.009	23605	0	486	13.651	17372	83.4	262.1
		0.5N + CH	70	13.708	11755	0	486	13.433	8887	74.4	270.7
		0.25N + CH	70	13.399	5877	0	486	13.411	5811	77.0	280.8

FA = 25% - w/cm = 0.45
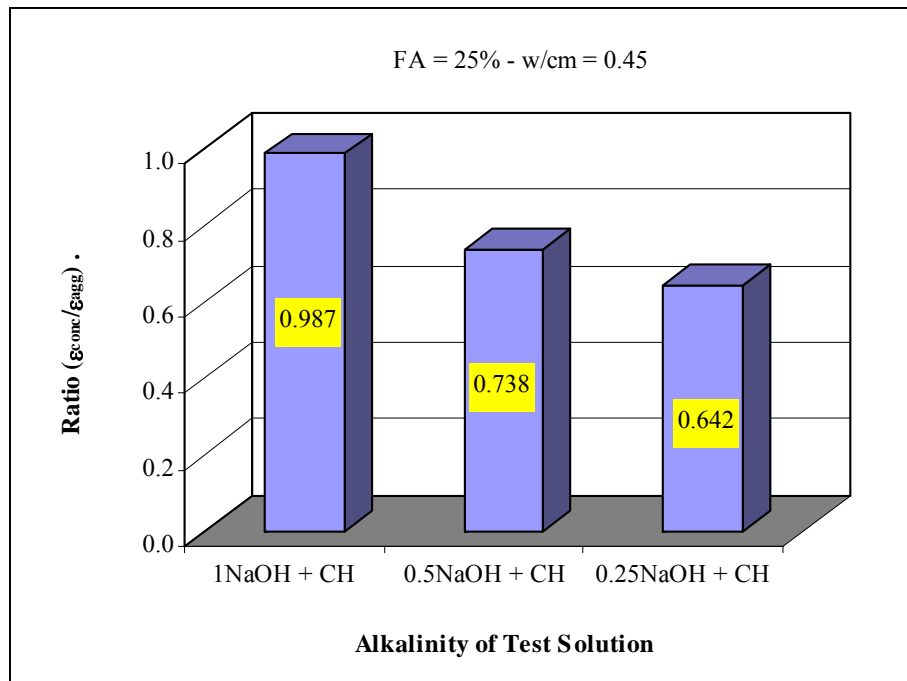
Figure 6.3 Effect of Alkalinity on the Expansion Ratio $\left[\dfrac{\varepsilon_0(conc)}{\varepsilon_0(agg)}\right]$ of NMR Concrete.

It appears that the concrete remains highly permeable to ions coming from outside the matrix, resulting in an excessive expansion (more porous and permeable concrete may allow more ion migration, thereby inducing a higher rate of reaction but it can also offer more space to accommodate the gel that is formed and thereby, may cause less expansion. The high recorded volumetric expansion of the NMR concrete indicates that the pozzolanic reaction is still at its early age.

Another complementary explanation to the similar volume expansion of aggregate and concrete is the presence of an alkali gradient. It is known that the pH of the pore solution of concrete is around 13.5 and this corresponds to a value between the 0.5N NaOH + CH and 0.25 NaOH + CH solutions. For the concrete test conducted at 1NaOH + CH, the pH of the alkali solution is slightly higher than 14 while the pH of the pore solution is expected to be around 13.25-13.5. Consequently, an alkali gradient was developed leading to the forced migration of hydroxyl ions. The pH decreases from 14.009 to 13.718 toward the inner of concrete in order to achieve equilibrium. The above

mentioned gradient is demonstrated by a sharp decrease in the Na^+ concentration from 23605 ppm to 18770 ppm at the end of the test; this is equivalent to a 20% decrease. As a result of the above two possible explanations, the concrete resistance is weakened by 1) the presence of fly ash and 2) the presence of an alkali gradient.

For the second concrete test performed at 0.5N NaOH + CH, the ultimate expansion of the concrete decreases from 0.1126 % to 0.0756% and the expansion ratio r decreases as well from 0.987 to 0.738. This was expected as the effect of the alkali gradient is reduced to a minimum since the difference in pH between the alkali solution and the pore solution of the concrete is also reduced. Solution chemistry confirms this gradient decrease as the Na^+ concentration decreases from 11755 ppm to 9883 ppm and this corresponds to a 15.9% reduction.

For the third concrete test conducted in a 0.25 N NaOH + CH solution, the gradient is expected to occur in the opposite direction (i.e. the alkali concentration of the pore solution is higher than the alkali concentration of the test solution). As a result, the ultimate expansion was recorded at 0.0345% and the expansion ratio decreases again from 0.738 to 0.642. This point of view is supported from the results of Table 6.2 as there is very little difference in the pH value before and after the test (13.399 versus 13.354). A similar deduction can be made concerning the Na^+ concentration (5877 ppm before the test versus 5962 ppm after the test). This suggests that equilibrium is achieved between the pore solution of concrete and soak solution. It should be mentioned here that the volume expansion of concrete is a result of hydroxyl and alkali attack coming from two different sources: the first from the cement itself and the second from the alkali solutions in which the concrete is immersed.

Platte River Gravel

For the concrete made with Platte River Gravel (PRG), ASTM C1260 molds were used during casting. In order to make a comparison between the NMR and PRG results, similar mix design factors were selected; i.e. (CF = 6, w/cm = 0.45). To illustrate the significance of the alkali solutions on the PRG mortar, two experiments at 70^0C were performed at 1 NaOH + CH and 0.5 NaOH + CH. The volumetric expansion results of

the PRG concrete are shown in Figure 6.4. It should be noted that each plot is an average of two as each test was repeated twice to check the repeatability of the procedure. As shown in the plots, both curves at both alkalinities show similar characteristic patterns. Almost no expansion is measured in the first couple of hours. This first phase can be called the dormant period as alkali ions from the soak solutions begin to diffuse through the interior of the concrete and attack the reactive siliceous gravel. The second period extends from the 10-15 hrs up to the 100 hrs where the % expansion reaches 0.035% and 0.02% for PRG conducted at 1 NaOH + CH and 0.5 NaOH + CH solutions, respectively. As shown from the plots, the alkali content of the soak solution has a significant influence on the expansion of mortar bars.

In order to make a quantitative comparison of the effect of alkalinity on mortar, the expansion characteristics were calculated using the numerical model proposed previously for the aggregate. The parameters of the model were calculated using the system identification method. The calculated expansion data were superimposed on the measured data in Figure 6.4 it can be seen that the model fits the data well. The PRG mortar characteristics are presented in Table 6.3. As shown from the table, the consequence of increasing the alkalinity of the soak solution is evident in the ultimate expansion (ε_0), the theoretical initial time (t_0) and on the rate constant (β); i.e. at in the 1 NaOH + CH solution, the ε_0 is 0.035% while it is 0.024% in the 0.5 NaOH + CH solution (Figure 6.4) and β also goes up as well from 1.274 to 1.332. This is explained as follows: as higher alkalinity indicates a higher abundance of hydroxyl ions in soak solution, the sooner the hydroxyl ions penetrate through the mortar pores, the sooner the ASR is started and gel is formed. Consequently, a greater amount of expansion is recorded by the data acquisition system. This is manifested by a higher rate constant and lower initiation time at higher alkalinity (t_0 =7.48 hrs at 1 NaOH + CH versus t_0 = 8.379 hrs at 0.5 NaOH + CH).
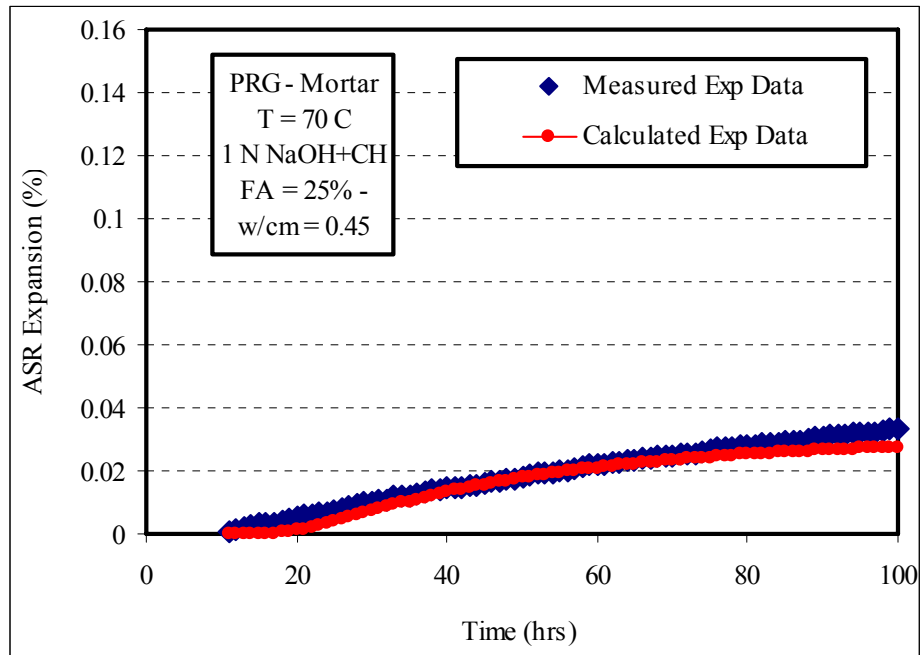
(a) PRG expansion in 1N NaOH + CH solution
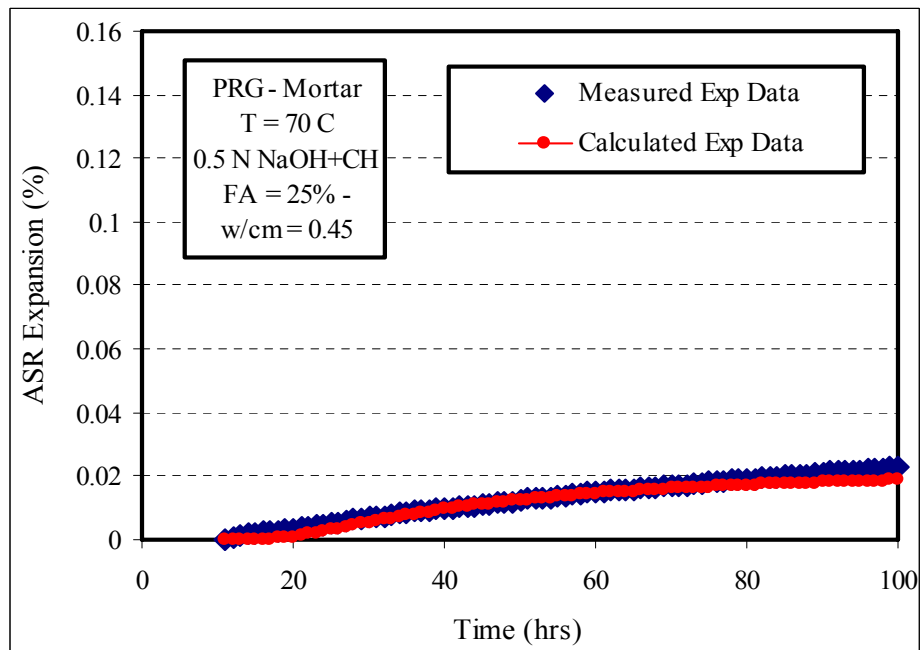
(b) PRG expansion in 0.5N NaOH + CH solution

Figure 6.4 Mortar Expansion.

Table 6.3 PRG Mortar Parameters Results (First Set).

PRG Mortar - Type I/II cement - 25% FA (class F) - w/cm = 0.45		
	Alkalinity of Test Solution	
	0.5N NaOH + CH	1N NaOH + CH
ε_u	0.0236	0.0353
ρ	26.962	29.493
t_e	8.379	7.480
β	1.274	1.332

The previous explanation is supported by the chemistry of the soak solutions before and after the tests. The results are presented in Table 6.4. As shown in the table, pH values decreases from 14.009 before the test to 13.805 after the test. This corresponds to a 20% decrease in hydroxyl ion concentration. This indicates that hydroxyl ions were consumed in the reaction. However, it is important to observe that the pH values did not change after the test for the PRG mortar conducted at 0.5 NaOH + CH (13.708 before versus 13.709 after), although measured expansion was recorded. This is a clear indication that mortar made with reactive aggregate can be expansive despite the use of low alkali cement (type I/II) and 25% class F fly ash. This suggests that mortar is still permeable at this stage and therefore a higher percentage of supplementary cementitious materials may be needed or this may be an indication that the pozzolanic reaction did not yet achieve its peak. The occurrence of the reaction is further manifested by the decrease of Na^+ ions after the test with both alkalinities. For example, for PRG conducted at 1 NaOH + CH, the Na^+ ions concentration drops down from 23605 ppm to 21164 ppm, this is equivalent to 2441 ppm while the decrease is 1280 ppm for PRG conducted at 0.5 NaOH + CH. Thus it can be concluded that increasing alkalinity enhances ASR, as the power of diffusion of alkali ions becomes higher and faster and consequently, a higher ultimate expansion is expected. Results of ASR characteristics support this point of view (Figure 6.5).It can also be seen from Table 6.4 that (K^+) ions were measured after the test although the initial alkali soak solution did not contain potassium. This suggests that (K^+) ions leach out from the mortar bars.

Table 6.4 PRG Soak Solution Chemistry Before and After the Test.

Aggregate type	Test Conditions	Alkalinity (NaOH)	Temp (^{0}C)	pH	Alkali Concentration (ppm) before testing			pH	Alkali Concentration (ppm) after testing		
					Na$^+$	K$^+$	Ca^{+2}		Na$^+$	k$^+$	Ca^{+2}
Platte River Gravel	w/cm = 0.45 FA =25%	1N + CH	70	14.009	23605	0	486	13.805	21164	27.8	259.5
		0.5N + CH	70	13.708	11755	0	486	13.709	10475	23.2	267.3
	w/cm = 0.45 FA =50%	1N + CH	70	14.009	23605	0	486	13.985	23878	25.4	415.2
		0.5N + CH	70	13.708	11755	0	486	13.703	11603	15.9	427.5
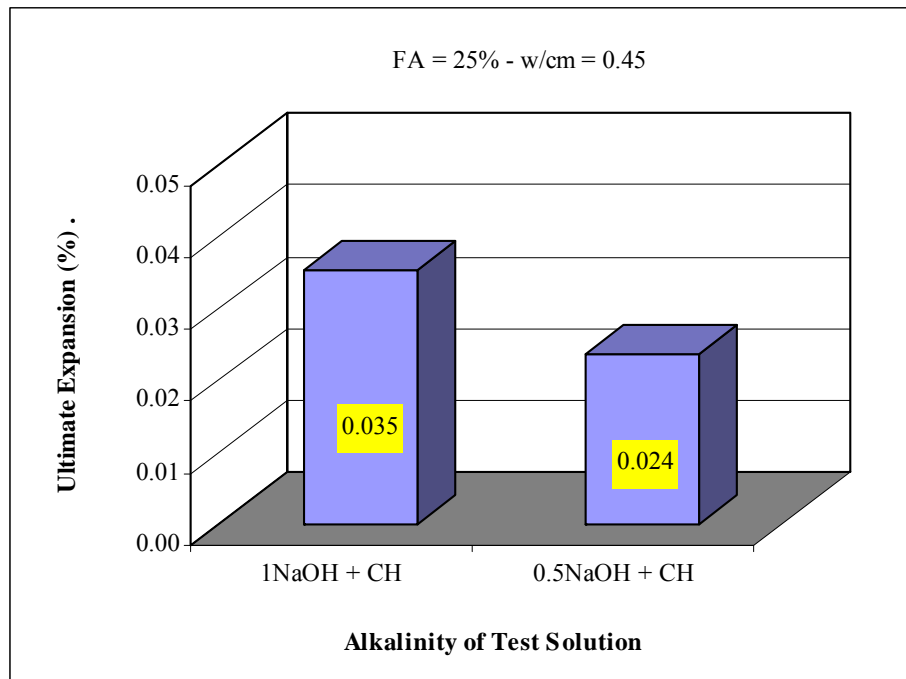
Figure 6.5 Effect of Test Solution Alkalinity on the ε_0 of PRG Mortar (with FA).

A comparison is made between the ultimate expansion of NMR concrete and PRG mortar. This is possible since all mix design parameters are the same. By comparing Figures 6.2 and 6.5 for tests conducted at 1N NaOH + CH, the ε_0 for NMR concrete was 0.112 % while it was 0.035% for PRG mortar. Similar deduction can be made for tests performed at 0.5N NaOH + CH. Therefore it can be deduced that NMR concrete is more reactive than PRG mortar. The results of NMR concrete and PRG mortar corroborated the previous results shown in Chapter V. In other words, the above comparison of the ε_0 of NMR concrete and PRG mortar is very consistent with ASR aggregate characteristics results determined at 70^0C earlier in Chapter V where the ε_0 of NMR aggregate (0.1134 %) is much higher than the ε_0 of PRG aggregate (0.036 %). A similar deduction is also possible by comparing the E_a of both aggregates (46.46 KJ/mol for PRG versus 10.72 KJ/mol for NMR). Consequently, it can be concluded that the type of reactive aggregate used in concrete mixtures is the main parameter that determines the expansion that may occur in concrete pavement. Although, the above comparison is made, it is

necessary to comment that the ε_0 comparison may not be entirely appropriate because the NMR and PRG molds are different.

In a previous part of this study, the PRG aggregates were tested in the dilatometer at 70 ^{0}C at two different alkali solutions (1 NaOH + CH and 0.5 NaOH + CH) similar to the concrete testing. Calcium hydroxide was added to the NaOH solution to simulate the pore solution of the concrete. The ultimate expansion of the aggregate was equal to 0.034 %, 0.036 %, for 1 NaOH + CH and 0.5 NaOH + CH solutions, respectively. As in the previous section, the expansion ratio $r = \left[\dfrac{\varepsilon_0(conc)}{\varepsilon_0(agg)} \right]$ was determined. It should be stated here that the factors that effect ASR is different for each. When the PRG aggregate is tested in the dilatometer, the progress of the chemical reaction is totally determined by the degree of crystallinity and the number of the reaction sites exposed to alkali hydroxide ions. On the other side, the reaction in mortar samples depends on the availability of alkali ions in the matrix in addition to the permeability of the mortar. Temperature is also a factor in both cases.

The expansion ratio results are presented in Figure 6.6. Several points need to point out based on the plots. The ratio r for both experiments is 0.957 and 0.868 for tests performed with 1 NaOH + CH and 0.5 NaOH + CH solutions, respectively. This is considered significantly high. This can be explained as the combined effects of two concurrent causes: the first is that it is known that siliceous gravel has a smooth surface texture. This will lead to the formation of weak bond between the cement paste and the aggregate. This weaker bond will eventually help the formation of a weak transition zone. Thus, the permeability of concrete will increase by providing channels to the alkali ions in the soak solution to diffuse through the interior of the concrete. Another possible reason is as follows: in general, in concrete mixtures, solid materials settle while excess water migrates to the surface. Although this will result in the formation of a thin weak layer at the surface of the pavement, it is highly possible that this surface can provide a shielding effect for the top surface, avoiding direct contact between aggressive ions from the environment and the interface zone at top of the concrete pavement. In the case of the NMR concrete and PRG mortar, this possible protective layer does not exist since the dimensions of the molds (1×1×1.25") doesn't permit this stratum to be formed and

consequently, the aggregate surface is in direct contact with the alkali ions from the solutions, resulting in a higher diffusion rate and as a result higher permeability of the concrete. Therefore, restraint provided by the cement paste is at a minimum relative to concrete.
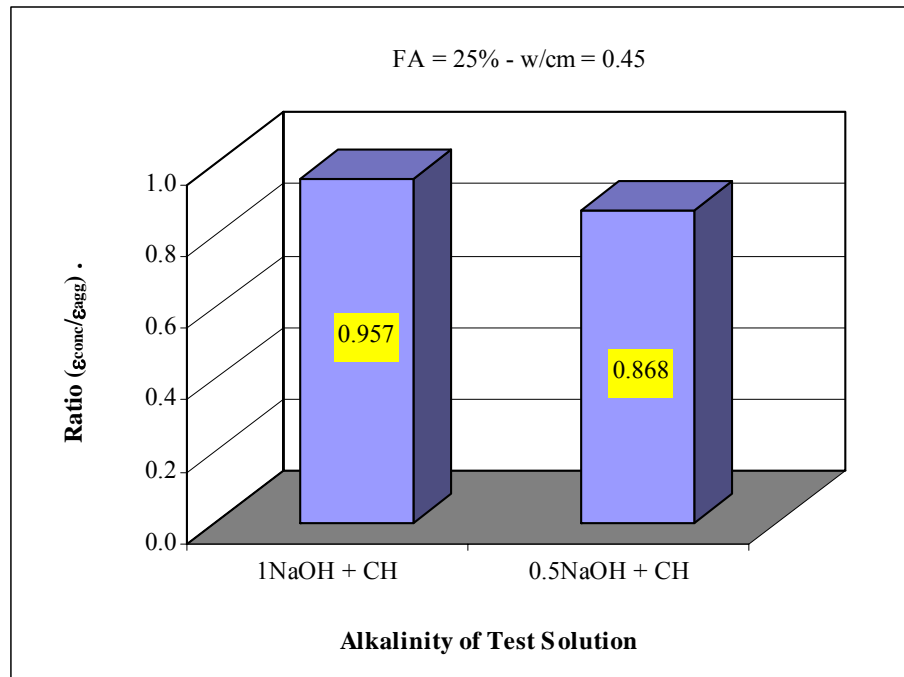
Figure 6.6 Effect of Alkalinity on the Ratio $\left[\dfrac{\varepsilon_0(conc)}{\varepsilon_0(agg)}\right]$ of PRG Mortar (with FA).

Determination of E_a Matching with Field Conditions of Alkalinity - NMR

To formulate concrete mixtures highly resistant to ASR, the aggregate activation energy (E_a), alkalinity, and the concrete mixture design parameters (water cement ratio, fly ash, etc) need to be linked through a robust and reliable approach. The first step in this approach is to link the alkalinity of the soak solution and the (E_a) of aggregate. In the test program outlined in Chapter III, NMR aggregates were tested at three different alkalinities (1 NaOH + CH, 0.5 NaOH + CH, 0.25 NaOH + CH). This corresponds to pH values between 13.39 and 14. The pore solution in concrete may achieve these high values depending on a) the form of reactive silica in the aggregate (amorphous, etc), b)

the permeability of the concrete and c) the availability of alkali ions in the matrix. However, in other cases where the presence of supplementary cementitious materials binds the movement of alkali ions in the matrix, the concentration of hydroxyl ions drops down to achieve equilibrium and therefore the pH of the solution goes down as well. Since the dilatometer test is unlikely to be conducted at a very low alkalinity (i.e. less than 0.1N NaOH or pH =13) because no measurable expansion can be recorded within a reasonable period of time. Consequently, it becomes vital to predict the activation energy needed to initiate ASR at lower pH values.

To achieve this objective, the following model; linking the alkali of the soak solution and alkalinity; introduced initially in Chapter IV is used.

$$E_a = E_{a_0} + \frac{C_1}{C^n} \tag{6.1}$$

where:

E_a = Activation Energy $\left[\dfrac{KJ}{mol} \right]$

E_{a_0} = Activation Energy - Threshold $\left[\dfrac{KJ}{mol} \right]$

C_1 = Activation Energy Curvature Coefficient $\left[\dfrac{KJ}{(mol)^{1-n}} \right]$

n = Activation Energy Curvature Exponent

C = Alkalinity (mol)

As shown from the proposed model, the E_a and C are known values and those correspond to the activation energy of the aggregate at a specific levels of alkalinity. Those were determined previously in Chapter V. The parameters to be determined are E_{a_0}, C_1, and n. System identification method was used in this case. For this reason, the sensitivity matrix, change vector and residual vectors were defined and set up. Since the process of determining those parameters is an iteration process, a matlab routine was developed for that purpose. The detailed description of the algorithm followed is presented in Chapter IV. The results obtained are presented below:

$E_{a_0} = 5.956$, $C_1 = 4.821$, $n = 1.327$

By substituting the above calculated parameters in the model, Eq. 6.1 becomes as follows

$$E_a = 5.95 + \frac{4.82}{C^{1.33}} \qquad\qquad (6.2)$$

To demonstrate the accuracy of the proposed model, the predicted E_a is plotted versus the measured E_a. Results are presented in Figure 6.7. As shown from the plots, the model fit to the measured data is appropriate and accurate.

The shape of the curve ("POWER CURVE") is important and illustrates the effect of alkalinity on E_a. As shown, the alkalinity and the E_a have an inversely proportional relationship. For example, the E_a is 34.2 kJ/mol at 0.25 N NaOH+CH whereas it is 10.7 KJ/mol at 1 N NaOH+CH. Two valuable pieces of information can be noticed by looking at the values of E_a at low (i.e. less than 0.25N) and at high alkalinity (i.e. higher than 1N).

The first point noticed is that the E_a values decrease slightly once the alkalinity increases above 1N as it approaches the threshold value of 5.95 KJ/mol. For example, at the 1N levels, the E_a is 10.7 KJ/mol while it is 7.9 KJ/mol from the predicted model at 2 N. This can be explained as follows: the amount of aggregate tested in the dilatometer is constant and therefore the total surface area of the reactive aggregate is constant as well. Therefore increasing the alkalinity beyond a specific amount will not decrease the amount of E_a significantly since the reaction sites on the surface of the aggregate were fully saturated by the hydroxyl ions coming from the soak solutions. Thus increasing alkalinity will induce only minimal change on the E_a values.

On the other side, the E_a values increase greatly as alkalinity of the soak solutions decreases below 0.25 N. For example, the E_a is 34.27 KJ/mol at 0.25 N while it is 108.5 KJ/mol (from the predicted model) at 0.1N. This significant increase can be explained as follows: at lower alkalinity (0.1N), the amount of hydroxyl ions is smaller than at higher alkalinity (0.25N) and therefore the number of aggregate reaction sites is considerably lower than the number at higher alkalinity. To compensate for this decrease, larger values of E_a are expected. It should be mentioned that from a theoretical point of view, the necessary E_a may reach infinity at very low alkalinity. These two above

explanations are very consistent with the definition of E_a mentioned earlier in Chapter V, as the energy required to initiate ASR.
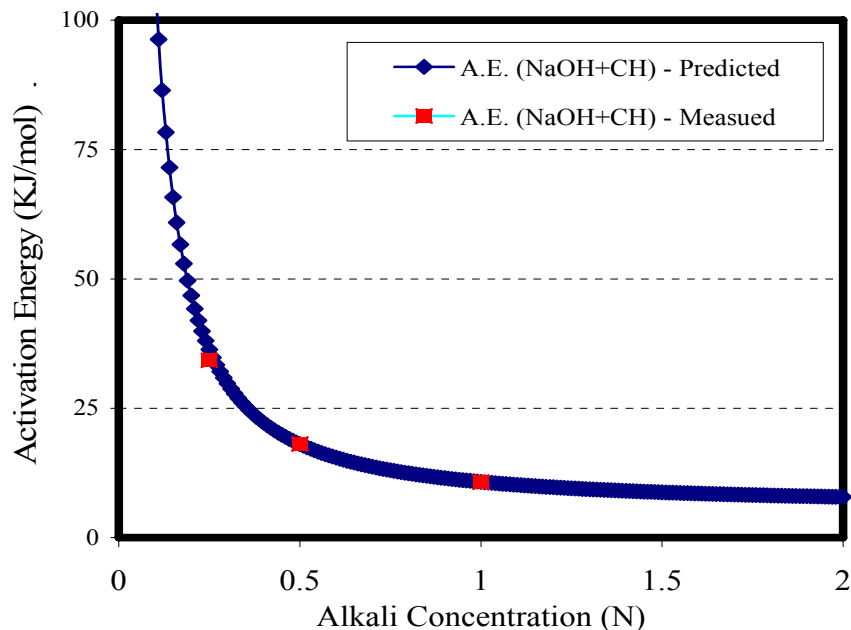
Figure 6.7 Effect of Alkalinity on the E_a of NMR.

Development of a Reaction Signature for NMR Combined Concrete Materials

The price of repairing and/or demolishing concrete structures has increased over the years. Therefore, it becomes vital to select for our concrete mixtures, sound materials resulting in maintenance free service structures that last for long periods of time.

As mentioned before in Chapter II, ASR is a durability problem. The main parameter that affects durability of concrete is its permeability. Higher permeability indicates that alkali ions can move freely though the concrete matrix. The main parameter that controls the permeability of concrete is the water cement ratio (w/cm) as higher w/cm results in highly permeable concrete and consequently, structures will be more susceptible to ASR.

To mitigate the detrimental effects of ASR, agencies and contractors used supplementary cementitious materials (SCM's) (e.g. fly ash) in different amounts based

on previous field performance, but their selection is mainly empirical and the effect of adding different amount of those SCM's on ASR remains unknown. Therefore, it becomes very beneficial for designers to have a tool and/or test protocol within their hands to predict the effect of the main factors (w/cm, SCM's) that control ASR in concrete structures.

To achieve this objective, a model was developed following the Juarez-Badillo procedure (Juarez-Badillo 1981). The deduction of the model was presented in details in Chapter IV. The proposed model below links the expansion ratio r, the E_a of the aggregate, w/cm and the % of fly ash used in concrete mixtures.

$$r = \frac{r_{min} + r_{max}\left[C.(\frac{f}{f_{max}-f})^\beta.(\frac{E_a-E_{a_{min}}}{E_{a_{max}}-E_a})^\alpha.(\frac{w-w_{min}}{w_{max}-w})^\gamma\right]}{1+C.(\frac{f}{f_{max}-f})^\beta.(\frac{E_a-E_{a_{min}}}{E_{a_{max}}-E_a})^\alpha.(\frac{w-w_{min}}{w_{max}-w})^\gamma)} \tag{6.3}$$

Where:

$r = (\frac{\varepsilon_u}{\varepsilon_a})$

$\varepsilon_u =$ Ultimate Expansion of Concrete (%)

$\varepsilon_a =$ Ultimate Expansion of Aggregate (%)

$f =$ % of Fly Ash used in the Mixture

$f_{max} =$ Max % of Fly Ash

$E_a =$ Activation Energy $\left[\dfrac{KJ}{mol}\right]$

$E_{a_{min}} =$ Min. Activation Energy $\left[\dfrac{KJ}{mol}\right]$

w = Water cement ratio (w/cm)

$w_{min} =$ Min. w/cm

$w_{max} =$ Max. w/cm

C, β, α, γ = non dimensional parameters of proportionality

As shown from the proposed model, the E_a and r are known values and those corresponds to the activation energy of aggregate and the expansion ratio at a specific alkalinity. Those were determined in the previous section of this chapter. The parameters

to be determined are C, β, α and γ. Before determining, the boundary conditions were set up as follows:

(a) It is known that the first component of ASR is the dissolution of silica from the aggregate. The amount dissolved is directly related to the pH of the pore solution as high pH values increases the dissolution process. Tang and Su-Fen in 1980 found that the solubility of amorphous silica increases dramatically from 10 mm/L at pH 12.6 to 70 mm/L at pH 13. Therefore, pH values of 12.6 were chosen as a threshold for the pore solution of concrete and this corresponds to an E_a equal to 400 (based on the previous model). Thus $E_{a_{max}}$ = 400 KJ/mol.

(b) As noted earlier, the use of fly ash is common to control ASR and to improve the durability of concrete. Chatterji, et al. 1986 mentioned that if sufficient amount of mineral admixtures are added, ASR may be restrained as calcium hydroxide is consumed during the pozzolanic reaction. Therefore, there is interest in predicting the effect of high dosage of fly ash on ASR. So, the f_{max} (Max % of Fly Ash) was assumed to be 55%.

(c) The presence of water is essential for ASR gel to expand and this is governed by the amount of water available in the concrete matrix after hydration occurs. The minimum and maximum water cement ratio were selected close to ones used in concrete mixture on the job-site ($w_{min} = 0.4$ $w_{max} = 0.55$).

By substituting the values of w_{min}, w_{max}, $E_{a_{min}}$, $E_{a_{max}}$ f_{max} in the proposed model, Eq. (6.3) becomes as follows:

$$r = \frac{C.\left[\frac{5}{6}\right]^{\beta}.\left[\frac{1}{2}\right]^{\gamma}\left[\frac{(E_a - 5.95)}{(400 - E_a)}\right]^{\alpha}}{1 + C.\left[\frac{5}{6}\right]^{\beta}.\left[\frac{1}{2}\right]^{\gamma}\left[\frac{(E_a - 5.95)}{(400 - E_a)}\right]^{\alpha}} \tag{6.4}$$

To determine C, β, α and γ, the system identification method is used. The detailed description of the algorithm followed is presented in Chapter IV. A matlab routine was developed to facilitate the calculation of the parameters. The results obtained are presented below:

$C = 2.617, \ \beta = -2.823, \ \gamma = 4.905, \ \alpha = -0.925$

By substituting the calculated parameters in the generalized model (Eq 6.3), the expression becomes as follows:

$$r = \frac{2.6178 \cdot \left[\dfrac{f}{0.55-f}\right]^{-2.8234} \cdot \left[\dfrac{w-0.4}{0.55-w}\right]^{4.9051} \left[\dfrac{(E_a-5.95)}{(400-E_a)}\right]^{-0.925}}{1 + \left[2.6178 \cdot \left[\dfrac{f}{0.55-f}\right]^{-2.8234} \cdot \left[\dfrac{w-0.4}{0.55-w}\right]^{4.9051} \left[\dfrac{(E_a-5.95)}{(400-E_a)}\right]^{-0.925}\right]} \tag{6.5}$$

The above equation can be expressed as follows:

$$\left(\frac{\varepsilon_u}{\varepsilon_a}\right) = \text{function } (f, E_a, w) \tag{6.6}$$

where:

f = fly ash

E_a = activation energy of aggregate at a specific alkalinity

w = water cement ratio

For NMR concrete mixtures, the amount of fly ash and water cement ratio is known from the design combinations (w/cm = 0.45 and FA = 25%) and therefore, those variables are constant in Eq. 6.6 which yields the following:

$$\text{(a) } \left(\frac{\varepsilon_u}{\varepsilon_a}\right) = \text{function } (f, E_a) \tag{6.7}$$

Eq. 6.7 can be expanded as follows:

$$r = \frac{87.36 \times 10^{-3} \cdot \left[\dfrac{f}{0.55-f}\right]^{-2.8234} \cdot \left[\dfrac{(E_a-5.95)}{(400-E_a)}\right]^{-0.925}}{1 + \left[87.36 \times 10^{-3} \cdot \left[\dfrac{f}{0.55-f}\right]^{-2.8234} \cdot \left[\dfrac{(E_a-5.95)}{(400-E_a)}\right]^{-0.925}\right]} \tag{6.8}$$

$$\text{(b) } \left(\frac{\varepsilon_u}{\varepsilon_a}\right) = \text{function } (E_a, w) \tag{6.9}$$

Eq. 6.9 can be expanded as follows:

$$r = \frac{4.38 \times \left[\dfrac{w-0.4}{0.55-w}\right]^{4.9051} \cdot \left[\dfrac{(E_a - 5.95)}{(400 - E_a)}\right]^{-0.925}}{1 + \left[4.38 \times \left[\dfrac{w-0.4}{0.55-w}\right]^{4.9051} \cdot \left[\dfrac{(E_a - 5.95)}{(400 - E_a)}\right]^{-0.925}\right]} \qquad (6.10)$$

Each of the above equations (6.8) and (6.10) leads to the development of

i)   A set of curves between $(\dfrac{\varepsilon_u}{\varepsilon_a})$ and E_a for different FA content (w = 0.45) (Figure 6.8).

ii) A set of curves between $(\dfrac{\varepsilon_u}{\varepsilon_a})$ and E_a for different w/cm (f = 25%) (Figure 6.9).

Figure 6.8 displays a set of relationships between the activation energy (E_a) and the expansion ratio (r) for NMR concrete mixtures with a w/cm = 0.45. As shown in the figure, some points are important to observe. The ratio r decreases as the E_a of the rock increases. A decrease in E_a is an indication that the rock is more reactive, thus the ε_u of NMR concrete will be higher, while the ε_a of aggregate will remain constant at a specific alkalinity and consequently r increases. The above deduction can be made irrespective of the amount of fly ash in the mixture.

Since the whole objective of this study is to find ways to mitigate ASR, the effect of SCM's (i.e. Fly ash, class F in this case) on ASR is of paramount importance. Thus, two comparisons can be made: a) The first between mixtures with and without fly ash and b) between concrete mixtures with different percents of fly ash content. Those comparisons can be made looking at the r values at a specific values of E_a. For example, at E_a = 150KJ/mol, the expansion ratio r is equal to 0.99 for concrete mixtures without fly ash, while it is 0.91 at 10% fly ash content. This is illustrated in Figure 6.8. This is likely due to the fact that the fly ash has reacted with the calcium hydroxide. As a result, the structure of the hydrated cement paste becomes denser, which blocks the movement of ions from one place to another. This decrease may also be due from the preferential reaction of the alkali coming from the fly ash and these alkalis may not be available to react with the dissolved silica of the rock (K. Wesche 1991). One has to mention here that fly ash also contains alkali, but only 16.66% of those are water soluble and therefore can

potentially contribute to ASR and the remaining alkalis are combined (Neville 1996). In addition, P.J. Nixon et al. 1986 mentioned fly ash alkali contribution to the pore water in concrete depends on the alkalinity of the cement used.

The second comparison is possible by comparing the r values at higher fly ash contents. For example, in Figure 6.8 at E_a = 150KJ/mol, the expansion ratio r is equal to 0.98, 0.91, 0.69, 0.41, 0.19, 0.07, 0.02 for mixtures containing 5%, 10%, 15%, 20%, 25%, 30%, 35% Fly Ash Class F respectively (Figure 6.8). It should be noticed here that the decrease in r values becomes negligible once the fly ash content reaches the 30% level (i.e. r is equal to 0.07 at 30% FA whereas it is 0.02 at 35% FA). This may be an indication that calcium hydroxide is almost consumed in the pozzolanic reaction at this percent of the fly ash amount.

Figure 6.9 exhibits a set of relationship between the activation energy (E_a) and the expansion ratio (r) for NMR concrete mixtures with 25 % fly ash. As shown in the figure, two points need to be mentioned. Similar to Figure 6.8, it can be observed that the expansion ratio r increases when E_a decreases. This is a clear indication that the boundary conditions were set properly using the Juarrez-Badillo Transform, as a higher value of E_a suggests that the aggregate reactivity is low. So, concrete mixtures made with this type of rock will display minimum expansion if any and therefore lower r values are obtained.
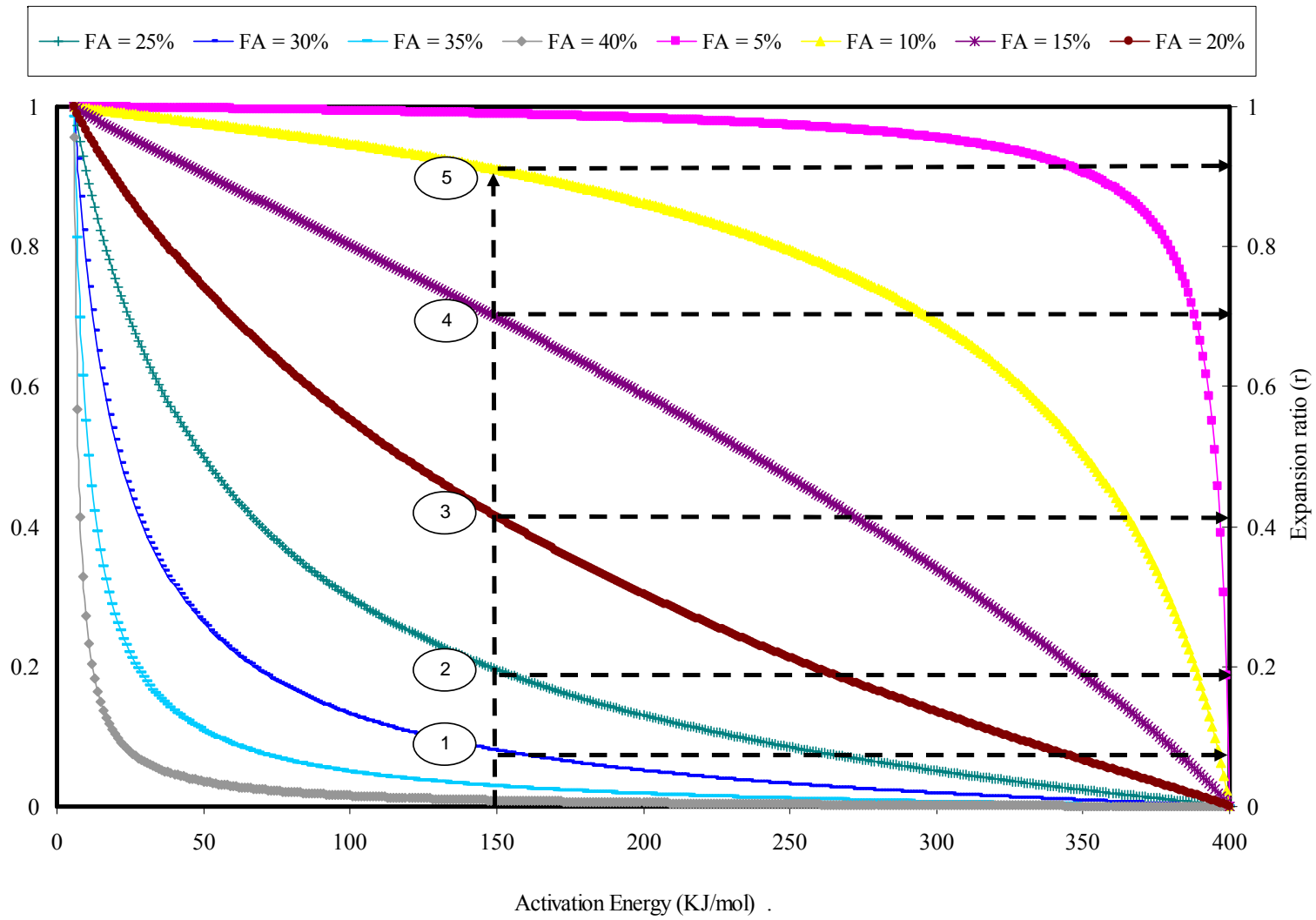
Figure 6.8 NMR Concrete Model (w/cm = 0.45).
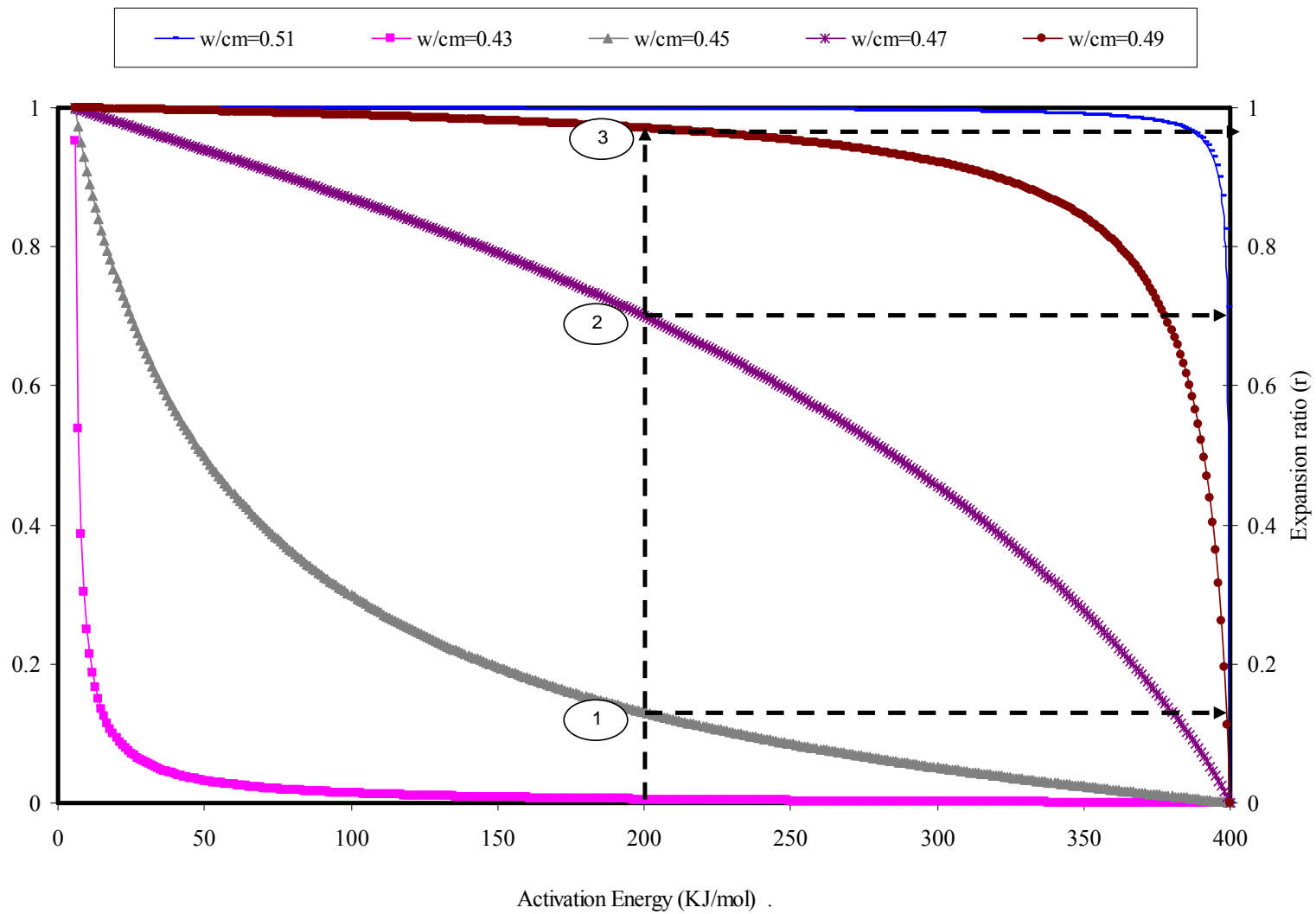
Figure 6.9 NMR Concrete Model (FA = 25%).

To be deleterious, ASR gel needs to be expansive. For ASR gel to swell, it needs to be in the vicinity of moisture. The water in concrete is found in the capillary and gel pores. The pores should be interconnected for water to diffuse toward the reaction sites around the aggregates. Therefore, high permeability is required for ASR to proceed. The water cement ratio (w/cm) is the main factor controlling the permeability, as high w/cm yields a highly porous system and therefore the movement of water molecules and other aggressive agents is rapid. As a result of the above, the effect of different w/cm on ASR characteristics is important to observe. For example, at E_a = 200KJ/mol, the expansion ratio r is equal to 0.048, 0.127, 0.694, 0.969, 0.998 for concrete mixtures at w/cm 0.43, 0.45, 0.47, 0.49, 0.51 respectively (Figure 6.9). It can be seen from the results that there is a sharp increase in r values at a w/cm ratios in excess of 0.45. One has to mention here that high r values indicate high concrete permeability as the ε_a of aggregate tested in the dilatometer is close to those of concrete. Neville 1996 mentioned that it is possible that the mature paste around the 0.4 w/cm ratio becomes segmented so that there is a huge difference in permeability above and below this number. Powers et al (1954) mentioned that the coefficient of permeability increases exponentially for mature cement paste at w/cm ratios higher than 0.45. The above are possible reasons for the high r values obtained for mixtures with w/cm above 0.45.

Validation of the NMR Concrete Model

To corroborate the previous NMR concrete model, $r_{measured}$ values should be compared with $r_{predicted}$ values. To accomplish this task, three concrete tests were conducted at 1 NaOH + CH, 0.5 NaOH + CH, and 0.25 NaOH + CH. Concrete was mixed at a water cement ratio of 0.45. Type I/II low alkali cement and non reactive sand were used in the mixture and the coarse aggregate factor was 0.7. No fly ash was used. The cement: fly ash: fine aggregate: coarse aggregate ratio was 1.00:0.00:5.51:1.48 (volumetric). All tests were conducted at 70 ^{0}C. The volume expansion test results for the NMR concrete are shown in Figure 6.10. In the initial hours, no expansion is recorded. This was followed by a rapid increase in the volume expansion until the end of the testing period of 100 hrs. The occurrence of the ASR is confirmed by comparing the pH of the alkali solution before and after the test (Table 6.2). For example, for the NMR concrete tested in the 1 NaOH + CH solutions, the pH was 14.009 at the beginning of the test, and then dropped down to 13.651, indicating that hydroxyl ions were consumed in the reaction and therefore, their concentration in the soak solutions were diminished. Similar pH observation can be made for NMR tested at 0.5 NaOH + CH while the difference in pH values before and after the test at 0.25 NaOH + CH is negligible. This maybe due to the equilibrium maintained between the pore solution of concrete and alkali soak solutions.

The time expansion data for NMR at 1N NaOH+CH and 0.5N NaOH+CH shows a sign of "double hump". The second abrupt expansion occurs at time equal to 70 and 78 hrs for NMR concrete tested at 1 and 0.5N NaOH+CH respectively. Those times corresponds to 550-650 micro-strains. This could be very well due to microcracking. To check this possibility, the nature of the linear trend between $Ln\left[-Ln\left(\varepsilon/\varepsilon_0\right)\right]$ and $Ln(t-t_0)$ is examined. Results are shown in Figure 6.11. It should be mentioned that the slope of the line represents the rate constant (β).
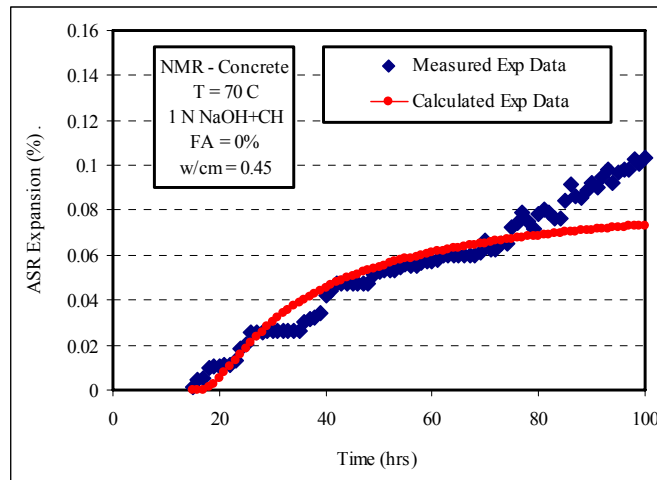
(a) NMR expansion at 1N NaOH + CH
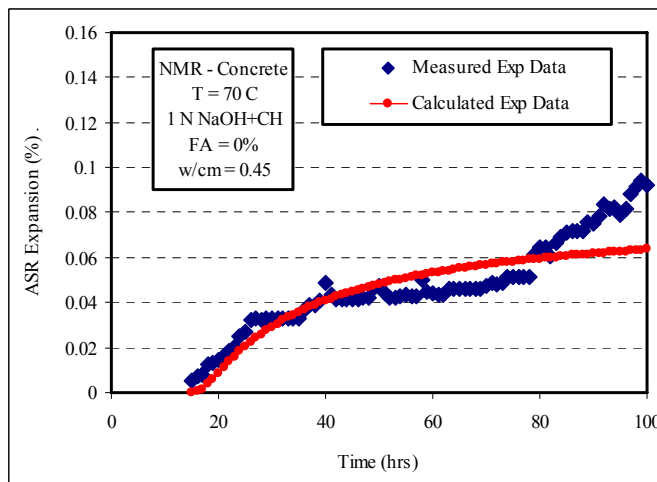
(b) NMR expansion at 0.5N NaOH + CH
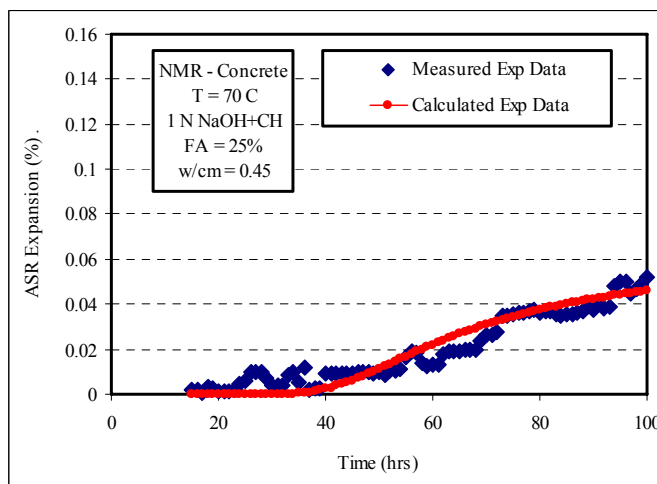
(c) NMR expansion at 0.25N NaOH + CH

Figure 6.10 Concrete NMR Expansion.
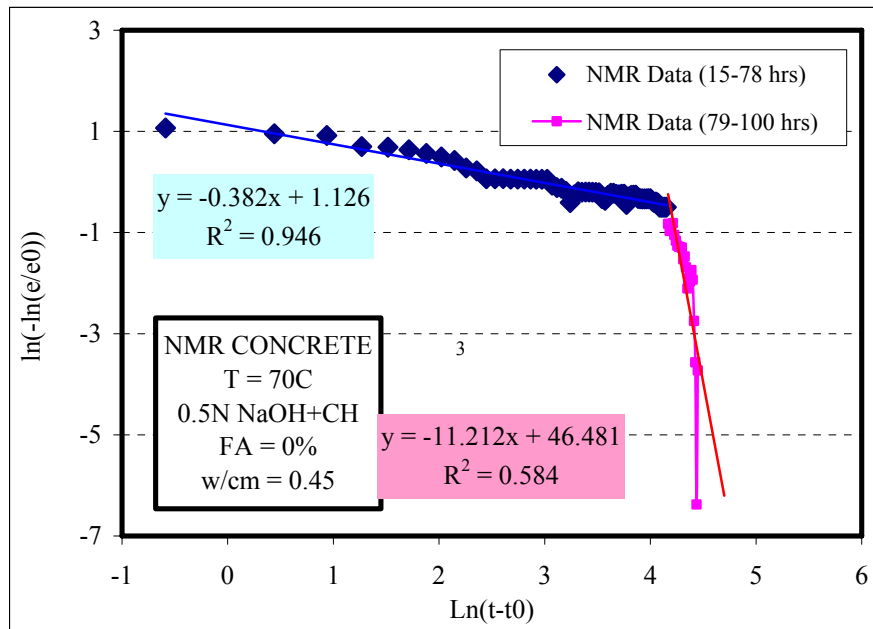
(a) NMR - 0.5N NaOH+CH
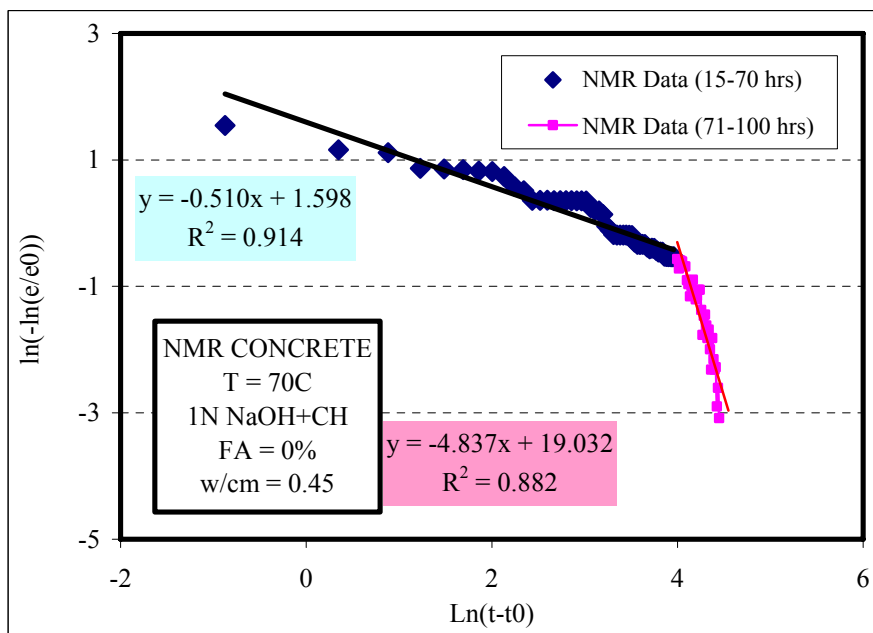
(b) NMR - 1N NaOH+CH

Figure 6.11 Determination of NMR Threshold Level of Expansion.

The plots indicate a major deviation in β values after 78 hrs for NMR tested at 0.5 N NaOH+CH. For example, the rate constant is 0.382 for the (15-78 hrs) time expansion data whereas it is 11.21 for the (79-100 hrs) data. Similar observation was noticed for NMR tested at 1 N NaOH+CH (i.e. β is equal to 0.51 for the first 70 hrs). This was followed by a dramatic jump (i.e. 19.032) in the second 71-100 hrs time expansion data. This huge difference in (β) values is probably due to microcracking that either: a) allows for a higher rate of expansion due to a reduction in stiffness of the matrix or b) allows for a higher rate of reaction due to increased fresh surfaces and chemical reactivity. Based on the above findings, we can deduct that the threshold level of expansion where cracking maybe initiated, occurs in the concrete structures at 550-650 micro-strains.

To determine the effect of alkalinity on the ε_u of concrete, ASR characteristics were determined using system identification method. The measured data were fitted using the same model proposed previously for the aggregate. The model parameters [ε_0, ρ, t_0, β] corresponding to the calculated expansion are presented in Table 6.5. Looking at the results obtained, it can be seen that the level of alkalinity has a significant effect on the ε_u of concrete. For example, the ε_u is equal to 0.1084 % at 1 N NaOH + CH whereas it is 0.0498 % at 0.25 N NaOH + CH. This is mainly due to the abundance of alkali ions in the soak solutions leading to higher alkali gradient at higher alkalinity. This is confirmed by the soak solution chemistry conducted after the test. The (Na^+) ions decreases from 23605 ppm to 17372 ppm at 1 N NaOH + CH (26.4% decrease) whereas this reduction is almost non-existent at 0.25 N NaOH + CH (5877 ppm before versus 5811 ppm after).

Table 6.5 NMR Concrete Parameters Results (Second Set).

NMR Concrete - Type I/II cement - 0% FA (class F) - w/cm = 0.45			
	Alkalinity of Test Solution		
	0.25N NaOH + CH	0.5N NaOH + CH	1N NaOH + CH
ε_0	0.0498	0.0944	0.1084
ρ	46.297	18.895	20.898
t_0	9.656	14.445	14.583
β	2.453	0.617	0.757

Since the ε_u of concrete is determined, r-values determinations for all alkalinities is possible. The results are shown in Figure 6.12. One crucial point can be made from the plots: the calculated r values are close to 1 irrespective of the alkalinity of the soak solutions. One has to mention here that high r values indicate that the concrete tested is permeable which is highly undesirable in field conditions. The results suggest that he mortar surrounding the rock provides minimal restraint at a water cement ratio of 0.45. Since the absence of fly ash in all three tests is characterized by a high ultimate expansion and consequently high r values, it can be concluded that the presence of a mineral admixture is essential in concrete mixtures to mitigate ASR. The recommended percent of fly ash used in concrete mixture to mitigate ASR is presented in the following section.

A comparison is made between the measured and predicted r values. The results are presented in Table 6.6. It is evident from the results that the $r_{measured}$ values are very close to $r_{predicted}$ values. This comparison leads us to conclude that the proposed NMR concrete model has the capability of capturing with high accuracy the combined effects of concrete materials (aggregate reactivity, diffusion, w/cm, % fly ash, on ASR expansion).
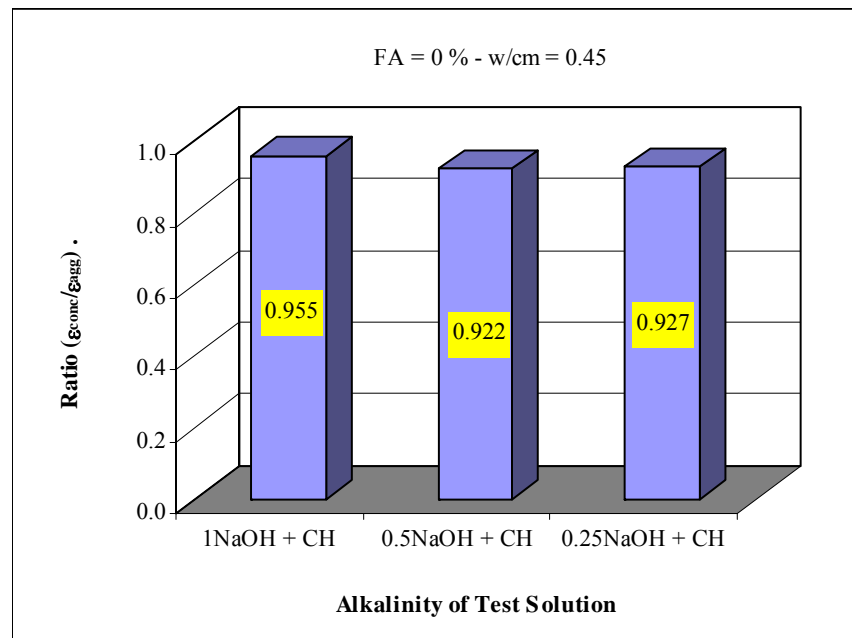

Figure 6.12 Effect of Alkalinity on the Ratio $\left[\dfrac{\varepsilon_0(conc)}{\varepsilon_0(agg)} \right]$ of NMR Concrete (w/o FA).

Table 6.6 Comparisons of Measured Versus Predicted r Values (NMR).

Alkalinity	$r_{measured}$	$r_{predicted}$
1 NaOH + CH	0.955	0.999
0.5 NaOH + CH	0.922	0.999
0.25 NaOH + CH	0.927	0.998

Development of a Threshold Alkalinity for Design (NMR)

In the previous sections of this chapter, two models were proposed. Each model was generated from a different set of tests. The first model which links the E_a of the aggregate and the alkalinity of the pore solution at levels close to those at field conditions was brought forth by a set of aggregate-solution tests representing aggregate reactivity with pore solution in concrete without the presence of mortar. The second model developed using the Juarez-Badillo transform which links the expansion ratio r and the E_a of the aggregate for different water cement ratios and fly ash contents was generated by conducting concrete tests simulating the effect of SCM's, w/cm, diffusion, etc as in concrete in field conditions. To determine the threshold alkalinity for design for NMR concrete for water cement ratio equal to 0.45, the concrete (Figure 6.8) and the aggregate model (Figure 6.7) were combined together in the same plot where the x axis represents the activation energy for both models as shown in Figure 6.13. The procedure for determining the threshold alkalinity for a concrete mixture is described below:

a) The concrete designer will select the appropriate expansion ratio r. R may represent the percentage cracking over the lifetime of the concrete structure. The expansion ratio may also be selected based on field experience accumulated over the years. It should be mentioned here that theoretically, the designer would like to select an r equal to zero and this corresponds to no cracking in the pavement. To achieve that purpose, one has to select a type of cement with no alkali content and therefore removing an essential component needed for the development of the gel. Since cement plants will not be able to produce this type of cement because the raw materials used in the cement manufacture already contain alkalis, it becomes necessary to select an appropriate value of r based on field experience. For demonstration purposes, r is selected in this case to be equal to 0.4. Therefore, a

dotted horizontal line is drawn at r = 0.4 (Figure 6.13). The points where this line crosses the curves for the different levels of fly ash are indicated as steps 1.1, 2.1, 3.1, 4.1, and 5.1. The -.1 indicates the first step in this process.

b) Practically, the designer will select one optimum percent of fly ash needed to control the alkalinity of the pore solution of the concrete. In this demonstration, several fly ash contents are selected: 10%, 15%, 20%, 25%, 30%. The -.2 indicates the second step in this process. The dotted line at r equal to 0.4 crosses the $(r\text{-}E_a)$ curves at five points. Those correspond to E_a equal to 367 (1.2), 277 (2.2), 156 (3.2), 70 (4.2), 29 (5.2) KJ/mol respectively. From each of the five points, a vertical dotted line was drawn. Those lines cross the aggregate reactivity model at five points. Those are equivalent to 0.04N (1.3), 0.05N (2.3). 0.075N (3.3), 0.14N (4.3), 0.31N (5.3) respectively. The -.3 indicates the third, and final step in this process.

c) Since the total amount of cement alkali is generally expressed in terms of "sodium equivalent", the determined threshold alkalinities for different fly ash content were converted to % $Na_2O_{equivalent}$. The results are as follows: for concrete mixtures with a w/cm equal to 0.45, the % $Na_2O_{equivalent}$ is equal to 0.046%, 0.0575%, 0.086%, 0.161% and 1.18% for mixtures containing 10%, 15%, 20%, 25%, 30% class F fly ash respectively. It is important to mention that the threshold alkali content, above which ASR expansion occurs, is not a fixed value. In fact, it depends on the type of reactive aggregate.
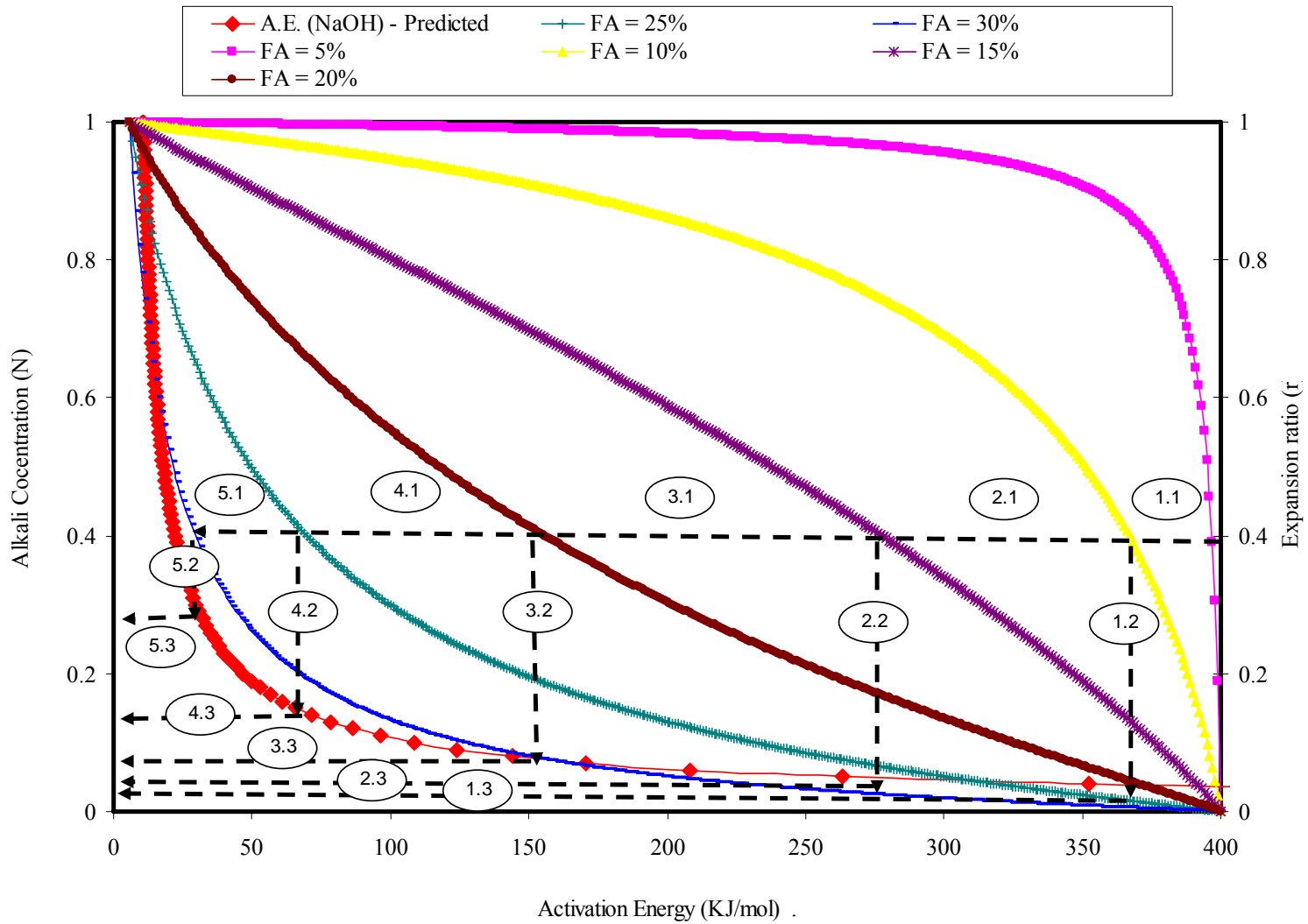
Figure 6.13 NMR Threshold Design for Alkalinity (w/cm = 0.45).

One has to state that the type I/II cement used in this research program contains 0.54% $Na_2O_{equivalent}$. This number is well above the threshold alkalinities mentioned above. Since alkalis can come from many sources, like cement, SCM's, aggregate, etc, achieving a total threshold alkalinity below 0.28% is not possible. Consequently, it maybe from a practical point of view better to select the type of cement that contains the minimum amount of alkali (Type I/II) or select the total allowed alkalinity of the pore solution and determine the percent of fly ash required to keep r values to minimum.

It is mentioned earlier that dissolution of silica is a function of the pH of the pore concrete solution. pH is directly related to alkalinity of the solution. Lab tests have shown that although limited expansion is possible using total alkali content below 3 kg/m^3, concrete structures in the field have displayed damage at lower alkali values, specially when aggregate and other sources (i.e. deicing salts) has contributed to the total alkali of the mixtures (Folliard et al, 2006). Therefore, there is interest in keeping the total alkali content below the 3 kg/m^3 (5 lb/yd^3).

For example, the total alkali is chosen to be equal to 0.648 lb/yd^3. Assuming a cement factor equal to 6, this corresponds to a 0.1N NaOH pore solution and a pH of 13. Therefore, a horizontal dotted line is drawn (Figure 6.14-step 1) at 0.1 N alkalinity. The designer will have the option to choose the minimum % of fly ash to obtain reasonable r values. The r values determined by the second step from the combined material model are as follows: 0.993, 0.941, 0.786, 0.528, 0.278, 0.12, and 0.045 for NMR concrete mixtures with 5%, 10%, 15%, 20%, 25%, 30% and 35% class F fly ash content respectively. The results obtained indicate the importance of SCM's (i.e. fly ash) to mitigate ASR as r values decrease significantly above 15% replacement levels. Although the higher % of fly ash is used, the lower r values are obtained, the designer while making his selection should take into consideration some of the disadvantages of using fly ash. It is known that the use of pozzolan reduces the heat of hydration of the concrete and thus concrete mixtures take more time to attain the required strength. Therefore the possibility of opening the structures (pavement, bridge deck, etc) to traffic is impeded. In general, the nature of the structure and its lifetime play a major role in controlling the design.
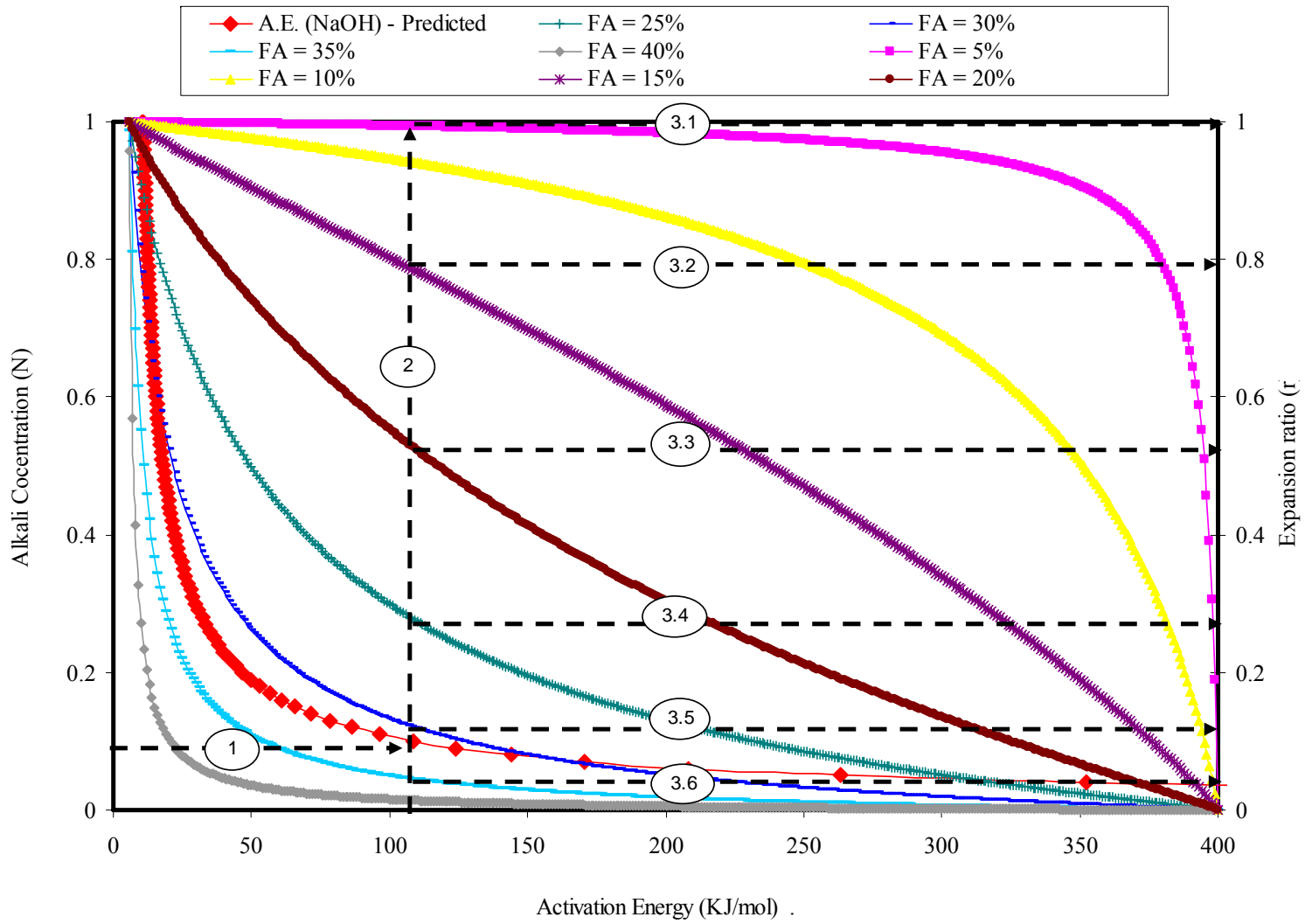
Figure 6.14 Combined Concrete and Aggregate Model for NMR (w/cm = 0.45).

American Standard of Testing and Materials (ASTM) C150 specifications limits is 0.6% $Na_2O_{equivalent}$ for low alkali cement (type I/II). One of the advantages of using fly ash in the mixtures is that the alkalis in fly ash are less soluble than those in cement and consequently, the total amount of alkalis of the blend (cement + fly ash) is less than that in the cement alone. To be on the safe side, one can assume that all alkalis in the fly ash will eventually dissolve into the pore solution of concrete. Assuming that cement with 0.3% $Na_2O_{equivalent}$ is used, this is equivalent to 0.26 N alkaline solutions. Therefore the same steps outlined above can be followed (Figure 6.15). The r values obtained are as follows: 0.98, 093, 0.81, 0.60, 0.35, 0.15, and 0.05 for NMR concrete mixtures with 5%, 10%, 15%, 20%, 25%, 30%, 35% and 40% class F fly ash content respectively. The results obtained re-assured the importance of fly ash in mitigating ASR as fly ash blocks the capillary voids which in turn reduces the permeability of concrete. In this particular case 35% fly ash is needed to bring the expansion ratio to reasonable values (r = 0.15).
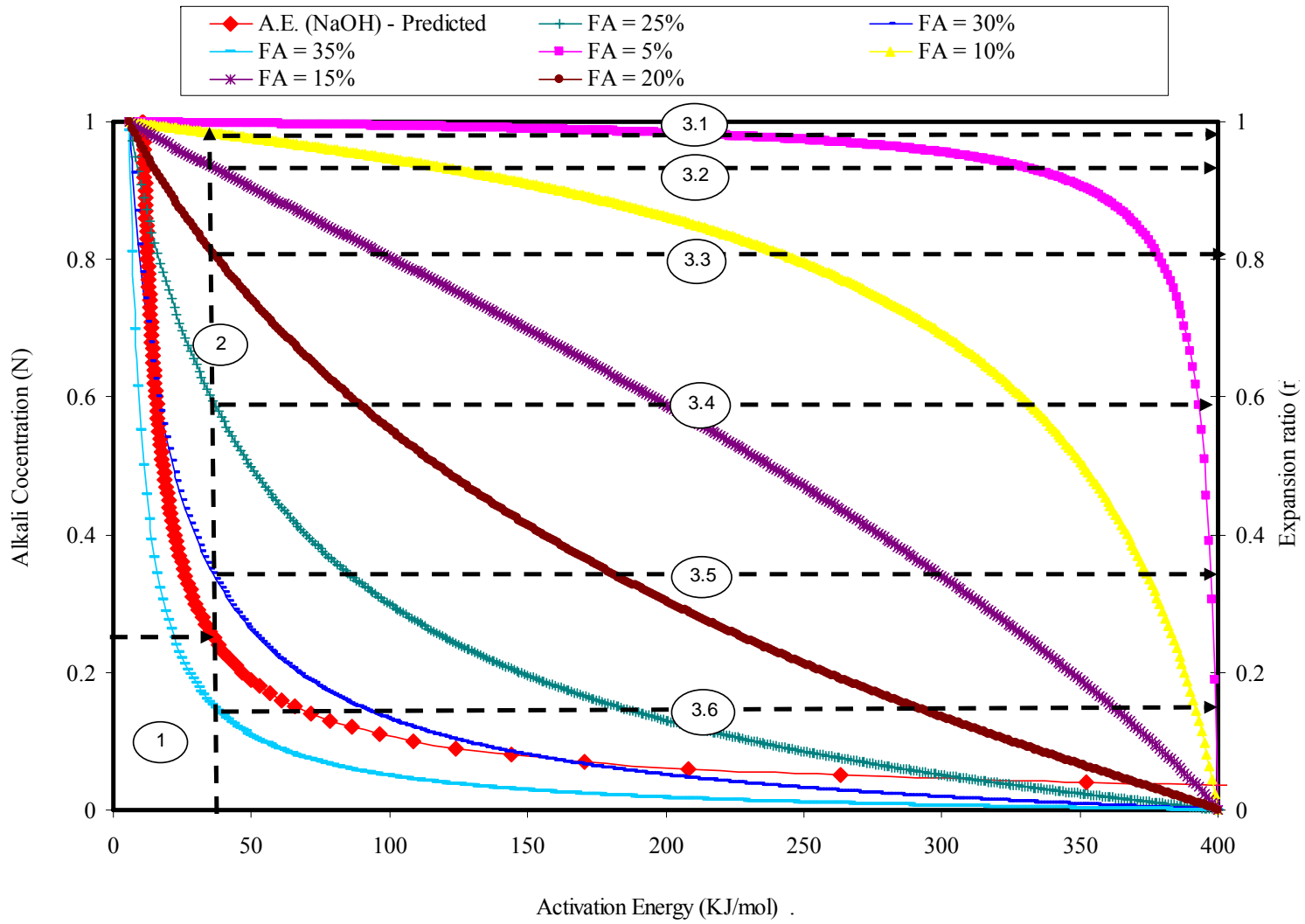
Figure 6.15 – Design Procedure for NMR Using ASTM C150 (w/mc = 0.45).

A similar procedure is used to determine the threshold alkalinity for design for NMR concrete mixtures containing 25% fly ash. To achieve this objective, the concrete (Figure 6.9) and the aggregate model (Figure 6.7) were combined together in the same plot where the x axis represents the E_a for both models as shown in Figure 6.16. The threshold alkalinity is determined as follows:

a) r value is selected. For illustration propose, r was selected equal to 0.4. Therefore, a dotted horizontal line is drawn at r = 0.4 (Figure 6.16 - step1). The line crosses the (r-E_a) curves at three points. These correspond to w/cm = 0.49, 0.47, and 0.45 and to E_a = 394, 317, and 69 KJ/mol respectively (step 2).

b) The designer selects among one the above w/cm's. Theoretically, he can select the minimum water cement ratio (i.e. 0.4 in this case) and determine its threshold total alkalinity. Low w/cm will reduce the permeability of the concrete and impede the movement of the moisture inside the concrete and consequently, mitigating ASR. However, selecting low w/cm will decrease the workability of the concrete and therefore its placement. Thus, it maybe more appropriate to select the max water cement ratio possible while keeping the alkalinity of the pore solution in check by adding mineral admixtures.

c) The threshold level alkalinities for concrete mixtures with a w/cm of 0.49, 0.47 and 0.45 are 0.035N, 0.045N, and 0.145N respectively (step 3). Those values are equivalent to 0.04, 0.05, and 0.166 Na_2O_{eq}. Those values are below the threshold values (3 kg/m^3) mentioned by researchers that expansion is unlikely to occur below this value. Therefore, the user can chose any w/cm values between 0.4 and 0.5 with 25% class F fly ash. A comparison among the threshold alkalinities indicate that lower w/cm is associated with higher threshold. In other words, there is more tolerance concerning the level of alkalinity in the solution when low w/cm is used in the mixture, as low w/cm values yield concrete with low permeability and therefore the movement of alkali ions even in high concentrations is impeded by the denser concrete matrix.
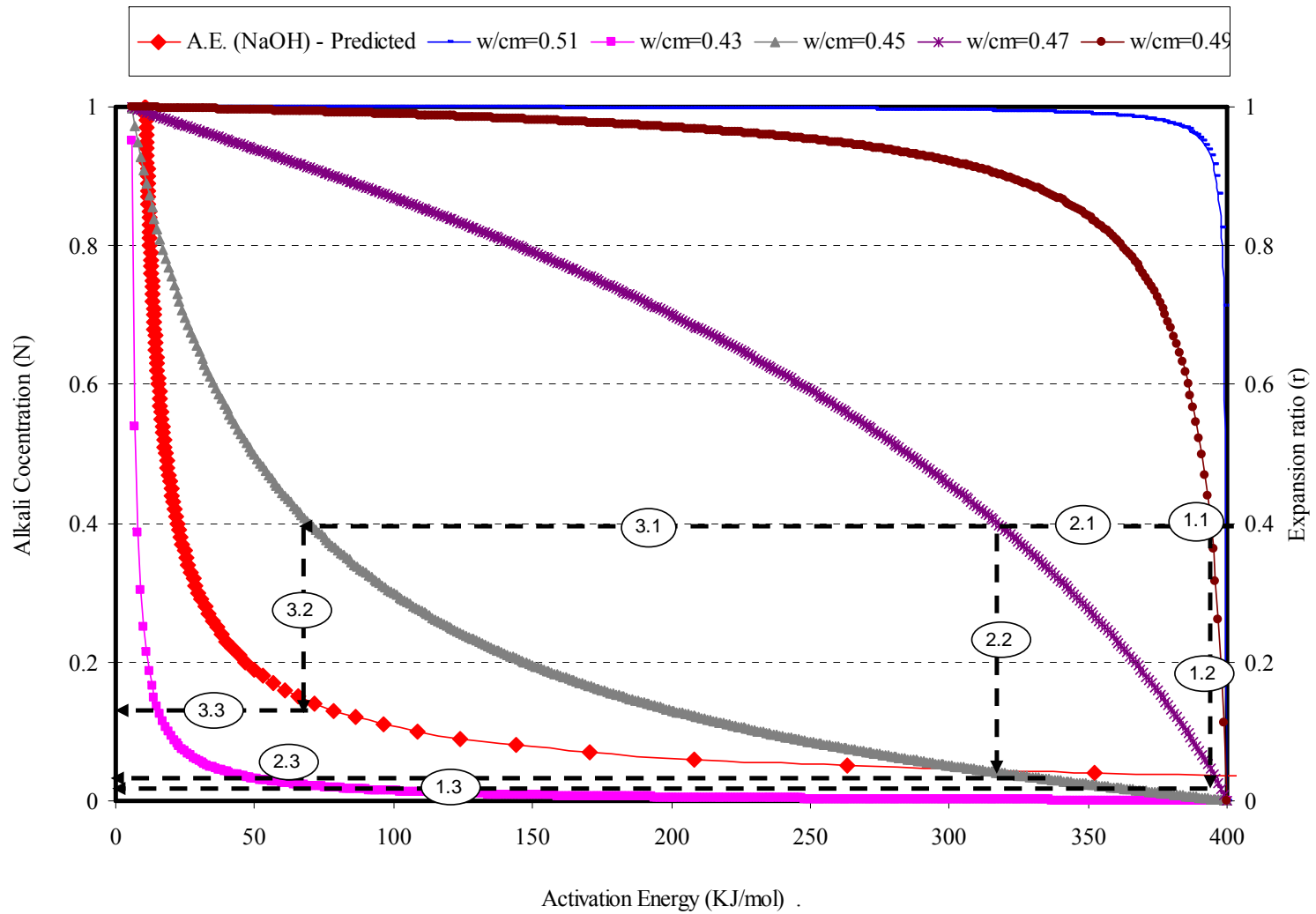
Figure 6.16 NMR Threshold Design for Alkalinity (fly ash = 25%).

Determination of E_a Matching with Field Conditions of Alkalinity - PRG

For PRG aggregates, similar steps were followed as in the NMR case. To anticipate the activation energy needed to initiate ASR at lower pH values, the alkalinity of the soak solutions and the E_a of the aggregate were connected using the previously proposed model (Eq 6.1).

$$E_a = E_{a_0} + \frac{C_1}{C^n} \tag{6.1}$$

For PRG gravel, the aggregates tests were conducted at two alkalinities: 1N NaOH + CH and 0.5N NaOH + CH and thus two E_a values were determined. The data is fitted using equation 6.1.

The results obtained are presented below:

$E_{a_0} = 40.7, \; C_1 = 5.79, \; n = 1.451$

By substituting the above calculated parameters in the model, Eq. 6.1 becomes as follows

$$E_a = 40.7 + \frac{5.79}{C^{1.45}} \tag{6.11}$$

The predicted E_a values are plotted versus the measured E_a values. The results are presented in Figure 6.17. A good fit between the measured and predicted E_a values is manifested and this demonstrates the applicability of the proposed model. As shown from the plot, as alkalinity increases, the E_a decreases underlining the relationship between these two variables.

As in the NMR case, two major and similar observations can be made from Figure 6.17: a) it appears that there exists a threshold level of alkalinity for PRG above which the effect of alkalinity on the E_a is minimum. For example, at the 1N+CH solution the E_a is 46.5 KJ/mol whereas it is 42.8 KJ/mol from the predicted model at 2 N. This is equivalent to 7.95% decrease. This is likely attributed to the saturation of the reaction sites by hydroxyl ions at the aggregate surfaces at high alkalinity, b) on the other side, the relationship between the E_a and alkalinity (below 0.5 N+CH) seems to follow a power curve. For example, the E_a is 84 KJ/mol at 0.25 N+CH while it is 56.5 KJ/mol at 0.5N+CH from the predicted model at 2 N. This is equivalent to a 48.9% increase. This is attributed to the fact that much more energy is needed a low alkalinity. It is also possible

that temperature becomes the major factor that determines the rate of reaction at low alkalinity. The previous statement is supported by the PRG characteristics determined in Chapter V. The rate constant β at 1N+CH increases from 1.37 at 60^0C to 3.55 at 80^0C. This is equivalent to 159.1% increase. On the other side, β growth from 60 to 80^0C is 221.1% at 0.5N+CH. This comparison emphasizes the importance of temperature on the E_a of the rock at low alkali levels.
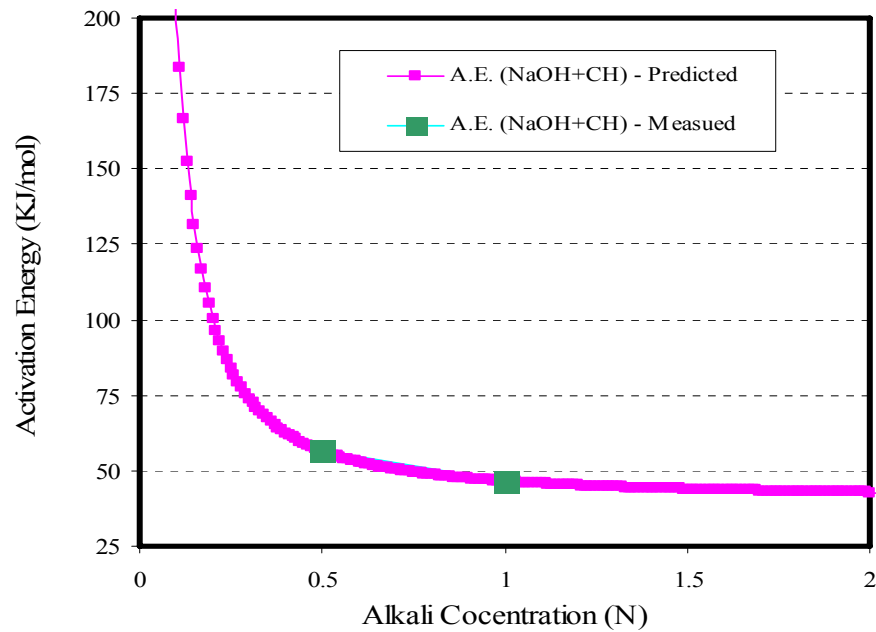

Figure 6.17 Alkalinity versus Activation Energy (PRG).

Development of a Reaction Signature for PRG Combined Concrete Materials

To predict the combined effect of concrete materials on ASR, the Juarez-Badillo transform was used to generate the PRG concrete model.

$$r = \frac{r_{min} + r_{max}\left[C.(\frac{f}{f_{max} - f})^{\beta}.(\frac{E_a - E_{a_{min}}}{E_{a_{max}} - E_a})^{\alpha}.(\frac{w - w_{min}}{w_{max} - w})^{\gamma}\right]}{1 + C.(\frac{f}{f_{max} - f})^{\beta}.(\frac{E_a - E_{a_{min}}}{E_{a_{max}} - E_a})^{\alpha}.(\frac{w - w_{min}}{w_{max} - w})^{\gamma})} \tag{6.3}$$

The E_a values for PRG were determined in Chapter V and the expansion ratio values "r" were calculated in the first section of this chapter. The parameters to be determined are C, β, λ and γ. Before proceeding with the calculation, the boundary conditions were chosen as follows:

$w_{min} = 0.4$, $w_{max} = 0.55$, $E_{a_{min}} = 40.7$, $E_{a_{max}} = 400$ and $f_{max} = 0.55$

By substituting the values of the above parameters in the proposed concrete model, Eq. (6.3) becomes as follows:

$$r = \frac{C.\left[\frac{5}{6}\right]^{\beta}.\left[\frac{1}{2}\right]^{\gamma}\left[\frac{(E_a - 40.7)}{(400 - E_a)}\right]^{\alpha}}{1 + C.\left[\frac{5}{6}\right]^{\beta}.\left[\frac{1}{2}\right]^{\gamma}\left[\frac{(E_a - 40.7)}{(400 - E_a)}\right]^{\alpha}} \tag{6.12}$$

The parameters C, β, α and γ were determined using system identification procedure. The results obtained are presented below:

$C = 3.566$, $\beta = -2.942$, $\gamma = 4.331$, $\alpha = -1.008$

By substituting the calculated parameters in the generalized model (Eq 6.3), the expression becomes as follows:

$$r = \frac{3.566.\left[\frac{f}{0.55 - f}\right]^{-2.942}.\left[\frac{w - 0.4}{0.55 - w}\right]^{4.331}\left[\frac{(E_a - 40.7)}{(400 - E_a)}\right]^{-1.008}}{1 + \left[3.566.\left[\frac{f}{0.55 - f}\right]^{-2.942}.\left[\frac{w - 0.4}{0.55 - w}\right]^{4.331}\left[\frac{(E_a - 40.7)}{(400 - E_a)}\right]^{-1.008}\right]} \tag{6.13}$$

The above equation can be expressed as follows:

$$\left(\frac{\varepsilon_u}{\varepsilon_a}\right) = \text{function } (f, E_a, w) \tag{6.14}$$

where:

f = fly ash

E_a = activation energy of aggregate at a specific alkalinity

w = water cement ratio

For PRG concrete mixtures, the amount of fly ash and water cement ratio is known from the design combinations (w/cm = 0.45 and FA = 25%) and therefore, those variables are constant in Eq. 6.13 which yields the following:

$$\text{(a) } \left(\frac{\varepsilon_u}{\varepsilon_a}\right) = \text{function } (f, E_a) \tag{6.15}$$

Eq. 6.15 can be expanded as follows:

$$r = \frac{177.2\times10^{-3}\cdot\left[\dfrac{f}{0.55-f}\right]^{-2.942}\cdot\left[\dfrac{(E_a-40.7)}{(400-E_a)}\right]^{-1.008}}{1+\left[177.2\times10^{-3}\cdot\left[\dfrac{f}{0.55-f}\right]^{-2.942}\cdot\left[\dfrac{(E_a-40.7)}{(400-E_a)}\right]^{-1.008}\right]} \tag{6.16}$$

$$\text{(b) } \left(\frac{\varepsilon_u}{\varepsilon_a}\right) = \text{function } (E_a, w) \tag{6.17}$$

Eq. 6.17 can be expanded as follows:

$$r = \frac{6.1\times\left[\dfrac{w-0.4}{0.55-w}\right]^{4.331}\cdot\left[\dfrac{(E_a-40.7)}{(400-E_a)}\right]^{-1.008}}{1+\left[6.1\times\left[\dfrac{w-0.4}{0.55-w}\right]^{4.331}\cdot\left[\dfrac{(E_a-40.7)}{(400-E_a)}\right]^{-1.008}\right]} \tag{6.18}$$

Each of the above equations (6.16) and (6.18) leads to the development of:

i) A set of curves between $\left(\frac{\varepsilon_u}{\varepsilon_a}\right)$ and E_a for different FA content (w = 0.45) (Figure 6.18).

ii) A set of curves between $\left(\frac{\varepsilon_u}{\varepsilon_a}\right)$ and E_a for different w/cm (f = 25%) (Figure 6.19).
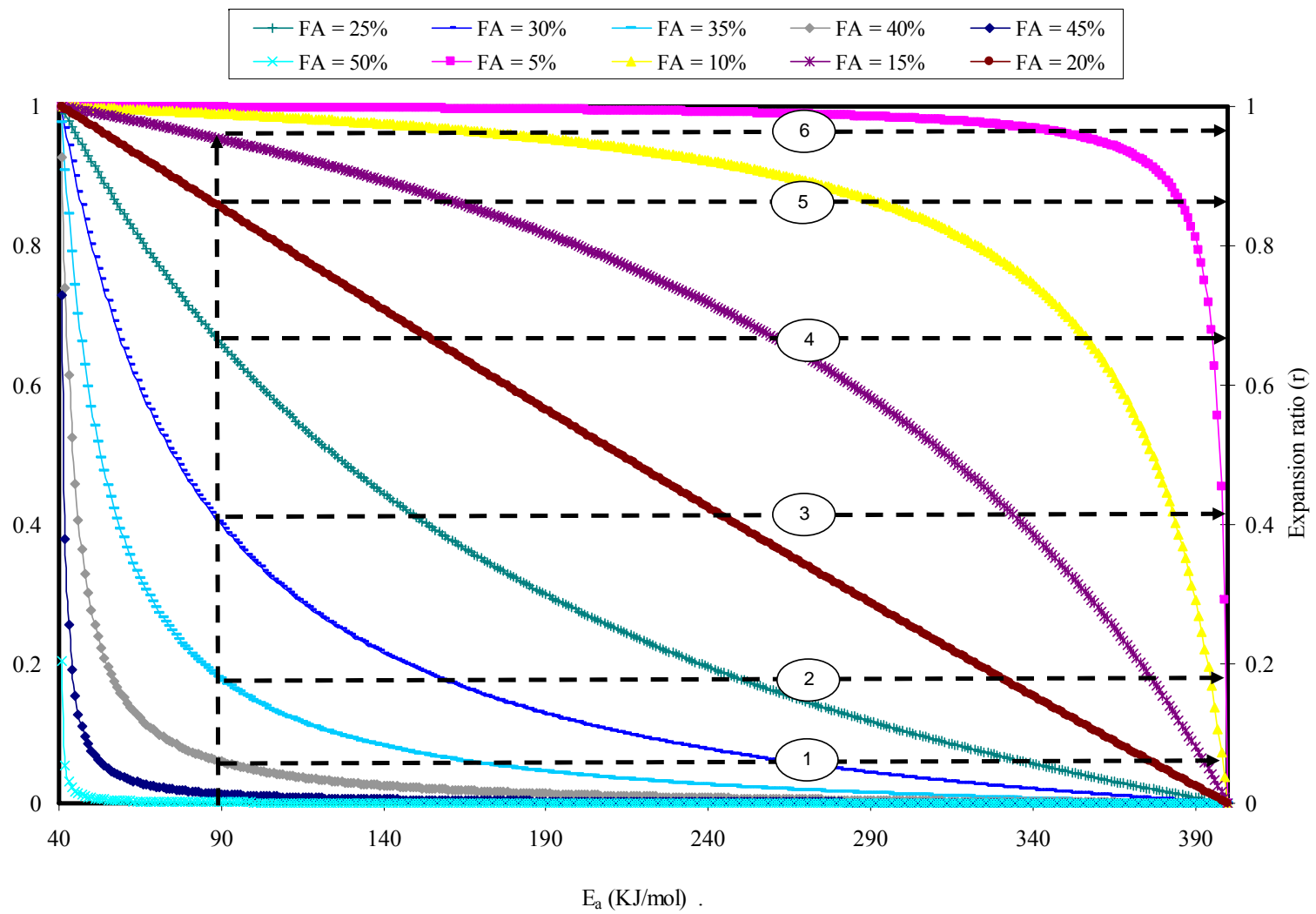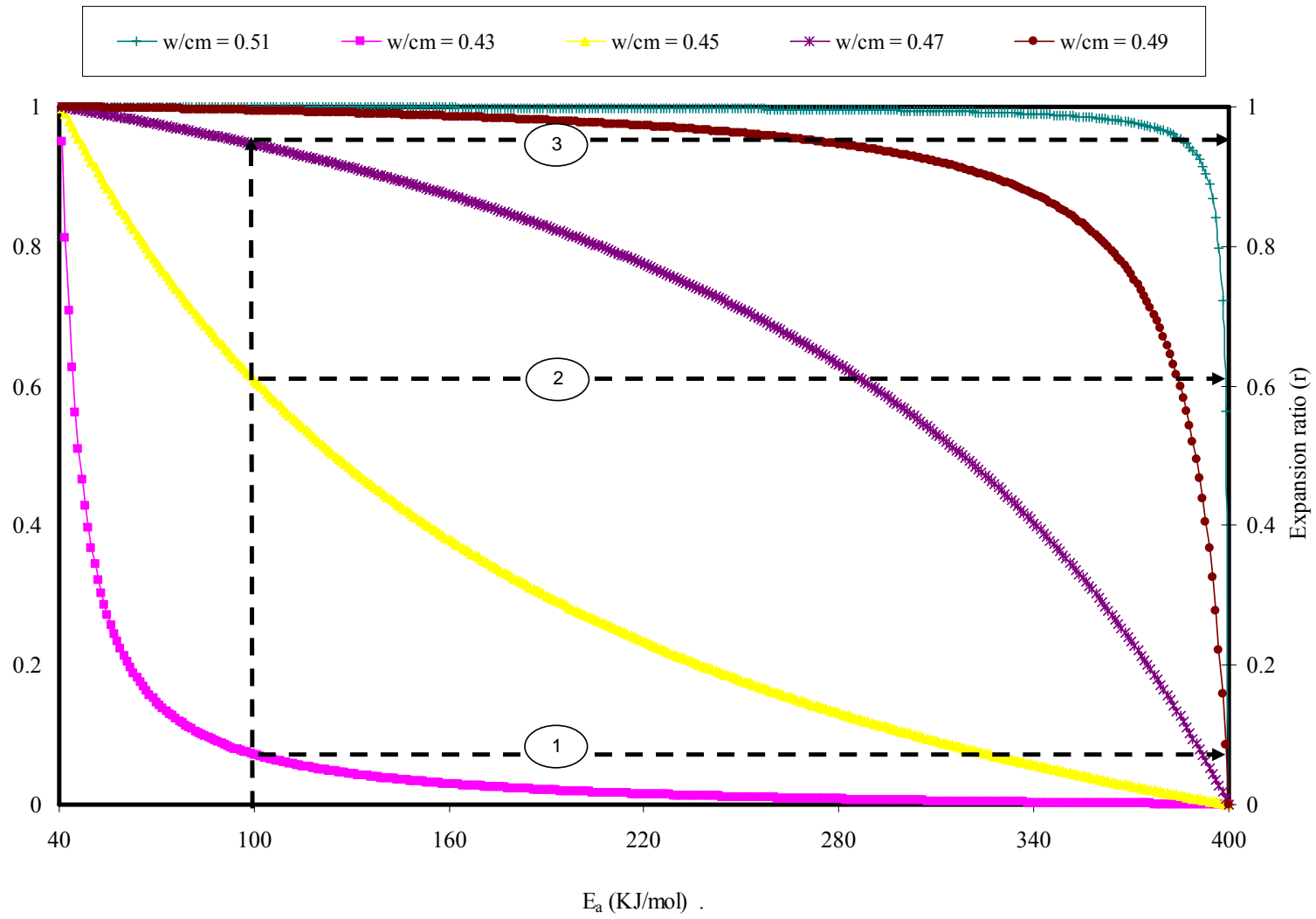
Figure 6.18 PRG Mortar Model (w/cm = 0.45).

Figure 6.19 PRG Mortar Model (w/cm = 0.45).

Figure 6.18 exhibits a set of theoretical curves between E_a and r for PRG mortar with a w/cm equal to 0.45. In general, similar observations can be made as in the case of NMR. As shown in the figure, the relationship between these two parameters is inversely proportional irrespective of the amount of fly ash in the mixture. A low E_a value indicate that the aggregate is very reactive and since reactivity of aggregate is the major factor that determine the ultimate expansion in the field, he expansion ratio "r" is expected to be close to one as the alkali levels govern the rate of expansion. The previous statement is manifested by the high expansion ratio obtained previously at 25% fly ash. It is also possible that these high "r" values are due to the presence of alkali gradient between the pore solution of the mortar and the alkali of the soak solutions. On the other side, at higher E_a values, the ratio is at its minimum as the pH of the pore solution of mortar will likely be higher than the alkalinity of the soak solution and therefore, the presence of alkali gradient mentioned above is practically not existent.

The presence of class F fly ash on concrete characteristics is again demonstrated by its effects on the "r" values. For example, at E_a = 90KJ/mol, the pH of the alkali solution is 13.36. From the theoretical curves, the corresponding expansion ratios r are equal to 0.953, 0.854, 0.659, 0.399, 0.178, 0.059, for mixtures containing 15%, 20%, 25%, 30%, 35% and 40% Fly Ash Class F respectively. As shown from the results, the ratios decrease as the percent of fly ash increase. This is maybe due to the occurrence of the pozzolanic reaction. Furthermore, it is known that fly ash solid particles are finer than those of concrete. Therefore, concrete permeability will decrease since the movement of alkali ions in the concrete matrix will be much more restricted. The amount of fly ash needed is also a point of interest. It seems that 15 to 20% fly ash has a minimum effect as the expansion ratio remains high. On the other side, increasing the amount of fly ash above 35%, yields only minimal amelioration on the "r" values. Thus, preliminary results indicate that 30% fly ash appears to be the optimum number.

A set of theoretical curves between E_a and r for PRG mortar with 25% class F fly ash at different water cement ratios are presented in Figure 6.19. As shown, the consequence of adding or reducing slightly the w/cm yields huge variation in "r" values. For example, at E_a = 100KJ/mol, the expansion ratio r is equal to 0.0714, 0.608, 0.946

for concrete mixtures with w/cm equal to 0.43, 0.45, and 0.47 respectively (Figure 6.19). It appears that the 0.45 w/cm value is a transition phase between low and high permeable concrete as w/cm above 0.47 or lower than 0.41 generate almost similar "r values".

Validation of the PRG Mortar Model

To substantiate the previous PRG mortar model, additional tests were conducted to measure $r_{measured}$ and then compare it with $r_{predicted}$. To achieve this objective, two mortar tests were performed at 1 NaOH + CH, 0.5 NaOH + CH. Mortar was mixed at water cement ratio of 0.45. Type I/II low alkali cement was used in the mixture and 50% of the cement content was replaced with class F Fly ash. All tests were conducted at 70 ^{0}C.

The volume expansion test results for the PRG mortar are shown in Figure 6.20. It should be noted that each measured plot in Figure 6.20 represents an average of two replicas (each test was repeated twice to check the repeatability). As shown, measurable expansions are recorded for both tests from the 10 h period until the 100 hrs where the % expansion reaches 0.001% and 0.0005% for PRG conducted at 1 NaOH + CH and 0.5 NaOH + CH solutions, respectively. A critical observation can be made by comparing the chemistry of the soak solutions before and after the test. For example, for PRG mortar tested at 1 NaOH + CH solutions, the pH was 14.009 at the beginning of the test and then measured 13.985 at the end of the test (Table 6.4). Similar pH observation can be made for PRG mortar tested at 0.5 NaOH + CH. This difference in pH value is negligible and within the error of the pH meter. There is also no significant change in alkali concentration before (23605 ppm) and after (23878 ppm) the test. Consequently, two conclusions can be made: a) the hydroxyl and alkali ions of the alkali solutions did not penetrate the mortar matrix b) mortar can be expansive although type I/II low alkali cement is used.
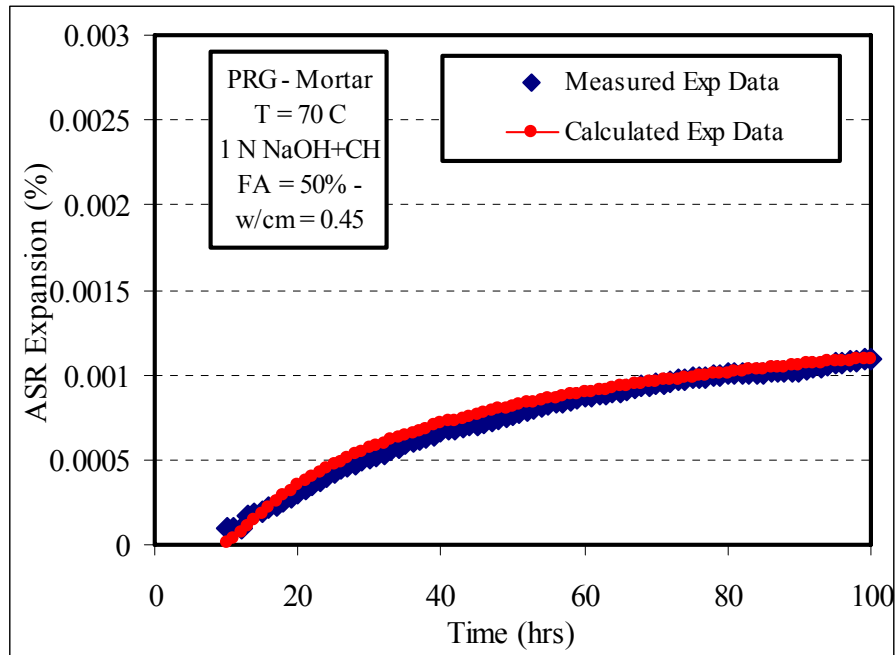
(a) PRG expansion at 1N NaOH + CH
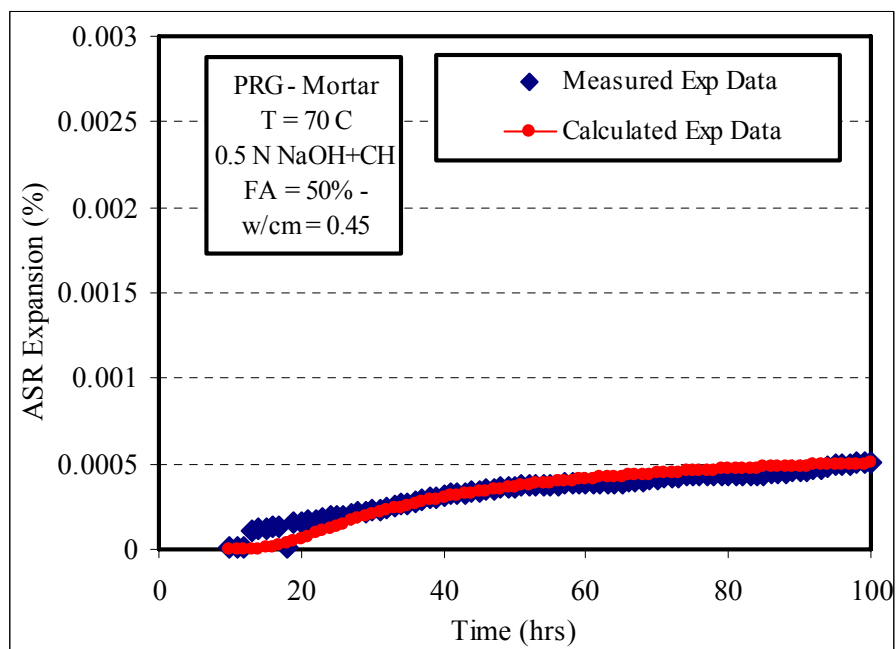
(b) PRG expansion at 0.5N NaOH + CH

Figure 6.20 Mortar PRG Expansion.

To calculate $r_{measured}$, the ultimate expansion of PRG at both alkalinities was determined. System identification procedure was used to find the mortar characteristics. Results are presented in Table 6.7. The calculated expansions are super-imposed on the measured expansion in Figure 6.20. A very good fit is manifested. The measured r values at both alkalinities are presented in Figure 6.21. Although the combined model capture to a reasonable degree the effect of the fly on the mortar characteristics as $r_{predicted}$ exhibits very small values similar to those $r_{measured}$, it underestimates the values (Table 6.8). This maybe due to the relatively limited applicability of the Juarez-Badillo procedure at values close to the boundary conditions set initially. Therefore, it is recommended that future tests be conducted at values close to the mid-range of the boundary conditions.

Table 6.7 PRG Mortar Parameters Results (Second Set).

PRG mortar - Type I/II cement - 50% FA (class F) - w/cm = 0.45		
	0.5N NaOH + CH	1N NaOH + CH
ε_0	0.0006	0.0032
ρ	22.1	59.8
t_0	8.0	9.1
β	1.2	3.0
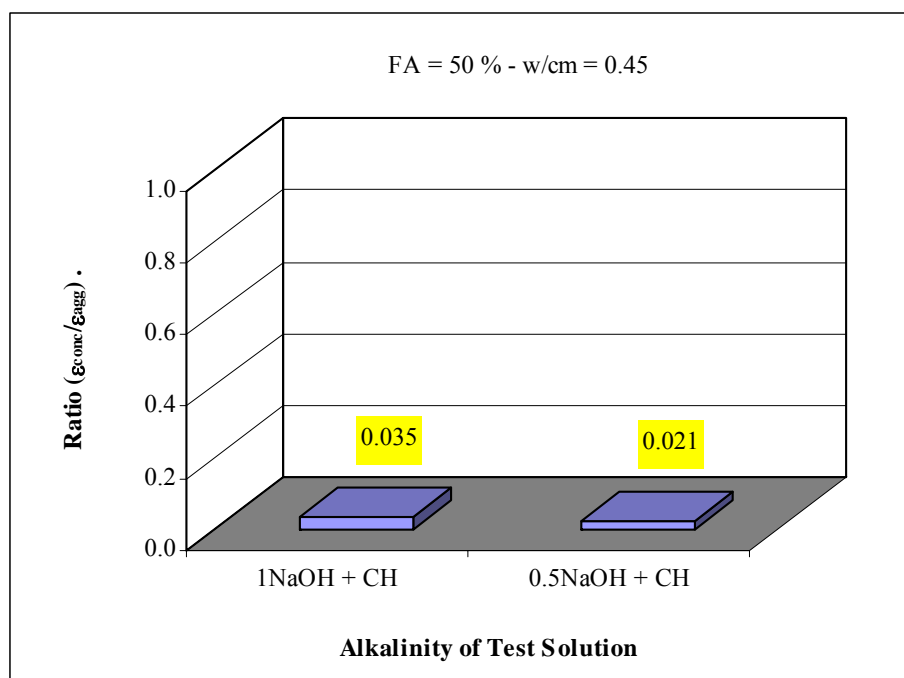
Figure 6.21 Effect of Alkalinity on the Ratio $\left[\dfrac{\varepsilon_0(conc)}{\varepsilon_0(agg)}\right]$ of PRG Mortar (with FA).

Table 6.8 Comparisons of Measured Versus Predicted r Values (PRG).

Alkalinity	$r_{measured}$	$r_{predicted}$
1 NaOH + CH	0.035	0.0138
0.5 NaOH + CH	0.021	0.00464

Development of a Threshold Alkalinity for Design (PRG)

The determination of a threshold alkali level under which ASR deleterious expansion will not occur, necessitate the connection between the E_a of the aggregate, the expansion ratio "r" and the alkalinity of soak solution. It should be mentioned that here the soak solution simulates the pore solution in concrete. To achieve the above target, the mortar model (Figures 6.18 and 6.19) and the aggregate model (Figure 6.17) were combined together in the same plot where the x axis represents the E_a for both models. The results are presented in Figures 6.22 and 6.23. As in the NMR case, a similar approach was

followed. The steps can be summarized as follows: the user selects the appropriate expansion ratio and determines from the mortar model the corresponding E_a. Once the E_a is determined, the calculation of the alkalinity of the soak is possible from the aggregate model. The alkalinity is then converted to % $Na_2O_{equivalent}$ or to lb/yd^3. The latest figures are considered the maximum total amount of alkalis allowed in the concrete matrix corresponding to the initial expansion ratio assumed earlier. An example is presented in Figures 6.22 and 6.23 and is elaborated below. It should be stated that values selected for the parameters in the example are subject to individual discretion or preference and the user doesn't have to abide by them:

(a) Based on the expected lifetime of the structure and its importance, the user selects an expansion ratio equal to 0.4 (step 1).

(b) From the (r- E_a) curves, the designer can select the amount of fly ash and its corresponding E_a. In this example, the E_a values are 334, 337, 248, 153 and 89 KJ/mol for mixtures containing 10%, 15%, 20%, 25% and 30%. Class F fly ash (step 2).

(c) The computed alkalinities from the aggregate model at the above E_a values are 0.06 N, 0.07N, 0.085, 0.13, and 0.23N respectively (step 3).

(d) Assuming the cement factor equal to 6, the above alkalinities are equivalent to 0.069%, 0.08%, 0.097%, 0.149% and 0.264% $Na_2O_{equivalent}$. These values are also equivalent to 0.23, 0.27, 0.32, 0.50 and 0.88 kg/m^3 respectively.

(e) The above threshold indicates that alkalinities can't exceed those levels for specific mixtures if the expansion ratio is assumed equal to 0.4.

(f) Assuming type I/II low alkali cement is used in the mixture, the maximum allowable by ASTM C150 is 0.6% $Na_2O_{equivalent}$. This number is well above most of the threshold alkali determined above.

(g) pH values of concrete depend on many factors. Assume that a minimum pH of concrete of 13.2 is required. This is equivalent to 0.575% $Na_2O_{equivalent}$. From the above results, only mixtures with 30% class F fly ash had a threshold above this value, while other mixtures with lower percents of fly ash will not be able to control the total

alkalinity for the mix as the expected $\%Na_2O_{equivalent}$ is higher than the threshold alkali level.

(h) From that specific example, it can be concluded that to maintain a 0.4 expansion ratio, 30% class F fly ash is needed to keep to alkalinity of the pore solution in check.

As seen from the above demonstrative examples in the NMR and PRG cases, the proposed combined approach is sufficiently flexible that the user has the choice of either: a) selecting the expansion ratio based on field experience, lifetime and/or importance of the structure, then choosing the appropriate amount of fly ash and determine the corresponding threshold alkalinity or b) choosing the maximum allowed alkalinity in the pore solution and then selecting the percent of fly ash to achieve the required expansion ratio.

One of the advantages of this approach is that the user does not have to select a specific water cement ratio or a percent fly ash. In fact, he can select any combination (w/cm & fly ash) that fits best his need or type of applications.

Another advantage of the proposed procedure is to allow the user to determine the effect of fly ash and water cement ratio on concrete characteristics without physically conducting the test. This efficiently assists agencies, contractors and material engineers in selecting the optimum concrete mixture combinations within the shortest period possible.
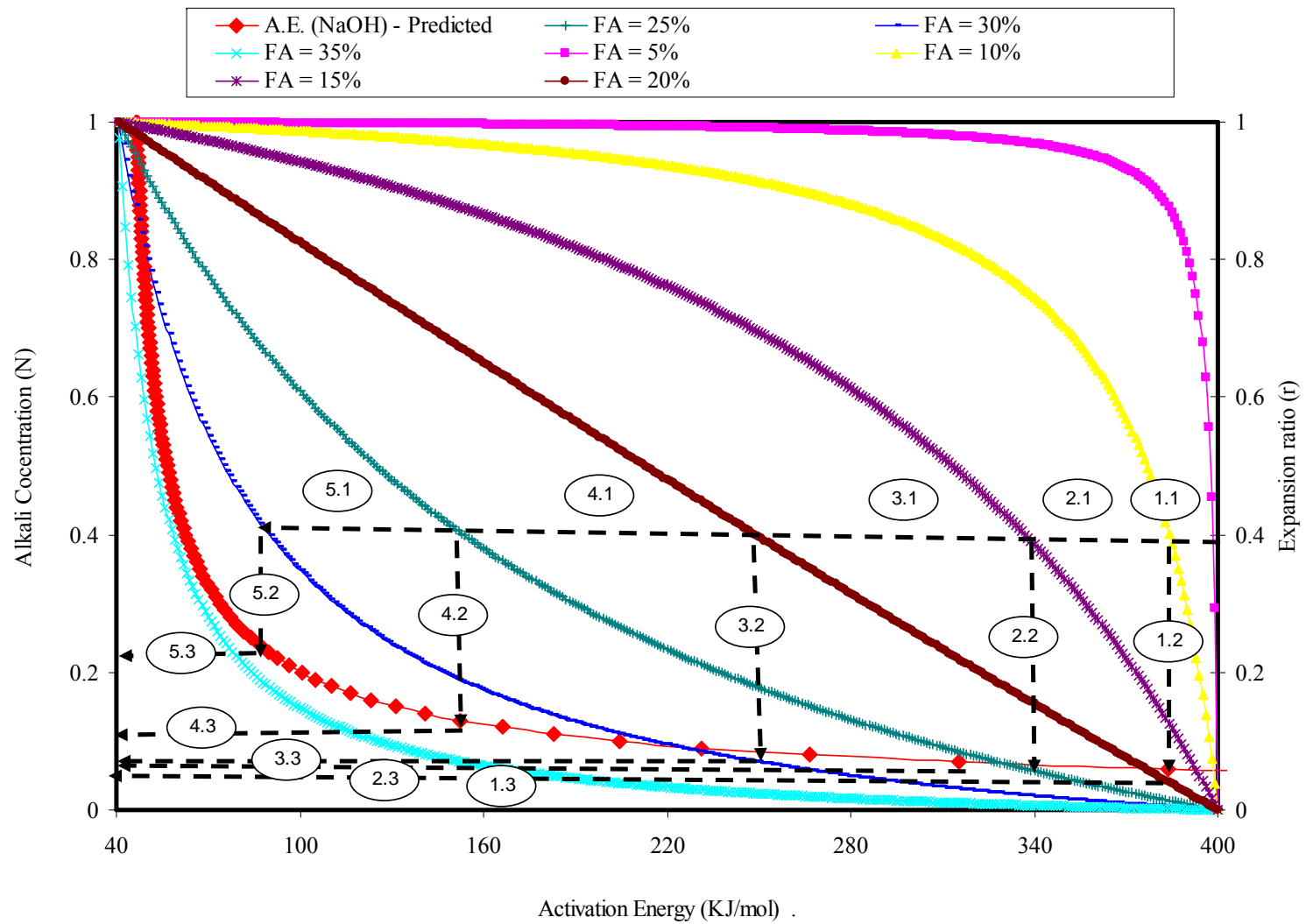
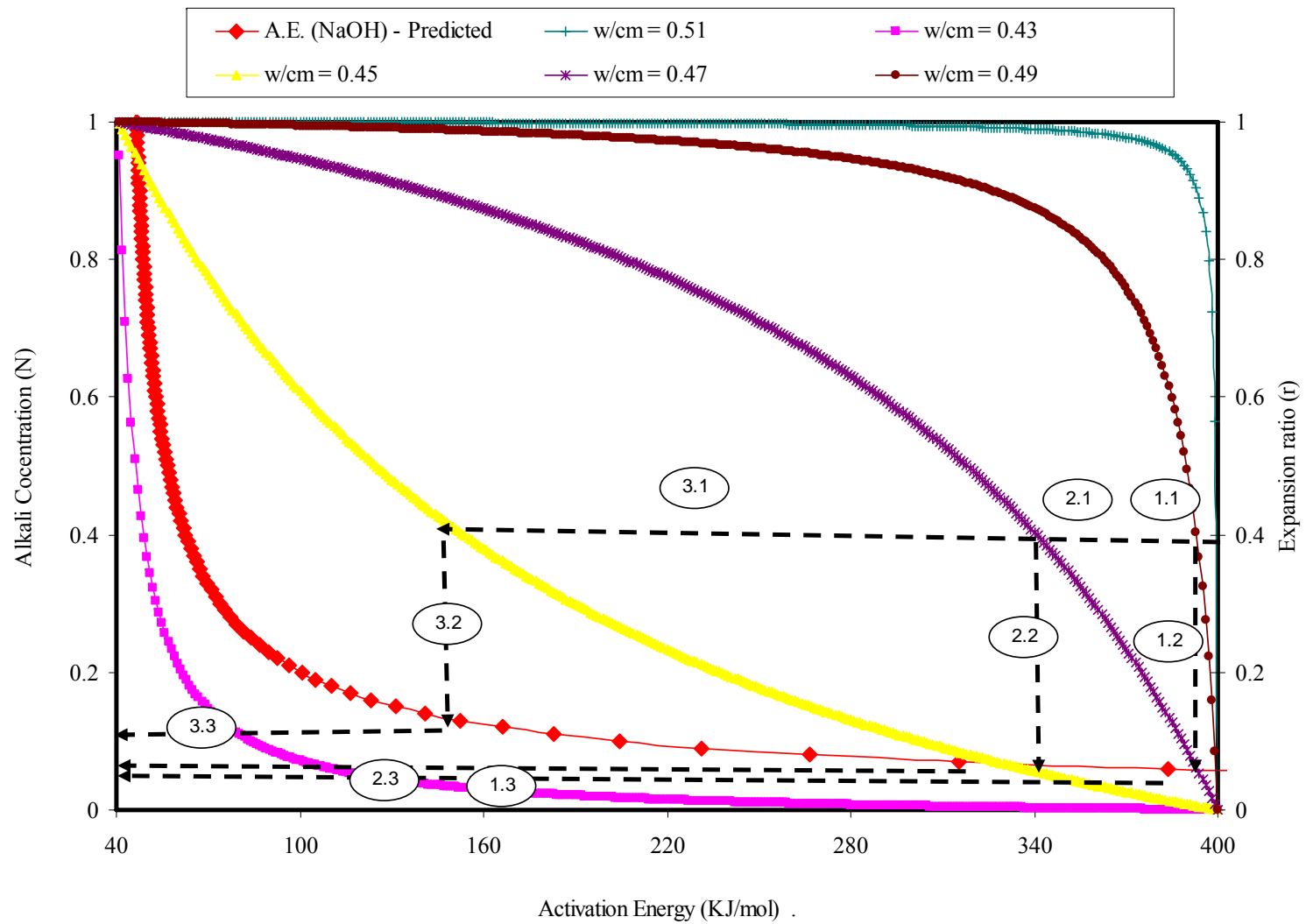Figure 6.22 PRG Threshold Design for Alkalinity (w/cm = 0.45).

Figure 6.23 PRG Threshold Design for Alkalinity (fly ash = 25%).

CHAPTER VII

CONCLUSIONS AND RECOMMENDATIONS

Introduction

Alkali-silica reaction has become in concrete structures (pavement, bridges, dams, etc) a growing and annoying problem for engineers, contractors and government agencies. As mentioned in Chapter II, the presence of a reactive siliceous component in some types of aggregate, high alkali content in the concrete matrix and a sufficient amount of moisture are the three major requirements needed for the ASR to initiate and spread. Therefore, the current logical approaches to tackle the problem were to use non-reactive aggregate, low alkali cement and to add a sufficient amount of supplementary cementitious materials (fly ash, etc) based on empirical history.

Laboratory standards tests are available and are currently used by researchers and agencies. The two most recognized tests are ASTM C1260 (Mortar- Bar Method) and ASTM C1293 (concrete prisms). The first test is a relatively short procedure and can be conducted within 16 days. But it is considered an aggregate test and its test conditions (i.e. crushing the aggregate and temperature) yield results that have very limited relevance to field conditions. The second standard procedure prism is very popular and is widely considered a good index of field performance. However, the minimum one year test duration is considered a serious setback. Consequently, a completely different approach; preferably a performance based approach is necessary.

To achieve this ultimate objective, a four year research project was conducted to develop a reliable test protocol that will assist the engineers, contractors and owners to identify and measure the potential for concrete pavement degradation because of ASR. Hence a comprehensive study on different types of aggregates of different reactivity was conducted to formulate a robust approach that takes into account the factors affecting ASR such as temperature, moisture, calcium concentration and alkalinity. This chapter presents the conclusions of this study based on the analysis of the results and discussions presented in chapters V and VI. In addition some recommendations for further research

and implementing this research into practical use are also provided at the end of this chapter.

Conclusions

Different series of expansion measurements were conducted on different types of aggregates (New Mexico Rhyolite, Platte River Gravel, Spratt Limestone, Sudbury Gravel) using a new apparatus developed at the Texas Transportation Institute referred to as "Dilatometer". A new model was proposed to determine ASR characteristics (the ultimate expansion of aggregates/concrete, the theoretical initial time of ASR expansion, the rate constant and the time scale parameter). The parameters were determined using a mathematical procedure entitled "System Identification Method". The ASR aggregates reactivity was predicted in terms of their activation energy using the Arrhenius equation. Some of the main findings from this part are:

a) All expansion-time plots display similar characteristic patterns. Almost no expansion was recordable in the initial hours (0-15 hrs). This was followed by a rapid increase in volume expansion up to 60-75 hrs. Then the expansion was stabilized around the four day period. This may be due to leaching of some calcium and potassium cations out of the aggregate. The gel absorbs those ions and blocks the dissolution of silica, and consequently impedes any further gel development.

b) Results indicate that alkalinity of the soak solution is a major factor that affects ASR expansion. An increase in alkalinity yields an increase in ASR expansion. This gain was attributed to the formation and then expansion of the ASR gel around the reaction sites of the aggregates.

c) The effect of temperature on ASR characteristics is very important to notice. It was observed for all types of aggregates at different alkalinities that increasing temperature from 60^0C to 70^0C, and 70^0C to 80^0C increases the rate constant. This indicates that ASR is a thermally activated process.

d) The importance of temperature as an accelerator of ASR is also evident. This can be observed by its effect on the theoretical on the time of expansion, t_0. This is explained from a kinetic point of view. As temperature increases, the amount of additional energy needed to initiate ASR decreases because the energy barrier that the system

has to overcome is much smaller at a higher temperature and therefore the time that it takes for ASR to initiate and develop is shorter.

e) Experimental results indicate that the addition of calcium hydroxide to the alkaline solution enhances ASR as more volumetric expansion was recorded. The previous is confirmed by the chemistry of the test solution where a sharp decline of sodium and hydroxyls ions was observed after the test compared to those in only sodium hydroxide solution.

f) From the analysis, it can be stated that ASR was found to be expansive without the presence of calcium hydroxide. Otherwise, both shrinkage and an increase in alkali ions would have been measured, which was not the case. The chemistry of the alkali solution supports this point of view.

g) To compare the reactivity of the aggregates in this study, the E_a of the rocks, determined using the Arrhenius equation, were compared against each other. From this comparison, it can be concluded that NMR is the most reactive aggregate tested in this research, followed by S.L, SuG and then PRG. By comparing the E_a at different alkalinities, it was also found that the E_a decreases when alkalinity increases. This observation signals the presence of a relationship between these two parameters and is very consistent with the definition of E_a as the minimum energy required to overcome for a chemical reaction to proceed.

h) To check the procedure validation and the laboratory proficiency, intra and inter-laboratory comparisons were conducted. Results are very promising as the covariance was less than 7% indicating that the results are highly repeatable and reliable. To check the capability of the new proposed kinetic model for distinguishing aggregates with different reactivity, hypothesis tests on the mean E_a of each type of aggregate at different alkalinity is conducted. Statistical results (two-samples T-Test) indicate that the means are different at 5% significance level. Therefore, it can be concluded that the E_a can serve as an overall indicator of ASR potential and can be used as a potential screening parameter for ASR in field performance.

In addition to the aggregate tests conducted, concrete samples with different w/cm's and fly ash contents using NMR and PRG aggregates were tested using the dilatometer at different alkalinities to determine concrete characteristics. By testing

concrete, as opposed to simply testing aggregates, realistic field and environmental effects are inherently considered when evaluating the resistance of different concrete mixtures to ASR. To relate the effect of material combinations to field performance, two models (aggregate and concrete) were combined together. The first model predicts the E_a of the aggregate at levels of alkalinity similar to field conditions. The second model, generated using the Juarez-Badillo transform, connects the concrete-to-aggregate expansion ratio, the w/cm, the fly ash content and the E_a of the aggregate. Some of the major findings from this part are:

a) Concrete expansion time plots show similar patterns. They begin with a dormant phase, followed by a steady increase. This was attributed to development of the gel in the concrete.

b) It was observed that concrete tested in a high alkali solution displays the highest ultimate expansion. This is likely due to the presence of an alkali gradient between the pore solution and the soak solution. This gradient in non existent at low alkalinity levels. Chemistry of the alkali before and after the test supports this point of view. Therefore, it can be concluded that concrete in the field subjected to a high alkali environment will display cracking earlier than to structures exposed to mild alkali conditions.

c) Experimental results show that the expansion ratio for NMR and PRG is close to one at 1N NaOH + CH. This can be explained as the combined effects of two concurrent causes: 1) The first is that the concrete is highly permeable at a water cement ratio of 0.45 and 2) the pozzolanic reaction is still at its early age. Thus, it can be stated that the expected restraining effects of the mortar around the aggregate is minimum in the initial period (2 weeks).

d) NMR concrete displays higher expansion than PRG at all alkalinities. The results are very consistent with ASR aggregate characteristics results (E_a). Therefore, it can be concluded that the type of reactive aggregate used in concrete mixtures is the main factor that determines the expansion that may occur in concrete pavement.

e) The relationship between the E_a and alkalinity appears to follow a "power curve". In other words, they have an inversely proportional relationship. The proposed model indicates that increasing the alkalinity of the solution beyond a certain level will only

induce minimal change on the E_a values. This is likely due to the fact that the reaction sites on the surface of the aggregate were fully saturated by the hydroxyl ions coming from the soak solutions at high alkalinity.

f) In all tests conducted for NMR and PRG, it appears that the absence of fly ash in all tests is characterized by a high ultimate expansion. Therefore, the use of mineral admixtures is vital to mitigate ASR as fly ash increases the durability of concrete through the pozzolanic reaction resulting in a denser concrete matrix and thus reducing its permeability.

g) A comparison conducted between $r_{measured}$ and $r_{predicted}$ values leads us to conclude that the proposed concrete model has the capability of capturing with high accuracy the combined effects of concrete materials (aggregate reactivity, diffusion, w/cm, % fly ash, on ASR expansion).

h) Through demonstrated numerical examples, it was seen that the proposed combined approach in this study is so flexible that the user can select the proper expansion ratio based on the importance of the structure and/or lifetime of the pavement and then select the percent fly ash needed to keep the total alkalinity level below the threshold of 5 lb/yd^3. Researchers have mentioned that expansion is unlikely to occur below this value. It was found in this study that concrete with water cement ratio of 0.45 and 30% class F fly ash are the optimum mixture combinations to mitigate ASR.

i) This new procedure will give the material engineer the capability of selecting any combination (w/cm & fly ash) that best fits his need or type of application, and of predicting its effect on the concrete characteristics (alkalinity of the pore solution, expansion ratio, etc) without physically conducting the dilatometer tests. This consistency and efficiency will help agencies save invaluable time.

Recommendations for Future Research

Based on the knowledge gained from this research project, it is recommended that the following additional studies be conducted to broaden the concepts and the strategies developed in this study to mitigate ASR:

a) This study was based on limited number of reactive aggregates, one type of cement and one type of fly ash. Additional sources of aggregates and different types of fly

ash should be investigated thoroughly before the findings from this research can be generalized on a broader scale.

b) The results obtained are based on four known high reactive aggregate. It is unlikely that the aggregates used across the states are as reactive as those in this study. Therefore, it is recommended that agencies conduct the dilatometer test using their local materials under local field conditions and determine the optimum mixture combinations using the procedures and theories introduced this study.

c) Although the mechanisms are not fully understood, current research indicates that the use of lithium compounds suppresses ASR expansion. Research is needed to determine the effect of lithium compounds on the activation energy of aggregate and consequently on the ultimate expansion of concrete. Since the exact amount of lithium needed to mitigate ASR is not known, it would be beneficial to conduct concrete tests treated with lithium products in the dilatometer and determine the minimum amount of lithium requited to reduce the alkalinity of the pore solution below the threshold level. The amount of lithium can be included in the Jauarez-Badillo transform as was the w/cm ratio, the fly ash content, and the activation energy.

d) Work should be furthered to normalize aggregate reactivity according to size distribution and other related factors.

e) Since crack initiation in some concrete mixtures was identified, it would be extremely beneficial to determine the minimum expansion ratio (r_L) as a function of the main concrete parameters that will lead to the identification of a boundary area for safe design.

REFERENCES

American Society for Testing Materials (ASTM). (2000a). "ASTM C 1293-95: Standard test method for concrete aggregates by determination of length change of concrete due to alkali-silica reaction." *Annual Book of ASTM Standards*, West Conshohocken, PA, 673-678.

American Society for Testing Materials (ASTM). (2000b). "ASTM C 1260-94: Standard test method for potential alkali reactivity of aggregate (mortar-bar method)." *Annual Book of ASTM Standards*, West Conshohocken, PA, 669-672.

American Society for Testing Materials (ASTM). (2000c). "ASTM C 227-97a: Standard test method for potential alkali reactivity of cement-aggregate combinations (mortar-bar method)." *Annual Book of ASTM Standards*, West Conshohocken, PA, 127- 131.

American Society for Testing Materials (ASTM). (2000d). "ASTM C 289-94: Standard test method for potential alkali reactivity of aggregate (chemical method)." *Annual Book of ASTM Standards*, West Conshohocken, PA, 154-160.

American Society for Testing Materials (ASTM). (2000e). "ASTM C 294-98: Standard Descriptive Nonmenclature for Constituents of Concrete Aggregates." *Annual Book of ASTM Standards*, West Conshohocken, PA, 164-172.

American Society for Testing Materials (ASTM). (2000f). "ASTM C 295-98: Standard guide for petrographic examination of aggregate for concrete." *Annual Book of ASTM Standards*, West Conshohocken, PA, 173-180.

American Society for Testing Materials (ASTM). (2000g). "ASTM C 441-97, Standard test method for effectiveness of mineral admixture or ground blast-furnace slag in preventing excessive expansion of concrete due to the alkali-silica reaction." *Annual Book of ASTM Standards*, West Conshohocken, PA, 225-227.

American Society for Testing Materials (ASTM). (2000h). "ASTM C 856-95, Standard practice for petrographic examination of hardened concrete." *Annual Book of ASTM Standards*, West Conshohocken, PA, 424-439.

American Society for Testing Materials (ASTM). (2000i) "ASTM C 342-97, Standard test method for potential volume change of cement-aggregate combinations." *Annual Book of ASTM Standards*, West Conshohocken, PA, 207-210.

American Society for Testing Materials (ASTM). (2000j) "ASTM C33-99a, Standard specification for concrete aggregates." *Annual Book of ASTM Standards*, West Conshohocken, PA, 10-17.

American Society for Testing Materials (ASTM). (2006) "ASTM C1567-04, Standard Test Method for Determining the Potential Alkali-Silica Reactivity of Combinations of Cementitious Materials and Aggregate (Accelerated Mortar-Bar Method)." *Annual Book of ASTM Standards*, West Conshohocken, PA, 772-776.

Andersen, K.T. and Thaulow, N. (1989). "The application of undulatory extinction angles (UEA) as an indicator of alkali-silica reactivity of concrete aggregates." *In* Okada K., Nishibayashi, S., and Kawamura, M. (Editors): *Proc., of the 8th International Conference on Alkali-Aggregate Reaction*, Kyoto, Japan, 489-494.

Barringer, W. L. (2000). "Application of accelerated mortar bar tests to New Mexico aggregates, *Proc., of 11th International Conference on Alkali-Aggregate Reactions in Concrete*, Quebec City, Quebec, Canada, 563-572.

Bellew, P. G., 1983, "Evaluation of test methods for alkali aggregate reactivity." *Proc., of the International Conference on Alkalis in Concrete: Research and Practice*, Copenhagen, Denmark, 303-314.

Berube, M., Duchesnea, J., Doriona, J.F., and Rivest, M. (2002). "Laboratory assessment of alkali contribution by aggregates to concrete and application to concrete structures affected by alkali–silica reactivity." *Cement and Concrete Research*, 32, 1215-1227.

Bleszynski, R., Thomas, M. D. A., and Hooton, D. (2000). "The efficiency of ternary cementitious systems for controlling expansion due to alkali-silica reaction in concrete." *Proc., of the 11th International Conference on Alkali-Aggregate Reaction*, Quebec, Canada, June 11-16, 583–592.

British Standard (1984). "BS 6100, British standard glossary of building and civil engineering terms, Section 5.2." British Standard Institution, London, UK.

British Standard (1989). "BS 812-Part 102, Testing aggregates. Methods for sampling." British Standards Institution (BSI), London, UK.

Canadian Standards Association (CSA), (2000). "Guide to the evaluation and management of concrete structures affected by alkali-aggregate reactions." CSA A864-00, 2000b, Ontario, Canada.

Carino, N. J. and Lew, H. S. (2001). "The maturity method: From theory to application." *Proc., the 2001 Structures Congress and Exposition*, Chang, P.C. ed., ASCE, Reston, VA., 1-19.

Chatterji, S. (1979). "The role of $Ca(OH)_2$ in the breakdown of Portland cement concrete due to alkali-silica reaction." *Cement Concrete Research*, 9(2), 185-188.

Chatterji, S. (1989). "Mechanisms of alkali-silica reaction and expansion." *Proc., 8th Int. Conf. on Alkali-Aggregate Reaction in Concrete*, Kyoto, 101-105.

Chatterji*, S., Jensen, A. D., Thaulow, N. and Christemsens, P. (1986). "Studies of alkali-silica reaction. Part 3. Mechanisms by which NaCl and Ca(OH)$_2$ affect the reaction." *Cement and Concrete Research*, 16(2), 246-254.

Chatterji, S., Thaulow, N. and Jensen, A.D. (1988). "Studies of alkali-silica reaction. Part 6. Practical implications of a proposed reaction mechanism." *Cement and Concrete Research*, 18, 363-366.

Chatterji, S, Thaulow, N., Jensen, A. D., and Christensen, P. (1986). "Mechanisms of accelerating effects of NaCl and Ca(OH)$_2$ on alkali-silica reaction." *Proc., of the 7th International Conference on Alkali-Aggregate Reaction in Concrete*, Ottawa, 115-119.

Dayah, M. (2009). <http://www.dayah.com/periodic> (Feb. 2, 2008).

Dent-Glasser, L. S. and Kataoka, N. (1981). "The chemistry of alkali-aggregate reactions." *Proceedings of the 5th International Conference on Alkali-Aggregate Reactions*, Cape Town, South Africa, S252/23, p. 66.

Desai, J. B. (2007). "Investigation into mitigation of alkali-silica reaction using selected SCM's in presence of potassium acetate deicer." Ph.D. Dissertation, Clemson University, SC.

Diamond, S. (1981). "Effects of two danish fly ashes on alkali contents of pore solutions of cement-fly ash pastes." *Cement and Concrete Research*, 11(3), 383–394.

Diamond, S. (1983). Alkali-reactions in concrete-pore solution effects. *Proc., of the 6th International Conference on Alkalis in Concrete*, Copenhagen, Denmark, 155–166.

Diamond, S. (1989). "ASR—Another look at mechanisms." *Proc., of the 8th International Conference on Alkali-Aggregate Reaction*, K. Okada, S. Nishibayashi, and M. Kawamura, eds., Kyoto, Japan, 83–94.

Dolar-Mantuani, L. (1978). Practical aspects of identifying alkali-reactive aggregates by petrographic methods. *Proc., of the 4th International Conference on Effects of Alkalis in Cement and Concrete*, West Lafayette, IA, 267–280.

Ebbing, D. D., and Gammon, S. D. (2005). *General chemistry*, 8th Edition, Houghton Mifflin, Boston, MA.

Folliard, K. J., Thomas, D.A., Fournier, B., Kurtis, K. E., and Ideker, J.H. (2006). *Interim recommendations for the use of lithium to mitigate or prevent alkali-silica reaction (ASR)*. FHWA-HRT-06-073, Federal Highway Administration, McLean, VA.

French, W. J. (1986). A review of some reactive aggregates from the U.K. with reference to the mechanism of reaction and deterioration. *Proc., of the 7th International Conference on Concrete Alkali-Aggregate Reactions*, Ottawa, Canada, 226–230.

Geiker, M., (1983). "Studies of Portland cement hydration: Measurement of chemical shrinkage and a systematic evaluation of hydration curves by means of the dispersion model." Ph.D. dissertation, Technical University of Denmark, Lyngby, Denmark.
Geiker, M. and Knudsen, T. (1985). "Chemical shrinkage" *Proc., Research on the Manufacture and Use of Cements*, Engineering Foundation, Denmark, 99-107.

Gillott, J. E., Duncan, M. A. G. and Swenson, E. G. (1973). "Alkali-aggregate reaction in Nova Scotia. IV. Character of the reaction." *Cement and Concrete Research*, 3, 521-535.

Gjorv, O. E. (1983). "Durability of Concrete Containing Condensed. Silica Fume." American Concrete Institute-SP-79, 2, 695–708.

Glasser, F. P. (1992). "Chemistry of the alkali-aggregate reaction." *The alkali-silica reaction in concrete,* R.N. Swamy ed., Blackie, London, United Kingdom, 96-121.

Grattan-Bellew, P. E. (1989). "Test methods and criteria for evaluating the potential reactivity of aggregates." *Proc., of the 8th International Conference on Alkali-Aggregate Reaction*, Kyoto, Japan, 279–294.

Hansen, W. C. (1944). "Studies relating to the mechanism by which the alkali-aggregate reaction proceeds in concrete." *Journal of the American Concrete Institute*, 15(3), 213-227.

Hooton, R. D. (1986). Effect of containers on ASTM C 441- Pyrex mortar bar expansions. *Proc., of the 7th International Conference on Alkali-Aggregate Reaction in Concrete*, Ottawa, Canada, 351-357.

Idorn, G. M. (1967). *Durability of concrete structures in Denmark*. Danish Technical Press, Copenhagen.

Jensen, A. D., Chatterji, S., Christensen, P., and Thaulow, N. (1984). "Studies of alkali-silica reaction part 2 effect of air-entrainment on expansion." *Cement and Concrete Research*, 14(3) 311-314.

Johnston, D. P, Stokes, D., and Surdahl, R. (2000). "A kinetic-based method for interpreting ASTM C 1260." *Cement Concrete Aggregate*, 22(2), 142-149.

Juarez-Badillo, E. (1981). "General compressibility equation for soils." *10th International Conference on Soil Mechanics and Foundation Engineering,* Stockholm, Sweden, 171-178.

Knudsen, T. (1986). "A continuous, quick chemical method for the characterization of the alkali-silica reactivity of aggregates." *Proc., the 7th International Conference on Concrete Alkali-Aggregate Reactions*, Ottawa, 289-293.

McGowan, J. K., and Vivian, H. E. (1952). "Studies in cement-aggregate reaction: Correlation between crack development and expansion of mortars." *Australian Journal of Applied Science*, 3, 228–232.

Mindess, S., Young, J. F., and Darwin, D. (2006). *Concrete*, 2nd Ed., Prentice Hall, Upper Saddle River, NJ.

Monteiro, P. J. M., Wang, K., Sposito, G., dos Santos M. C., and de Andradef , W. P. (1997). "Influence of mineral admixtures on the alkali –aggregate reaction." *Cement and Concrete Research*, 27(12), 1899-1909.

Montgomery, D. C., and Runger, G. C. (2002). *Applied statistics and probability for engineers*, 2th Ed. Wiley, New York.

Mukhopadhyay, A., Shon, C., and Zollinger, D. (2006). "Activation energy of alkali-silica reaction and dilatometer method." *Journal of the Transportation Research Board*, 1-11.

Neville, A. M. (1996). *Properties of concrete*, 4th Ed., Pearson Education, Singapore.

Nixon, P.J., Page, C.L., Bollinghaus, R., and Canham, I. (1986). "The effect of pfa with a high total alkali content on pore solution composition and alkali silica reaction." *Magazine Concrete Research*, 38(134), 30-35.

Nixon, P. J., and Sims, I., (1992). "RILEM TC106 alkali aggregate reaction – accelerated tests interim report and summary of survey of national specifications." *Proc., of the 9th International Conference on Alkali-Aggregate Reaction in Concrete*, Concrete Society, Slough, UK, 2, 731–738.

Oberholster, R. E. and Davies, G. (1986). "An accelerated method for testing the potential alkali reactivity of siliceous aggregates." *Cement and Concrete Research*, 16, 181-189.

Odler, I. (2000). "Special inorganic cements." *Modern Concrete Technology Series*, Ed. E&FN Spon, New York, 8, 115-133.

Pedneault, A. (1996). "Development of testing and analytical procedures for the evaluation of the residual potential of reaction, expansion, and deterioration of concrete affected by ASR." M.Sc. Memoir, Laval University, Québec City, Canada.

Powers, T.C. (1935). "Adsorption of water by Portland cement paste during the hardening process." *Industrial and Engineering Chemistry*, 27, 790-794.

Powers, T. C., Copeland L. E., and Mann H. M. (1954). "Permeability of Portland cement paste." *Journal of American Concrete Institute*, 51, 285-298.

Powers, T. C., and Steinour, H. H. (1955). "An investigation of some published researches on alkali-aggregate reaction: I. the chemical reactions and mechanism of expansion." *Journal of the American Concrete Institute*, 26(6), 497–516.

Prezzi, M., Monteiro, P. J. M., and Sposito, G. (1997). Alkali-silica reaction - Part 1: Use of the double-layer theory to explain the behavior of the reaction product gels." *ACI Journal*, 94(1), 10-17.

Prezzi, M., Monteiro, P. J. M., and Sposito, G. (1998). Alkali-silica reaction - Part 2: The effect of chemical additives." *ACI Journal*, 95(1), 3-10.

Rangaraju, P. R., and Olek, J. (2007). "Potential for acceleration of ASR in presence of pavement deicing chemicals." Rep. *01-G-002-03-9*, Innovative Pavement Research Foundation, Skokie, IL.

Rodrigues, F. A., Monteiro, P. J. M., and Sposito, G. (1999). "The alkali-aggregate reaction: The surface charge density of silica and its effect on the expansive pressure." *Cement and Concrete Research*, 29(4), 527-530.

Rodrigues, F. A., Monteiro, P. J. M. and Sposito, G. (2001). "The alkali–silica reaction: The effect of monovalent and bivalent cations on the surface charge of opal." *Cement and Concrete Research*, 31(11) 1549–1552.

Rogers, C. (1999). "Multi-laboratory study of accelerated mortar bar test (ASTM C 1260) for alkali-silica reaction." *Cement, Concrete and Aggregates*, 21(2), 191-200.

Rogers, C. A. and Hooton, R. D. (1989). Leaching of alkalis in alkali-aggregate reaction testing. *Proc., of the 8th International Conference on Alkali-Aggregate Reaction*, Kyoto, Japan, 327–332.

Sarkar, S. L., Zollinger, D. G., Mukhopadhyay, A. K., and Seungwook, L. (2004). Appendix 1- Handbook for Identification of Alkali-Silica Reactivity." *Airfield Pavement, Advisory Circular No. 150/5380-8*, U.S. Department of Transportation Federal Aviation Administration.

Shon, C. (2008). "Performance-based approach to evaluate alkali-silica reaction potential of aggregate and concrete using dilatometer method." Ph.D. dissertation, Texas A&M University, College Station, TX.

Sorrentino, D., Clement, J. Y., and Golberg, J. M. (1992). "A new approach to characterize the chemical reactivity of the aggregates." *Proc., of the 9th International Conference on Alkali-Aggregate Reaction in Concrete*, Slough, UK, 1009-1016.

Stanton, T. E. (1940). "Expansion of concrete through reaction between cement and aggregate". *Proc. ASCE*, 66, 1781–1811.

Stark, D., and Bhatty, M. S. Y. (1986). "Alkali-silica reactivity: Effect of alkali in aggregate on expansion." Alkalies in Concrete, ASTM STP 930, American Society for Testing and Materials, Philadelphia, PA, 16–30.

Stewart, R. (2005). "Characterization of an alkali-silica-reaction system" Unpublished paper, Texas A&M University, College Station.

Strategic Highway Research Program, (1991). *SHRP C-315, Handbook for the identification of alkali-silica reactivity in highway structures,* Washington, D.C.

Swamy, R. N. (1992). *The alkali-silica reaction in concrete*, Van Nostrand Reinhold, New York.

Swamy, R. N. and Al-Asali, M. M. (1986). New test methods for alkali-silica reaction. *Proc., of the 7th International Conference on Concrete Alkali-Aggregate Reactions*, Ottawa, Canada, 324–329.

Swamy, R. N. and Al-Asali, M. M. (1988). "Expansion of concrete due to alkali-silica reaction." *ACI Materials Journal* 85, 33-40.

Tang, M. (1981). "Some remarks about alkali-silica reactions." *Cement and Concrete Research*, 33(117) 208–219.

Tang, M. S., and Su-Fen, H. (1980). "Effect of $Ca(OH)_2$ on alkali-silica reaction." *Proc., of the Eight International Congress of Cement Chemistry*, Paris, France, 2, 94–99.

Thomas, M. D. A., Blackwell, B. Q., and Pettifer, K. (1992). "Suppression of damage from alkali silica reaction by fly ash in concrete dams." *Proc., of the 9th International Conference on Alkali-Aggregate Reaction in Concrete*, Concrete Society, Slough, London, United Kingdom, Concrete Society, Slough, 2, 1059–1066.

Thomas, M. D. A. and Bleszynski, R. F. (2001). "The use of silica fume to control expansion due to alkali-aggregate reactivity in concrete - A review." *Materials Science of Concrete VI*, Eds. J. Skalny and S. Mindess, American Ceramic Society, Westerville, OH.

Thomas, M. D. A., Fournier, F., Folliard, K. J., Ideker, J.H., and Resendez, Y. (2007). "The use of lithium to prevent or mitigate alkali-silica reaction in concrete pavements and structures." FHWA-HRT-06-133, Federal Highway Administration, McLean, VA.

Tordoff, M. A. (1990). Assessment of prestressed concrete bridges suffering from alkali silica reaction. *Cement and Concrete Composites,* 12(3) 203–210.

Unbehauen, U. (1982). "Introduction to system identification using parameter estimation methods." *Identification of vibrating structures*. Ed. by H.G. Natke, Springer Verlag, Germany.

Wesche, K. (1991). (Ed.), "Fly ash in Concrete," RILEM Report of Technical Committee 67-FAB, section 3.1.5 by I. Jawed and J. Skalny, 59-62 E&FN Spon, London.

Young, J. F., Mindess, S., Gray, R. J., and Bentur, A. (1998). *The science and technology of civil engineering materials*, Prentice Hall, Upper Saddle River, NJ.

VITA

Hassan A. Ghanem was born in Tripoli - Lebanon. He did his elementary and high school in a private French school in Lebanon and received his diploma from Lycee Franco Libanais – Tripoli in 1994. He attended Beirut Arab University to pursue a degree in engineering. He received his B.E. with a major in civil engineering in 1999. He continued his education in his alma mater and completed his M.E. specializing in structural and geotechnical engineering in January 2002. While pursuing his graduate studies in Lebanon, he worked for the Technical Engineering and Contracting Office for three years on projects involving design and construction of residential buildings.

A yearning for more advanced studies in civil engineering forced him to travel overseas. He attended Texas Tech University, Lubbock, TX in Fall 2002 and received his M.S. in civil engineering specializing in structural and wind engineering in August 2004. His Ph.D. studies began in 2004 at Texas A&M University in College Station under the direction of Dr. Dan Zollinger in the development of ASR mitigation techniques and graduated in May 2009.

His permanent address is: Lebanon – Tripoli – Abou Samra – Place Saadoun – Bldg Zapher Sayadi – Sixth Floor